Some theory and phenomenology of neutrino masses and the baryon asymmetry

MOFFAT, KRISTIAN,PASCAL

Some theory and phenomenology of neutrino masses and the baryon asymmetry

Kristian Moffat

A thesis presented for the degree of
Doctor of Philosophy

Institute for Particle Physics Phenomenology
Department of Physics
Durham University
United Kingdom

October 2019

Some theory and phenomenology of neutrino masses and the baryon asymmetry

Kristian Moffat

Submitted for the degree of Doctor of Philosophy

October 2019

Abstract: This thesis provides some theoretical and phenomenological work on two of the outstanding problems in modern physics, namely, the extreme smallness of neutrino masses and the relative abundance of matter over antimatter. A theorem is developed relating the smallness of the light neutrino masses to the degree of lepton number violation in some seesaw extensions of the Standard Model of particle physics. It is shown that for exactly massless light neutrinos there must be an exact lepton number symmetry. Then the viability of thermal leptogenesis as a resolution to the baryon asymmetry problem at different scales is assessed using more sophisticated numerical tools than have previously been applied. It is shown that, if fine-tuned solutions are allowed, the scale may be lowered to $\sim 10^6$ GeV. Using these results, it is shown that, if CP violation comes purely from the phases of the PMNS matrix, thermal leptogenesis may still be viable over a range of scales covering 10^6 — 10^{13} GeV. It is also shown that thermal leptogenesis is viable in the Neutrino Option, in which the Higgs potential has its dimensionful parameter provided by loop corrections from the heavy Majorana neutrinos in the type I seesaw at a mass scale $\sim 10^6$ GeV.

Contents

List of Figures

List of Tables

Declaration

The work in this thesis is based on research carried out in the Department of Physics at Durham University. No part of this thesis has been submitted elsewhere for any degree or qualification.

- Chapter 4 is based on [4] to be published presently
- Chapter 5 is based on [5] published as
  Three-flavored nonresonant leptogenesis at intermediate scales
  K. Moffat, S. Pascoli, S.T. Petcov, H. Schulz and J. Turner, Phys. Rev. D **98**, 015036
- Chapter 6 is based on [6] published as
  Leptogenesis from Low Energy CP Violation,
  K. Moffat, S. Pascoli, S. T. Petcov and J. Turner, JHEP **03** (2019) 034
- Chapter 7 is based on [7] accepted for publication in JHEP

Acknowledgements

Now that I have completed this work and it is almost time for me to release it into the world, I have first the enjoyable task of thanking those who enabled me to reach this point.

I have been fortunate to have been the student of Silvia Pascoli whose contributions have inarguably improved every project we have worked on. Every student ought to have a supervisor capable of such sharp insights and scientific integrity.

Perhaps it's the competitive nature of the field, but I've also been fortunate to have had only good collaborators in Cédric, Jessica, Holger, Serguey and Ilaria. In particular I would like to let Jessica know how much I have appreciated her kindness, and that she has made the work we did together thoroughly enjoyable.

I managed to spend these four years in the company of some amazing friends. I was glad to find no distance had grown between me and my old schoolfriend Carl and to have three more years in his company. And I made many wonderful new friends with whom I've shared many laughs and adventures, including: Alexis, Andrés, Andrew, Dan, Fernando, Jack, Jacob, Maddy, Matheus, Phil, Piotr and Tom. I especially want to thank Jack and Matheus for the depth of their friendship.

I must mention the constant remote presence of David which has been so important to me.

Finally I want to thank Mom, Dad and Dougal for their endless support and love.

What one fool can do, another can.

— from *Calculus Made Easy* by Silvanus P. Thompson

What one fool can understand, another can.

— from *QED: The Strange Theory of Light and Matter* by Richard P. Feynman

Dedicated to

Karen, Jim and Daniel

Chapter 1

Introduction

Elementary particle physics and cosmology are mature fields — they both have a standard model that elegantly explains most observations. However, there are experimental observations which do not fit in these standard models. Unexplained phenomena include: the identity of dark matter, the origin of dark energy, the baryon asymmetry of the universe, the strong CP problem, the existence of neutrino masses, the hierarchy problem, etc.[1] Solutions to any of these questions will necessarily constitute profound revisions to the established body of scientific knowledge. This thesis addresses two of them in detail:

1. The origin of neutrino masses. Massive fermions must have left- and right-chiral components but the Standard Model of particle physics, in its most minimal form, does not include right-chiral neutrino fields. Thus the observed neutrino masses are without explanation. Simply including these fields in the Standard Model is not very satisfactory, as the observed neutrino masses are very small and would thus require exceedingly small couplings. In order to avoid such fine-tuned parameters, more nuanced extensions of the Standard Model have been proposed that naturally explain the smallness of these masses.

[1] A glance over new submissions to arXiv.org on any given weekday gives some indication of which problems attract the most attention.

2. The baryon asymmetry of the universe or the measured excess of matter over antimatter in the universe. The Standard Model of particle physics does not predict a quantitatively correct asymmetry and thus extensions must be sought that can remedy this. A particularly appealing feature of some of these extensions is that they can simultaneously explain the baryon asymmetry and the origin of the small neutrino masses.

This thesis is written from my current perspective on the subjects I touched during my PhD and assumes the level of knowledge I had as a PhD student when I began my research in particle physics. There are two introductory chapters, Chapters 2 and 3, which provide the necessary background for the original research presented in Chapters 4, 5, 6 and 7. It concludes in Chapter 8 with a discussion of its relevance to the body of particle physics knowledge at large. Chapter 2 introduces the basic ideas of neutrino physics that are necessary for this thesis. Chapter 3 introduces one mechanism by which the baryon asymmetry is produced, namely leptogenesis. Following the convention for most particle physics PhD theses, the middle chapters are heavily based on my research papers. Chapter 4 introduces a theorem relating lepton number violation and neutrino masses in some Standard Model extensions (based on [4]). Chapter 5 looks at the energy scales for which thermal leptogenesis may be viable (based on [5]). Chapter 6 explores the possible origins of CP violation in thermal leptogenesis (based on [6]). Chapter 7 asks if successful leptogenesis is possible in the context of a model called the Neutrino Option [2, 8] which purports to simultaneously solve the hierarchy problem and to explain neutrino masses (based on [7]).

Chapter 2

Massive neutrinos

The observed neutrinos are exceedingly light elementary fermions whose weak interactions are described by the Standard Model (SM) of particle physics. Their small masses have the rare property of being an experimental fact that is not comfortably explained by the Standard Model. Naturally, much contemporary research aims to provide mechanisms by which neutrinos may obtain such small masses.

In this chapter, we shall review both the successes and failures of the Standard Model in explaining neutrino phenomena. We shall then take a panoramic survey of the relevant extensions of the Standard Model before focusing in on the type I seesaw extension which is prominent in the later chapters of this thesis.

2.1 The Standard Model and neutrinos

The Standard Model

The Standard Model is a quantum field theory described by a path integral with gauge symmetry group $\mathrm{SU}(3)_c \times \mathrm{SU}(2)_L \times \mathrm{U}(1)_Y$ and with a renormalisable Lagrangian which may be decomposed according to its field content as

$$\mathcal{L}_{\mathrm{SM}} = \mathcal{L}_{\mathrm{Gauge}} + \mathcal{L}_{\mathrm{Higgs}} + \mathcal{L}_{\mathrm{Fermion}} + \mathcal{L}_{\mathrm{Yukawa}}. \tag{2.1.1}$$

This field content is summarised in Table 2.1. The Standard Model is the current best explanation of electromagnetism, the weak interactions and the strong interactions. Gravitation, the remaining fundamental interaction is not incorporated into it.

The strong interactions result from the local $\mathrm{SU}(3)_c$ symmetry whose *colour charge* is carried by the quarks, Q_i, u_{iR} and d_{iR} [9–11]; and the gluons G which are the corresponding gauge boson. The gauge coupling runs to zero with increasing energies and is large at small energies. This means that high-energy processes are amenable to a perturbative analysis whereas the low-energy processes require fundamentally different techniques. At low energies, composite objects with overall zero colour charge will emerge — the mesons and baryons, with the quarks being permanently confined within them [12, 13].

The *electroweak interactions* are the result of the local $\mathrm{SU}(2)_L \times \mathrm{U}(1)_Y$ symmetry whose gauge bosons are W and B respectively. The quarks Q_i, u_{iR} and d_{iR}, the leptons L_α, $l_{\alpha R}$ and the Higgs ϕ carry the hypercharge of $\mathrm{U}(1)_Y$. Under $\mathrm{SU}(2)_L$, the doublets are: $Q_i = (u_{iL}, d_{iL})^T$ containing left-chiral up and down type quarks; $L_\alpha = (\nu_{\alpha L}, l_{\alpha L})^T$ which contains the left-chiral neutrino and charged lepton fields and $\phi = (\phi^\pm, \phi^0)$. In the SM, the Higgs field dynamically breaks the $\mathrm{SU}(2)_L \times \mathrm{U}(1)_Y$ symmetry to the symmetry of electromagnetism: $\mathrm{U}(1)_{\mathrm{em}}$. After this *electroweak symmetry breaking*, the massless W and B bosons are no longer mass eigenstates but instead mix to form the massive $W^\pm$ and Z bosons of the weak interactions and the massless photon A of electromagnetism.

Let us examine the terms in Eq. (2.1.1):

$\mathcal{L}_{\mathrm{Gauge}}$ contains purely gauge-boson fields G, W, B in kinetic or self-interaction terms:

$$\mathcal{L}_{\mathrm{Gauge}} = -\frac{1}{4} G^a_{\mu\nu} G_a^{\mu\nu} - \frac{1}{4} W^i_{\mu\nu} W_i^{\mu\nu} - \frac{1}{4} B_{\mu\nu} B^{\mu\nu}, \tag{2.1.2}$$

in which

$$G^a_{\mu\nu} \equiv \partial_\mu G^a_\nu - \partial_\nu G^a_\mu - g_1 f^{abc} G^b_\mu G^c_\nu, \tag{2.1.3}$$

$$W^i_{\mu\nu} \equiv \partial_\mu W^i_\nu - \partial_\nu W^i_\mu - g_2 \epsilon_{ijk} W^j_\mu W^k_\nu, \tag{2.1.4}$$

	$SU(3)_c$	$SU(2)_L$	$U(1)_Y$
Q_i	3	2	$+\frac{1}{3}$
L_α	1	2	-1
u_{iR}	3	1	$+\frac{4}{3}$
d_{iR}	1	1	$-\frac{2}{3}$
$l_{\alpha R}$	1	1	-2
G	8	1	0
W	1	3	0
B	1	1	0
ϕ	1	2	1

Table 2.1: The field content of the Standard Model. For $SU(3)_c$ and $SU(2)_L$, the non-Abelian groups, the dimension of the representation is shown. For $U(1)_Y$ the charge under that group (hypercharge, Y) is shown. The generational indices are $i \in \{1, 2, 3\}$ and $\alpha \in \{e, \mu, \tau\}$ and subscripts L and R denote left and right chirality respectively.

$$B_{\mu\nu} \equiv \partial_\mu B_\nu - \partial_\nu B_\mu. \tag{2.1.5}$$

Where here the roman alphabet is used for $SU(2)_L$, $SU(3)_c$ indices (in W and G), g_1, g_2 and g_3 are coupling constants of $SU(3)_c$, $SU(2)_L$ and $U(1)_Y$ respectively and ϵ_{ijk}, f^{abc} are the structure constants for $SU(2)_L$ and $SU(3)_c$ respectively.

$\mathcal{L}_{\text{Fermion}}$ contains the kinetic and gauge-interaction terms of the fermionic field content:

$$\mathcal{L}_{\text{Fermion}} = \overline{Q} i \not{D} Q + \overline{u_R} i \not{D} u_R + \overline{d_R} i \not{D} d_R + \overline{L} i \not{D} L + \overline{l_R} i \not{D} l_R, \tag{2.1.6}$$

in which the generational indices are hidden and

$$D_\mu = \partial_\mu + i g_1 G^a_\mu \frac{\lambda^a}{2} + i g_2 W^i_\mu \frac{\tau^i}{2} + i g_3 B_\mu \frac{Y}{2}, \tag{2.1.7}$$

where λ is the generator of $SU(3)_c$, τ^i are $SU(2)_L$ generators (the Pauli matrices), Y is the hypercharge operator. A field which is a singlet of a given gauge group should have the generator taken as 0.

$\mathcal{L}_{\text{Higgs}}$ contains the kinetic and self-interaction terms for the Higgs field ϕ:

$$\mathcal{L}_{\text{Higgs}} = \left(D^\mu \phi\right)^\dagger \left(D_\mu \phi\right) + \lambda \phi^\dagger \phi \left(v^2 - \phi^\dagger \phi\right), \tag{2.1.8}$$

in which v is the vacuum expectation value (VEV) of the Higgs field. When it

acquires a VEV, the Higgs field gives masses to the gauge bosons through

$$\begin{aligned} |D_\mu\langle\phi\rangle|^2 &= \left|\frac{1}{2}\begin{pmatrix} g_3B_\mu + g_2W_\mu^3 & g_2\left(W_\mu^1 - iW_\mu^2\right) \\ g_2\left(W_\mu^1 + iW_\mu^2\right) & g_3B_\mu - g_2W_\mu^3 \end{pmatrix}\begin{pmatrix} 0 \\ v \end{pmatrix}\right|^2, \\ &= \frac{g_2^2v^2}{2}W_\mu^+W^{-\mu} + \frac{v^2}{4}\left(g_2^2+g_3^2\right)Z_\mu Z^\mu, \end{aligned} \tag{2.1.9}$$

where $W_\mu^\pm \equiv (W_\mu^1 \mp iW_\mu^2)/\sqrt{2}$ and $Z_\mu \equiv (g_3B_\mu - g_2W_\mu^3)/\sqrt{g_2^2+g_3^2}$. The linearly independent counterpart to Z_μ is the photon $A_\mu \equiv (g_2B_\mu + g_3W_\mu^3)/\sqrt{g_2^2+g_3^2}$.

$\mathcal{L}_{\text{Yukawa}}$ is the fermion-Higgs interaction terms or *Yukawa terms* (with hidden generational indices)

$$\mathcal{L}_{\text{Yukawa}} = -\left(\overline{Q}\tilde{\phi}\right)Y_uu_R - \left(\overline{Q}\phi\right)Y_dd_R - \left(\overline{L}\phi\right)Y_ll_R + \text{h.c.}, \tag{2.1.10}$$

where $\tilde{\phi} \equiv i\tau_2\phi^*$ and through which the fermions can gain a mass once the Higgs acquires a VEV:

$$\begin{aligned} \mathcal{L}_{\text{Fermion mass}} &= -vY_u^{\alpha\beta}\overline{u_L^\alpha}u_R^\beta - vY_d^{\alpha\beta}\overline{d_L^\alpha}d_R^\beta - vY_l^{\alpha\beta}\bar{l}_L^\alpha l_R^\beta + \text{h.c.}, \\ &= -m_u^{\alpha\beta}\overline{u_L^\alpha}u_R^\beta - m_d^{\alpha\beta}\overline{d_L^\alpha}d_R^\beta - m_l^{\alpha\beta}\bar{l}_L^\alpha l_R^\beta + \text{h.c.}, \end{aligned} \tag{2.1.11}$$

where $m_a^{\alpha\beta}$ is the mass matrix for field a.

The Lagrangian of the Standard Model written in Eq. (2.1.1) includes all renormalisable terms consistent with the imposed symmetries. However, one can construct higher-dimensional operators consistent with the imposed symmetries of the Standard Model that are suppressed by a large mass scale (see for example Eq. (2.3.2)). The restriction to the renormalisable part is justified as an effective low-energy approximation.[1] When the non-renormalisable terms are neglected, the remaining operators exhibit some extra accidental symmetries beyond those imposed. That is because the violation of these symmetries only occurred in the non-renormalisable

[1]Renormalisability is not a requirement of a theory in itself: effective theories are not generally renormalisable but may be handled by assuming a cutoff in energy beyond which they are not accurate. This cutoff suppresses the non-renormalisable terms and this is the spirit in which they are ignored in Eq. (2.1.1). These terms have dimensions higher than four and include, for example, the dimension six operators which lead to proton decay and which are suppressed by the inverse square of the cutoff.

terms. Examples include the baryon and lepton numbers, B and L, that count the charge of baryons and leptons (where quarks carry $B = 1/3$). In fact, at the level of the Lagrangian both $B - L$ and $B + L$ are symmetries, however, of these two, the path integral of the SM is only invariant under $B - L$ and not $B + L$ (which is therefore anomalous). Violation of the latter occurs only in non-perturbative processes, an example of which is discussed in Appendix C.

The historical successes of the Standard Model include its prediction of the tau lepton [14], the $W^{\pm}$ and Z bosons [15–18], the top quark [19, 20] and the Higgs boson [21,22]. In fact, the Standard Model along with the general theory of relativity constitute our best theories of the fundamental interactions — in principle, all physical phenomena of everyday life are explained by these two theories. However there are good reasons to think that the Standard Model needs modification. Among them: it does not correctly predict the abundance of matter over antimatter in the universe; it does not account for the accelerating expansion of the universe; none of its particle content is a good candidate for a dark matter particle; it incorrectly predicts that neutrinos are without mass.

This thesis is primarily about the two of these shortcomings — the problem of the matter-antimatter asymmetry and the problem of neutrino masses. Let us turn now to the Standard Model prediction of massless neutrinos and the evidence against it.

Neutrinos in the Standard Model

In the Standard model there are three distinct left-handed fermionic fields to describe the neutrinos: ν_{eL}, $\nu_{\mu L}$ and $\nu_{\tau L}$ which are incorporated into a left-handed $\mathrm{SU}(2)_L$ doublet with the corresponding charged lepton l_e, l_μ or l_τ. Consider a typical neutrino produced by tritium beta decay in a weak interaction in an atomic nucleus with an energy $E_\nu \sim 5$ keV. At these low energies, the mediating W boson mass is extremely large, $m_W \sim 80$ GeV $\gg E_\nu$ and we can use the Fermi effective theory [23] to describe

subsequent interactions of the neutrino with matter. The effective coupling is [24]

$$G_F = \frac{\sqrt{2}}{8}\frac{g_2^2}{m_W^2} \approx 1.1663787(6) \times 10^{-5}\ \text{GeV}^{-2}, \tag{2.1.12}$$

so from dimensional analysis we expect the neutrino-matter cross-sections to behave as

$$\sigma \propto G_F^2 s, \tag{2.1.13}$$

where s is the squared centre-of-mass energy Mandelstam variable, which gives us an extremely small interaction cross-section $\sigma \sim 10^{-21}\ \text{GeV}^{-2}$. Thus, the Standard Model neutrinos come as a set of three left-handed fields that very rarely interact with matter, and that are created or destroyed in weak interactions, each associated with a charged lepton.

The Standard Model (in its simplest form) does not have any right-handed neutrino fields. For this reason one cannot write down a fermionic mass term for the neutrinos and so the Standard Model predicts that neutrinos have no mass (notice the lack of an m_ν in Eq. (2.1.11)). Historically this picture of massless neutrinos was first challenged in experiments intended to count the number of neutrinos from the sun. Neutrinos in the sun would be produced in the electron flavour and a detector would capture them via inverse beta decay [25, 26]. Although the number of neutrinos produced in the solar cycle was known, it was found that the number of detected neutrinos was lower than predicted. Later on, a similar anomaly was discovered in the flux of neutrinos from the upper atmosphere. Here the ratio of muon neutrinos to electron neutrinos was smaller than the prediction. With further experimental and theoretical work it was shown that the phenomenon of neutrino oscillations [27–31] could explain these experimental anomalies. This is when a neutrino created in a given flavour state may change flavour as it propagates (and thus cause detectors sensitive to only one flavour to undercount the total number of neutrinos). To make this explanation work at least two of the observed neutrinos must be massive with an extremely small mass scale at least $\mathcal{O}(10^6)$ times smaller than the electron mass. In addition the mass and flavour states of neutrinos must be misaligned. Let us consider

the implications of these extremely small masses now (however it is that they come about). In particular let us try to understand in some detail the phenomenon of neutrino oscillations through which the massive nature of neutrinos was discovered.

2.2 Properties of massive neutrinos

The neutrinos created or destroyed in weak interactions are not identical with the eigenstates of mass. To be totally general we can start in a basis in which the charged lepton masses are not diagonalised and write

$$\nu_{\alpha L} = V^{\nu}_{\alpha k}\nu_{kL}, \tag{2.2.1}$$

where V^{ν} is a unitary matrix used to relate the mass ν_{kL} and flavour $\nu_{\alpha L}$ eigenstates of neutrinos and

$$l_{\alpha L} = V^{l}_{\alpha k}l_{kL}, \tag{2.2.2}$$

where V^{l} is the equivalent of V^{ν} for charged leptons. The charged current interaction terms coming from Eq. (2.1.6) are

$$\mathcal{L}_{\rm CC} = -\frac{g_2}{\sqrt{2}}\sum_{\alpha,k,j}\left(V^{\nu *}_{\alpha k}\overline{\nu}_{kL}\gamma^{\rho}V^{l}_{\alpha j}l_{jL}W_{\rho} + \text{h.c.}\right) \tag{2.2.3}$$

and so V^{ν} and V^{l} always appear in the combination

$$V^{\dagger} \equiv V^{\nu\dagger}V^{l}. \tag{2.2.4}$$

Thus we lose no information by making the simplifying choice of defining V^{l} to be an identity matrix. Then we have [27, 28, 31][2]

$$\nu_{\alpha L} = V_{\alpha k}\nu_{kL}, \tag{2.2.5}$$

Let us attempt to find a general parametrisation of the matrix V by counting the number of physical parameters on which it depends.

[2]A similar story exists for the quark sector where one finds the CKM matrix relating down-type quark flavour and mass eigenstates [32, 33].

A 3×3 unitary matrix has $3 \times 3 = 9$ complex parameters or 18 real parameters. Unitarity imposes the constraint

$$V^\dagger V = 1, \tag{2.2.6}$$

which means that each column of U has Euclidean norm of 1 and are each orthogonal. The former imposes 3 real constraints (one for each column), the latter imposes 3 complex constraints (one for each pair of columns). Thus there are

$$18 - 3 - 2 \times 3 = 9, \tag{2.2.7}$$

real parameters in this matrix. We need not add in extra constraints by consideration of rows as these are derived from transposition of the constraints already considered. A completely general parametrisation of the 3×3 unitary matrix may be written as

$$V = \mathrm{diag}\left(e^{-i(\psi+\rho_e)}, e^{-i(\psi+\rho_\mu)}, e^{-i\psi}\right) U,$$

for some real phases ψ, ρ_e, ρ_μ where by convention [24]

$$U \equiv \begin{pmatrix} c_{12}c_{13} & s_{12}c_{13} & s_{13}e^{-i\delta} \\ -s_{12}c_{23} - c_{12}s_{23}s_{13}e^{i\delta} & c_{12}c_{23} - s_{12}s_{23}s_{13}e^{i\delta} & s_{23}c_{13} \\ s_{12}s_{23} - c_{12}c_{23}s_{13}e^{i\delta} & -c_{12}s_{23} - s_{12}c_{23}s_{13}e^{i\delta} & c_{23}c_{13} \end{pmatrix} \begin{pmatrix} 1 & 0 & 0 \\ 0 & e^{i\frac{\alpha_{21}}{2}} & 0 \\ 0 & 0 & e^{i\frac{\alpha_{31}}{2}} \end{pmatrix}, \tag{2.2.8}$$

with $c_{ij} \equiv \cos\theta_{ij}$ and $s_{ij} \equiv \sin\theta_{ij}$ for some real parameters θ_{ij} and is called the PMNS matrix. We define $\mathcal{P}_M \equiv \mathrm{diag}(1, e^{i\frac{\alpha_{21}}{2}}, e^{i\frac{\alpha_{31}}{2}})$ to be the matrix containing the *Majorana phases* α_{21} and α_{31}. Together with the *Dirac phase* δ, these parameters control CP violation in the light neutrino sector. If we insert this form for V into the charged current Lagrangian, written schematically as

$$(\overline{\nu}_1, \overline{\nu}_2, \overline{\nu}_3)\, e^{i\psi} \underbrace{U^\dagger \begin{pmatrix} e^{i\rho_e} & 0 & 0 \\ 0 & e^{i\rho_\mu} & 0 \\ 0 & 0 & 1 \end{pmatrix}}_{\text{General } 3\times 3 \text{ unitary matrix}} \begin{pmatrix} l_e \\ l_\mu \\ l_\tau \end{pmatrix}, \tag{2.2.9}$$

we can see that the diagonal matrix containing the phase factors $e^{i\rho_e}$ and $e^{i\rho_\mu}$ can be absorbed into the charged lepton fields on the right along with the overall phase $e^{i\psi}$. This leaves just U with its 6 real parameters as the physically relevant matrix transforming between the neutrino flavour and mass bases:

$$\nu_{\alpha L} = U_{\alpha k}\nu_{kL}. \tag{2.2.10}$$

The accurate determination of the parameters of this matrix constitute one of the main goals of experimental neutrino physics. Now that we have a precise understanding of the mass-flavour mixing, we are in a position to understand neutrino oscillations.

Oscillations

The essential physical ideas of neutrino oscillations can be best explained by calculating the probability for transition of a neutrino from one flavour α to a distinct flavour β after traversing some distance $\mathcal{D}$. To compute the amplitude for this probability, we should expand a one-particle neutrino state of flavour α into its constituent mass states, evolve the state to the space-time location of observation, and project a state of flavour β on to it [26, 34, 35].

Ordinarily, we assume that free particles travelling large distances are well-described by plane waves with only one possible value of momentum. For propagating neutrinos in oscillation experiments, it is physically clearer and more accurate to use a wave packet description in which a neutrino with mass m_i has amplitudes to propagate with momentum in a small spread around some value P_i. This might arise because the neutrino results from a decay $\pi^+ \to \mu^+\nu_i$, where the initial pion is confined in a box and thus has amplitude to decay with different momenta[3][4]. Thus we write

$$|\nu_\alpha\rangle = \frac{1}{\pi^{\frac{3}{4}}\sigma^{\frac{3}{2}}} \sum_i \int d^3p e^{-\frac{(p-P_i)^2}{2\sigma^2}} U_{\alpha i}|\nu_i, p\rangle, \tag{2.2.11}$$

where the Gaussian factor was chosen merely as a mathematically convenient way to describe the wave packet. The precise shape of the wave packet will be irrelevant to our final result. Evolving this in space and time, it becomes

$$|\nu_\alpha(x,t)\rangle = \frac{1}{\pi^{\frac{3}{4}}\sigma^{\frac{3}{2}}} \sum_i \int d^3p e^{-\frac{(p-P_i)^2}{2\sigma^2}} e^{-i(E_i t - px)} U_{\alpha i}|\nu_i, p\rangle, \tag{2.2.12}$$

where $E_i \equiv \sqrt{p^2 + m_i^2}$. We choose to project this onto the final state of flavour β:

$$|\nu_\beta\rangle = \frac{1}{\pi^{\frac{3}{4}}\sigma^{\frac{3}{2}}} \sum_i \int d^3q e^{-\frac{(q-Q_i)^2}{2\sigma^2}} U_{\beta i}|\nu_i, q\rangle, \tag{2.2.13}$$

[3] If the initial pion were a plane wave such that the momentum is definite, then one could determine the pion and muon mass to infer the mass of the emitted neutrino and the interference necessary for oscillation would be lost — only one neutrino contributes. This is because the creation point is now very widely (infinitely) spread out in space over a region much larger than the oscillation length and so no oscillation pattern could be detected.

[4] The finite lifetime of the unstable pion produces an additional spread that may be incorporated similarly to our inclusion of the spatial momentum spread.

which, for simplicity has been written with the same wave packet structure. After doing so and simplifying the integrals and summations with the resulting Dirac and Kronecker deltas, we arrive at

$$\langle \nu_\beta | \nu_\alpha(x,t) \rangle = \frac{1}{\pi^{\frac{3}{2}}\sigma^3} \sum_i \int d^3p e^{-\frac{(p-P_i)^2}{\sigma^2}} e^{-i(E_i t - px)} U_{\alpha i} U^*_{\beta i}. \tag{2.2.14}$$

We now take advantage of the relative smallness of neutrino masses compared with their energies and use

$$E_i \approx p + \frac{m_i^2}{2p}, \tag{2.2.15}$$

to obtain

$$\langle \nu_\beta | \nu_\alpha(x,t) \rangle = \frac{1}{\pi^{\frac{3}{2}}\sigma^3} \sum_i \int d^3p e^{-\frac{(p-P_i)^2}{\sigma^2}} e^{-ip(t-x)} e^{-i\frac{m_i^2}{2p}t} U_{\alpha i} U^*_{\beta i}. \tag{2.2.16}$$

When, $t - x$ is large, the factor $e^{-ip(t-x)}$ will rapidly oscillate with p and cause the integral to vanish, thus we evaluate the amplitude for $t = x = \mathcal{D}$

$$\langle \nu_\beta | \nu_\alpha(x=\mathcal{D}, t=\mathcal{D}) \rangle = \frac{1}{\pi^{\frac{3}{2}}\sigma^3} \sum_i \int d^3p e^{-\frac{(p-P_i)^2}{\sigma^2}} e^{-i\frac{m_i^2}{2p}x} U_{\alpha i} U^*_{\beta i}. \tag{2.2.17}$$

If the Gaussians are narrow, then we may take $e^{-i\frac{m_i^2}{2p}x}$ outside of the integral with $p \to P_i$ and perform the integral, to obtain

$$\langle \nu_\beta | \nu_\alpha(x=\mathcal{D}, t=\mathcal{D}) \rangle \approx e^{-i\frac{m_1^2}{2P_1}} \sum_i e^{-i\left(\frac{m_i^2}{2P_i} - \frac{m_1^2}{2P_1}\right)\mathcal{D}} U_{\alpha i} U^*_{\beta i}. \tag{2.2.18}$$

Taking the pion decay example to be concrete, we have

$$P_i^2 = \frac{m_\pi^2}{4}\left(1 - \frac{m_\mu^2}{m_\pi^2}\right)^2 - \frac{m_i^2}{2}\left(1 + \frac{m_\mu^2}{m_\pi^2}\right) + \frac{m_i^4}{4m_\pi^2}, \tag{2.2.19}$$

such that

$$\frac{m_i^2}{2P_i} - \frac{m_1^2}{2P_1} \approx \frac{m_i^2 - m_1^2}{\left(\frac{m_\mu^2 - m_\pi^2}{m_\pi}\right)} + \mathcal{O}\left(m_i^4\right) \approx \frac{m_i^2 - m_1^2}{2E} + \mathcal{O}\left(m_i^4\right) \tag{2.2.20}$$

with E the energy when the neutrino mass is neglected. This corresponds to an

oscillation probability

$$P\left(\nu_\alpha \to \nu_\beta\right) \approx \left|\sum_i e^{-i\frac{\Delta m^2_{i1}}{2E}\mathcal{D}} U_{\alpha i} U^*_{\beta i}\right|^2, \tag{2.2.21}$$

with $\Delta m^2_{ij} \equiv m^2_i - m^2_j$.

We see that it is the presence both of different neutrino masses and their misalignment with the flavour basis that leads to the phenomenon of neutrino oscillations. Observing such a phenomenon with the charged leptons is much more difficult (if we do not define them to be diagonal) due to the large uncertainty of energies that would be necessary to create a coherent superposition of mass states.

From Eq. (2.2.21) we see why it is that the differences in the squared masses for neutrinos are measured in the oscillation experiments and not the absolute masses. This is no surprise — being an interference phenomenon, neutrino oscillations are not sensitive to the absolute mass scale as this is appears as a common phase. Further we can see that if the exponentials were put into the form of a diagonal matrix $\mathcal{E}$, then the oscillation probability is

$$P\left(\nu_\alpha \to \nu_\beta\right) \approx \left|\left(U\mathcal{E}U^\dagger\right)_{\alpha\beta}\right|^2, \tag{2.2.22}$$

and so the Majorana phase matrix $\mathcal{P}_M$ in U will cancel out of the description $\left(\mathcal{P}_M\mathcal{E}\mathcal{P}^\dagger_M = \mathcal{P}_M\mathcal{P}^\dagger_M\mathcal{E} = \mathcal{E}\right)$.

The individual mass states of neutrinos travel at slightly different speeds v with the difference in speed Δv given, in terms of the squared mass splitting Δm^2 and energy E by

$$\Delta v \approx \frac{\Delta m^2}{2E^2}. \tag{2.2.23}$$

This means that the different components will spread out and no longer overlap after some time. For accelerator neutrinos with energy $E = 1$ GeV, and a wave packet of length determined by the pion decay width, using $\Delta m^2 = 2.4 \times 10^{-3}$ eV^2, the wave packets separate after 10^{20} km. We can ignore this and assume oscillation is always present. However, in a supernova, $E \sim 10$ MeV and the wave packet width

is about the same as the inter-nucleon distance. Separation occurs at 10^3 km and so neutrinos from supernovae are not oscillating by the time they get to us. With SN 1987 A the time difference in the arrival of the different components could have been as large as 10^{-4} s.

Direct mass bounds

As we have seen, neutrino oscillation experiments can only provide information on the differences of the squares of the neutrino masses. The absolute mass scale must be determined by other means. Two such complementary probes of neutrino masses are cosmological observations and beta decay experiments.

The cosmological bound may be determined from the fact that the evolution of the universe is sensitive to the sum of the light neutrino masses. After making certain assumptions about the cosmological model, the bound is [36]

$$\sum_i m_i < [0.120, 0.160] \text{ eV}$$

at the 95% confidence level. Given the dependence on assumptions about cosmology in this bound, it has been worthwhile to turn to a separate means of determining the neutrino mass scale.

An alternative method is the beta decay experiments which study the kinematics of beta decay processes. KATRIN [37] for example, the most sensitive such experiment at present, looks at the process

$$^3\text{H} \rightarrow {}^3\text{He} + \text{e}^- + \overline{\nu}_\text{i} \tag{2.2.24}$$

with $i = 1, 2, 3$, although the principle is the same no matter the particular beta decay reaction. The larger the mass of m_i, the smaller the maximum electron energy with each neutrino mass state providing a different energy threshold. The current experimental limits do not distinguish the different neutrino thresholds but rather

an averaged quantity

$$\langle m_\beta \rangle = \sqrt{\sum_i |U_{ei}|^2 m_i^2}. \tag{2.2.25}$$

The current bounds come from the Troitsk and Mainz experiments [38, 39] and give

$$\langle m_\beta \rangle \leq 2.05\,\text{eV}.$$

Dirac or Majorana?

Due to their electrical neutrality, neutrinos are the only elementary fermions that may be their own antiparticles making them *Majorana* fermions. A Majorana neutrino field may be written

$$\nu = \nu_L + \nu_L^c \tag{2.2.26}$$

where for some field ψ

$$\psi^c \equiv C\overline{\nu}^T, \tag{2.2.27}$$

with C the charge conjugation matrix. That is to say that the left- and right- chiral components of a Majorana field are not independent but that one may be constructed from the other. In the mass basis, a mass term in the Lagrangian connects the left- and right-handed fields as

$$\mathcal{L}_m^\nu = -\sum_i m_i \overline{\nu}_{iL} \nu_{iR} + \text{h.c.} \tag{2.2.28}$$

If these particles are Dirac, we may use the Majorana phase matrix to define new fields such that $\nu_{iL} = \mathcal{P}_M \tilde{\nu}_{iL}$ and $\nu_{iR} = \mathcal{P}_M \tilde{\nu}_{iR}$. The mass term is invariant under this and so if we work with $\tilde{\nu}_i$ in place of ν_i, the Majorana phases are stripped from the PMNS matrix. That is to say, they are rendered unphysical. This is not the case for Majorana particles for which $\nu_R = C\overline{\nu}_L^T$ and so the left- and right-chiral field redefinitions cannot be made independently. In this case the Majorana phases are physical as no convention can remove them — this is why we call them Majorana phases (see Appendix B for further properties of Majorana fermions).

Generically, the distinction between Dirac and Majorana particles must vanish when

their masses go to zero. This means that the difference in amplitudes for processes involving one or the other must be suppressed by powers of m/E (the mass over the energy). This parameter is exceptionally small for neutrinos and would appear to make the experimental verification of the Dirac or Majorana nature very difficult. Adding to that, as we have seen, neutrino oscillation experiments cannot determine the Majorana phases and so provide no information either.

However it may be possible to resolve the nature of neutrinos by looking for lepton number violation. One may rephase the Dirac fields with a constant factor: $\nu_L \to e^{i\theta}\nu_L$ and $\nu_R \to e^{i\theta}\nu_R$ and leave the Lagrangian invariant. This global symmetry at the level of the action corresponds to the conservation of lepton number. In the Majorana case, because of the interdependence of the chiral components, this symmetry no longer holds and the Majorana mass term violates lepton number by two units.

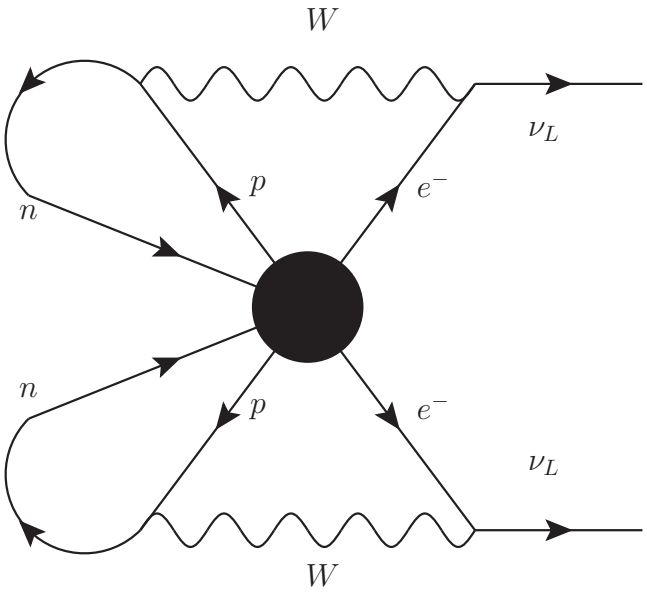

Figure 2.1: *Schechter-Valle theorem: If in some theory, neutrinoless double beta decay may occur, then an effective Majorana mass exists for the light neutrinos.*

An experimental test of this is neutrinoless double beta decay ($0\nu\beta\beta$). This is the simultaneous occurrence of a pair of beta decays in one nucleus in which there are no neutrinos in the final state — thus violating lepton number by two units.

Experiments probing double beta decay can provide information on the CP-violating Majorana phases of the PMNS matrix.

The rate of neutrinoless double beta decay is given by [40]

$$\frac{\Gamma_{0\nu\beta\beta}}{\log 2} = \frac{G_{01}}{m_e^2}|\mathcal{A}|^2, \tag{2.2.29}$$

where G_{01} is a kinematic factor, m_e the electron mass and $\mathcal{A}$, the amplitude for the process. One finds that

$$\mathcal{A} \propto \langle m_\nu \rangle \equiv m_1 U_{e1}^2 + m_2 |U_{e2}|^2 e^{i\alpha_{21}} + m_3 |U_{e3}|^2 e^{i(\alpha_{31}-2\delta)}, \tag{2.2.30}$$

where $\langle m_\nu \rangle$ is the neutrinoless double beta decay effective Majorana mass in the case of 3-neutrino mixing. The most stringent upper bound on $|\langle m_\nu \rangle|$ was reported by the KamLAND-Zen collaboration [41] searching for neutrinoless double beta decay of ^{136}Xe:

$$|\langle m_\nu \rangle| < (0.061 - 0.165) \text{ eV}, \tag{2.2.31}$$

where the uncertainty in the knowledge of the nuclear matrix element of ^{136}Xe decay have been accounted for. The best lower limits on the half-lives for neutrinoless double beta decay are $T_{1/2}^{0\nu} > 8.0 \times 10^{25}$ yr (GERDA-II collaboration), $T_{1/2}^{0\nu} > 1.5 \times 10^{25}$ yr (Cuoricino, CUORE-0, and CUORE), and $T_{1/2}^{0\nu} > 1.07 \times 10^{26}$ yr (KamLAND-Zen collaboration), with all these limits given at the 90% CL. A new generation of experiments aims to be sensitive to $|\langle m_\nu \rangle| \sim [0.01, 0.05]$ eV [42, 43].

In complete generality, as can be seen in Fig. 2.1, no matter the mechanism by which it is allowed, the presence of double beta decay implies an effective Majorana mass (barring fine-tuned cancellations between contributions). Although this is a four-loop process and hence well-suppressed, its implications for the nature of neutrinos is significant. Notice that no amount of non-observation of neutrinoless double beta decay can prove that neutrinos are Dirac as it is possible for instance that the amplitudes contributing to the decay rate cancel.

Status of neutrino measurements

θ_{13} (°)	θ_{12} (°)	θ_{23} (°)	δ (°)	Δm^2_{21} (10^{-5}eV^2)	Δm^2_{31} (10^{-3}eV^2)
$8.61^{+0.12}_{-0.13}$	$33.82^{+0.78}_{-0.76}$	$49.7^{+0.9}_{-1.1}$	217^{+40}_{-28}	$7.39^{+0.21}_{-0.20}$	$2.525^{+0.033}_{-0.031}$

Table 2.2: Normal ordering best fit values and 1σ ranges from a global fit to neutrino data [1].

θ_{13} (°)	θ_{12} (°)	θ_{23} (°)	δ (°)	Δm^2_{21} (10^{-5}eV^2)	Δm^2_{32} (10^{-3}eV^2)
$8.65^{+0.12}_{-0.13}$	$33.82^{+0.78}_{-0.75}$	$49.7^{+0.9}_{-1.0}$	280^{+25}_{-28}	$7.39^{+0.21}_{-0.20}$	$-2.512^{+0.034}_{-0.031}$

Table 2.3: Inverted ordering best fit and 1σ ranges from a global fit to neutrino data [1].

In Table 2.2 and Table 2.3, we have the best fit values for the neutrino parameters. Currently, the ordering of the masses is not determined and there are two possibilities: normal ordering, in which $m_1 < m_2 < m_3$ and inverted ordering in which $m_3 < m_1 < m_2$, hence the duplication of tables. It is useful to realise that ν_1 is the neutrino with the largest amount of ν_e, ν_2, the second highest and ν_3 the third highest. The values of $|\langle m_\nu \rangle|$ probed by the new generation of $0\nu\beta\beta$ experiments correspond to quasi-degenerate light neutrino spectra and inverted ordering [44]. The angle θ_{23} has large enough errors that the octant is still somewhat undetermined. Accurate measurements of this angle are of significance to flavour models for which the particular octant is of great significance. Recently, some information about the CP-violating phase δ has been obtained, but it is very poorly constrained as may be seen by examination of the corresponding errors in Table 2.2 and Table 2.3. Finally we note that the Majorana phases remain completely undetermined.

2.3 Overview of speculative theories of neutrinos

By modifying the features of the SM, a large set of speculative theories, many of which predict light neutrino masses, has been generated. Such modifications may

affect the particle content or the symmetry structure or both. In this section we provide a cursory summary of these extensions of the SM.

Theories which retain the gauge structure of the SM

Perhaps the simplest extension is to add right-handed neutrinos ν_R to the SM particle content. Then, a neutrino Yukawa-term with coupling y is permitted which provides a mass term

$$\frac{v}{\sqrt{2}} y \overline{\nu}_L \nu_R, \tag{2.3.1}$$

corresponding to a neutrino mass $m_\nu = \frac{v}{\sqrt{2}} y$ after electroweak symmetry breaking.

If we assume, based on the cosmological mass bounds or on the oscillation data, that $m_\nu \sim \mathcal{O}\left(10^{-11}\right)$ GeV, then we require $y \sim 10^{-13}$. When the goal of the theory is to explain the smallness of the neutrino masses, a theory in which the extreme smallness is merely transferred from m to y is unsatisfying. Furthermore, this theory has no explanation as to why one would exclude the Majorana mass term $\overline{\nu}_R \nu_R^c$.

A set of simple extensions to the Standard Model can be formulated by considering the lowest-dimension non-renormalisable operator of the Standard Model — the dimension-5 Weinberg operator [45, 46]

$$\frac{1}{2} c_{\alpha\beta} \left(\overline{L_\alpha^c} \tilde{\phi}^* \right) \left(\tilde{\phi}^\dagger L_\beta \right) + \text{h.c.}, \tag{2.3.2}$$

where the coefficient $c_{\alpha\beta}$ has dimensions 1/energy. This can generate a Majorana mass for neutrinos once the Higgs gains a vacuum expectation value.

A more complete theory than the SM might generate this term after integrating out a new field S. As a reminder, integrating out a field means assuming that it is massive enough that its derivative terms, proportional to the momentum, may be neglected in comparison with its mass. Its appearance in the action of a path integral is then of the same form as ordinary Gaussian integrals and may be performed analytically by the usual technique of completing the square and changing variables. In schematic

form, we would like to generate a term $(L\phi)^2$ in the Lagrangian[5] by integrating out the field S which has mass term[6] BS^2. This means that we have something of the form

$$\int dS e^{AS+BS^2}, \tag{2.3.3}$$

with A some coefficient of S potentially containing fields. After completing the square we have

$$\int dS e^{B\left(S+\frac{1}{2B}A\right)^2-\frac{1}{4B}A^2} \propto e^{-\frac{1}{4B}A^2}. \tag{2.3.4}$$

In this toy model, we wish for this resultant term to contain $(L\phi)^2$. Thus we may choose

$$AS \to y\,(L\phi)\,S + \text{h.c}, \tag{2.3.5}$$

or

$$AS \to y_1\,(LL)\,S + y_2\,(\phi\phi)\,S + \text{h.c.} \tag{2.3.6}$$

In Eq. (2.3.5), $L\phi$ may be an $\mathrm{SU}(2)_L$ singlet or a triplet, meaning that S must be a singlet or triplet also. From Lorentz invariance we are required to take S to be fermionic.

In Eq. (2.3.6) we may similarly have LL and $\phi\phi$ singlet or triplet meaning that S must be a scalar singlet or triplet. Consider the case of a scalar singlet field S. In the quadratic L term, in order that it is not zero as a result of two fields of the same chirality multiplying, it must have a form $\overline{L^c}LS$ which requires S to have hypercharge 2. The Higgs has hypercharge 1 and so to form a structure with hypercharge -2 in the second term of Eq. (2.3.6) we can have ϕ^* or $\tilde{\phi}$ leading to the combinations: $\phi^\dagger\phi^*$, $\phi^\dagger\tilde{\phi}$ and their Hermitian conjugates. The former is not invariant under $\mathrm{SU}(2)_L$ transformations and so we must select $\phi^\dagger\tilde{\phi}S$ which gives zero when the Higgs takes on its VEV and thus does not contribute to the neutrino mass [47].

In summary there are three possibilities that may generate neutrino masses, conven-

[5]We trust from context this L will not be confused with lepton number.

[6]This is meant schematically, such that S^2 maybe be the square of a scalar field, and B the mass squared, or S^2 may be a fermionic product $\overline{\psi}\psi$ and B simply the mass.

tionally named

- Type I Seesaw: An $SU(2)_L$ singlet fermion [48],
- Type II Seesaw: An $SU(2)_L$ triplet scalar [49, 50],
- Type III Seesaw: An $SU(2)_L$ triplet fermion [51].

The seesaw mechanisms mentioned above provide an ultraviolet completion of the Weinberg operator. Due to the method in which we constructed them, they connect the lepton and Higgs through a new particle propagator at tree-level. Integrating out these new fields is equivalent to contracting the propagator line to a point and using an effective vertex corresponding to the Weinberg operator coupling. These are not the only possibilities for increasing the particle content however. For example, there exist theories of neutrino masses in which the new particle content provides neutrino masses at loop-level in Feynman diagrams [52, 53].

Theories with modified symmetries

There are many ways one may choose to modify the symmetries of the Standard Model and many of these introduce new particle content at the same time. We mention a handful of important theories here:

- The left-right symmetric model which contains the gauge group $\mathrm{SU}(2)_L \times \mathrm{SU}(2)_R \times \mathrm{U}(1)_{B-L}$ [54–56], has the property that all left-handed fermions have a right-handed partner and thus automatically leads to the possibility neutrino mass terms. Alternatively, some models contain the gauge-group $\mathrm{SU}(2)_L \times \mathrm{U}(1)_{B-L}$ and allow for the breaking of $\mathrm{U}(1)_{B-L}$ to generate naturally small neutrino masses [57] (see also [58] and the references within).

- Grand unified theories are those in which the Standard Model gauge structure is a subset of a larger and simpler group. A common example is SU(5), which, in its simplest form contains an exact $B - L$ symmetry and predicts massless neutrinos. Another example is SO(10) which contains the gauge group $\mathrm{SU}(2)_L \times \mathrm{SU}(2)_R \times \mathrm{SU}(4)$ and thus contains right-handed neutrinos allowing for the natural generation of their masses [59–61].

- Supersymmetric theories are those in which a symmetry between bosons and fermions is introduced. If one does not allow for the violation of a symmetry called R-parity, which among other things prevents proton decay, then the minimal supersymmetric standard model conserves lepton and baryon number to all orders in perturbation theory and therefore predicts massless neutrinos. However, if one does allow for a small violation, lepton and baryon number may be violated and naturally small neutrino masses may be generated [62–64]. This small violation must be done without introducing too large a proton decay rate.

- Theories with extra dimensions may include right-handed neutrinos with a wave function that has only a small overlap with the leptonic doublet thus explaining the smallness of the neutrino masses [65–67].

2.4 Aspects of the type I seesaw

Light and heavy neutrinos

We have now completed our survey of neutrino theory. For the purposes of explaining the work presented in this thesis, let us look in more detail at the type I seesaw.

As already mentioned, the type I seesaw adds some number n_N of heavy gauge singlet neutrinos N_i ($i \in \{1, 2, \dots n_N\}$) to the Standard Model. After electroweak symmetry breaking the neutrino mass terms of the Lagrangian are given by

$$\begin{aligned} \mathcal{L}_m &= -\frac{1}{2}\left(\bar{\nu}_L, \overline{N_R^c}\right)\begin{pmatrix} 0 & vY \\ vY^T & m_R \end{pmatrix}\begin{pmatrix} \nu_L^c \\ N_R \end{pmatrix} + \text{h.c.}, \\ &= -\frac{1}{2}\left(\bar{\nu}_L, \overline{N_R^c}\right)\begin{pmatrix} 0 & m_D \\ m_D^T & m_R \end{pmatrix}\begin{pmatrix} \nu_L^c \\ N_R \end{pmatrix} + \text{h.c.}, \end{aligned} \tag{2.4.1}$$

where Y is the neutrino Yukawa matrix which couples the heavy Majorana neutrinos to the leptonic and Higgs doublets and m_R is the $n_N \times n_N$ Majorana mass matrix which is usually assumed to be much larger than the Dirac mass terms $m_D \equiv vY$.

If we call the mass matrix appearing in Eq. (2.4.1) $\mathcal{M}$, and the vector of neutrino fields simply $\mathcal{X}_L \equiv (\nu_L, N_R^c)^T$, then we may write

$$\mathcal{L}_m = -\frac{1}{2}\overline{\mathcal{X}}_L \mathcal{M} \mathcal{X}_L^c + \text{h.c.}, \tag{2.4.2}$$

and define $\mathcal{Y}_L \equiv \mathcal{U}\mathcal{X}_L$ with $\mathcal{U}$ a unitary matrix (a generalisation of the PMNS matrix U), then we may write

$$\mathcal{L}_m = -\frac{1}{2}\overline{\mathcal{Y}}_L \mathcal{U}^\dagger \mathcal{M} \mathcal{U}^* \mathcal{Y}_L^c + \text{h.c.} \tag{2.4.3}$$

If we choose $\mathcal{U}$ so as to perform a singular value decomposition (in this case a Takagi factorisation), to make $\mathcal{M}$ into the positive diagonal matrix of masses $\hat{\mathcal{M}}$, then we have

$$\mathcal{L}_m = -\frac{1}{2}\overline{\mathcal{Y}}_L \hat{\mathcal{M}} \mathcal{Y}_L^c + \text{h.c.} \tag{2.4.4}$$

but the Hermitian conjugate term can be simply combined with the first term to

give

$$\mathcal{L}_m = -\frac{1}{2}\left(\overline{\mathcal{Y}}_L + \overline{\mathcal{Y}}_L^c\right)\hat{\mathcal{M}}\left(\mathcal{Y}_L + \mathcal{Y}_L^c\right). \tag{2.4.5}$$

And thus we may use the field $\psi_m \equiv \mathcal{Y}_L + \mathcal{Y}_L^c$ which satisfies the Majorana condition $\psi_M = \psi_M^c$ to describe the massive neutrinos in this theory. That is to say that the neutrinos are Majorana in the generic type I seesaw.

The matrix $\mathcal{U}$ may be factorised into two unitary matrices $\mathcal{U}'$ and $\mathcal{U}''$ such that

$$\mathcal{U} = \mathcal{U}'\mathcal{U}'' = \mathcal{U}'\begin{pmatrix} \mathcal{U}_\nu & 0 \\ 0 & \mathcal{U}_N \end{pmatrix}, \tag{2.4.6}$$

where $\mathcal{U}'$ performs the block-diagonalisation

$$\mathcal{U}'^T\mathcal{M}\mathcal{U}' = \begin{pmatrix} m_\nu & 0 \\ 0 & m_N \end{pmatrix}, \tag{2.4.7}$$

where m_ν and m_N are the light and heavy neutrino mass matrices respectively and the matrix $\mathcal{U}''$ acts to diagonalise the light and heavy mass matrices via $\mathcal{U}_\nu$ and $\mathcal{U}_N$ respectively:

$$\left(\mathcal{U}'\mathcal{U}''\right)^T\mathcal{M}\left(\mathcal{U}'\mathcal{U}''\right) = \begin{pmatrix} \hat{m}_\nu & 0 \\ 0 & \hat{m}_N \end{pmatrix}, \tag{2.4.8}$$

where $\hat{m}_\nu = \mathrm{diag}\left(m_1, m_2, m_3\right)$ and $\hat{m}_N = \mathrm{diag}\left(m_4, \ldots, m_{n_N+3}\right)$.

The light neutrino mass matrix is given by the approximate tree-level expression

$$m_\nu \approx -m_D m_R^{-1} m_D^T, \tag{2.4.9}$$

where we have neglected terms of higher order in m_D/m_R. For the heavy neutrinos we have tree-level expression

$$m_N \approx m_R, \tag{2.4.10}$$

which is correct to lowest order in m_D/m_R.

Note of course that it is the PMNS matrix U that puts the light neutrino mass matrix m_ν in diagonal form through the relation

$$\hat{m}_\nu = U^T m_\nu U. \tag{2.4.11}$$

Radiative corrections to the light masses

Here we consider the one-loop corrections contributing to the neutrino mass. When we are being careful, we shall use m_ν and m_N to denote the light and heavy neutrino mass matrices and m_ν^i and m_N^i to denote the ith loop contribution to these quantities. In particular we have $m_\nu = m_\nu^0 + m_\nu^1 + \cdots$ where m_ν^0 is the tree-level contribution.

A self-energy correction for the light neutrinos may be generated at one-loop as described in Appendix A and is given by [68–70]

$$m^1_{\nu ij} = \frac{\alpha_W}{16\pi m_W^2} C_{ik} C_{jk} f\left(m_k\right), \tag{2.4.12}$$

with $i,j \in \{1,2,3\}$, $k \in \{1,\ldots,n_N\}$, $\alpha_W \equiv g_2^2/4\pi$ and $C \equiv \mathcal{U}_L^T \mathcal{U}_L^*$, where $\mathcal{U}_L \equiv (\mathcal{H},\mathcal{I})$ which comes from the block-decomposition of $\mathcal{U}$

$$\mathcal{U} \equiv \begin{pmatrix} \mathcal{H} & \mathcal{I} \\ \mathcal{J} & \mathcal{K} \end{pmatrix}, \tag{2.4.13}$$

with $\mathcal{H}$ a 3×3 matrix and $\mathcal{K}$ an $n_N \times n_N$ matrix. The function f appearing in Eq. (2.4.12) is given by

$$f\left(m_k\right) = m_k \left(3m_Z^2 g_{kZ} + m_H^2 g_{kH}\right) \tag{2.4.14}$$

where

$$g_{ab} = \frac{m_a^2}{m_a^2 - m_b^2} \log \frac{m_a^2}{m_b^2}. \tag{2.4.15}$$

It is useful to define a diagonal matrix

$$F \equiv \mathrm{diag}(f(m_1), ..., f(m_{m+3})), \tag{2.4.16}$$

such that Eq. 2.4.12 may be rewritten in matrix form as

$$m^1_{\nu ij} = \frac{\alpha_W}{16\pi m_W^2} \left(CFC^T\right)_{ij}. \tag{2.4.17}$$

If we expand this result in m_D/m_R and take only the first term, we find, in the basis

where m_R is diagonal, the approximate matrix expression

$$m_\nu^1 \approx m_D \frac{m_R}{32\pi^2 v^2}\left(\frac{\log\left(\frac{m_R^2}{m_H^2}\right)}{\frac{m_R^2}{m_H^2}-1}+3\frac{\log\left(\frac{m_R^2}{m_Z^2}\right)}{\frac{m_R^2}{m_Z^2}-1}\right)m_D^T, \tag{2.4.18}$$

such that the light neutrino mass to one-loop is approximately[7]

$$m_\nu \approx -m_D\left(m_R^{-1}-h\left(m_R\right)\right)m_D^T, \tag{2.4.19}$$

where

$$h \equiv \frac{m_R}{32\pi^2 v^2}\left(\frac{\log\left(\frac{m_R^2}{m_H^2}\right)}{\frac{m_R^2}{m_H^2}-1}+3\frac{\log\left(\frac{m_R^2}{m_Z^2}\right)}{\frac{m_R^2}{m_Z^2}-1}\right). \tag{2.4.20}$$

The Casas-Ibarra parametrisation

When there are three heavy Majorana neutrinos, the neutrino Yukawa couplings can be parametrised as [71]

$$Y = \frac{i}{v}U\sqrt{\hat{m}_\nu}R^T\sqrt{\hat{m}_R}, \tag{2.4.21}$$

by consideration of the tree-level light mass matrix Eq. 2.4.9. In this expression, R is a 3×3 complex orthogonal matrix and $\hat{m}_\nu$ may be constructed with one free mass parameter and the measured mass squared differences in the normal ordered (NO) or inverted ordered (IO) cases. Explicitly, we may write

$$\begin{aligned}\hat{m}_\nu &= \mathrm{diag}\left(m_1,m_2,m_3\right) = \mathrm{diag}\left(m_1,\sqrt{\Delta m_{21}^2+m_1^2},\sqrt{\Delta m_{31}^2+m_1^2}\right) \quad \text{NO},\\ \hat{m}_\nu &= \mathrm{diag}\left(m_1,m_2,m_3\right) = \mathrm{diag}\left(\sqrt{-\Delta m_{32}^2+m_3^2-\Delta m_{21}^2},\sqrt{-\Delta m_{32}^2+m_3^2},m_3\right) \quad \text{IO},\end{aligned} \tag{2.4.22}$$

and use the general parametrisation for a complex orthogonal matrix

$$R = \begin{pmatrix}1 & 0 & 0\\ 0 & c_1 & s_1\\ 0 & -s_1 & c_1\end{pmatrix}\begin{pmatrix}c_2 & 0 & s_2\\ 0 & 1 & 0\\ -s_2 & 0 & c_2\end{pmatrix}\begin{pmatrix}c_3 & s_3 & 0\\ -s_3 & c_3 & 0\\ 0 & 0 & 1\end{pmatrix}, \tag{2.4.23}$$

[7] Usually a loop-correction is smaller than the tree-level contribution because there are two extra factors of a coupling and the loop factor $1/(16\pi^2)$. However, for the light neutrinos there is only the additional loop factor because the tree-level result was already quadratic in the Yukawa couplings.

where $c_i = \cos w_i$, $s_i = \sin w_i$ and the complex angles are given by $w_i = x_i + iy_i$ ($i \in \{1, 2, 3\}$).

By simple analogy, it is possible to extend the Casas-Ibarra parametrisation to include both the tree-level and one-loop correction to the light neutrino masses Eq. (2.4.19) with [72]

$$Y = \frac{i}{v} U \sqrt{\hat{m}_\nu} R^T \sqrt{h(\hat{m}_R)^{-1}}. \tag{2.4.24}$$

If one is working in a theory with only two heavy Majorana neutrinos, then it is possible to use a simpler expression for the R-matrix that depends on only one complex parameter θ by assuming that N_3 is decoupled from all other particles. The assumption of N_3 decoupling implies that we may take $m_1 = 0$ for the NO spectrum (at tree-level). Correspondingly we have for the $R-$matrix:

$$R = \begin{pmatrix} 0 & \cos\theta & \sin\theta \\ 0 & -\sin\theta & \cos\theta \\ 1 & 0 & 0 \end{pmatrix}, \tag{2.4.25}$$

where $\theta = x + iy$. This in turn leads to (after dropping the column of zeroes corresponding to N_3)

$$U^\dagger Y = \frac{i}{v} \begin{pmatrix} 0 & 0 \\ \sqrt{M_1}\sqrt{m_2}\cos\theta & -\sqrt{M_2}\sqrt{m_2}\sin\theta \\ \sqrt{M_1}\sqrt{m_3}\sin\theta & \sqrt{M_2}\sqrt{m_3}\cos\theta \end{pmatrix}. \tag{2.4.26}$$

Similarly, for IO spectrum we have $m_3 = 0$ and subsequently

$$R = \begin{pmatrix} \cos\theta & \sin\theta & 0 \\ -\sin\theta & \cos\theta & 0 \\ 0 & 0 & 1 \end{pmatrix}. \tag{2.4.27}$$

In this case

$$U^\dagger Y = \frac{i}{v} \begin{pmatrix} \sqrt{M_1}\sqrt{m_1}\cos\theta & -\sqrt{M_2}\sqrt{m_1}\sin\theta \\ \sqrt{M_1}\sqrt{m_2}\sin\theta & \sqrt{M_2}\sqrt{m_2}\cos\theta \\ 0 & 0 \end{pmatrix}. \tag{2.4.28}$$

Low-scale seesaw variants

The type I seesaw predicts a light neutrino mass with size $m_\nu \sim m_D^2/m_R$. Assuming $\mathcal{O}(1)$ Yukawa couplings, yields $m_D \equiv vY \sim \mathcal{O}(100)$ GeV and assuming $m_\nu \sim 10^{-11}$ GeV, yields $m_R \sim 10^{15}$ GeV. This suggests that type I seesaw scenarios are far beyond the reach of current colliders. In particular, it is impossible to produce an on-shell heavy Majorana neutrino if their masses are as large as this and on top of that the active-heavy mixing is $\mathcal{O}(m_D/m_R) \sim 10^{-13}$.

The seesaw scenario as we have considered it makes three neutrinos light by making the other neutrinos very heavy. It is the $1/m_R$ dependence of the light neutrino masses that ensures they are small. However, another possibility is that each heavy neutrino contributes to the mass in such a way that there are cancellations between contributions. Then they do not need to be extremely heavy in order to make the light neutrinos so light.

Constructing a toy-model to do this is easy. Let us take one light neutrino and two heavy — the $(1+2)$ scenario. The mass matrix in the basis where m_R is diagonal is

$$\mathcal{M} = \begin{pmatrix} 0 & vy_1 & vy_2 \\ vy_1 & a & 0 \\ vy_2 & 0 & b \end{pmatrix}, \tag{2.4.29}$$

and the corresponding tree-level light neutrino mass is

$$m_\nu \approx -v^2 \left(\frac{y_1^2}{a} + \frac{y_2^2}{b} \right).$$

This can be made as small as we like, even exactly zero if we choose $y_1/\sqrt{a} = \pm i y_2/\sqrt{b}$. Once the tree-level light neutrino masses are set to zero, the one-loop contribution to the mass is the dominant contribution. However, as may be understood by substitution into Eq. (2.4.18), the one-loop mass may be set to zero if, in addition to $y_1/\sqrt{a} = \pm i y_2/\sqrt{b}$, we impose $a = b$. This leads to the radiatively stable mass

matrix

$$\mathcal{M} = \begin{pmatrix} 0 & vy_1 & \pm ivy_1 \\ vy_1 & a & 0 \\ \pm ivy_1 & 0 & a \end{pmatrix}. \tag{2.4.30}$$

A change of basis puts this in the form

$$\begin{aligned} \mathcal{M}' &= \begin{pmatrix} 1 & 0 & 0 \\ 0 & \frac{\mp 1}{\sqrt{2}} & \frac{\mp 1}{\sqrt{2}} \\ 0 & \frac{i}{\sqrt{2}} & -\frac{i}{\sqrt{2}} \end{pmatrix} \begin{pmatrix} 0 & vy_1 & \pm ivy_1 \\ vy_1 & a & 0 \\ \pm ivy_1 & 0 & a \end{pmatrix} \begin{pmatrix} 1 & 0 & 0 \\ 0 & \frac{\mp 1}{\sqrt{2}} & \frac{i}{\sqrt{2}} \\ 0 & \frac{\mp 1}{\sqrt{2}} & -\frac{i}{\sqrt{2}} \end{pmatrix}, \\ &= \begin{pmatrix} 0 & \mp\sqrt{2}vy_1 & 0 \\ \mp\sqrt{2}vy_1 & 0 & a \\ 0 & a & 0 \end{pmatrix}. \end{aligned} \tag{2.4.31}$$

If we take the neutrinos in this basis to be ν_L, ν_R^c, X^c, where X is a right-handed gauge-singlet, then we may assign lepton numbers -1, $+1$, $+1$ respectively (to the fields with conjugations as stated) and find that lepton number is a symmetry of the mass terms when the mass matrix is as given in Eq. (2.4.31). This symmetry ensures that all higher-order loop corrections to the light neutrino masses are also zero.

Classes of models exist, called low-scale seesaws [73–77] based around the mass matrix of Eq. (2.4.31). Generally they promote the elements to matrices of the appropriate size to describe realistic $(3 + n_N)$ situations. In order to make the cancellation in the light neutrino masses incomplete, such that they acquire some mass, all that is needed is small lepton-number violating parameters, for instance, the inverse seesaw [73–75] (a prominent low-scale seesaw model) has the texture

$$\mathcal{M} = \begin{pmatrix} 0 & vy_1^T & 0 \\ vy_1 & \mu & M \\ 0 & M^T & \mu' \end{pmatrix},$$

with μ, $\mu' \ll vy_1 \ll M$ and predicts a tree-level light neutrino mass matrix propor-

tional to the lepton number violating parameter μ'

$$m_\nu \approx v^2 \left(M^{-1} y_1\right)^T \mu' M^{-1} y_1.$$

The neutrino masses are naturally small because they are due to a small violation of a symmetry. In this context the Yukawas may be $\mathcal{O}(1)$ and the heavy neutrinos as light as 1 TeV. The low-scale seesaws are much more easily testable than the naive type I seesaw scenario due to their enhanced active-heavy mixing and their lowered mass scale for production of on-shell heavy neutrinos.

In the $(3+2)$ scenario, with ν_R and X, we see that when there is an exact lepton number symmetry, $\mu = \mu' = 0$, the mass terms of the Lagrangian are

$$\mathcal{L}_m \ni -\frac{1}{2} M \left(\overline{\nu_R^c} X + \overline{X} \nu_R^c + \overline{X^c} \nu_R + \overline{\nu}_R X^c\right), \tag{2.4.32}$$

$$= -M \left(\overline{X^c} \nu_R + \overline{\nu}_R X^c\right), \tag{2.4.33}$$

$$= -M \overline{\psi_D} \psi_D, \tag{2.4.34}$$

where $\psi_D \equiv \nu_R + X^c$. This means that the physical heavy neutrino here is a Dirac neutrino ψ_D with a Dirac mass term and no Majorana mass term. When there is a small amount of lepton number violation by the parameters μ and μ', the two Majorana components have a mass splitting $\approx \mu$ and are called a pseudo-Dirac neutrino. More generally, the $(3 + n_N)$ scenario leads to multiple pseudo-Dirac neutrinos in the inverse seesaw.

Chapter 3

Baryogenesis through leptogenesis

The world is composed of matter and not antimatter. In everyday life, objects are made of atoms and never anti-atoms. Even at cosmological scales where the galaxies are the infinitesimal constituents of structures, we find the same thing: matter galaxies not antimatter galaxies. Precise cosmological observations have quantified this excess of matter in the baryonic component of the universe and show that it is orders of magnitude larger than predicted by the Standard Model. Therefore a successful explanation of the observed matter-antimatter asymmetry of the universe requires new physical ideas beyond those of the Standard Model.

In this chapter we review leptogenesis — one class of mechanisms by which the baryon asymmetry may have been produced. First we shall examine the evidence for a cosmological baryon asymmetry, then introduce a quantitative description of leptogenesis distilled to its essential features. For its relevance to the original research to be presented later in this thesis, we then incorporate decoherence due to flavour effects into the description.

3.1 The baryon asymmetry

The baryon asymmetry is often expressed in terms of the parameter η_B which is defined in terms of particle number densities n to be

$$\eta_B \equiv \left.\frac{n_B - n_{\overline{B}}}{n_\gamma}\right|_0$$

with the subscripts B, $\overline{B}$ and γ referring to baryons, antibaryons and photons and the subscript 0 indicating the present-day value. There appears to be no antimatter component to the universe: if there were patches of matter and patches of antimatter of any size, there would be gamma rays resulting from annihilation at their boundaries but these are not observed [78]. Furthermore cosmic rays which originate far away in our galaxy or even in other galaxies are almost entirely matter particles. The tiny proportion, about 0.01%, of antiparticle cosmic rays are consistently explained as being produced by matter particles undergoing interactions on their way to the Earth [79]. So we reasonably conclude that presently $n_{\overline{B}} = 0$.

We imagine that the matter-antimatter asymmetry was created very early in the history of the universe and that the antimatter component subsequently vanished in annihilations with some of the matter component. This annihilation process conserves the baryon number and so it is the density of the remaining baryons that quantifies the excess of matter over antimatter.[1] That is to say that $n_B - n_{\overline{B}}$ is unaffected by the annihilations that take $n_{\overline{B}} \to 0$. The baryon number density n_B and hence the baryon-to-photon ratio $\eta_B = n_B/n_\gamma|_0$ can be ascertained from studying the processes of big bang nucleosynthesis (BBN) [80–84] and baryon acoustic oscillations (BAO) [85, 86] which occurred long after the creation of the asymmetry.

Big bang nucleosynthesis occurred when the temperature of the universe fell below

[1] Of course, there may be an asymmetry in the leptons too. This lepton asymmetry would exist in the electrons and neutrinos of the universe at the present time given that heavier leptons would decay in to them. Given that we do not know the number nor the nature of neutrinos, the lepton asymmetry is unknown and poorly constrained although one might deduce the electronic component from the observed electrical neutrality of the universe. Given the uncertainties on the leptonic asymmetry, the baryon asymmetry is of primary interest currently in investigating the fundamental distinction between matter and antimatter in the universe.

$T \sim 1$ MeV. The mass fraction of the resulting ^{4}He, D, ^{3}He and ^{7}Li has been determined and it is known theoretically how each of these is dependent upon the baryon number density. Matching the predicted value to the measured one it has been determined that the 1σ range [87] is

$$\eta_{B\mathrm{BBN}} = (5.80 - 6.60) \times 10^{-10}.$$

The cosmic microwave background (CMB) contains information on the presence of sound waves (baryon acoustic oscillations) in the plasma of the early universe at the time when neutral hydrogen formed ($T \lesssim 1$ eV). As the plasma contained protons, electrons and photons, the sound speed, which determined the size of the structures in the CMB, was a function of the baryon number density. It has been inferred that the 1σ range [88] is

$$\eta_{B\mathrm{CMB}} = (6.02 - 6.18) \times 10^{-10}.$$

The excellent agreement of the BBN and CMB values is remarkable given that they are determined from independent processes occurring at temperatures differing by a factor of 10^6.

3.2 Simplest version of leptogenesis

Baryogenesis — the production of the excess of baryons over antibaryons — has been explained through various theoretical processes. We focus on one such category: leptogenesis, in which lepton number violating processes produce a lepton asymmetry which is subsequently converted in part into the baryon asymmetry. Leptogenesis is often appealing because of its ability to explain the baryon asymmetry using extensions of the Standard Model which also explain the smallness of neutrino masses.

In general, a baryon asymmetry may only be created in a theory if it satisfies Sakharov's conditions: C and CP violation, out-of-equilibrium processes and baryon number violation [89]. The Standard Model satisfies each of these with C violation in

the weak interactions, CP violation in the quark sector, out-of-equilibrium thermal processes in the electroweak phase transition and baryon number in the sphaleron processes [90–92]. However, when Standard Model baryogenesis is scrutinised, it is found to fail on the quantitative level. The CP violation is insufficient[2] and the electroweak phase transition is not sudden enough (see Fig. 3.1) [98–104]. This is why it must be new physics, beyond the Standard Model, that explains baryogenesis.

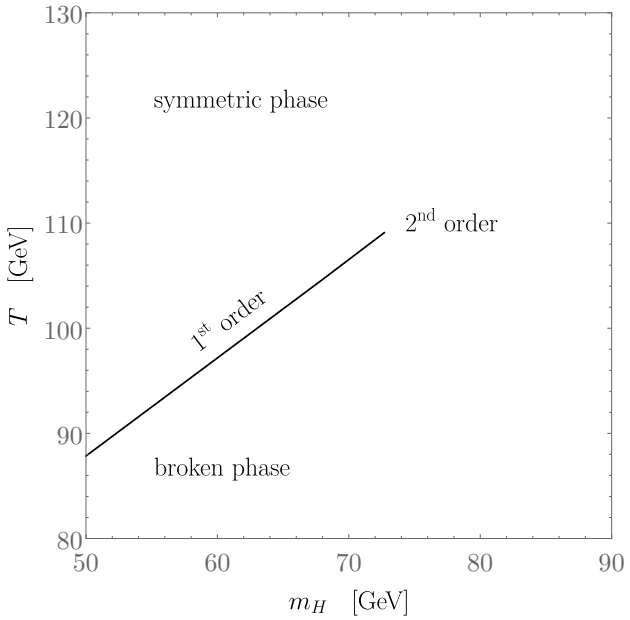

Figure 3.1: The phase diagram of the Higgs. A discontinuous first-order transition is only possible when the Higgs mass is less than about 72 GeV. Thus, the out-of-equilibrium condition is not realised in the purely SM baryogenesis processes.

In this thesis, we will only consider thermal leptogenesis [48, 105–107] in which the heavy neutrinos of the type I seesaw (Section 2.4) undergo lepton-number, C- and CP-violating decays out-of-equilibrium. We begin by developing the very simplest description of this kind of leptogenesis containing only the relevant physics to explain the mechanism of production of the baryon asymmetry and neglecting that which only tweaks the precision of the numerical predictions [108].

[2]One can estimate the size of the asymmetry by constructing a quantity called the Jarlskog invariant J [93, 94] (depending on the quark masses) which is zero when CP violation is zero. The dimensionless ratio $J/v^{12} \sim 10^{-20}$ is far too small to account for $\eta_B \sim 10^{-10}$ [95–97].

The basic rate equations for particles in an expanding universe

We begin very generically and consider a particle species X with number density ρ_X which may be affected either by the expansion of the universe with Hubble parameter H or through inelastic collision processes with quantum mechanical probability amplitudes $\mathcal{M}(X, Y \to Z)$ or $\mathcal{M}(Z \to X, Y)$ where by Y, Z we could mean a whole set of particles $X = a, b, \ldots$, $Z = i, j, \ldots$ Then the Boltzmann equation (more properly the rate equation) describing the evolution of the number density is (see for example [109])

$$\dot{\rho}_X + 3H\rho_X = -\sum_{Y,Z} \gamma(X, Y \to Z) + \sum_{Y,Z} \gamma(Z \to X, Y), \tag{3.2.1}$$

where the γ is the averaged rate of inelastic collision processes

$$\gamma(X, Y \to Z) = \int d\pi\, (2\pi)^4\, \delta^4(p_X + p_Y - p_Z)\, |\mathcal{M}(X, Y \to Z)|^2\, f_X f_Y g_Z, \tag{3.2.2}$$

and $\delta^4(p_X + p_Y - p_Z)$ conserves four-momentum when one integrates over the density of states $d\pi = d\pi_X d\pi_Y d\pi_Z$ in which

$$d\pi_A = \frac{d^3 p_A}{(2\pi)^3 2E_A}.$$

The factors of f_X, f_Y are the phase space densities (with f_Y possibly a product $f_a f_b \ldots$ since Y may be a set of particles) and g_Z is the quantum statistical factor $(1 \pm f_i)(1 \pm f_j)\ldots$, for $i, j, \ldots \in Z$ — the plus sign for bosons and the minus for fermions. An exactly similar expression holds for the inverse processes.

The collision terms can be made more manageable by eliminating the phase space densities in favour of the particle numbers. A pair of approximations make this possible. Firstly, let us assume that the phase space densities are small enough that the factors $1 \pm f$ may be replaced with unity[3]:

$$\gamma(X, Y \to Z) = \int d\pi\, (2\pi)^4\, \delta^4(p_X + p_Y - p_Z)\, |\mathcal{M}(X, Y \to Z)|^2\, f_X f_Y. \tag{3.2.3}$$

[3]On the basis that $f^{\mathrm{eq}} \approx e^{-E/T}$ and $\langle E \rangle \sim 3T$ such that $f \approx 0.05$ and can be neglected in comparison with 1 at the expense of $\mathcal{O}(0.1)$ errors.

Secondly, we assume that although inelastic collisions are changing particle numbers from their equilibrium value ($\rho_X \neq \rho_X^{\rm eq}$ in general), the *elastic* collisions quickly redistribute the energy such that the particles immediately return to the equilibrium distribution in energy $\propto e^{-\beta E_X}$. This means that we retain the Maxwell-Boltzmann distribution but give it a new normalisation

$$f_X = \frac{\rho_X}{\rho_X^{\rm eq}} e^{-\beta E_X}.$$

Equivalently, we could say that we have introduced a chemical potential $\mu = \log(\rho_X/\rho_X^{\rm eq})/\beta$ to control the particle numbers.

This means that the rates may be expressed as

$$\begin{aligned} \gamma\left(X, a, b, \ldots \to i, j, \ldots\right) &= \gamma^{\rm eq}\left(X, a, b, \ldots \to i, j, \ldots\right) \frac{\rho_X \rho_a \rho_b \cdots}{\rho_X^{\rm eq} \rho_a^{\rm eq} \rho_b^{\rm eq} \cdots} \\ \gamma\left(i, j, \ldots \to X, a, b, \ldots\right) &= \gamma^{\rm eq}\left(i, j, \ldots \to X, a, b, \ldots\right) \frac{\rho_i \rho_j \cdots}{\rho_i^{\rm eq} \rho_j^{\rm eq} \cdots}, \end{aligned} \tag{3.2.4}$$

where $\gamma^{\rm eq}$ is the same as γ for a given process but with the equilibrium distributions in the integrand. This is advantageous because the equilibrium distributions are just the standard ones of statistical mechanics. This leaves us with just the particle densities ρ to determine (as opposed to both particle densities and phase space densities). At this point it is natural to introduce the simplifying notation for normalised reaction rates

$$\Gamma\left(X, a, b, \ldots \to i, j, \ldots\right) \equiv \frac{\gamma^{\rm eq}\left(X, a, b, \ldots \to i, j\right)}{\rho_X^{\rm eq} \rho_a^{\rm eq} \rho_b^{\rm eq} \cdots}. \tag{3.2.5}$$

Before specialising to the case of leptogenesis, we make one further simplification by ridding ourselves of the term $3H\rho_X$ describing the dilution of particles due to the expansion of the universe, by normalising the densities such that they represent the number of particles in a comoving volume containing one ultra-relativistic heavy neutrino in thermal equilibrium (following the conventions of [110]). We denote the normalised density n and eliminate the ρ densities in favour of them.[4]

[4]When we defined η_B previously we did not specify the normalisation of the particle densities n because it cancels from the definition.

Heavy Majorana neutrinos in the expanding universe

In leptogenesis the heavy neutrinos undergo a decay $N \to l\,\overline{\phi}$ with (normalised) rate $\Gamma \equiv \Gamma\left(N \to l\,\overline{\phi}\right)$ or the conjugated equivalent $N \to \bar{l}\,\phi$ with rate $\overline{\Gamma} \equiv \Gamma\left(N \to \bar{l}\,\phi\right)$ in which ϕ is the Higgs doublet and l is a superposition of the different flavour lepton doublets L_e, L_μ and L_τ and $\bar{l}$ is the same but for antiparticles:

$$\begin{aligned} |l\rangle &\equiv \sum_\alpha c_{1\alpha}|L_\alpha\rangle, \\ |\bar{l}\rangle &\equiv \sum_\alpha \overline{c}_{1\alpha}|\overline{L}_\alpha\rangle, \end{aligned} \tag{3.2.6}$$

where $c_{1\alpha}$ and $\overline{c}_{1\alpha}$ are some model-dependent coefficients. Recall that this is before electroweak symmetry is broken and so the leptons and Higgs are essentially massless[5]. This also means that there is a charged Higgs so that the processes $N \to l^-\,\phi^+$ and $N \to l^+\phi^-$ are possible in addition to those involving the neutral Higgs and neutrinos. If CP is a symmetry, then $\Gamma = \overline{\Gamma}$, however, if CP is violated, the two decays of N may occur at different rates and their difference $\Gamma - \overline{\Gamma}$ is a measure of CP violation — a requirement for the production of a matter-antimatter asymmetry.[6] At tree-level (only) these rates are equal with $\Gamma = (Y^\dagger Y)_{11}M/(8\pi)$.

An initial population of heavy Majorana neutrinos will decay to leptons or antileptons in these two processes at different rates provided there is CP violation. In this way, a volume initially populated with equal numbers of particles and antiparticles may develop an excess of one or the other in the leptonic and Higgs components.

For simplicity let us assume that only one heavy Majorana neutrino undergoes such a decay. Then applying the Boltzmann equations to this physical scenario we have

$$\begin{aligned} \dot{n}_N = &\,\Gamma\left(N \to l\,\overline{\phi}\right) n_N + \Gamma\left(N \to \bar{l}\,\phi\right) n_N \\ &- \Gamma\left(l\,\overline{\phi} \to N\right) n n_{\overline{\phi}} - \Gamma\left(\bar{l}\,\phi \to N\right) \overline{n} n_\phi, \end{aligned}$$

[5]Except for an effective mass acquired from their propagation through a thermal bath.

[6]In general we may always use CPT to define antiparticles as it is always a symmetry of relativistic QFT. We have that $\left|\mathcal{M}\left(N \to l\,\overline{\phi}\right)\right| = \left|\mathcal{M}\left(\bar{l}\,\phi \to N\right)\right|$ from CPT symmetry. Then, if we also have CP symmetry, which implies T symmetry, we can reverse the ordering and find $\left|\mathcal{M}\left(N \to l\,\overline{\phi}\right)\right| = \left|\mathcal{M}\left(N \to \bar{l}\,\phi\right)\right|$. We see that, if there is a CP symmetry, the amplitudes of these processes would be equal and so would the rates in this case. If they are not equal then there is CP violation.

where here, n_N, n and n_ϕ are the normalised densities for heavy neutrinos, leptons and Higgs and those with overbars are the antiparticle densities. We emphasise that these densities are normalised such that they represent the particle numbers in a comoving volume containing one ultrarelativistic heavy neutrino (such that, e.g., $n_N^{\rm eq}\left(T \gg M\right) = 1$). We choose not to use a subscript on the lepton densities in order to make the equations more graceful later on.

The particles l and ϕ are essentially in equilibrium due to their fast gauge interactions; their small deviations from equilibrium being negligible in comparison with that of N. Later, when deriving equations for the asymmetry in the leptons, these small deviations will be essential features, but for now we neglect them by using the equilibrium distributions for l and ϕ. Further simplification is achieved by a pair of observations: we may relate the Γ factors by noting, firstly, that CPT invariance imposes

$$\left|\mathcal{M}\left(N \to l\,\overline{\phi}\right)\right|^2 = \left|\mathcal{M}\left(\overline{l}\,\phi \to N\right)\right|^2,$$

and secondly that the exponential form of the Maxwell-Boltzmann phase space densities and the conservation of energy give

$$f_N^{\rm eq} = f_l^{\rm eq} f_\phi^{\rm eq},$$

($e^{-\beta E_l} e^{-\beta E_\phi} = e^{-\beta E_N}$). Using these in the definitions of γ and Γ, (Eq. (3.2.2) and Eq. (3.2.5)) we get

$$\begin{aligned} \Gamma\left(N \to l\,\overline{\phi}\right) n_N^{\rm eq} &= \Gamma\left(l\,\overline{\phi} \to N\right) n^{\rm eq}, \\ \Gamma\left(N \to \overline{l}\phi\right) n_N^{\rm eq} &= \Gamma\left(l\,\overline{\phi} \to N\right) n^{\rm eq}, \end{aligned} \tag{3.2.7}$$

where we have eliminated $\overline{n}^{\rm eq}$ in the last step by using $\overline{n}^{\rm eq} = n^{\rm eq}$. We conclude

$$\frac{dn_N}{dt} = -\left(\Gamma\left(N \to l\,\overline{\phi}\right) + \Gamma\left(N \to \overline{l}\,\phi\right)\right)\left(n_N - n_N^{\rm eq}\right). \tag{3.2.8}$$

We recast this once more by changing from the time variable to the more useful $z \equiv M/T$, M being the heavy neutrino mass, which has the nice property of increasing with time. This allows for a direct comparison of the temperature with the other physical scale M making $z \sim 1$ the point at which leptogenesis processes

are typically most fervent. In practice, this means introducing factors $1/Hz$ for every rate $\Gamma(A \to B)$ so that the equation above is written

$$\begin{aligned} \frac{dn_N}{dz} &= -\frac{\Gamma + \overline{\Gamma}}{Hz}\left(n_N - n_N^{\mathrm{eq}}\right), \\ &= -D\left(n_N - n_N^{\mathrm{eq}}\right), \end{aligned} \tag{3.2.9}$$

where we have defined

$$D \equiv \frac{\Gamma + \overline{\Gamma}}{Hz} = Kz\frac{\mathcal{K}_1(z)}{\mathcal{K}_2(z)}, \tag{3.2.10}$$

in which

$$K \equiv \frac{\Gamma}{H(M)} = \frac{\tilde{m}}{m_*}, \tag{3.2.11}$$

is called the decay parameter. The effective neutrino mass is defined by [111]

$$\tilde{m} \equiv \frac{\left(Y^\dagger Y\right)_{11} v^2}{M}, \tag{3.2.12}$$

and

$$m_* \equiv \frac{16\pi^2 v^2}{3M_{\mathrm{Planck}}}\sqrt{\frac{g_*\pi}{5}} \approx 10^{-3}\ \mathrm{eV}. \tag{3.2.13}$$

A simple recipe gives the averaged decay rate Γ: first compute the vacuum decay rate at rest using the usual Feynman rules; multiply by the mass over energy M/E for N to boost it into the frame of a moving particle; finally take the thermal average by integrating it with a factor f_N^{eq}. The result for Γ contains a factor $\langle E^{-1}\rangle/n^{\mathrm{eq}} \propto \mathcal{K}_1(z)/\mathcal{K}_2(z)$ ($\mathcal{K}_i$ being modified Bessel functions of the second kind) and the Hubble parameter $H \propto 1/z$

Equation for $B - L$ asymmetry evolution

Now we should consider the evolution of the normalised lepton density n and anti-lepton density $\overline{n}$ as it is their difference $n_{B-L} = \overline{n} - n$ that we ultimately want to calculate. Their individual evolutions are

$$\begin{aligned} \frac{dn}{dz} &= \frac{\Gamma}{Hz}n_N - \frac{\Gamma^{\mathrm{ID}}}{Hz}n, \\ \frac{d\overline{n}}{dz} &= \frac{\overline{\Gamma}}{Hz}n_N - \frac{\overline{\Gamma}^{\mathrm{ID}}}{Hz}\overline{n}, \end{aligned} \tag{3.2.14}$$

where $\Gamma^{\rm ID} \equiv \Gamma\left(l\,\overline{\phi} \to N\right)$ and $\overline{\Gamma}^{\rm ID} \equiv \Gamma\left(\bar{l}\,\phi \to N\right)$. In the above, the Higgs has been taken to be in equilibrium for simplicity — we do not lose any essential physics for the production of a lepton asymmetry in doing so. This isn't an option for the leptons as the equilibrium distributions are the same for leptons and antileptons and it would be the same as setting the lepton asymmetry to zero for all time.

The production of n_{B-L} depends on the CP-violating difference $\Gamma - \overline{\Gamma}$. Let us try to be precise about the relative size of terms involving CP violation. If we consider the transition matrix $\mathcal{T} = i(1-\mathcal{S})$ where the $\mathcal{S}$ matrix being just e^{-iHt} is unitary, then the unitarity condition for S leads to

$$\mathcal{T}_{ij} - \mathcal{T}^*_{ji} = i\sum_k \mathcal{T}_{ik}\mathcal{T}^\dagger_{kj}.$$

Seeing as CP symmetry would imply that

$$|\mathcal{T}_{ij}|^2 = |\mathcal{T}_{ji}|^2,$$

we can consider CP violation by looking at

$$\begin{aligned} |\mathcal{T}_{ij}|^2 - |\mathcal{T}_{ji}|^2 &= \left|i\left(\mathcal{T}\mathcal{T}^\dagger\right)_{ij} + \mathcal{T}^*_{ji}\right|^2 - |\mathcal{T}_{ji}|^2 \\ &= -2\Im\left[\left(\mathcal{T}\mathcal{T}^\dagger\right)_{ij}\mathcal{T}^*_{ji}\right] + \left|\left(\mathcal{T}\mathcal{T}^\dagger\right)_{ij}\right|^2, \end{aligned} \tag{3.2.15}$$

and from this determine that whatever order in the perturbative expansion $\mathcal{T}$ appears at, the CP asymmetries only appear at the next order or higher.

For leptogenesis, at tree-level, the two rates Γ and $\overline{\Gamma}$ are given by the absolute square of Yukawa matrix elements or the absolute square of their complex conjugates. These must be equal and so the tree-level CP-violation is zero. And so, in accordance with Eq. (3.2.15), we are forced to compute the decay rates to the level of loops which is of fourth order in Yukawa couplings. The loop-level corrections to the decay process are depicted in Fig. 3.2 where we can clearly see an unavoidable dependence on all the heavy Majorana neutrinos in the theory. In fact, if there is only one heavy Majorana neutrino, there is no CP violation because the combination of Yukawa couplings becomes real — two or more heavy Majorana neutrinos are needed if leptogenesis is

to work[7].

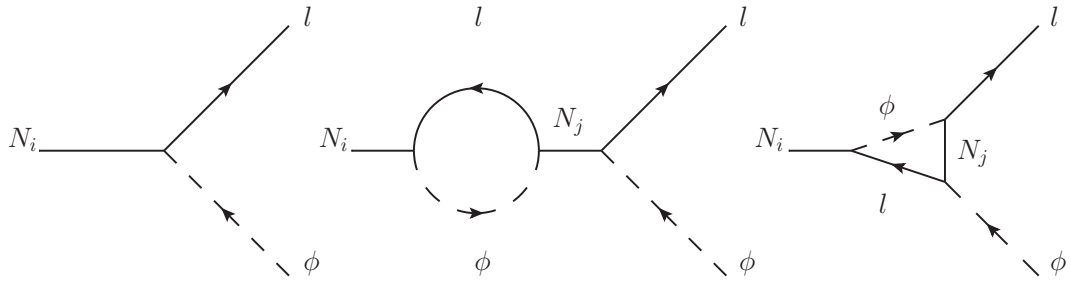

Figure 3.2: The diagrams contributing to the CP asymmetry of the $N_i \to l\,\phi$ decay process. The loop-level contributions are necessary for a non-vanishing asymmetry.

If we define

$$\epsilon \equiv -\frac{\Gamma - \overline{\Gamma}}{\Gamma + \overline{\Gamma}},$$

to be the CP asymmetry and use the amplitudes calculated from the diagrams of Fig. 3.2 we find [112–116]

$$\epsilon = \frac{3}{16\pi} \sum_{k \neq i} \frac{\Im\left[\left(Y^\dagger Y\right)^2_{ik}\right]}{\left(Y^\dagger Y\right)_{ii}} \frac{\xi\left(x_{ki}\right)}{\sqrt{x_{ki}}},$$

with $x_{ki} = \left(\frac{M_k}{M_i}\right)^2$ and

$$\xi\left(x\right) \equiv \frac{2}{3} x \left[\left(1+x\right) \log\left(\frac{1+x}{x}\right) - \frac{2-x}{1-x}\right].$$

In these diagrams we need to include the contributions of at least one other heavy Majorana neutrino $N_j = N_2,\, N_3, \ldots$ as intermediate states. We don't need to consider these other heavy Majorana neutrinos in the initial or final states in order to get a framework that predicts a lepton asymmetry so for now we ignore their contributions except when they appear here as virtual particles — we are only hoping to arrive at the very simplest functioning description of leptogenesis. For those who doubt that the self-energy contribution is necessary, then notice that in the limit where the N_j are much heavier than $N = N_1$, contraction of the propagators in the

[7]At least two heavy Majorana neutrinos are also needed in the type I seesaw if one is to match the neutrino oscillation data on the squared mass differences.

self-energy and vertex contributions of Fig. 3.2 make the diagrams identical and thus both are to be included if either is.

Using the relations of Eq. (3.2.7) in Eq. (3.2.14) to get an expression for $d\overline{n}/dz - dn/dz$ gives

$$\frac{dn_{B-L}}{dz} = \epsilon D n_N + \frac{n_N^{\rm eq}}{n^{\rm eq}}\overline{\Gamma} n - \frac{n_N^{\rm eq}}{n^{\rm eq}}\Gamma \overline{n}. \tag{3.2.16}$$

This is not yet satisfactory as it depends not just on n_{B-L} but also on n and $\overline{n}$. One way to view this is that we are looking to change variables from n and $\overline{n}$ to a new pair of variables including $n_{B-L} \equiv \overline{n} - n$. The other variable being of course $n + \overline{n}$ — the linearly independent combination. Taking this view, we should write the previous equation as

$$\begin{aligned}\frac{dn_{B-L}}{dz} &= \epsilon D n_N - \frac{n_N^{\rm eq}}{n^{\rm eq}}\Gamma\left(\frac{1}{2}n_{B-L} + \frac{1}{2}\left(n+\overline{n}\right)\right) + \frac{n_N^{\rm eq}}{n^{\rm eq}}\overline{\Gamma}\left(\frac{1}{2}\left(n+\overline{n}\right) - \frac{1}{2}n_{B-L}\right), \\ &= \epsilon D\left(n_N + \frac{1}{2}\frac{n_N^{\rm eq}}{n^{\rm eq}}\left(n+\overline{n}\right)\right) - \frac{1}{2}\frac{n_N^{\rm eq}}{n^{\rm eq}} n_{B-L}\left(\Gamma + \overline{\Gamma}\right).\end{aligned}$$

At this stage we have an equation for the evolution of n_N in addition to the above equation for the evolution of n_{B-L}. For a closed set of differential equations that may actually be solved, we must find one for $n + \overline{n}$. We find this equation by adding dn/dz and $d\overline{n}/dz$:

$$\frac{d\left(n+\overline{n}\right)}{dz} = D n_N - D\frac{n_N^{\rm eq}}{n^{\rm eq}}\frac{n+\overline{n}}{2} + \frac{1}{2}\epsilon D\frac{n^{\rm eq}}{n^{\rm eq}} n_{B-L}.$$

Neglecting the last term as it is $\mathcal{O}\left(\epsilon n_{B-L}\right)$, we arrive at

$$\frac{d\left(n+\overline{n}\right)}{dz} = D\left(n_N - \frac{n_N^{\rm eq}}{n^{\rm eq}}\frac{n+\overline{n}}{2}\right).$$

Technically, we now have a complete set of equations describing leptogenesis, however, from the $1 \leftrightarrow 2$ processes, we know that

$$\Delta n_N = -\left(\Delta n + \Delta\overline{n}\right),$$

from which we see that, by comparison with dn_N/dz

$$\frac{n+\overline{n}}{2} = n^{\rm eq} + \mathcal{O}\left(\epsilon n_{B-L}\right).$$

Then by substitution in the equation for n_{B-L}, we can eliminate $n+\overline{n}$ altogether:

$$n = \frac{1}{2}(n+\overline{n}) + \frac{1}{2}(n-\overline{n}) \approx n^{\rm eq} - \frac{1}{2}n_{B-L},$$
$$\overline{n} = \frac{1}{2}(n+\overline{n}) - \frac{1}{2}(n-\overline{n}) \approx n^{\rm eq} + \frac{1}{2}n_{B-L},$$

and arrive at

$$\frac{dn_{B-L}}{dz} = \epsilon D\left(n_N + n_N^{\rm eq}\right) - W n_{B-L}, \tag{3.2.17}$$

where

$$W \equiv \frac{1}{2}\frac{\Gamma^{\rm ID} + \overline{\Gamma}^{\rm ID}}{Hz} = \frac{1}{4}K\mathcal{K}_1(z)\, z^3, \tag{3.2.18}$$

is called the washout term and is expressed in terms of the washout parameter K Eq. (3.2.11).

Addressing the overcounting

As the CP asymmetries force us to go to fourth order in the Yukawa couplings for one process, we need to be consistent and incorporate other processes at the same order. So we include $2 \leftrightarrow 2$ scattering processes (show in Fig. 3.3) in the Boltzmann equations. In these $2 \leftrightarrow 2$ processes, when the intermediate states go on shell, we end up double counting the $1 \leftrightarrow 2$ processes, so it is then necessary to subtract these on-shell contributions from the decays. In other words, when the intermediate N that mediates $l\overline{\phi} \to \bar{l}\phi$ goes on shell, the process is the same as $l\overline{\phi} \to N$ followed by $N \to \bar{l}\phi$ which we have already accounted for. Without fixing this counting error our equations produce an asymmetry even when the heavy neutrinos are in thermal equilibrium, in contradiction with the general rules of Sakharov (think about setting $n_N = n_N^{\rm eq}$ in Eq. (3.2.17)) [109, 117, 118].

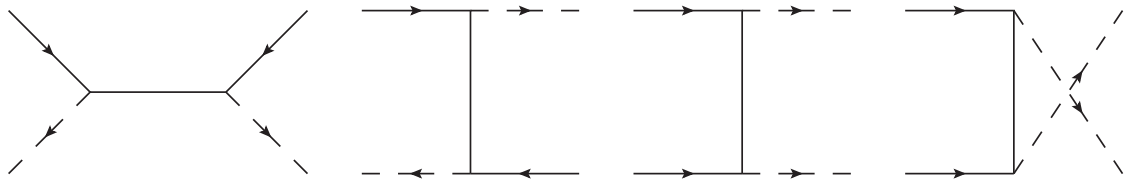

Figure 3.3: $2 \to 2$ scatterings involving only N, l and ϕ.

Now we should add in the $l\,\overline{\phi} \leftrightarrow \bar{l}\,\phi$ and $ll \leftrightarrow \phi\phi$ processes. For the former, we

must subtract from these the real intermediate states which instead contribute to $N \to l\,\overline{\phi}$. The on-shell part is

$$\gamma^{\text{eq, OS}}\left(l\,\overline{\phi} \to \bar{l}\,\phi\right) = \gamma^{\text{eq}}\left(l\,\overline{\phi} \to N\right)\text{BR}\left(N \to \bar{l}\,\phi\right).$$

Substituting $\text{BR}\left(N \to \bar{l}\,\phi\right) = (1+\epsilon)/2$ and $\gamma^{\text{eq}}\left(N \to \bar{l}\,\phi\right) = \gamma^{\text{eq}}\left(l\overline{\phi} \to N\right) = (1+\epsilon)\gamma_D/2$, where $\gamma_D = Hzn_N^{\text{eq}}D$, then the corrected $2 \to 2$ rate is

$$\gamma^{\text{eq, sub}}\left(l\,\overline{\phi} \to \bar{l}\,\phi\right) = \gamma^{\text{eq}}\left(l\,\overline{\phi} \to \bar{l}\,\phi\right) - \frac{(1+\epsilon)^2}{4}\gamma_D. \tag{3.2.19}$$

Similarly for the conjugate process

$$\gamma^{\text{eq, sub}}\left(\bar{l}\,\phi \to l\,\overline{\phi}\right) = \gamma^{\text{eq}}\left(\bar{l}\,\phi \to l\,\overline{\phi}\right) - \frac{(1-\epsilon)^2}{4}\gamma_D. \tag{3.2.20}$$

If we now use the unitarity relation[8]

$$\left|\mathcal{M}\left(l\,\overline{\phi} \to \bar{l}\,\phi\right)\right|^2 + \left|\mathcal{M}\left(l\,\overline{\phi} \to l\,\overline{\phi}\right)\right|^2 = \left|\mathcal{M}\left(l\,\overline{\phi} \to l\,\overline{\phi}\right)\right|^2 + \left|\mathcal{M}\left(\bar{l}\,\phi \to l\,\overline{\phi}\right)\right|^2,$$

we find that the first terms on the right-hand sides of Eq. (3.2.19) and Eq. (3.2.20) are equal: $\gamma^{\text{eq}}\left(l\,\overline{\phi} \to \bar{l}\,\phi\right) = \gamma^{\text{eq}}\left(\bar{l}\,\phi \to l\,\overline{\phi}\right)$. And consequently, the new $\Delta L = 2$ terms to add to Eq. (3.2.17) are

$$\frac{dn}{dz} = \cdots - 2\frac{\gamma_{\Delta L=2}}{n^{\text{eq}}Hz}n + \frac{1}{2}Dn^{\text{eq}} + \epsilon Dn^{\text{eq}},$$
$$\frac{d\overline{n}}{dz} = \cdots - 2\frac{\gamma_{\Delta L=2}}{n^{\text{eq}}Hz}\overline{n} + \frac{1}{2}Dn^{\text{eq}} - \epsilon Dn^{\text{eq}}.$$

This modifies Eq. (3.2.17) to

$$\frac{dn_{B-L}}{dz} = \cdots - \frac{2\gamma_{\Delta L=2}}{n^{\text{eq}}}n_{B-L} - 2\epsilon Dn^{\text{eq}}.$$

The new washout term $\frac{2\gamma_{\Delta L=2}}{n^{\text{eq}}}n_{B-L}$ can be safely neglected in most regimes and so we drop it (at least for the sake of simplicity). We finally write [109]

$$\frac{dn_{B-L}}{dz} = \epsilon D\left(n_N - n_N^{\text{eq}}\right) - Wn_{B-L},$$

which is now consistent with Sakharov's conditions and therefore an acceptable

[8] Consider $\mathcal{S}\mathcal{S}^\dagger$ and $\mathcal{S}^\dagger\mathcal{S}$.

description of leptogenesis.

Solutions of the equations

Now we have a pair of equations with a single model-dependent parameter K:

$$\begin{aligned} \frac{dn_N}{dz} &= -D\left(n_N - n_N^{\mathrm{eq}}\right), \\ \frac{dn_{B-L}}{dz} &= \epsilon D\left(n_N - n_N^{\mathrm{eq}}\right) - W n_{B-L}. \end{aligned} \tag{3.2.21}$$

Approximate analytical solutions may be found for the two extreme cases, $K \ll 1$ called the *weak washout regime*, and $K \gg 1$ called the *strong washout regime*. Here we will study these limiting cases in order to gain some intuition.

The first equation in Eq. (3.2.21) says that, the heavy Majorana neutrinos, which are taken to begin at some initial $z = z_0$ with value $n_N(z_0)$, are driven towards the equilibrium distribution $n_N^{\mathrm{eq}}(z)$ (which evolves with z)[9], generally overshooting and performing an overdamped oscillation about it. The larger the value of K, the more quickly this process plays out. The choice of numerical values z_0 and $n_N(z_0)$ depends on the physical assumptions by which the initial state is produced but, as we shall see, in the strong washout regime these choices are very significant. Typically the initial temperature is somewhat higher than the mass of some of the heavy neutrinos so that $z_0 \sim 0.1$.

In the second equation in Eq. (3.2.21), we can regard the asymmetry as being produced by a source term $S(z) = \epsilon D\left(n_N - n_N^{\mathrm{eq}}\right)$ and diminished by a sink term $W(z)\, n_{B-L}$:

$$\frac{dn_{B-L}}{dz} = S(z) - W(z)\, n_{B-L}.$$

In the strong washout regime, this can settle into a balanced situation — analogous to reaching a state of terminal velocity where n_{B-L} is the velocity, $W n_{B-L}$ is a velocity-dependent resistance and $S(z)$ is the weight. In this case, the acceleration

[9] In the special case that $n_N(z_0) = n_N^{\mathrm{eq}}(z_0)$, the evolving nature of the equilibrium distribution means that this condition won't be maintained at later values of z and so even here a lepton asymmetry may be generated.

dn_{B-L}/dz is nearly zero and we have $S(z) \approx W(z)\, n_{B-L}$ or

$$n_{B-L} \approx \frac{S(z)}{W(z)} = -\frac{\epsilon}{W}\frac{dn_N}{dz} \approx -\frac{\epsilon}{W}\frac{dn_N^{\rm eq}}{dz}.$$

After some sufficiently large z (call it z_f), $W(z_f) < 1$, and the processes affecting n_{B-L} fall out of equilibrium, essentially ceasing. The asymmetry is fixed after this point at[10]

$$n_{B-L} \approx -\frac{\epsilon}{W}\frac{dn_N^{\rm eq}}{dz}\bigg|_{z=z_f} = \frac{3}{2Kz_f}\epsilon. \tag{3.2.22}$$

In the weak washout regime, this balance cannot be established and so the final asymmetry is dynamical (as opposed to an equilibrium value) and necessarily dependent upon the choice of initial conditions as well as the value of K.[11]

The source term has all the features one would expect from Sakharov's conditions for producing a lepton asymmetry: C and CP violation in ϵ; lepton number violation in D describing the rate of $N \to l\,\overline{\phi}$ or its conjugate; dependence on out-of-equilibrium particles in needing $n_N - n_N^{\rm eq} \neq 0$ to produce an asymmetry. The washout term can reduce the asymmetry even without needing to treat particles and antiparticles differently — a box with 100 antiparticles and 90 particles can undergo decays of both kinds of particle so that they halve in number at the same rate, the asymmetry of $100 - 90 = 10$ is reduced to $50 - 45 = 5$. This is reflected in the sufficiency of treating the inverse decays at tree-level and not incorporating the CP violations in them (after all such a correction would be $\mathcal{O}(\epsilon n_{B-L})$).

Even once n_{B-L} has been generated we still predict $n_B = 0$ as we have not included any baryon number violating processes. However sphalerons (which are in equilibrium below $T \sim 10^{12}$ GeV) quickly process part of the lepton asymmetry into a baryon asymmetry with efficiency $n_B = (28/79)n_{B-L}$ (see Appendix C). To convert to η_B we must divide by the photon density, accounting for the change in density between

[10] In Chapter 5, we argue that this implies a lower bound on M for successful leptogenesis. This was originally derived in [119], (see also [120, 121]).

[11] Taking the terminal velocity idea further we'd have an equation $\frac{dv}{dt} = g - \xi v$ with solution $v = \frac{g}{\xi}(1 - e^{-\xi t})$. Scaling g and ξ by a factor α is like changing K to $K\alpha$ and gives $v = \frac{g}{\xi}(1 - e^{-\alpha\xi t})$. If $\alpha > 1$ the terminal velocity g/ξ is reached faster. This suggests that for small washout, the terminal value of n_{B-L} won't be reached before z_f.

the end of leptogenesis and recombination:

$$\eta_B \approx 0.013 n_{B-L}.$$

3.3 The density matrix approach

So far the only leptons we have considered are the left-handed $|l\rangle$ (and $|\bar{l}\rangle$) that are produced in the decay of N and which are a superposition of flavour states $|l\rangle = \sum_\alpha c_{1\alpha}|\alpha\rangle$, $\alpha \in \{e, \mu, \tau\}$. However, once an l is produced, Higgs particles in the early universe plasma can scatter different flavour components out of l (and into their right-handed counterparts via the fermion-Higgs couplings of the SM) at different rates, with τ being the most frequently scattered due to it having the largest SM Yukawa coupling. Let us assume that there are only τ scatterings for now. The result is that the coherent combination of e, μ, τ that constituted l is spoiled and the e/μ- (which we'll call β) and τ-components of l behave as separate particles [117, 118, 122–139].

It is quite difficult to include interactions of this kind in the description we have given so far because we are simply counting the number of l particles in some volume as a function of time. In order to write things in terms of flavour states, we should rework our description into one that explicitly mentions the single-particle quantum states $|l\rangle$ and the orthogonal state $|m\rangle$ (defined by $\langle l|m\rangle = 0$). Once we have this, we may transform to the flavour basis which we take to consist of $|\tau\rangle$ and its orthogonal $|\beta\rangle$. Then we can easily include these flavour-dependent interactions.

Let us introduce the density matrix

$$\mathbf{n} = n \begin{pmatrix} 1 & 0 \\ 0 & 0 \end{pmatrix},$$

in the basis of the vectors $|l\rangle$ and $|m\rangle$. We may alternatively write it in terms of dyads as $\mathbf{n} = n|l\rangle\langle l| + 0|l\rangle\langle m| + 0|m\rangle\langle l| + 0|m\rangle\langle m|$.

If we want to describe the time-evolution of the density matrix due to forward decays on the heavy Majorana neutrinos (we'll consider the inverse decays in a moment), then we simply need to embed them in the (l, l) component of the matrix as

$$\begin{aligned} \frac{d\mathbf{n}}{dz} &= \frac{\Gamma}{Hz} n_N S + \ldots, \\ \frac{d\overline{\mathbf{n}}}{dz} &= \frac{\overline{\Gamma}}{Hz} n_N \overline{S} + \ldots, \end{aligned} \tag{3.3.1}$$

where $S \equiv \mathrm{diag}\,(1, 0)$ in the basis $|l\rangle\ |m\rangle$ and $\overline{\mathbf{n}}$ is the antilepton density matrix defined in analogy to $\mathbf{n}$ with $\overline{S} \equiv \mathrm{diag}\,(1, 0)$ in the basis $|\bar{l}\rangle\ |\overline{m}\rangle$. There is no new physics in this because we do not include the heavy Majorana neutrino states in the density matrix. All that has happened is we have written the forward decay terms in a more complicated way than we previously did.

The evolution of the density matrix is given by $\mathbf{n}\,(t) = e^{-i\mathcal{H}t}\mathbf{n}\,(0)\,e^{i\mathcal{H}^\dagger t}$ (as a result of the dyad structure). By taking the time t to be infinitesimal, we can find the differential equation for the time evolution of the density matrix

$$\dot{\mathbf{n}} = i[\mathbf{n}, \mathcal{H}_R] + \{\mathbf{n}, \mathcal{H}_I\}, \tag{3.3.2}$$

where $\mathcal{H} = \mathcal{H}_R + i\mathcal{H}_I$ is the Hamiltonian partitioned into its real and imaginary parts. Now we can include inverse decays by considering them to be a dissipative or imaginary part of the Hamiltonian, we write

$$\frac{d\mathbf{n}}{dz} = \frac{\Gamma}{Hz} n_N S - \frac{1}{2}\frac{\Gamma^{\mathrm{ID}}}{Hz}\{S, \mathbf{n}\}, \tag{3.3.3}$$

and

$$\frac{d\overline{\mathbf{n}}}{dz} = \frac{\overline{\Gamma}}{Hz} n_N \overline{S} - \frac{1}{2}\frac{\overline{\Gamma}^{\mathrm{ID}}}{Hz}\{\overline{S}, \overline{\mathbf{n}}\}. \tag{3.3.4}$$

To transform these equations to the particle flavour basis $|\tau\rangle$, $|\beta\rangle$ ($\langle\beta|\tau\rangle = 0$) and antiparticle flavour basis $|\overline{\tau}\rangle$, $|\overline{\beta}\rangle$ ($\langle\overline{\beta}|\overline{\tau}\rangle = 0$) requires two unitary matrices $\mathcal{C}$ ($|l\rangle$, $|m\rangle \to |\tau\rangle$, $|\beta\rangle$) and $\overline{\mathcal{C}}$ ($|\bar{l}\rangle$, $|\overline{m}\rangle \to |\overline{\tau}\rangle$, $|\overline{\beta}\rangle$). Explicitly

$$\mathcal{C} \equiv \begin{pmatrix} \langle\tau|l\rangle & -\langle\beta|l\rangle \\ \langle l|\beta\rangle & \langle l|\tau\rangle \end{pmatrix} = \begin{pmatrix} c_{1\tau} & -c_{1\beta} \\ c^*_{1\beta} & c^*_{1\tau} \end{pmatrix} = \underbrace{\frac{1}{\sqrt{(Y^\dagger Y)_{11}}} \begin{pmatrix} Y_{\tau 1} & -Y_{\beta 1} \\ Y^*_{\beta 1} & Y^*_{\tau 1} \end{pmatrix}}_{\text{at tree-level}}$$

and

$$\overline{\mathcal{C}} \equiv \begin{pmatrix} \langle\overline{\tau}|\bar{l}\rangle & -\langle\overline{\beta}|\bar{l}\rangle \\ \langle\bar{l}|\overline{\beta}\rangle & \langle\bar{l}|\overline{\tau}\rangle \end{pmatrix} = \begin{pmatrix} \overline{c}_{1\tau} & -\overline{c}_{1\beta} \\ \overline{c}^*_{1\beta} & \overline{c}^*_{1\tau} \end{pmatrix} = \underbrace{\frac{1}{\sqrt{(Y^\dagger Y)_{11}}} \begin{pmatrix} Y^*_{\tau 1} & -Y^*_{\beta 1} \\ Y_{\beta 1} & Y_{\tau 1} \end{pmatrix}}_{\text{at tree-level}},$$

with which we define

$$\begin{aligned} P &\equiv \mathcal{C} S \mathcal{C}^\dagger, \\ \overline{P} &\equiv \overline{\mathcal{C}}\, \overline{S}\, \overline{\mathcal{C}}^\dagger. \end{aligned} \tag{3.3.5}$$

Taking the difference to get an equation in $\mathbf{n}^{B-L} \equiv \overline{\mathcal{C}}\overline{\mathbf{n}}\overline{\mathcal{C}}^\dagger - \mathcal{C}\mathbf{n}\mathcal{C}^\dagger$ and neglecting terms of $\mathcal{O}(\epsilon n_{B-L})$ we find

$$\frac{d\mathbf{n}^{B-L}}{dz} = \epsilon D \left(n_N + n_N^{\rm eq}\right) P^0 + \frac{P - \overline{P}}{2} D \left(n_N - n_N^{\rm eq}\right) - \frac{1}{2} W \{P^0, \mathbf{n}^{B-L}\}, \tag{3.3.6}$$

where P^0 is P or $\overline{P}$ computed using the tree-level approximations for $\mathcal{C}$ or $\overline{\mathcal{C}}$. To compute the lepton asymmetry from this, one solves for the matrix $\mathbf{n}^{B-L}$ and takes the trace $n_{B-L} = \mathrm{Tr}(\mathbf{n}^{B-L})$.

Clearly the physics of this equation is incorrect. When $n_N = n_N^{\rm eq}$, no asymmetry can be produced according to Sakharov's conditions, but the asymmetry generating term (containing ϵ) in Eq. (3.3.6) is not zero. This is the same problem as was found in the derivation of Eq. (3.2.21). Namely, the issue of consistently incorporating $2 \to 2$ scatterings by carefully subtracting the real intermediate states to avoid double-counting [117]. When this is done, the equation is corrected to [110,117,118,136,140]

$$\frac{d\mathbf{n}^{B-L}}{dz} = \epsilon D \left(n_N - n_N^{\rm eq}\right) \left(P^0 + \frac{P - \overline{P}}{2\epsilon}\right) - \frac{1}{2} W \{P^0, \mathbf{n}^{B-L}\}.$$

This gives a generalisation of the CP asymmetry to the matrix expression [110, 118, 123, 140]

$$\boldsymbol{\epsilon} = \epsilon \left(P^0 + \frac{P - \overline{P}}{2\epsilon}\right).$$

Thermal widths

Now we've made it to the flavour basis, we can include the flavour effects which scatter the left-handed τ with rate Γ_τ.[12] Using Eq. (3.3.2), we get a contribution

$$\begin{aligned} \mathcal{C}\frac{d\mathbf{n}}{dz}\mathcal{C}^\dagger &= \ldots - \frac{1}{2}\frac{\Gamma_\tau}{Hz}\{S, \mathbf{n}\}, \\ \overline{\mathcal{C}}\frac{d\overline{\mathbf{n}}}{dz}\overline{\mathcal{C}}^\dagger &= \ldots - \frac{1}{2}\frac{\Gamma_\tau}{Hz}\{S, \overline{\mathbf{n}}\}. \end{aligned} \tag{3.3.7}$$

In taking the difference, we get,

$$\frac{d\mathbf{n}^{B-L}}{dz} = \ldots - \frac{1}{2}\frac{\Gamma_\tau}{Hz}\{S, \mathbf{n}^{B-L}\},$$

where

$$\frac{1}{2}\frac{\Gamma_\tau}{Hz}\{S, \mathbf{n}^{B-L}\} = \frac{1}{2}\frac{\Gamma_\tau}{Hz}\begin{pmatrix} 2n^{B-L}_{\tau\tau} & n^{B-L}_{\tau\beta} \\ n^{B-L}_{\beta\tau} & 0 \end{pmatrix}.$$

However, if we are including the transition of left-handed to right-handed taus, then the inverse process should also be accounted for by tracking asymmetry in the right-handed taus. This changes the expression for $\mathbf{n}^{B-L}$ by adding

$$\frac{d\mathbf{n}^{B-L}}{dz} = \ldots - \frac{\Gamma_\tau}{Hz}\begin{pmatrix} \overline{n}_{\tau_R\tau_R} - n_{\tau_R\tau_R} & 0 \\ 0 & 0 \end{pmatrix}, \tag{3.3.8}$$

and also produces an extra Boltzmann equation for the asymmetry in τ_R [141]

$$\frac{d(n_{\tau_R\tau_R} - \overline{n}_{\tau_R\tau_R})}{dz} = \frac{1}{2}\frac{\Gamma_\tau}{Hz}\left((n_{\tau\tau} - \overline{n}_{\tau\tau}) - 2(n_{\tau_R\tau_R} - \overline{n}_{\tau_R\tau_R})\right). \tag{3.3.9}$$

Below from $T \sim 10^{12}$ GeV, Γ_τ/Hz is large and we have to a good approximation

$$\frac{d(n_{\tau_R\tau_R} - \overline{n}_{\tau_R\tau_R})}{dz} = 0, \tag{3.3.10}$$

which provides the condition

$$(n_{\tau\tau} - \overline{n}_{\tau\tau}) = 2(n_{\tau_R\tau_R} - \overline{n}_{\tau_R\tau_R}),$$

[12] It may be worth mentioning that there is also a real non-dissipative contribution to the Hamiltonian from the thermal self-energy which we neglect. It ends up in a commutator, as opposed to anticommutator, with $\mathcal{C}(\mathbf{n} + \overline{\mathbf{n}})\mathcal{C}^\dagger$ and it may be argued to be negligible due to the diagonalising effects of gauge interactions.

leaving us with the simple expression [110, 117, 118, 136, 140, 141]

$$\begin{aligned}\frac{d\mathbf{n}^{B-L}}{dz} &= \boldsymbol{\epsilon} D\left(n_N - n_N^{\rm eq}\right) - \frac{1}{2} W\{P^0, \mathbf{n}^{B-L}\} - \frac{1}{2}\frac{\Gamma_\tau}{Hz}\begin{pmatrix} 0 & n_{\tau\beta}^{B-L} \\ n_{\beta\tau}^{B-L} & 0 \end{pmatrix}, \\ &= \boldsymbol{\epsilon} D\left(n_N - n_N^{\rm eq}\right) - \frac{1}{2} W\{P^0, \mathbf{n}^{B-L}\} - \frac{1}{2}\frac{\Gamma_\tau}{Hz}[S, [S, \mathbf{n}^{B-L}]].\end{aligned} \tag{3.3.11}$$

The nature of the solutions of the density matrix equations

Let us expand the density matrix equations into its components

$$\begin{aligned}\frac{dn_{\tau\tau}^{B-L}}{dz} &= \epsilon_{\tau\tau} D(n_N - n_N^{\rm eq}) - W\left(|c_{1\tau}|^2 n_{\tau\tau}^{B-L} + \Re\left[c_{1\tau}^* c_{1\beta} n_{\tau\beta}^{B-L}\right]\right) \\ \frac{dn_{\beta\beta}^{B-L}}{dz} &= \epsilon_{\beta\beta} D(n_N - n_N^{\rm eq}) - W\left(|c_{1\beta}|^2 n_{\beta\beta}^{B-L} + \Re\left[c_{1\beta}^* c_{1\tau}\left(n_{\tau\beta}^{B-L}\right)^*\right]\right) \\ \frac{dn_{\tau\beta}^{B-L}}{dz} &= \epsilon_{\tau\beta} D(n_N - n_N^{\rm eq}) - \frac{1}{2} W\left(n_{\tau\beta}^{B-L}\left(|c_{1\tau}|^2 + |c_{1\beta}|^2\right) + c_{1\beta}^* c_{1\tau}\left(n_{\tau\tau}^{B-L} + n_{\beta\beta}^{B-L}\right)\right) \\ &\quad - \frac{1}{2}\frac{\Gamma_\tau}{Hz} n_{\tau\beta}^{B-L}.\end{aligned} \tag{3.3.12}$$

Let us consider two extreme cases: $\Gamma_\tau \to 0$ and $\Gamma_\tau \to \infty$. In the former, when the flavour effects are negligible, it is not immediately clear if Eq. (3.3.12) is equivalent to Eq. (3.2.21), where we recall $n_{B-L} = n_{\tau\tau} + n_{\beta\beta}$. In Appendix J, we demonstrate that this is indeed the case, and that the physical distinction between the two equations comes from flavour effects.

In the opposite limit where $\Gamma_\tau \to \infty$, the flavour effects kill the off-diagonal density matrix elements. Crudely this goes as $e^{-(\Gamma_\tau/Hz)z}$, where Γ_τ/Hz is constant with z (see Fig. 3.4). The surviving equations are [117] [118, 122, 123]

$$\begin{aligned}\frac{dn_{\tau\tau}^{B-L}}{dz} &= \epsilon_{\tau\tau} D(n_N - n_N^{\rm eq}) - W|c_{1\tau}|^2 n_{\tau\tau}^{B-L}, \\ \frac{dn_{\beta\beta}^{B-L}}{dz} &= \epsilon_{\beta\beta} D(n_N - n_N^{\rm eq}) - W|c_{1\beta}|^2 n_{\beta\beta}^{B-L},\end{aligned} \tag{3.3.13}$$

which are called the *two-flavour Boltzmann equations*. The τ and β components of l no longer interfere in the processes of leptogenesis and instead act like independent particles. One way to imagine this, which is not totally captured in the equations, is that the l particle is produced in the decays of N as a wave packet which propagates

through the early universe. Then, upon encountering a Higgs particle, the left-handed τ component is scattered as a right-handed τ and can no longer contribute to the amplitude for the inverse decay process. For this reason a projection probability factor must appear multiplying the washout terms in Eq. (3.3.13).

Aside from the interesting particle physics and cosmology in the above equations, there is also a worthwhile remark about quantum mechanics to be made. We note the analogy with a simple two-state quantum mechanical system s with state vector

$$|s\rangle = \alpha|u\rangle + \beta|d\rangle,$$

and density matrix

$$|s\rangle\langle s| = |\alpha|^2|u\rangle\langle u| + |\beta|^2|d\rangle\langle d| + \alpha\beta^*|u\rangle\langle d| + \alpha^*\beta|d\rangle\langle u|, \tag{3.3.14}$$

which interacts with a measuring device that determines the state of this system. We describe the measuring device S as another quantum mechanical system with the defining property

$$\begin{aligned} |u\rangle|S\rangle &= |u\rangle|U\rangle, \\ |d\rangle|S\rangle &= |d\rangle|D\rangle, \end{aligned} \tag{3.3.15}$$

that is, it is forced into distinguishable states by interaction with the microscopic system — this is what is meant by measurement in quantum mechanics. Then the density matrix of the combined system is

$$|s,S\rangle\langle s,S| = |\alpha|^2|u\rangle\langle u||U\rangle\langle U| + |\beta|^2|d\rangle\langle d||D\rangle\langle D| + \alpha\beta^*|u\rangle\langle d||U\rangle\langle D| + \alpha^*\beta|d\rangle\langle u||D\rangle\langle U|.$$

If we now want to describe only the microscopic system, we should trace out the detector states[13] to find the reduced density matrix which is an effective density matrix for the microscopic system

$$|s\rangle\langle s|_{\text{eff}} \equiv \text{Tr}_S|s,S\rangle\langle s,S| = |\alpha|^2|u\rangle\langle u| + |\beta|^2|d\rangle\langle d|.$$

[13]Imagine the density matrix of two non-interacting systems. To get the density matrix of just one, we could trace out the other.

Thus, the act of measurement of a microscopic system is one in which the off-diagonal elements of the density matrix are reduced to zero by some means (compare with Eq. (3.3.14)). What we have in Eq. (3.3.11) is an explicit description of the same in which the dynamical processes that lead to this state of measurement, a system with diagonal density matrix, have been included in the system, rather than assumed as in Eq. (3.3.15). In other words, the plasma of the early universe acts as a measuring device determining the τ or β nature of the leptons.[14]

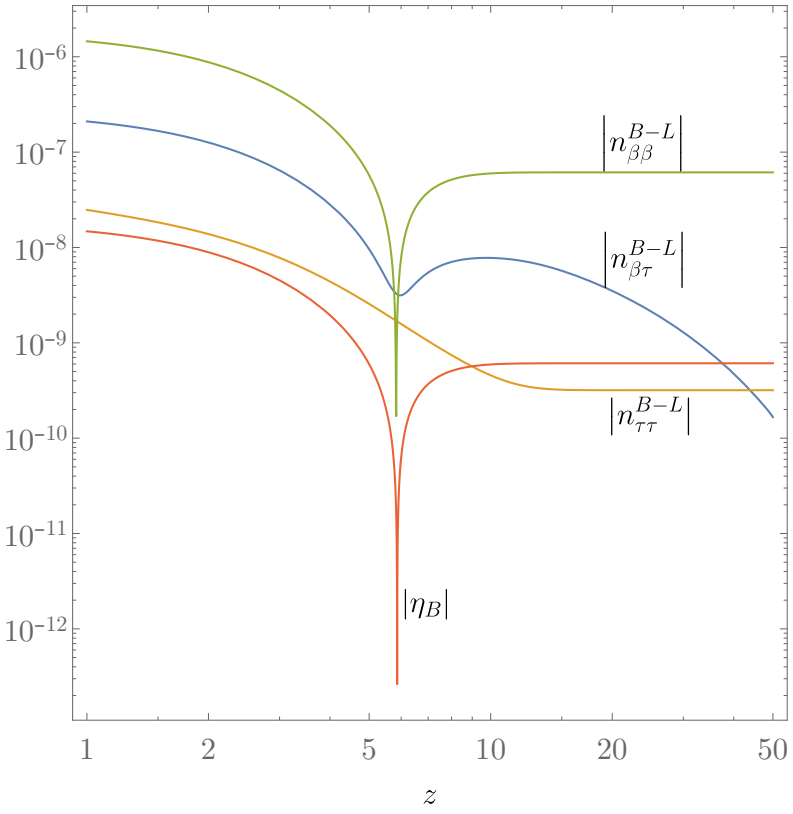

Figure 3.4: The evolution of the different components of the lepton asymmetry density matrix $\mathbf{n}^{B-L}$ demonstrating in particular the damping of the off-diagonal elements of n.

[14]In terms of measurement devices and microscopic systems, we should interpret this as there being identical measuring devices (and corresponding experimenters) one of which encounters $|u\rangle$ and the other encountering $|d\rangle$. After some interactions between system and measurement device, the microscopic system has caused one measuring device to be in the $|U\rangle$ state where the experimenter reads "U" and the other $|D\rangle$ with the experimenter reading "D".

Adding in more heavy Majorana neutrinos and flavour effects

Allowing all the heavy Majorana neutrinos to decay and adding the muon and electron flavour effects is very straightforward as it is mostly a matter of duplication of terms. In this scenario, we're allowing

$$N_i \to l_i\overline{\phi}, \quad N_i \to \bar{l}_i\phi,$$

and

$$l_i\overline{\phi} \to N_i, \quad \bar{l}_i\phi \to N_i,$$

where

$$|l_i\rangle = \sum_\alpha c_{i\alpha}|l_\alpha\rangle, \quad |\bar{l}_i\rangle = \sum_\alpha \overline{c}_{i\alpha}|\bar{l}_\alpha\rangle.$$

We add indices to the different quantities appearing in the equations of leptogenesis to indicate which heavy Majorana neutrino they each correspond to. We now have n_{N_i} $(i = 1, 2, 3, \ldots)$ as the abundance of the ith heavy Majorana neutrinos, $n_{N_i}^{\rm eq}$ as the equilibrium distribution of the ith heavy Majorana neutrino, D_i (W_i) denoting the decay (washout) corresponding to the ith heavy Majorana neutrino, which are given by [142]

$$D_i(z) = K_i x_i z \frac{\mathcal{K}_1(z_i)}{\mathcal{K}_2(z_i)}, \tag{3.3.16}$$

and

$$W_i(z) = \frac{1}{4} K_i \sqrt{x_i} \mathcal{K}_1(z_i) z_i^3, \tag{3.3.17}$$

with $\mathcal{K}_1$ and $\mathcal{K}_2$ the modified Bessel functions of the second kind with

$$x_i \equiv M_i^2/M_1^2, \quad z_i \equiv \sqrt{x_i} z,$$

where $\hat{m}_N \approx \hat{m}_R = \mathrm{diag}(M_1, M_2, \cdots)$ and

$$K_i \equiv \frac{\Gamma_i}{H(T = M_i)}, \quad \Gamma_i = \frac{M_i \left(Y^\dagger Y\right)_{ii}}{8\pi}. \tag{3.3.18}$$

Finally, the $P_{\alpha\beta}^{0(i)} \equiv c_{i\alpha} c_{i\beta}^*$, are the projection matrices. The CP-asymmetry matrix describing the decay asymmetry generated by N_i is denoted by $\epsilon_{\alpha\beta}^{(i)}$.

The general density matrix equations of leptogenesis are[15] [110, 117, 118, 136, 140]

$$\begin{aligned}
\frac{dn_{N_i}}{dz} =& - D_i(n_{N_i} - n_{N_i}^{\rm eq}) \\
\frac{dn_{\alpha\beta}^{B-L}}{dz} =& \sum_i \left(\epsilon_{\alpha\beta}^{(i)} D_i(n_{N_i} - n_{N_i}^{\rm eq}) - \frac{1}{2} W_i \left\{P^{0(i)}, n^{B-L}\right\}_{\alpha\beta}\right) \\
& - \frac{\Gamma_\tau}{2Hz}\left[\begin{pmatrix} 1 & 0 & 0 \\ 0 & 0 & 0 \\ 0 & 0 & 0 \end{pmatrix}, \left[\begin{pmatrix} 1 & 0 & 0 \\ 0 & 0 & 0 \\ 0 & 0 & 0 \end{pmatrix}, n^{B-L}\right]\right]_{\alpha\beta} \\
& - \frac{\Gamma_\mu}{2Hz}\left[\begin{pmatrix} 0 & 0 & 0 \\ 0 & 1 & 0 \\ 0 & 0 & 0 \end{pmatrix}, \left[\begin{pmatrix} 0 & 0 & 0 \\ 0 & 1 & 0 \\ 0 & 0 & 0 \end{pmatrix}, n^{B-L}\right]\right]_{\alpha\beta} \\
& - \frac{\Gamma_e}{2Hz}\left[\begin{pmatrix} 0 & 0 & 0 \\ 0 & 0 & 0 \\ 0 & 0 & 1 \end{pmatrix}, \left[\begin{pmatrix} 0 & 0 & 0 \\ 0 & 0 & 0 \\ 0 & 0 & 1 \end{pmatrix}, n^{B-L}\right]\right]_{\alpha\beta}.
\end{aligned} \tag{3.3.19}$$

Where we note that the flavour effects for τ, μ and e come into equilibrium when $M \sim 6 \times 10^{11}$ GeV, $M \sim 2 \times 10^9$ GeV, $M \sim 1 \times 10^7$ GeV respectively.

The CP-asymmetry parameters are [110, 118, 123, 140]

$$\begin{aligned}
\epsilon_{\alpha\beta}^{(i)} = \frac{3}{32\pi \left(Y^\dagger Y\right)_{ii}} \sum_{j\neq i} \Bigg\{ & i[Y_{\alpha i} Y_{\beta j}^* (Y^\dagger Y)_{ji} - Y_{\beta i}^* Y_{\alpha j} (Y^\dagger Y)_{ij}] f_1\left(\frac{x_j}{x_i}\right) \\
& + i[Y_{\alpha i} Y_{\beta j}^* (Y^\dagger Y)_{ij} - Y_{\beta i}^* Y_{\alpha j} (Y^\dagger Y)_{ji}] f_2\left(\frac{x_j}{x_i}\right) \Bigg\},
\end{aligned} \tag{3.3.20}$$

where

$$f_1\left(\frac{x_j}{x_i}\right) \equiv \frac{\xi\left(\frac{x_j}{x_i}\right)}{\sqrt{\frac{x_j}{x_i}}}, \quad f_2\left(\frac{x_j}{x_i}\right) \equiv \frac{2}{3\left(\frac{x_j}{x_i} - 1\right)}. \tag{3.3.21}$$

The diagonal components of the $\epsilon^{(i)}$ matrix simplify to the following form

$$\epsilon_{\alpha\alpha}^{(i)} = \frac{3}{16\pi \left(Y^\dagger Y\right)_{ii}} \sum_{j\neq i} \Bigg\{ \Im\left[{Y_{\alpha i}}^* Y_{\alpha j} (Y^\dagger Y)_{ij}\right] f_1\left(\frac{x_j}{x_i}\right) + \Im\left[{Y_{\alpha i}}^* Y_{\alpha j} (Y^\dagger Y)_{ji}\right] f_2\left(\frac{x_j}{x_i}\right) \Bigg\}. \tag{3.3.22}$$

[15] We're using a notation where the matrices $\mathbf{n}^{B-L}$ and $\boldsymbol{\epsilon}$ are in bold-face unless their indices are shown where it is obvious that they are matrices. This is to make it difficult to mistake them for n_{B-L} and ϵ.

The flavoured Boltzmann equations in this new notation are

$$\begin{aligned} \frac{dn_{N_i}}{dz} &= -D_i(n_{N_i} - n_{N_i}^{\rm eq}), \\ \frac{dn_{\alpha\alpha}^{B-L}}{dz} &= \sum_i \left(\epsilon_{\alpha\alpha}^{(i)} D_i(n_{N_i} - n_{N_i}^{\rm eq}) - p_{i\alpha} W_i n_{\alpha\alpha}^{B-L}\right). \end{aligned} \tag{3.3.23}$$

where $p_{i\alpha} \equiv |c_{i\alpha}|^2$, $\overline{p}_{i\alpha} \equiv |\overline{c}_{i\alpha}|^2$ are the projection probabilities. If the τ interactions are in equilibrium then $\alpha = \tau, \beta$ and these are the two flavoured Boltzmann equations. If τ and μ are both in equilibrium then $\alpha = \tau$, μ, e and these are the three-flavoured Boltzmann equations.

3.4 Summary

In this chapter we have derived the basic equations of thermal leptogenesis (Eq. (3.2.21)) where heavy Majorana neutrinos N decay into leptons: $l\overline{\phi}$ or $\overline{l}\phi$. In doing so we made a number of simplifying assumptions with the justification that we were looking for the simplest description of leptogenesis. The resulting pair of equations describe the evolution of heavy Majorana neutrino densities and the lepton asymmetry, which, after accounting for a technical difficulty of over-counting, satisfy Sakharov's conditions.

We then developed the formalism to incorporate flavour effects and extra heavy Majorana neutrinos and to arrive at Eq. (3.3.19). The flavour effects come from purely SM interactions between leptons and the Higgs in the early universe plasma. The interactions have a strength that depends on the flavour component in the leptons and that causes decoherence between these components. These equations are sufficiently accurate for a variety of phenomenological studies. In Appendix D, we make some attempt to discuss what was left out and justify the approximations made in this chapter.

Chapter 4

Massless neutrinos

In the type I seesaw, the largeness of the mass scale of the heavy Majorana neutrinos makes testing the theory very difficult. This is because the right-handed neutrinos provide only a very small contribution to the light mass states and because they are too massive to produce on-shell in experiments.

Low-scale variants of the type I seesaw have been proposed [68,73,74,76,77,143–164] (see also [165,166] and references therein) which do not suppress the active component of the heavy neutrinos. This is possible because they allow for cancellations between the mass contributions from the different heavy Majorana neutrinos such that any one contribution (and therefore the active-heavy mixing) may be large. This also means that the heavy neutrino mass scale may be lower than in the naive type I seesaws — the smallness of the light masses is achieved by cancellation of potentially large contributions and not because of division by the large mass scale. This opens up the possibility of observable signatures of the heavy neutrinos at current colliders or in low-energy experiments studying meson decays or lepton flavour violation.

A natural way to test the type I seesaw and its variants is by looking for lepton number violation (LNV). LNV does not occur in the SM and so searches for LNV signatures have very low backgrounds [167–172]. The inverse [73–75] and linear [68, 144] seesaws introduce an approximate lepton number symmetry in order to achieve the aforementioned cancellation in the light neutrino masses but this usually leads to

a reduced rate for LNV signals (see Eq. (2.4.31) and the surrounding discussion). In the extended seesaw [155] there is an accidental cancellation (not associated with a symmetry) of the light neutrino masses. Here though, radiative corrections may spoil these cancellations and lead to large light neutrino masses so that one would need to impose restrictions on the mixing in order to stay within experimental constraints. In this case the LNV signatures are again suppressed[1].

Kersten and Smirnov showed that, in models with three or fewer heavy neutrinos of equal mass, requiring an exact radiatively stable cancellation of the first term of the seesaw expansion is equivalent to requiring the conservation of lepton number [174]. This extends earlier results which did not consider the effects of radiative corrections [175, 176]. However, their result cannot be directly applied or extended to many phenomenologically important models such as the inverse seesaw model which require a larger number of heavy neutrinos. Additionally, the requirement of equal masses is obtained from the running of the Weinberg operator under the assumption that the Higgs boson is lighter than all heavy neutrinos.

In this chapter, we show that for models with an arbitrary number of sterile neutrinos that may or may not be lighter than the Higgs boson, then the masslessness of light neutrinos requires lepton number conservation (LNC) at the level of the Lagrangian. This provides a basis to the requirement of a nearly conserved lepton number symmetry in low-scale seesaw models and implies that any symmetry leading to massless light neutrinos contains lepton number as a subgroup or an accidental symmetry.

4.1 A brief overview of the argument

As the full argument is somewhat technical, it is best to give a schematic version of it here along with some general remarks. We remember that we want to consider

[1] A possible exception exists in the form of resonances in the Breit-Wigner distribution when pairs of heavy Majorana neutrinos have mass splitting close to their decay rates (see, e.g. [173]).

the type I seesaw with an arbitrary number of right-handed neutrinos and in which cancellations lead to three exactly massless light neutrinos to all orders in the radiative expansion.

We expand the light neutrino mass m_ν in a radiative expansion in m_ν^i, where i denotes the number of loops of the given contribution:

$$m_\nu = m_\nu^0 + m_\nu^1 + m_\nu^2 + ...$$

This is then set to zero:

$$m_\nu = 0.$$

In order to avoid fine-tuned solutions, we do not allow cancellations between different orders of the expansion, e.g. $m_\nu^1 = -m_\nu^2$. Instead we must have that at each order i, $m_\nu^i = 0$. We take that this condition is equivalent to requiring that one can rescale the heavy neutrino masses $m_N \to \Lambda m_N$ without ruining $m_\nu = 0$ (note that each m_ν^i is a function of m_N). By considering the explicit forms of the tree-level light neutrino masses m_ν^0 and the one-loop masses m_ν^1, we show that the only solution for which both are equal to zero independently of the scaling parameter Λ is one in which the total mass matrix exhibits a lepton number symmetry.

4.2 Theorem

Under the assumption that conditions 1), 2) and 3) (below) are obeyed, the necessary and sufficient condition for three exactly massless neutrinos to all radiative orders when an arbitrary number of gauge-singlet neutrino fields are added to the SM is that the neutrino mass matrix is given by

$$\widetilde{\mathcal{M}} = \begin{pmatrix} 0 & \alpha & \pm i\alpha & 0 \\ \alpha^T & A & 0 & 0 \\ \pm i\alpha^T & 0 & A & 0 \\ 0 & 0 & 0 & B \end{pmatrix}, \tag{4.2.1}$$

in which A and B are diagonal matrices with positive entries and α is a generic complex matrix. The conditions that must hold are:

1. there is no cancellation between different orders of the seesaw expansion,

2. there are no cancellations between different orders of the loop expansion,

3. a rescaling of the neutrino mass matrix cannot affect the condition for massless light neutrinos[2].

The former is a necessary requirement to satisfy phenomenological constraints as mixing cannot be of order one (see appendix F.1). The latter means that these fine-tuned cancellations cannot be achieved solely by specific textures of the neutrino mass matrix (see appendix F.2).

The mass matrix of Eq. (4.2.1) may be related to those arising in the common low-scale seesaw variants [68, 73, 74, 76, 77, 143–166]. Starting with the neutrino mass matrix $\widetilde{M}$, one can always find a unitary matrix

$$Q = \begin{pmatrix} 1 & 0 & 0 & 0 \\ 0 & \pm\frac{i}{\sqrt{2}}D & \frac{1}{\sqrt{2}}D & 0 \\ 0 & \frac{1}{\sqrt{2}}D & \pm\frac{i}{\sqrt{2}}D & 0 \\ 0 & 0 & 0 & 1 \end{pmatrix}, \tag{4.2.2}$$

with D unitary. This may be used to change basis and perform a congruent transformation from the matrix of Eq. (4.2.1) to

$$Q^T\widetilde{\mathcal{M}}Q = \begin{pmatrix} 0 & \pm i\sqrt{2}(D^T\alpha^T)^T & 0 & 0 \\ \pm i\sqrt{2}D^T\alpha^T & 0 & \pm iD^TAD & 0 \\ 0 & \pm iD^TAD & 0 & 0 \\ 0 & 0 & 0 & B \end{pmatrix}. \tag{4.2.3}$$

[2]It is likely that this condition this is equivalent to the requirement that there is no fine-tuned cancellation between different orders of the loop expansion —- assumption 2). An updated version of [4] will make the connection precise.

The latter is of the form

$$\begin{pmatrix} M_{\rm LNC} & 0 \\ 0 & B \end{pmatrix}, \tag{4.2.4}$$

where $M_{\rm LNC}$ is of the same form as the lepton number conserving mass matrix $\mathcal{M}'$ in Eq. (2.4.31).

Thus, there is a one-to-one correspondence between the lepton number conserving limit of the low-scale seesaw variants and the non-decoupled block of the mass matrix $\widetilde{\mathcal{M}}$ of the theorem here presented. The lepton number of the decoupled singlet neutrinos may be arbitrarily chosen without any phenomenological consequences, with zero leading to a lepton number conserving model. Therefore the theorem we are going to prove is equivalent to: *The most general gauge-singlet neutrino extensions of the SM with no cancellation between different seesaw or radiative orders, and which lead to three massless neutrinos (independently of rescaling the total neutrino mass matrix) are lepton number conserving.*[3].

4.2.1 Proof

The light neutrino masses receive contributions from both tree-level and radiative corrections and can be expanded in two convenient ways: *i*) in the perturbative series in the couplings of the interaction Lagrangian giving radiative corrections where each of these terms can be further expanded in *ii*) the expansion in m_D/m_R (the seesaw expansion).

If one chooses to cancel terms in the radiative expansion with one another then one finds that an extreme fine-tuning is necessary [72] (see appendix F.2). We shall

[3]It is worth emphasizing that we do not extend the Standard Model gauge group and thus no symmetry forbids a (Majorana) mass term for the right-handed neutrinos in our initial assumptions. More importantly, one of the hypotheses of our theorem requires the seesaw expansion to remain perturbative (see appendix F.1) and we do not concern ourselves with the trivial scenario where this expansion and thus the mixing between active and sterile neutrinos is zero. Our theorem thus applies to seesaw models where by construction light neutrinos are Majorana particles. In particular, this excludes the scenario that apparently contradicts our theorem where light neutrinos are massive and Dirac particles.

ignore such fine-tuned solutions and conclude that we must set the light masses to zero at tree-level, then set them to zero at one-loop and so on. It shall turn out to be necessary only to consider up to one-loop to achieve an all-orders massless result. This is because, once the one-loop result is considered, a lepton number symmetry is imposed on the model and from this symmetry we conclude that the massless condition must be true to all orders.

At each order of the perturbative expansion we disregard the possibility of having a cancellation between different orders of the seesaw expansion since it would lead to an active-heavy mixing larger than the experimental upper bounds (see appendix F.1). This problem does not occur if each term of the expansion is set to zero and we proceed to impose this condition in our proof.

The matrix $\widetilde{\mathcal{M}}$ as a sufficient condition for massless light neutrinos: $\widetilde{\mathcal{M}} \implies \hat{m}_\nu = 0$

The matrix $\widetilde{\mathcal{M}}$ automatically leads to $m_\nu = 0$ due to conservation of lepton number as demonstrated in section 4.2. We provide an explicit proof below.

Consider the first term of the seesaw expansion at tree-level for the light neutrinos using the mass matrix of Eq. (4.2.1). Here we have,

$$m_D = (\alpha, \pm i\alpha, 0)\,, \tag{4.2.5}$$

and

$$m_R^{-1} = \begin{pmatrix} A^{-1} & 0 & 0 \\ 0 & A^{-1} & 0 \\ 0 & 0 & B^{-1} \end{pmatrix}. \tag{4.2.6}$$

Thus, the tree-level light mass at first order is

$$m_D m_R^{-1} m_D^T = (\alpha, \pm i\alpha, 0) \begin{pmatrix} A^{-1} & 0 & 0 \\ 0 & A^{-1} & 0 \\ 0 & 0 & B^{-1} \end{pmatrix} \begin{pmatrix} \alpha^T \\ \pm i\alpha^T \\ 0 \end{pmatrix} \tag{4.2.7}$$

$$= \alpha A^{-1}\alpha^T + (\pm i)^2\, \alpha A^{-1}\alpha^T \tag{4.2.8}$$

$$= 0. \tag{4.2.9}$$

Therefore, from Eq. (2.4.9) we have

$$m_\nu^0 = 0, \tag{4.2.10}$$

considering only the first term of the seesaw expansion. Following [177, 178], we define

$$Z = m_R^{-1} m_D^T \tag{4.2.11}$$

and take

$$U' = \begin{pmatrix} \left(1 + Z^\dagger Z\right)^{-\frac{1}{2}} & Z^\dagger \left(1 + ZZ^\dagger\right)^{-\frac{1}{2}} \\ -\left(1 + ZZ^\dagger\right)^{-\frac{1}{2}} Z & \left(1 + ZZ^\dagger\right)^{-\frac{1}{2}} \end{pmatrix}, \tag{4.2.12}$$

which is unitary and block-diagonalises $\mathcal{M}$ provided that Eq. (4.2.16) holds. With this notation, we find that

$$m_\nu^0 = -\left(1 + Z^T Z^*\right)^{-\frac{1}{2}} m_D Z \left(1 + Z^\dagger Z\right)^{-\frac{1}{2}}, \tag{4.2.13}$$

where the presence of $m_D Z = m_D m_R^{-1} m_D^T = 0$ ensures that the entire seesaw expansion is zero. That is that $m_\nu^0 = 0$ to all orders in the seesaw expansion.

Now lepton number conservation implies that this massless condition is maintained at all orders in the loop expansion. We conclude from this that the mass matrix of Eq. (4.2.1) leads to three massless neutrinos to all orders.

The matrix $\widetilde{\mathcal{M}}$ as a necessary condition for massless light neutrinos: $\hat{m}_\nu = 0 \implies \widetilde{\mathcal{M}}$

From

$$\hat{m}_\nu = 0, \tag{4.2.14}$$

and the fact that we may always perform the singular value decomposition of m_ν (that is, U_ν always exists), we have that

$$m_\nu = U_\nu^* \hat{m}_\nu U_\nu^\dagger = 0. \tag{4.2.15}$$

Thus by consideration only of the first order in both expansions we have the condition[4]

$$m_D m_R^{-1} m_D^T = 0, \tag{4.2.16}$$

which, as stated above is sufficient to obtain $\hat{m}_\nu^0 = 0$ to all orders in the seesaw expansion.

Let us now consider the one-loop contribution to $\hat{m}_\nu$. We computed the one-loop induced mass for neutrinos and found it to agree with [68], giving

$$m_{\nu ij}^1 = \frac{\alpha_W}{16\pi m_W^2} C_{ik} C_{jk} f\left(m_k\right), \tag{4.2.17}$$

which is written in terms of quantities defined in Section 2.4. Let us define

$$F \equiv \mathrm{diag}(f(m_1), ..., f(m_{m+3})), \tag{4.2.18}$$

$$= \begin{pmatrix} 0 & 0 \\ 0 & F_h \end{pmatrix}, \tag{4.2.19}$$

such that Eq. (4.2.17) may be rewritten in matrix form as

$$m_\nu^1 = \frac{\alpha_W}{16\pi m_W^2} CFC^T. \tag{4.2.20}$$

Imposing zero masses for the light neutrinos implies that the total one-loop self-energy must be set to zero[5]. This implies that the $(1,1)$ block of $CFC^T = 0$, that is

$$\left(CFC^T\right)_{11} = \mathcal{H}^T \mathcal{I}^* F_h \mathcal{I}^\dagger \mathcal{H} = 0, \tag{4.2.21}$$

[4]Recall that we bar cancellations between different orders of the radiative and seesaw expansions.

[5]Massless neutrinos must have zero imaginary parts for their self energy as they cannot decay and thus they have zero total self-energy.

which may equivalently be written as

$$U_\nu^T \left(1 + Z^T Z^*\right)^{-1} Z^T U_N^* F_h U_N^\dagger Z \left(1 + Z^\dagger Z\right)^{-1} U_\nu = 0. \tag{4.2.22}$$

This reduces to

$$Z^T U_N^* F_h U_N^\dagger Z = 0 \tag{4.2.23}$$

upon the left and right multiplication by

$$\left(1 + Z^T Z^*\right) U_\nu^*$$

and

$$U_\nu^\dagger \left(1 + Z^\dagger Z\right)$$

respectively.

Since m_R is diagonal and positive, we have to the first order in the seesaw expansion

$$U_N \approx 1. \tag{4.2.24}$$

Thus, again treating the terms of the seesaw expansion independently, from Eq. (4.2.23) we arrive at

$$Z^T F_h Z = 0, \tag{4.2.25}$$

from the first term.

We shall now consider the implication of Eq. (4.2.25) for the form of the neutrino mass matrix and prove that it leads to Eq. (4.2.1). We use the tree-level expression for Z. Allowing for degenerate masses in m_R, in the flavour-basis the mass matrix can be written

$$\mathcal{M} = \begin{pmatrix} 0 & m_{D1} & m_{D2} & \dots & m_{Dn} \\ m_{D1}^T & \mu_1 I_1 & 0 & \dots & 0 \\ m_{D2}^T & 0 & \mu_2 I_2 & \dots & \vdots \\ \vdots & \vdots & \vdots & \ddots & 0 \\ m_{Dn}^T & 0 & \dots & 0 & \mu_n I_3 \end{pmatrix}, \tag{4.2.26}$$

where I_i is an $n_i \times n_i$ identity matrix. Correspondingly, we may write

$$Z = m_R^{-1} m_D^T \tag{4.2.27}$$

$$= \begin{pmatrix} \mu_1^{-1} m_{D1}^T \\ \mu_2^{-1} m_{D2}^T \\ \vdots \\ \mu_n^{-1} m_{Dn}^T \end{pmatrix}. \tag{4.2.28}$$

In this notation Eq. (4.2.25) becomes

$$Z^T F_h Z = \sum_{i=1}^{n} \mu_i^{-2} m_{Di} m_{Di}^T f(\mu_i) = 0. \tag{4.2.29}$$

Now, if the texture of the neutrino mass matrix is to determine the condition for massless neutrinos, an overall scaling

$$\mathcal{M} \to \Lambda \mathcal{M} \tag{4.2.30}$$

does not affect the form of the mass matrix or the condition[6] $\hat{m}_\nu = 0$. We shall show that this scaling leads to the condition

$$m_{Di} m_{Di}^T = 0. \tag{4.2.31}$$

In fact the above scaling implies

$$U^* \hat{\mathcal{M}} U^\dagger \to \Lambda U^* \hat{\mathcal{M}} U^\dagger = U^* \Lambda \hat{\mathcal{M}} U^\dagger, \tag{4.2.32}$$

and since U is unitary by construction it cannot be redefined to absorb the scaling. As a consequence, the scaling promotes

$$f(m_i) \to f(\Lambda m_i) \tag{4.2.33}$$

[6]Such a scaling removes the possibility of fine-tuned solutions in which a particular numerical choice of entries (in given units) for the mass matrix may lead to a cancellation. We attempt to quantify the degree of fine-tuning in appendix F.2.

and, in the limit of the first term of the seesaw expansion in which $\hat{m}_N = m_R$

$$f(\mu_i) \to f(\Lambda\mu_i). \tag{4.2.34}$$

We notice that f is a monotonically increasing strictly convex function, as shown in appendix E.2. Thus one may choose $k > n$ (with n defined in Eq. (4.2.26)) distinct values for Λ and obtain as many distinct equations of the form

$$\sum_{i=1}^{n} \mu_i^{-2} m_{Di} m_{Di}^T f(\Lambda\mu_i) = 0 \tag{4.2.35}$$

These equations form a system of linearly independent equations for the coefficients

$$\mu_i^{-2} m_{Di} m_{Di}^T f(\mu_i).$$

Since none of the μ_i are zero by construction, the only solution of this system of equations is[7]

$$m_{Di} m_{Di}^T = 0. \tag{4.2.36}$$

We shall now see that the condition of Eq. (4.2.36) is equivalent to having the neutrino mass take the form of Eq. (4.2.1). First, we express each m_{Di} in terms of vectors u^i, v^i, w^i as

$$m_{Di}^T = \left(u^i, v^i, w^i\right). \tag{4.2.37}$$

Then, we have

$$m_{Di} m_{Di}^T = \begin{pmatrix} u^{iT}u^i & u^{iT}v^i & u^{iT}w^i \\ v^{iT}u^i & v^{iT}v^i & v^{iT}w^i \\ w^{iT}u^i & w^{iT}v^i & w^{iT}w^i \end{pmatrix} \tag{4.2.38}$$

and

$$u^{iT}u^i = 0 \tag{4.2.39}$$

[7]It may appear here that we are are neglecting cancellations at a given order in the loop expansion and thus restricting ourselves further than the two caveats require. However, cancellations at each given order in the loop expansion impose an infinite set numerical constraints on the parameters of the theory and leave only the trivial solution of decoupled neutrinos. We neglect these solutions.

$$v^{iT}v^i = 0$$

$$w^{iT}w^i = 0$$

$$u^{iT}v^i = 0$$

$$u^{iT}w^i = 0$$

$$w^{iT}v^i = 0.$$

From a vector u^i such that $u^{iT}u^i = 0$, it is always possible to construct an orthogonal block-diagonal matrix $R_u = \text{diag}\,(R_u^1, \ldots, R_u^n)$ (appendix E.1) such that

$$\left(u^i, v^i, w^i\right) \to \left(u^{i'}, v^{i'}, w^{i'}\right) \tag{4.2.40}$$

$$= \left(R_u^i u^i, R_u^i v^i, R_u^i w^i\right), \tag{4.2.41}$$

in which

$$u^{i'} = \left(u_1^{i'}, \pm i u_1^{i'}, 0, \ldots, 0\right)^T. \tag{4.2.42}$$

As a special case, if the original vector u^i has only real components, then $u^{i'} = 0$. Such a transformation leaves m_R unaffected as

$$\begin{aligned} m'_R &= \text{diag}\left(R_u^1 \mu_1 I_1 R_u^{1T}, \ldots, R_u^n \mu_n I_n R_u^{nT}\right) \\ &= \text{diag}\,(\mu_1 I_1, \ldots, \mu_n I_n) \\ &= m_R. \end{aligned} \tag{4.2.43}$$

Under this transformation, we have

$$u^{iT}v^i = 0 \to u^{i'T}v^{i'} = 0, \tag{4.2.44}$$

leading us to conclude that

$$v^{i'} = \left(v_1^{i'}, \pm i v_1^{i'}, v_3^{i'}, v_4^{i'}, \ldots, v_{n_i}^{i'}\right)^T. \tag{4.2.45}$$

Similarly, we construct a second matrix R_v acting on $\left(v_3^{i'}, v_4^{i'}, \ldots, v_{n_i}^{i'}\right)^T$ such that $v^{i'}$ is reduced to

$$v^{i''} = \left(v_1^{i'}, \pm i v_1^{i'}, v_3^{i''}, \pm i v_3^{i''}, 0, \ldots, 0\right)^T. \tag{4.2.46}$$

Finally, this process is repeated with R_w such that

$$w^{i'''} = \left(w_1^{i'}, \pm i w_1^{i'}, w_3^{i''}, \pm i w_3^{i''}, w_5^{i'''}, \pm i w_5^{i'''} \ldots, 0\right)^T . \tag{4.2.47}$$

Each block of m_D thus takes the form

$$m_{Di} = \begin{pmatrix} u_1^{i'} & \pm i u_1^{i'} & 0 & 0 & 0 & 0 & 0 & \ldots & 0 \\ v_1^{i'} & \pm i v_1^{i'} & v_3^{i''} & \pm i v_3^{i''} & 0 & 0 & 0 & \ldots & 0 \\ w_1^{i'} & \pm i w_1^{i'} & w_3^{i''} & \pm i w_3^{i''} & w_5^{i'''} & \pm i w_5^{i'''} & 0 & \ldots & 0 \end{pmatrix} . \tag{4.2.48}$$

By rearranging the columns and rows, we may write the flavour-basis mass matrix as

$$\mathcal{M} = \begin{pmatrix} 0 & \alpha & \pm i\alpha & 0 \\ \alpha^T & A & 0 & 0 \\ \pm i\alpha^T & 0 & A & 0 \\ 0 & 0 & 0 & B \end{pmatrix} = \widetilde{\mathcal{M}}, \tag{4.2.49}$$

where α are blocks constructed from a permutation of the columns of m_D and A and B are positive diagonal matrices made from the same permutation of the diagonal entries of the $\mu_i I_i$.

We conclude that this neutrino mass matrix appears in any extensions of the Standard Model which introduce only new fermionic gauge singlets and in which the three light neutrinos are exactly massless (subject to the conditions previously discussed).

4.3 Conclusions

In this chapter we have shown that having all three light neutrinos massless at all orders in perturbation theory is equivalent to taking the neutrino mass matrix to be that of Eq. (4.2.1). As a corollary, we found that this is equivalent to requiring lepton number conservation. This extends the result of Kersten and Smirnov which was limited to three heavy neutrinos or fewer with equal masses. This is particularly important since it provides the basis to the requirement of a nearly conserved lepton number symmetry in low-scale seesaw models. It also implies that any symmetry

leading to massless light neutrinos contains lepton number as a subgroup or an accidental symmetry.

Since neutrino oscillations imply that at least two of the three light neutrinos are not massless, then lepton number is not conserved. And indeed many low-scale seesaw models relate the smallness of the light neutrino masses to the size of lepton number violation. Because of the smallness of the light neutrino masses, this means that one necessarily has either suppression of LNV signatures from a large mass scale or due to an approximate lepton number symmetry. The observability of LNV in neutrinoless double beta decay was discussed in [72, 179–183] but the collider implications we defer to a later article.

Chapter 5

Intermediate scale leptogenesis

The final baryon asymmetry in leptogenesis is ordinarily proportional to the CP asymmetry (Eq. (3.2.22)),

$$\epsilon^{(i)} \equiv -\frac{\Gamma_i - \overline{\Gamma}_i}{\Gamma_i + \overline{\Gamma}_i}.$$

As discussed in Chapter 3, the numerator depends on the sensitive loop-level cancellation at $\mathcal{O}(Y^4)$ whereas the denominator, which does not depend on a cancellation, is dominated by $\mathcal{O}(Y^2)$ tree-level contributions. This means that as the Yukawas are reduced in size, the maximum possible CP asymmetry and therefore the maximum final baryon asymmetry must reduce with them. From the seesaw relation, lowering the heavy Majorana neutrino mass scale M_1 requires a reduction in the Yukawas in order to keep the light neutrino masses within experimental bounds, then there must be a smallest value of M_1 for which successful leptogenesis is compatible with the observed neutrino masses.[1] In this chapter we explore the assumptions behind this bound and the possibility of going below it within thermal leptogenesis.

[1] It might be objected that actually $\eta_B \propto \epsilon/K$ but naively K varies like the light neutrino masses which we are taking to be constant to keep them within experimental bounds.

5.1 The lower bound on thermal leptogenesis

This bound, the *Davidson-Ibarra* bound, was found to have a value $M_1 \approx 10^9$ GeV [119]. Detailed numerical studies have confirmed the original estimate and require $M_1 \geq 10^9$ GeV [120, 121] when the light neutrino mass is $m_1 \leq 0.1$ eV [120, 142, 184].

Three assumptions limit the applicability of the Davidson-Ibarra bound:

- Only N_1, the lightest heavy Majorana neutrino, decays,
- The heavy Majorana neutrino mass spectrum is hierarchical: $M_1 \ll M_2,\ M_3$,
- Flavour effects are ignored.

In this chapter, we relax all of these conditions, although we shall require a mild hierarchy of heavy masses[2], and perform a numerical search for a bound on the scale of viable leptogenesis, by the application of the density matrix equations (Eq. (3.3.19)). Our main conclusion will be that the viable parameter space becomes extremely constricted for scales below $M_1 \approx 10^6$ GeV. Given the existence of leptogenesis models at the TeV scale, we shall refer to leptogenesis at $M_1 \sim 10^6$ GeV as *intermediate-scale* leptogenesis.

There are multiple reasons to consider intermediate-scale leptogenesis. For example, the addition of heavy neutrinos to the SM leads to a loop-level correction to the Higgs mass which may be unnaturally large. The correction to m_H^2 is proportional to the light neutrino masses and to M^3, with M the heavy Majorana neutrino mass scale [185]. Avoiding corrections to m_H^2 larger than ~ 1 TeV^2 requires the lightest pair of heavy Majorana neutrino masses to satisfy $M_1 < 4 \times 10^7$ GeV and $M_2 < 7 \times 10^7$ GeV [186]. Alternatively, baryogenesis models tend to reside at the GeV- or GUT-scales such that intermediate scales are under-explored.

It has been found that the scale of leptogenesis may be lowered below the Davidson-Ibarra bound through the introduction of a symmetry to the Standard Model. In

[2]Without the assumption of some hierarchy in the heavy Majorana neutrino masses there is technically no lower bound on M_1 if one uses the expressions for the CP asymmetry of Chapter 3.

[187], non-resonant thermal leptogenesis is explored at intermediate scales in the context of small $B-L$ violation. It is shown that the Davidson-Ibarra bound may be evaded with the scale lowered to 10^6 GeV, in this context because, the lepton number conserving part of the CP asymmetries, which are not related to light neutrino masses, may be enhanced. An alternative approach is to introduce supersymmetry in which one may also find viable leptogenesis at intermediate scales. In this context, the bound on the magnitude of the CP asymmetry is greatly enhanced over that found by Davidson and Ibarra. Consequently, the mass scale bound is lowered allowing for the possibility of intermediate scale leptogenesis [188]. Thermal leptogenesis at intermediate scales may solve a problem that arises in theories with gravitinos in their particle spectrum. The interaction strength of gravitinos is suppressed by the Planck scale and so they are long-lived particles that tend to persist into the nucleosynthesis era. Their decay products can destroy ^{4}He and D nuclei [189, 190] and spoil the successful predictions of nucleosynthesis. In order reduce the number of gravitinos present during nucleosynthesis, one requires a reheating temperature less than $\mathcal{O}(10^9)$ GeV (depending on the gravitino mass) [191].

In this chapter, we ask the question *how low can the scale of thermal leptogenesis go when we do not make the simplifying assumptions of Davidson and Ibarra?* We present an in-depth numerical study of the dependence of the baryon asymmetry produced from non-supersymmetric thermal leptogenesis on the low and high-scale model parameters and produce a new bound on the lowest scales for successful leptogenesis.

5.2 Physical assumptions of this chapter

In our work, we shall assume that:

- There are three heavy Majorana neutrinos N_i, with a mildly hierarchical mass spectrum in which $M_2 > 3M_1$ and $M_3 > 3M_2$ [192]. This avoids the possibility of *resonant enhancement* of the CP asymmetries [193].

- We shall parametrise the light neutrino mass matrices according to Eq. (2.4.22), using the best-fit data for the mass splittings.

- The sum of the neutrino masses is constrained by the cosmological bound. To account for varying analyses and underlying cosmological models we shall impose a constraint[3]

$$\sum m_\nu \leq 1.0 \text{ eV},$$

throughout this work.

- We safely neglect lepton number-changing scatterings on the basis that we are in the strong-washout regime (see Appendix D).

- We include the flavour effects due to tau, muon and electron Yukawa couplings on the charged lepton products of heavy Majorana neutrino decay (see the discussion of Section 3.3).

Before presenting our results it is useful to make a few definitions.

The parameter space, which is determined by the Casas-Ibarra parametrisation of Eq. (2.4.24), is 18-dimensional. We denote a point in this parameter space by $\mathbf{p} \equiv (\theta_{12}, \theta_{23}, \theta_{13}, \delta, \alpha_{21}, \alpha_{31}, x_i, y_i, m_i, M_i)$ with $i \in \{1, 2, 3\}$.

Anticipating our results, we define a parameter that quantifies the degree of fine-tuning for a given $\mathbf{p}$:

$$\mathcal{F} \equiv \frac{\sum_{i=1}^{3} \hat{m}^1_{\nu ii}}{\sum_{i=1}^{3} \hat{m}_{\nu ii}}. \tag{5.2.1}$$

To the accuracy of our calculations, the neutrino mass matrix m_ν is the sum of the tree- and one-loop contributions: $m_\nu = m^0_\nu + m^1_\nu$. A cancellation between the two leads to $\mathcal{F} > 1$ whereas in the limit that the tree-level contribution dominates, $\mathcal{F}$ tends to zero. Thus $\mathcal{F}$ fulfills some of the requirements of a measure of fine-tuning.

As the higher-order radiative corrections are not incorporated into the Casas-Ibarra parametrisation we must take care that the two-loop contribution is not large in

[3]None of our best-fit points exceed $\sum m_\nu = 0.63$ eV (see Appendix G) and thus all are in within the more stringent cosmological bound $\sum m_\nu < 0.72$ eV provided by *Planck* TT + lowP [88].

comparison with the one-loop correct light neutrino mass matrix. In Appendix G we make some estimates to justify that this has been achieved in our results.

5.3 Computational methods

The computational core of this work involves solving the set of coupled differential equations of Eq. (3.3.19), namely the density matrix equations of thermal leptogenesis with flavour effects. We use the PYTHON interface for complex differential equations [194] to the LSODA algorithm [195] that is available in SCIENTIFIC PYTHON [196].

We aim to find regions of the parameter space in which $\eta_B(\mathbf{p})$ is consistent with $\eta_{B_{\rm CMB}} = (6.10 \pm 0.04) \times 10^{-10}$. This necessitates the use an efficient sampling method. This is mainly for two reasons. Firstly, there are enough independent parameters that naive brute-force approaches will not suffice. Secondly, the function $\eta_B(\mathbf{p})$ tends to vary rapidly with some of the parameters in $\mathbf{p}$. This is especially true of the fine-tuned solutions which rely on precise numerical relations between the parameters and where the predicted final asymmetry may change by orders of magnitude or sign after a small shift in a parameter value.

We used MULTINEST [197–199], in particular, PYMULTINEST [200] which is a wrapper around MULTINEST written in PYTHON. The MULTINEST algorithm is a nested sampling algorithm that calculates Bayesian posterior distributions. We shall use the latter to define our regions of confidence.

In all our scenarios, MULTINEST uses a flat prior and the following log-likelihood

$$\log L = -\frac{1}{2}\left(\frac{\eta_B(\mathbf{p}) - \eta_{B_{\rm CMB}}}{\Delta\eta_{B_{\rm CMB}}}\right)^2 . \tag{5.3.1}$$

When a MULTINEST run was finished, we used SUPERPLOT [201] to visualise the projection of the posterior onto a two-dimensional plane.

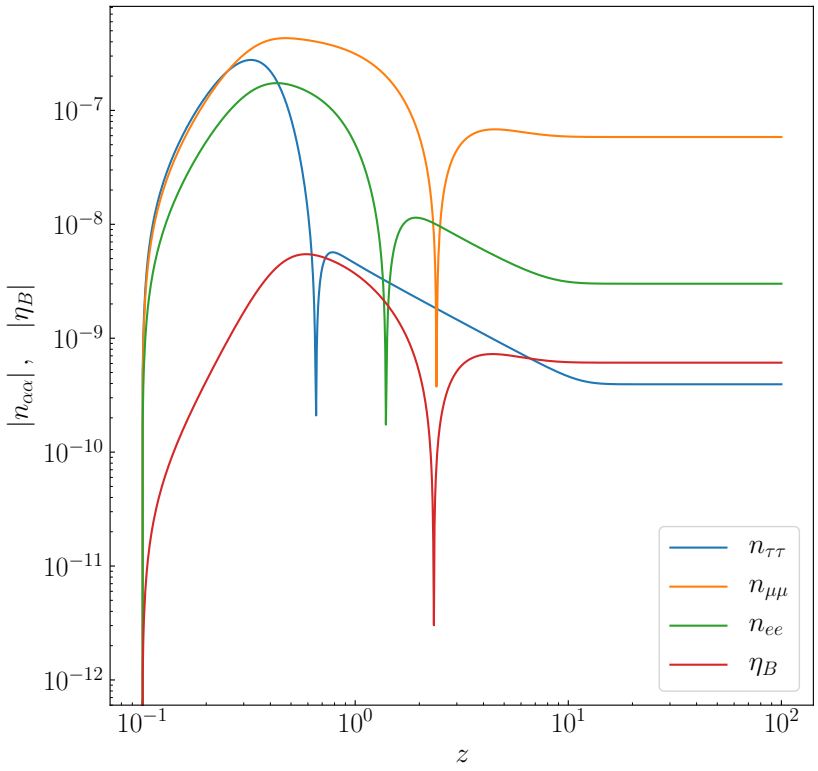

Figure 5.1: A typical plot showing the evolution of the different flavour components of the lepton asymmetry and the total asymmetry as a function of z. Leptogenesis is typically finished after $z \sim 10$.

5.4 Results

We present the viable solutions for thermal leptogenesis at intermediate scales for the case of one and two decaying heavy Majorana neutrinos in Section 5.4.1 and Section 5.4.2, respectively, the latter being a better approximation. The inclusion of both allows for a comparison of the effects of different numbers of decaying heavy Majorana neutrinos. Adding the decays of the third heavy Majorana neutrino does not appreciably affect the numerics and so we do not present those results.

	θ_{23} (°)	δ (°)	α_{21} (°)	α_{31} (°)	x_1 (°)	y_1 (°)	x_2 (°)	y_2 (°)	x_3 (°)	y_3 (°)	$m_{1(3)}$ (eV)	M_1 (GeV)	M_2 (GeV)	M_3 (GeV)
S_1	46.24	281.21	181.90	344.71	132.23	179.88	87.81	2.88	−30.25	177.5	0.120	$10^{6.0}$	$10^{6.5}$	$10^{7.0}$
S_2	46.57	88.26	116.07	420.44	44.36	171.78	86.94	2.96	97.01	174.30	0.079	$10^{6.5}$	10^{7}	$10^{7.5}$
S_3	46.63	31.71	130.95	649.65	−72.33	170.54	86.96	2.22	−1.86	178.31	0.114	$10^{6.5}$	$10^{7.2}$	$10^{7.9}$
$\overline{S_1}$	40.56	158.51	157.48	511.0	−16.23	179.29	90.04	1.29	−107.14	179.22	0.0047	$10^{6.0}$	$10^{6.5}$	$10^{7.0}$
$\overline{S_2}$	43.67	201.02	238.77	658.33	−39.88	178.68	88.12	2.46	53.97	158.01	0.0133	$10^{6.5}$	$10^{7.0}$	$10^{7.5}$
$\overline{S_3}$	43.64	57.28	179.87	292.95	86.58	174.40	91.11	1.61	134.48	173.74	0.012	$10^{6.5}$	$10^{7.2}$	$10^{7.9}$
$S_{m_\nu^1}$	44.59	140.04	537.15	291.89	164.06	−149.85	178.99	49.15	93.39	−14.50	0.15882	$10^{9.0}$	$10^{9.5}$	10^{10}
$S_{m_\nu^0}$	43.81	31.59	681.96	276.19	271.56	−125.27	14.95	−11.50	344.87	5.22	0.0041	$10^{9.0}$	$10^{9.5}$	10^{10}

Table 5.1: The best-fit points for the leptogenesis scenarios in Fig. 5.4-Fig. 5.11, corresponding to S_1 to $\overline{S}_3$, are given and are all consistent with $\eta_B = (6.10 \pm 0.04) \times 10^{-10}$, $\theta_{13} = 8.52°$ and $\theta_{12} = 33.63°$. The upper (lower) three rows are the best-fit points for normal (inverted) ordering. The final two rows are the best fit points for normal ordering in the loop and tree-level dominated scenarios.

5.4.1 Results from N_1 Decays

In this section we solve the density matrix equations Eq. (3.3.19) under the approximation that we may neglect the contributions of N_2 and N_3 except in the expressions for the CP asymmetry. As explained in Section 5.3, solving the density matrix equations Eq. (3.3.19) over regions of 18-dimensional parameter space is numerically challenging. However, given that the solar (θ_{12}) and reactor (θ_{13}) mixing angles are relatively precisely measured so we can fix them at their best-fit values from global fit data [202]. Similarly, although we allow the lightest neutrino mass (m_1 for NO and m_3 for IO) to vary within the constraints from the sum of neutrino masses, the other two light masses are determined from the best-fit values of Δm^2_{21}, Δm^2_{31} and Δm^2_{32} from global fit data [202]. Finally, in any one parameter scan, but not between them, we fix the heavy Majorana mass spectrum leaving only 11 of the 18 parameters to be varied.

In all scenarios we choose a set of initial values for M_1, M_2 and M_3, then explore the parameter space to find the regions consistent with $\eta_{B_{\rm CMB}}$ to 1σ and 2σ confidence. By calculating the fine-tuning $\mathcal{F}$ in the regions of 1σ agreement, we decide either to lower the scale of M_1 or not (while keeping the ratios M_2/M_1 and M_3/M_2 fixed). As the scale is lowered the fine-tuning increases the significance of higher-order

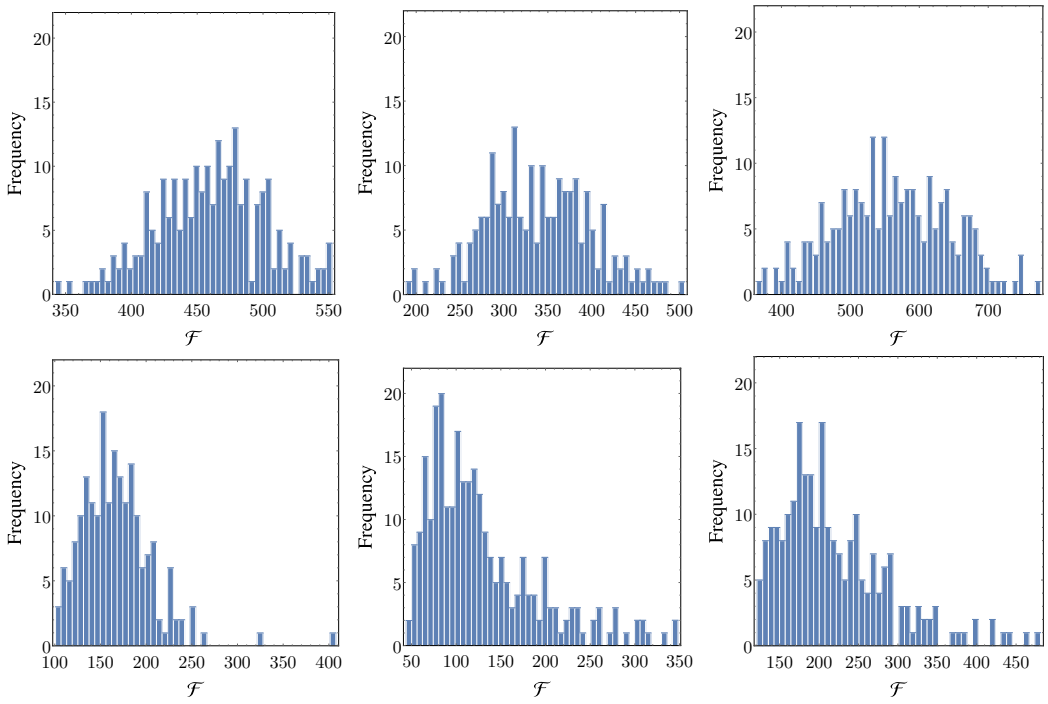

Figure 5.2: The top (bottom) three plots from left to right show the fine-tuning $\mathcal{F}$ for regions of the model parameter space within 1σ of measured η_B for S_1, S_2 and S_3 ($\overline{S_1}$, $\overline{S_2}$ and $\overline{S_3}$) respectively.

corrections in the light neutrino masses is greater. We do not further lower the scale when either the two-loop contributions becomes greater than a few percent or when the fine-tuning exceeds $\mathcal{O}(1000)$ (see Appendix G). If one were to incorporate the effects of higher radiative orders, the parameter space could be explored at even lower scales where the fine-tuning is greater. Thus, the lower bounds that we ultimately find are somewhat approximate as they depend upon the degree of fine-tuning. However, as we shall show, the viable parameter space rapidly diminishes with lowering scale and so our lower bounds must be approximations to the true lower bounds.

We choose to present the results of six scenarios for a single decaying heavy Majorana neutrino called

- S_1, $\overline{S_1}$: $M_1 = 10^6\,\text{GeV}$, $M_2/M_1 \simeq 3.15$, $M_3/M_2 \simeq 3.15$,
- S_2, $\overline{S_2}$: $M_1 = 10^{6.5}\,\text{GeV}$, $M_2/M_1 \simeq 3.15$, $M_3/M_2 \simeq 3.15$,

- S_3, $\overline{S_3}$: $M_1 = 10^{6.5}\,\text{GeV}$, $M_2/M_1 \simeq 5$, $M_3/M_2 \simeq 5$,

where no overline indicates NO and an overline indicates IO. Scenarios S_1 ($\overline{S_1}$) and S_2 ($\overline{S_2}$) have the same mass ratios, but with the former at the lowest acceptable mass scale and the latter presented for comparison at a higher mass scale. S_3 ($\overline{S_3}$) corresponds to the lowest scale for its given set of mass ratios.

In Fig. 5.1, we provide the temperature evolution of the absolute magnitude of the lepton asymmetry number densities, $|n_{\alpha\alpha}|, \alpha = e, \mu, \tau$ typical to each scenario. In particular, with this plot we justify our numerical choice to take the final value of $z \geq 100$ as n_{B-L} has long-since stopped appreciably evolving by this point. We solve the density matrix equations assuming a vanishing initial abundance of N_1.

Parameter space of S_1

The plots in Fig. 5.4 show two-dimensional projections of the eleven-dimensional posterior corresponding to S_1[4]. The dark (light) blue contours correspond to the regions of parameter space consistent with 68% (95%) confidence levels. In addition to the two-dimensional posterior plots we provide the best-fit point for each heavy Majorana neutrino mass spectrum scenario as shown in Table 5.1 where the upper (lower) three rows of the table correspond to normal (inverted) ordering.

We allow the PMNS matrix parameters to vary within a 3σ range of their best-fit value: $\delta \in [0, 360]^\circ$, $\theta_{23} \in [38.6, 52.5]^\circ$ and $\alpha_{21}, \alpha_{31} \in [0, 720]^\circ$. For the two-dimensional posterior plots of scenario S_1 shown in Fig. 5.4, the 1σ region favours larger values of the CP-violating Dirac phase: $120 \leq \delta(^\circ) \leq 360$. The likelihood function is more sensitive to α_{21} than α_{31}: from Fig. 5.4, we observe $80 \leq \alpha_{21}(^\circ) \leq 270$ while $65 \leq \alpha_{31}(^\circ) \leq 720$ is consistent with the measured baryon asymmetry to a 1σ level. Although θ_{23} may take most values within its 3σ range, the likelihood function prefers values near to 45° and in the upper octant. The values of the

[4]As each individual plot of the triangle plots is relatively small, we provide the following link to view each individually: `https://gitlab.dur.scotgrid.ac.uk/leptogenesis-public/thermal/wikis/home`

lightest neutrino mass tend to be close to the upper limit, which for normal ordering is $m_1 \simeq 0.332$ eV. The strong dependence of η_B on the lightest neutrino mass agrees with work which investigated two-flavoured thermal leptogenesis [203].

The likelihood function is somewhat insensitive to the values of x_1 and x_3 (hence their exclusion from the posterior plots[5]) but highly sensitive to x_2 with preferred values of approximately 90°. The complex components of the R-matrix are likely to be within a small range: $y_1 \simeq 180°$, $y_2 \simeq 3°$ and $y_3 \simeq 180°$ where the explanation for this structure has been given in Section 5.5. The mass of the decaying heavy Majorana neutrino is relatively small and so it might be expected that large phases of the PMNS and R-matrix are needed to compensate by keeping the Yukawa couplings sufficiently large.

Parameter space of S_2 and S_3

The parameter plots for larger M_1 and the more hierarchical heavy Majorana neutrino spectra of S_2 and S_3 are shown in Fig. 5.6 and Fig. 5.8 respectively. Unsurprisingly, on comparison of scenario S_1 and S_2 (which share the same mass splitting but different absolute scales) we observe the scenario with the larger heavy Majorana neutrino masses has a larger viable region of the model parameter space. Moreover, the constraints on the R- and PMNS-matrix parameters in scenario S_2 are weaker yet qualitatively similar to S_1. In particular, the m_1-dependence in S_2 is less severe than in the scenario of S_1. For example in Fig. 5.4 the 2σ allowed region for the lightest neutrino mass is $0.125 \leq m_1(\text{eV}) \leq 0.332$ while for Fig. 5.6, $0.0316 \leq m_1(\text{eV}) \leq 0.332$. For smaller values of m_1, successful leptogenesis is possible for larger values of the heavy Majorana neutrino mass M_1. For larger heavy Majorana neutrino mass splittings, we anticipate a reduction of the viable parameter space because the CP asymmetry is increasingly suppressed for larger mass splittings. This is confirmed upon comparison of Fig. 5.6 and Fig. 5.8 where the former has milder mass splitting.

[5] Although they are included in the plots found by following the aforementioned link.

Finally, note that in contrast to S_1, in the case of both S_2 and S_3, the likelihood function prefers values of θ_{23} close to 45° and in the lower octant.

Parameter space of $\overline{S_1}$

The triangle plot showing the two-dimensional posterior distributions of the 11-dimensional model parameter space for $\overline{S_1}$ is shown in Fig. 5.5. The dark (light) red contours correspond to the regions of parameter space consistent with 68% (95%) confidence levels. As anticipated, the points of the model space consistent with the measurement are different from the normal ordering case and the volume of parameter space consistent with the measured $\eta_{B_{\rm CMB}}$ is less constrained. In particular we observe that the likelihood function is relatively insensitive to changes of δ, α_{31} and θ_{23}. This scenario displays a similar feature to S_1, where the likelihood function favours values of $\alpha_{21} \leq 360°$.

Additionally, the likelihood has a flat direction in the x_1 and x_3 parameters of the R-matrix (as discussed in Section 5.5). We observe that all values of x_1 and x_3 are consistent to a 2σ level with the measured η_B but that, again, the likelihood is very sensitive to x_2 with $x_2 \simeq 90°$. Similarly, to the normal ordering scenario the imaginary phases of R are constrained with $y_1 \simeq 180°$, $y_2 \simeq 2°$ and $y_3 \simeq 180°$.

Parameter space of $\overline{S_2}$ and $\overline{S_3}$

The triangle plots for larger values of M_1 and the more hierarchical spectra of $\overline{S_2}$ and $\overline{S_3}$ are shown in Fig. 5.7 and Fig. 5.9 respectively. As seen in the case of normal ordering, the scenario with the slightly more hierarchical mass spectrum ($M_2 = 5\,M_1$, $M_3 = 5\,M_2$) has a slightly smaller volume of parameter space consistent with the data than the case of the milder hierarchy.

The fine-tuning of the scenarios

Although we allow for the possibility there exists a certain level of cancellation between the tree- and one-loop level contributions to the light neutrino masses, we avoid regions of the parameter space where the perturbative series no longer converges. We present the fine-tuning measure defined in Eq. (5.2.1) for the regions of the model parameter space within 1σ of the measured η_B. To be explicit, the top (bottom) three plots of Fig. 5.2 shows the distribution of the fine-tuning measure within the 1σ region of S_1, S_2 and S_3 ($\overline{S_1}$, $\overline{S_2}$ and $\overline{S_3}$) shown in Fig. 5.4, Fig. 5.6 and Fig. 5.8 (Fig. 5.5, Fig. 5.7 and Fig. 5.9) respectively. Moreover increasing the spread from 1σ to 5σ would allow for a broader spread of fine-tuning values, both smaller and larger.

In general, for normal ordering, the fine-tuning measure for points within 1σ is $\mathcal{O}(100)$ with minimal fine-tuning value in S_1 of $\mathcal{F} \approx 330$. Somewhat unsurprisingly, the scenario with the larger mass of decaying heavy Majorana neutrino, S_2, has smaller fine-tuning due to the fact the complex phases of the R-matrix may attain a broader range of values, and the minimum value of $\mathcal{F} \approx 180$. However, in the case of S_3 (where the decaying heavy Majorana neutrino mass is the same as S_2 the mass splitting between the heavy Majorana neutrinos is larger) the fine-tuning values are in general larger due to the increased mass of N_3.

The fine-tuning present in the case of inverted ordering is, in general, less than in the case of normal ordering, with minimum value in $\overline{S_1}$ of $\mathcal{F} \simeq 100$. Again, the same pattern emerges as in the case of normal ordering where the fine-tuning in $\overline{S_2}$ ($\overline{S_3}$) is less (greater) than $\overline{S_1}$. In fact, for $\overline{S_2}$ the minimum $\mathcal{F} \approx 40$. Again, we emphasise the fine-tuning we present here is for points $\mathbf{p}$ within 1σ of the best fit value of $\eta_{B_{\rm CMB}}$ and allowing for an increase in the spread around the best fit value would allow for smaller (and larger) values of fine-tuning.

Tree- and loop-dominated scenarios

At such scales, $T \ll 10^9$ GeV, it is impossible to have successful leptogenesis without some degree of cancellation between the tree- and one-loop-level contributions. However, we did investigate if there existed regions of parameter space such that thermal leptogenesis was viable (within 1σ of the central value of $\eta_{B_{\rm CMB}}$) where either the tree- or one-loop-level contribution dominates. In the latter scenario, where the radiative corrections dominate over the tree-level contributions, the fine-tuning measure should be close to unity as $|m_\nu^1|/|(m_\nu^0 + m_\nu^1)| \approx 1$ for $m_\nu^0 \ll m_\nu^1$. We applied the same numerical procedure to solve the density matrix equations with one decaying heavy Majorana neutrino and vetoed points $\mathbf{p}$ if the fine-tuning measure was not within $0.9 \leq \mathcal{F} \leq 1.1$. After scanning a series of differing heavy Majorana neutrino mass spectra, we found the loop-dominated scenario was possible, assuming normal ordering, for $M_1 = 10^9$ GeV with $M_2 = 3.15M_1$ and $M_3 = 3.15M_2$. The best-fit point is denoted as $S_{m_\nu^1}$ in Table 5.1 and the triangle plot of the two-dimensional posterior distributions may be found on the provided webpage. In the former scenario, where the tree-level contributions dominates, the fine-tuning measure will be close to zero. Using MULTINEST to search for regions of $\mathbf{p}$ consistent with tree-domination we required the fine-tuning to be within $0 \leq \mathcal{F} \leq 0.2$. We found no solutions compatible with this condition for $M_1 < 10^9$ GeV. However, we did find a single single point consistent with a fine-tuning $\mathcal{F} \approx 0.18$ for a mass spectrum of $M_1 = 10^9$ GeV, $M_2 \approx 3.15M_1$ and $M_3 \approx 3.15M_2$. Note that a two-dimensional projection of the posterior is not possible and we simply provide the value of this point as $S_{m_\nu^0}$ in Table 5.1. For larger values of M_1 more points will exist that satisfy the condition and so we regard $S_{m_\nu^0}$ as the solution of lowest M_1 in which the tree-level is the dominant contribution. The absolute values of the Yukawa matrix elements are listed, for reference, for all scenarios in Appendix G.2.

We note that it is possible to reduce the fine-tuning by considering the scenario where $M_2 = M_3$. Such a scenario may result from the introduction of a partial symmetry

into the type-I seesaw. In this section, we are considering the approximation that only N_1 decays so this does not lead to resonant leptogenesis. As an example, consider S_1 but with $M_2 = M_3 \approx 5.05 \times 10^6$ GeV. A point **p** satisfying this leads to $\eta_B = 6.1 \times 10^{-10}$, which is in good agreement with the experimental value. In this case, N_2 and N_3 act as two Majorana components of a pseudo-Dirac pair. The contribution of N_2 and N_3 to the tree-level mass is cancelled (as together they are lepton number conserving) and a dramatic reduction in our fine-tuning measure occurs, resulting in $\mathcal{F} \approx 2.1$. This is similar to the scenarios considered in [187] and will not be further discussed in this paper.

In summary, foregoing fine-tuning of the light neutrino masses $\gtrsim \mathcal{O}(10)$, it is possible to lower the scale of non-resonant thermal leptogenesis to $T \sim 10^6$ GeV with a mildly hierarchical heavy Majorana neutrino mass spectrum. At such intermediate scales, interactions mediated by the SM charged lepton Yukawa couplings are greater than the Hubble rate. We have properly accounted for such effects as we calculated the lepton asymmetry from three-flavoured density matrix equations. In the case of normally ordered light neutrinos, larger values of the δ are favoured in conjunction with an atmospheric mixing angle close to $\theta_{23} = 45^\circ$ (slightly above or below depending on the scenario, see Table 5.1). We observe that larger masses of m_1 are favoured as this compensates for decreasing M_1. In the scenario of an inverted ordered mass spectrum, the likelihood function shows little sensitivity to changes in the low-energy neutrino parameters. On the other hand, the R-matrix is comparatively highly constrained. In addition, we present the distribution of the fine-tuning measure within 1σ of the measured η_B and found the fine-tuning was in general smaller for inverted ordering than it was for normal ordering and usually took values $\sim \mathcal{O}(100)$. We find that the minimum observed value of the fine-tuning measure in the vicinity of the best-fit is $\mathcal{F} \sim$40. However, *at* the most likely point, $\mathcal{F}$ assumes values $\sim \mathcal{O}(100)$.

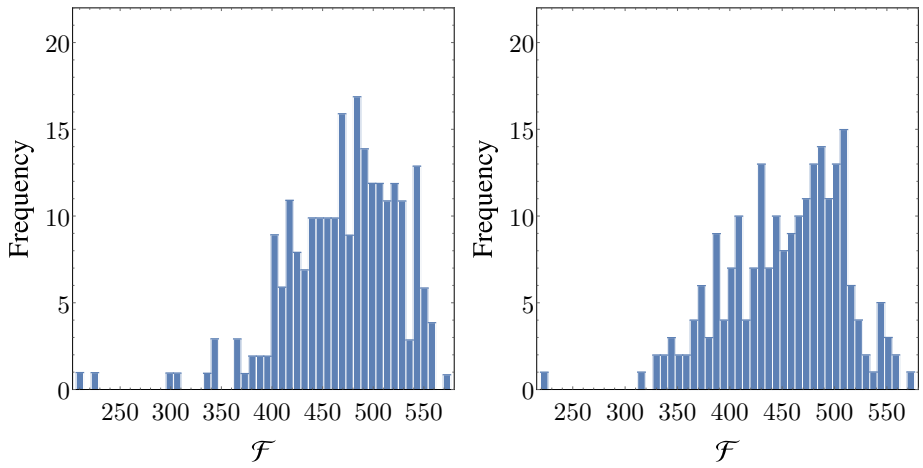

Figure 5.3: The left and right plots show the fine-tuning for regions of the model parameter space within 1σ of the measured η_B for S_4 and $\overline{S_4}$ respectively.

	θ_{23} (°)	δ (°)	α_{21} (°)	α_{31} (°)	x_1 (°)	y_1 (°)	x_2 (°)	y_2 (°)	x_3 (°)	y_3 (°)	$m_{1(3)}$ (eV)	M_1 (GeV)	M_2 (GeV)	M_3 (GeV)
S_4	47.85	105.65	133.40	367.99	−99.50	178.77	94.22	0.12	−9.59	172.53	0.208	$10^{6.7}$	$10^{7.5}$	$10^{8.1}$
$\overline{S_4}$	44.11	243.0	347.54	437.04	14.94	167.76	90.79	1.42	132.12	178.29	0.0084	$10^{6.7}$	$10^{7.5}$	$10^{8.1}$

Table 5.2: The best-fit points for the leptogenesis scenarios in Figs 5.10-5.11 are given and are all consistent with $\eta_B = (6.10 \pm 0.04) \times 10^{-10}$, $\theta_{13} = 8.52°$ and $\theta_{12} = 33.63°$. The upper (lower) row is the best-fit points for normal (inverted) ordering.

5.4.2 Results from N_2 Decays

In this section, we explore the possibility that the decay of two heavy Majorana neutrinos contributes to the baryon asymmetry. In this setup, the density matrix equations follow rather straightforwardly from Eq. (3.3.19) and the numerical procedure to find the two-dimensional posterior plots is the same as discussed in Section 5.4.1. The qualitative difference between this case and the former as discussed in Section 5.3 is that now N_2 may decay in addition to N_1. As $M_2 > M_1$, N_2 will decay before N_1 with the average time between the two decays determined by the hierarchy of their masses.

In [204] the authors explored thermal leptogenesis using the decay of two heavy Majorana neutrinos in the limit the third is decoupled from the theory. Using analytic estimates, they found the minimal mass of the lightest heavy Majorana neutrino, for

successful leptogenesis, to be $M_1 \sim 1.3 \times 10^{11}$ GeV assuming a mildly hierarchical mass spectrum. In this scenario, we explored a number of heavy Majorana neutrino mass scenarios and found the lowest mass of N_1 which allowed for successful leptogenesis was $M_1 = 10^{6.7}$ GeV with $M_2 \approx 6.3M_1$ and $M_3 \approx 4M_2$. We denote these two scenarios as S_4 and $\overline{S_4}$ for normal and inverted ordering respectively and the best-fit point and corresponding triangle plots are shown in Fig. 5.10 and Fig. 5.11. These results should be considered as more reliable than those of the previous section as they produced under the same set of approximations except the neglect of N_2 decays.

Naively, one would think that the decay of two heavy Majorana neutrinos would further lower the scale of leptogenesis as both may contribute to the final asymmetry. However, this is not the case as there may be cancellations between the contributions of N_1 and N_2. We note that contribution of the third heavy Majorana neutrino to the lepton asymmetry in these scenarios is negligible as the CP-asymmetry $\epsilon^{(3)}_{\alpha\beta}$ is several orders of magnitude lower than that of the other two and its washout term W_3 decays far faster.

Unlike in the previous section, we find the two-dimensional posterior projections in this case for both orderings do not appear to be too dissimilar. In both cases, the likelihood function is insensitive to δ. In addition, the atmospheric mixing angle can be in the lower or upper octant and there is strong dependence on large values of m_1 (m_3) in S_4 ($\overline{S_4}$). The dependence of the likelihood on the R-matrix parameters is similar to the cases discussed in Section 5.4.1; we find x_1 and x_3 may take any values while $x_2 \simeq 90°$. Likewise, two of the imaginary components of the R-matrix are constrained to be large $y_1, y_3 \simeq 180°$ while the other is nearly vanishing $y_2 \simeq 2.5°$. For reference, the corresponding absolute value Yukawa matrices are given in Section G.2. In a similar fashion to Section 5.4.1, we present the fine-tuning measure for the regions of the model parameter space within 1σ of the measured η_B. We observe for normal and inverted ordering the fine-tuning $\sim \mathcal{O}(100)$.

5.5 Discussion of Fine-tuned Results

We may gain an understanding of why fine-tuned solutions were found by the numerical machinery through inspection of the structure of the Yukawa matrix at the best-fit points. Looking at the solutions for one and two decaying heavy Majorana neutrino scenarios, we observe that generically $|y_1| \approx 180°$, $y_2 \approx 0°$, $|y_3| \approx 180°$ and $|x_2| \approx 90°$. Consider as a typical example S_1, for which the orthogonal R-matrix assumes the following form

$$R \approx \begin{pmatrix} -\frac{i}{2}e^{y_3}\cos x_2 & \frac{1}{2}e^{y_3}\cos x_2 & \sin x_2 \\ \frac{i}{2}e^{y_1+y_3} & -\frac{1}{2}e^{y_1+y_3} & \frac{1}{2}e^{y_1}\cos x_2 \\ \frac{1}{2}e^{y_1+y_3} & \frac{i}{2}e^{y_1+y_3} & -\frac{i}{2}e^{y_1}\cos x_2 \end{pmatrix},$$

which has the structure

$$R \approx \begin{pmatrix} R_{11} & R_{12} & R_{13} \\ -iR_{22} & R_{22} & R_{23} \\ -R_{22} & -iR_{22} & -iR_{23} \end{pmatrix}. \tag{5.5.1}$$

The appearance of y_1 and y_3 in the exponentials, and the proximity of x_2 to 90°, result in $|R_{13}| \sim 1$, $|R_{1i}| \ll |R_{22}|$ and $|R_{i3}| \ll |R_{22}|$.

In the case of the asymmetries $\epsilon^{(1)}_{\alpha\alpha}$, generated in the N_1 decays, and for the best-fit values of the parameters listed in Table 5.1, the leading term in the expansion of the function $f_1(x_j/x_1)$ in powers of $x_j/x_1 = M_1^2/M_j^2 \ll 1$, $j = 2, 3$, as can be shown, gives a sub-dominant contribution. The dominant contribution is generated by the next-to-leading term in the expansion of $f_1(x_j/x_1)$ as well as by the leading term in the expansion of the self-energy function $f_2(x_j/x_1)$ in powers of $x_j/x_1 = M_1^2/M_j^2 \ll 1$. Under the approximation $m_1 = m_2$, the part of the asymmetry proportional to f_1 (which we call $\epsilon^{(1)}_{\alpha\alpha}(f_1)$) is

$$\begin{aligned}\epsilon^{(1)}_{\alpha\alpha}(f_1) =& \frac{3}{16\pi\left(Y^\dagger Y\right)_{11}}\frac{M_1^2}{v^4}\frac{5}{9}\frac{M_1^2}{M_2^2}\Big(m_1^2|U_{\alpha1}+iU_{\alpha2}|^2\Im\left[\left(R_{11}^*R_{21}\right)^2\right] \\ &+m_1\sqrt{m_1m_3}\Im\left[R_{11}^*R_{21}^2U_{l3}^*R_{13}^*\left(U_{\alpha1}+iU_{\alpha2}\right)\right]\Big).\end{aligned}$$

and

$$\epsilon^{(1)}_{\alpha\alpha}(f_2) = \frac{3}{16\pi\,(Y^\dagger Y)_{11}}\frac{M_1^2}{v^4}\frac{2}{3}m_1^{\frac{3}{2}}\sqrt{m_3}|R_{21}|^2\left(\sum_{j=2,3}\frac{M_1}{M_j}\right)\Im\left[R_{11}R^*_{13}U^*_{l3}\left(U_{\alpha1}+iU_{\alpha2}\right)\right].$$

Numerical estimates at the best-fit values of Table 5.1 show that this second contribution (the resonance function contribution) is somewhat larger than the first one, although the baryon asymmetry in the cases studied by us is produced in the non-resonance regime.

In the density matrix equations, the CP-asymmetry parameters enter in the combinations

$$\epsilon^{(1)}_{\alpha\alpha}(f_1) + \epsilon^{(1)}_{\alpha\alpha}(f_2),$$

for $\alpha = e, \mu, \tau$ in the three-flavour regime.

Thus, although for our best-fit scenarios $\epsilon^{(1)}_{ee}(f_2) + \epsilon^{(1)}_{\mu\mu}(f_2) + \epsilon^{(1)}_{\tau\tau}(f_2)$ may be zero, this does not mean that the $\epsilon^{(1)}_{\alpha\alpha}(f_2)$ give a negligible contribution in the generation of the lepton (baryon) asymmetry.

We note that there is a factor $(Y^\dagger Y)^{-1}_{11}$ in the diagonal CP-asymmetries $\epsilon^{(1)}_{\alpha\alpha}$ (Eq. (3.3.20)) for the lightest heavy Majorana neutrino and a factor $(Y^\dagger Y)_{11}$ (Eq. (3.3.17)) appears in the washout term W_1. Thus, we naively expect that in order achieve successful leptogenesis, by reducing the washout, $(Y^\dagger Y)_{11}$ should be made small. Expanding this quantity, in terms of the R-matrix elements and the remaining CI parameters, we find

$$\left(Y^\dagger Y\right)_{11} = \frac{M_1}{v^2}\left(m_1|R_{11}|^2 + m_2|R_{12}|^2 + m_3|R_{13}|^2\right).$$

Thus, with the assumption that this quantity should be small, the relative smallness of the elements R_{1i} is explained and with it the values of x_2 and y_2.

Similarly, given the dependence on $|R_{21}|$ in $\epsilon^{(1)}_{\alpha\alpha}(f_2)$, it may be expected that we should maximise the values of y_1 and y_3. With these imaginary parts of ω_1 and ω_3 large, the values of the corresponding real parts x_1 and x_3 is immaterial. This is reflected in the relative flatness of their directions in the parameter space plots. The

dependence on m_1 in $(Y^\dagger Y)_{11}$ may initially lead one to expect m_1 to be minimised. That this is not the case is due to the factors m_1^2 or $m_1^{3/2}\sqrt{m_3}$ appearing in the expressions for $\epsilon^{(1)}_{\alpha\alpha}$. In order to maximise these CP-asymmetries, one would expect m_1 to be found at its largest allowed value (determined by the constraint on the sum of the neutrino masses).

Let us now examine how these choices of parameters affect the expressions for the tree- and one-loop light neutrino masses. We may estimate the light masses using the largest value of the Yukawa matrix ($\sim 10^{-2}$ in the case of S_1, see Appendix G.2) and the smallest heavy mass $M_1 = 10^6$ GeV:

$$m_\nu^0 \sim v^2 \frac{Y^2}{M_1} \sim \mathcal{O}\left(10^{-6}\text{ GeV}\right).$$

This mass is too large from the point of view of the experimental bound and yet the numerical machinery is enforcing neutrino masses which sum to < 1 eV. Let us investigate why this estimate fails. This structure of the R-matrix leads to the following structure for the Dirac mass matrix:

$$m_D\sqrt{f} = \begin{pmatrix} \delta_1, & u, & -iu + \delta_2 \end{pmatrix},$$

in which $|\delta_2| \ll |\delta_1| \ll |u|$ where each of δ_1, δ_2 and u are 3-component complex vectors. We may rewrite the tree- and one-loop masses in terms of this relatively simple matrix $m_D\sqrt{f}$

$$m_\nu^0 = \left(m_D\sqrt{f}\right) M^{-1} f^{-1} \left(m_D\sqrt{f}\right)^T,$$

where the commutativity of the diagonal matrices M and f has been exploited. For the one-loop contribution we find

$$m_\nu^1 = \left(m_D\sqrt{f}\right) \left(f - M^{-1}\right) f^{-1} \left(m_D\sqrt{f}\right)^T.$$

This ensures that their sum is

$$\begin{aligned} m_\nu &= m_D\sqrt{f}\left(m_D\sqrt{f}\right)^T \\ &= \delta_1\delta_1^T + u\delta_2^T + \delta_2 u^T + \delta_2\delta_2^T. \end{aligned}$$

Due to the relative smallness of the elements of δ_i, the light neutrino mass matrix may be considerably smaller than would be expected from a naive estimate based on the size of u. Neglecting terms containing a δ_i, we find that

$$m_\nu^0 = -m_\nu^1.$$

This is the mechanism by which the fine-tuned mass matrices are arrived at.

Although in this analysis, the results of S_1 were used, the other solutions differ essentially only in the sign used for y_i. This introduces a different pattern of minus signs in the matrix of Eq. 5.5.1 (and hence also in the expression for $m_D\sqrt{f}$) which does not affect the overall argument. Note that this argument is true even for the solutions of the two-decaying heavy Majorana neutrinos equations.

5.6 Summary and Conclusions

In this work we have explored the viable model parameter space of thermal leptogenesis associated with a type-I seesaw mechanism. To do so, we numerically solved the three-flavoured density matrix equations [110] for one and two-decaying heavy Majorana neutrinos. Of the eighteen dimensional model parameter space, seven parameters were fixed from neutrino oscillation data, cosmological constraints and consideration of a mildly hierarchical heavy Majorana neutrino mass spectrum.

To find the regions of parameter space consistent with the measured baryon-to-photon ratio we used pyMultiNest which implements a nested sampling algorithm to calculate Bayesian posterior distributions which are utilised to find regions of confidence. In addition, we ensured the Yukawa matrix entries respected perturbativity

and we protected against resonance effects by assuming a mildly hierarchical heavy Majorana neutrino mass spectrum. In the case of one decaying heavy Majorana neutrino, we found the lightest heavy Majorana neutrino mass that could successfully generate the baryon asymmetry, with our choice of upper bound on R-matrix components, to be $M_1 \simeq 10^6$ GeV. This is possible as regions of the parameter space which have levels of fine-tuning in the light neutrino mass matrix $> \mathcal{O}(10)$ were explored. In conjunction, eleven parameters were allowed to vary thus compensating for the smaller heavy Majorana neutrino masses. Moreover, with normal ordering, maximally CP-violating values of δ and θ_{23} close to 45° (in most cases slightly larger than 45°, see Table 5.1) is preferred. In addition, there was strong dependence on the mass of the lightest neutrino. On the other hand, we found in the case of inverted ordering there were no strong constraints on low energy neutrino parameters. For this scenario, the level of fine-tuning was $\sim \mathcal{O}(100)$. In the case of one decaying heavy Majorana neutrino, we found the scenario with the smallest fine-tuning, at intermediate scales, was $\overline{S_2}$, ($\mathcal{F} \sim 40$) with a heavy Majorana neutrino spectrum $M_1 = 10^{6.5}$ GeV, $M_2 \approx 3.15 M_1$ and $M_3 \approx 3.15 M_2$. We showed also that fine tuning would not be necessary at all if $M_2 = M_3$, when the one loop contribution to the light Majorana neutrino mass matrix is strongly suppressed. We also explored the possibility that either the tree or one-loop radiative corrections dominate the neutrino mass matrix. We found the lowest scale possible for this scenario, assuming a mildly hierarchical spectrum, was $M_1 = 10^9$ GeV. As discussed, a motivation for exploring leptogenesis at intermediate scales is to avoid large corrections to the Higgs mass. Although, we found regions of the parameter space of three-flavoured thermal leptogenesis consistent with the observed baryon asymmetry, we did not seek to minimise Δm_H^2 and relegate this to a future study.

Finally, we investigated the case of two decaying heavy Majorana neutrinos. We found the lowest scale for both normal and inverted ordering to be $M_1 = 10^{6.7}$ GeV. This scale is higher than in the one decaying heavy Majorana neutrino case because the scale of the washout is larger for N_2 and its CP-asymmetry is small in comparison

with N_1. Although the washout for N_2 decays much more quickly than for N_1, it still has an appreciable effect on the final lepton asymmetry and so one must raise the scale of the heavy Majorana neutrino masses to achieve successful leptogenesis. We did not include spectator effects which could potentially further lower the scale of thermal leptogenesis and may be investigated in future work.

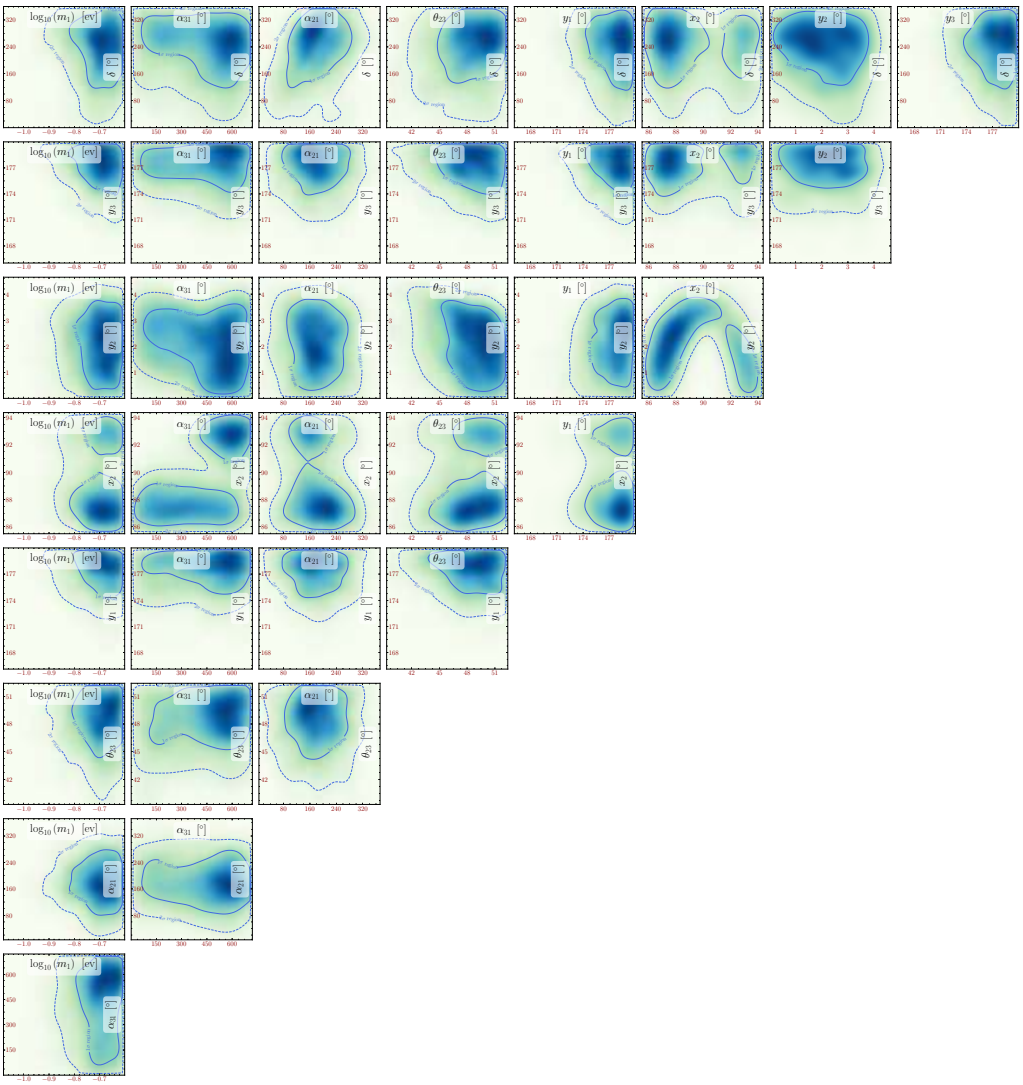

Figure 5.4: S_1: Triangle plot showing the two-dimensional projection of the 11-dimensional model parameter space for posterior distributions using normal ordering with one-decaying heavy Majorana neutrino and heavy Majorana neutrino mass spectrum: $M_1 = 10^6$ GeV, $M_2 = 3.15\,M_1$, $M_3 = 3.15\,M_2$. The contours correspond to 68% and 95% confidence levels respectively.

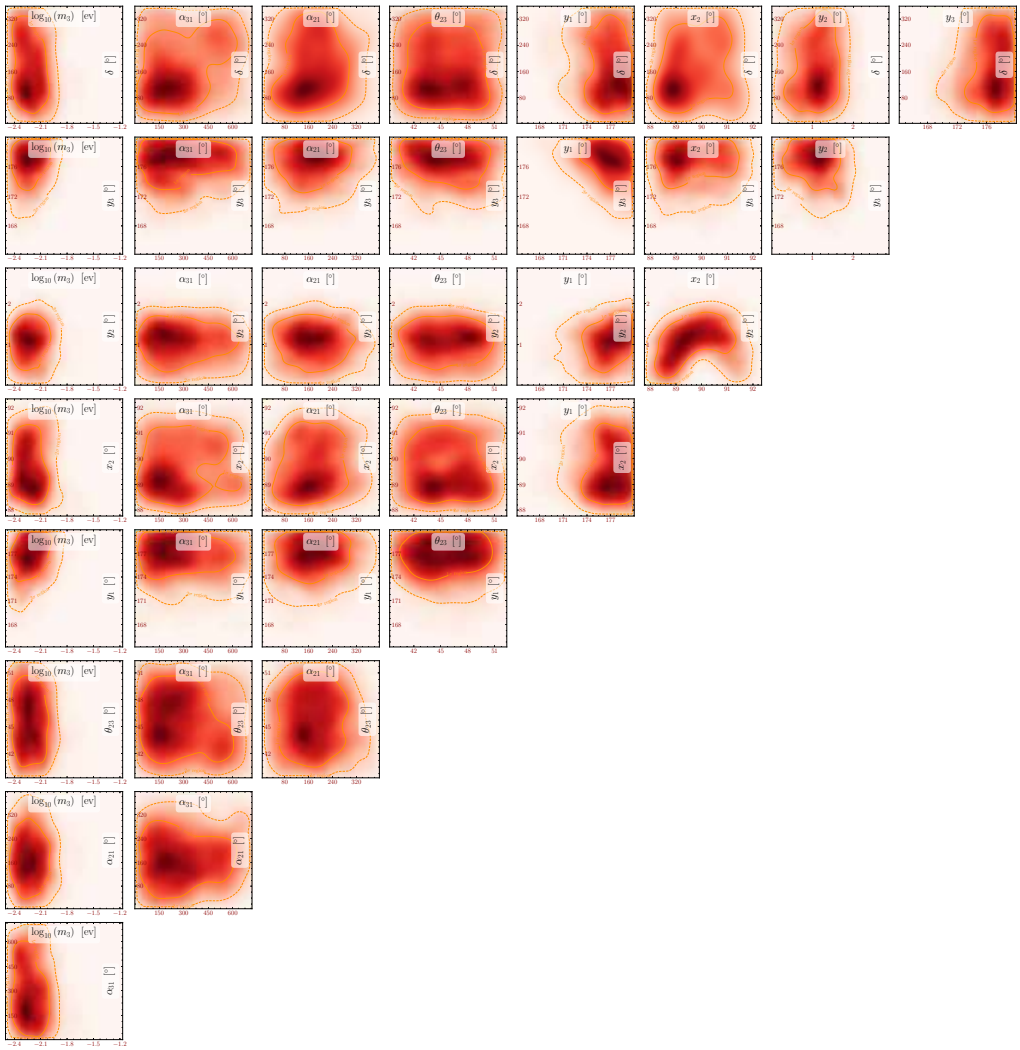

Figure 5.5: $\overline{S_1}$: Triangle plot showing the two-dimensional projection of the 11-dimensional model parameter space for posterior distributions using inverted ordering and with one-decaying heavy Majorana neutrino mass spectrum: $M_1 = 10^6$ GeV, $M_2 = 3.15\,M_1$, $M_3 = 3.15\,M_2$. The contours correspond to 68% and 95% confidence levels respectively.

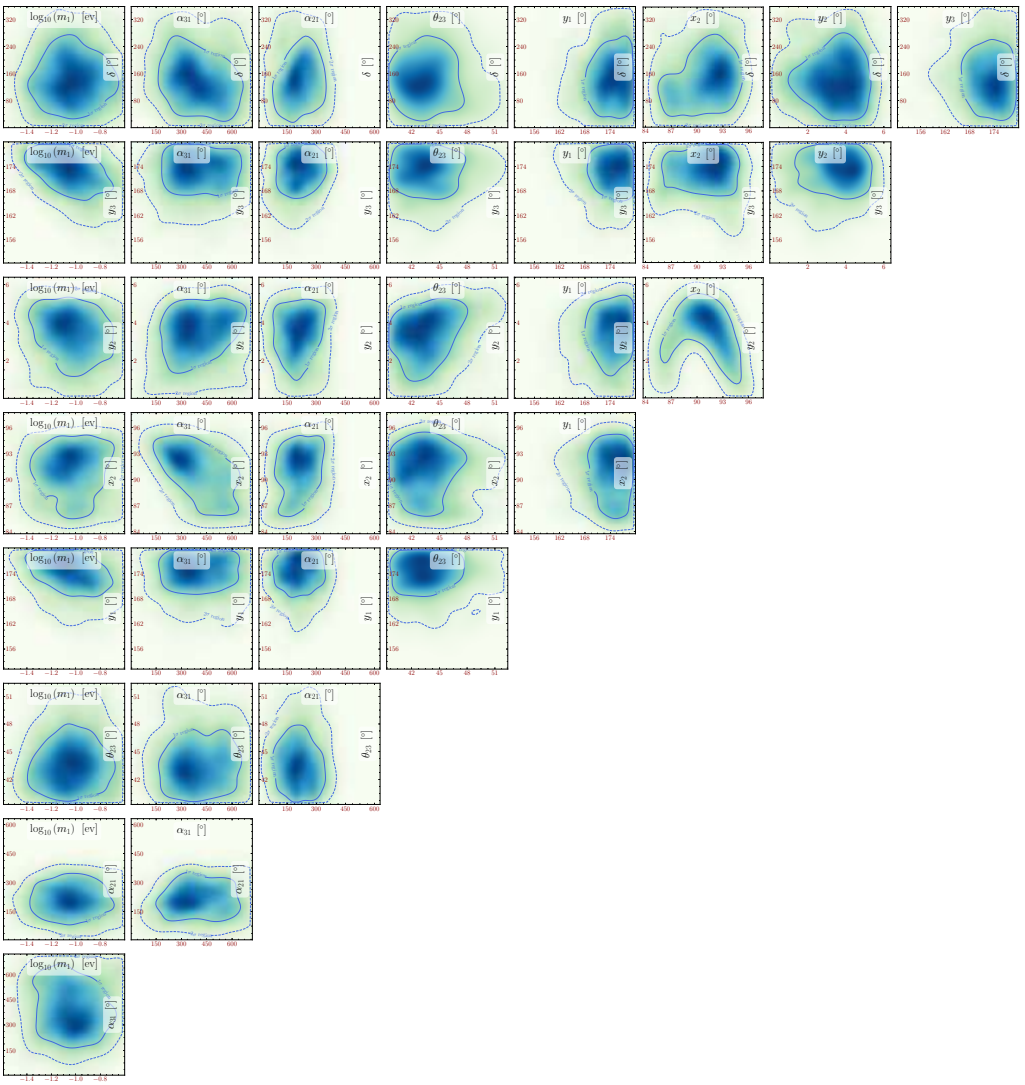

Figure 5.6: S_2: Triangle plot showing the two-dimensional projection of the 11-dimensional model parameter space for posterior distributions using normal ordering with one-decaying heavy Majorana neutrino and heavy Majorana neutrino mass spectrum: $M_1 = 10^{6.5}$ GeV, $M_2 = 3.15\,M_1$, $M_3 = 3.15\,M_2$. The contours correspond to 68% and 95% confidence levels respectively.

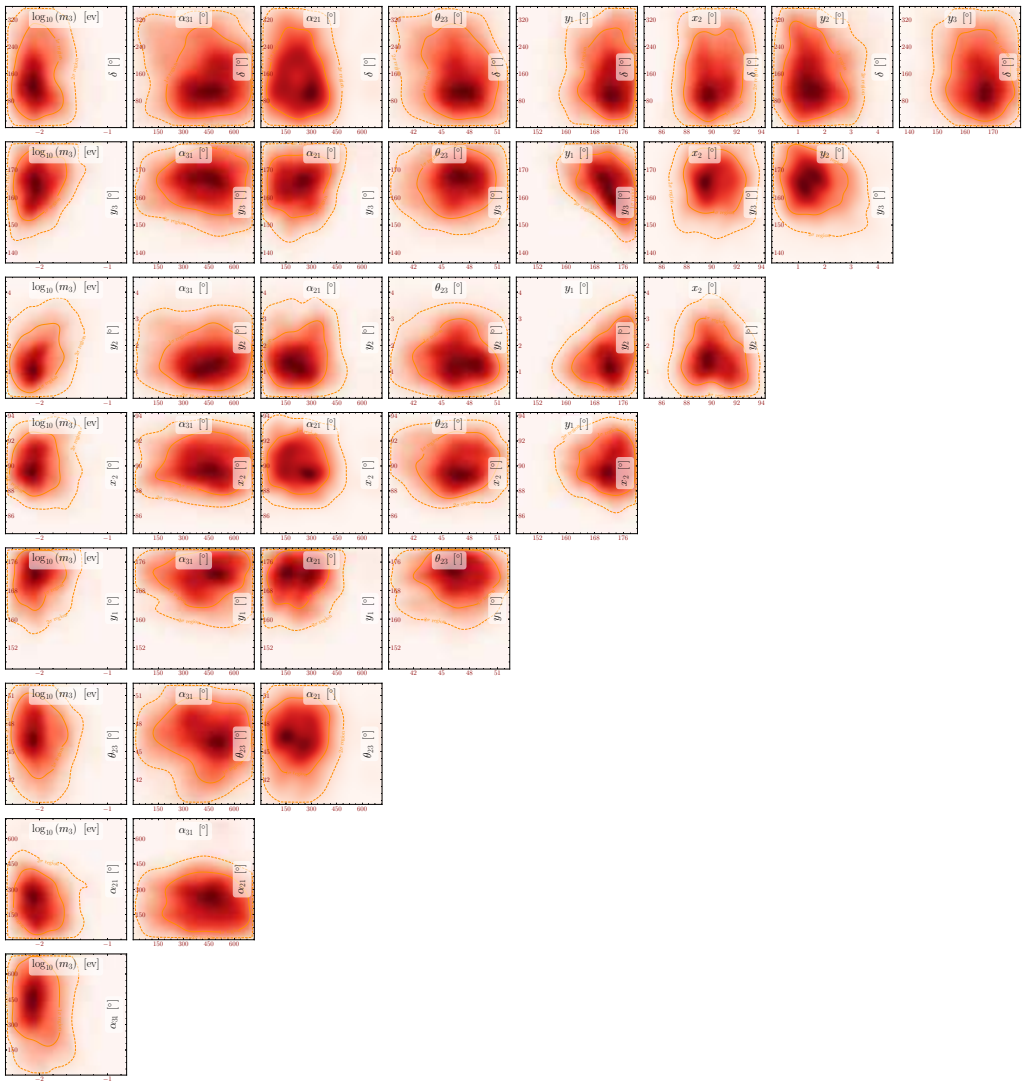

Figure 5.7: $\overline{S_2}$: Triangle plot showing the two-dimensional projection of the 11-dimensional model parameter space for posterior distributions using inverted ordering with one-decaying heavy Majorana neutrino and heavy Majorana neutrino mass spectrum: $M_1 = 10^{6.5}$ GeV, $M_2 = 3.15\, M_1$, $M_3 = 3.15\, M_2$. The contours correspond to 68% and 95% confidence levels respectively.

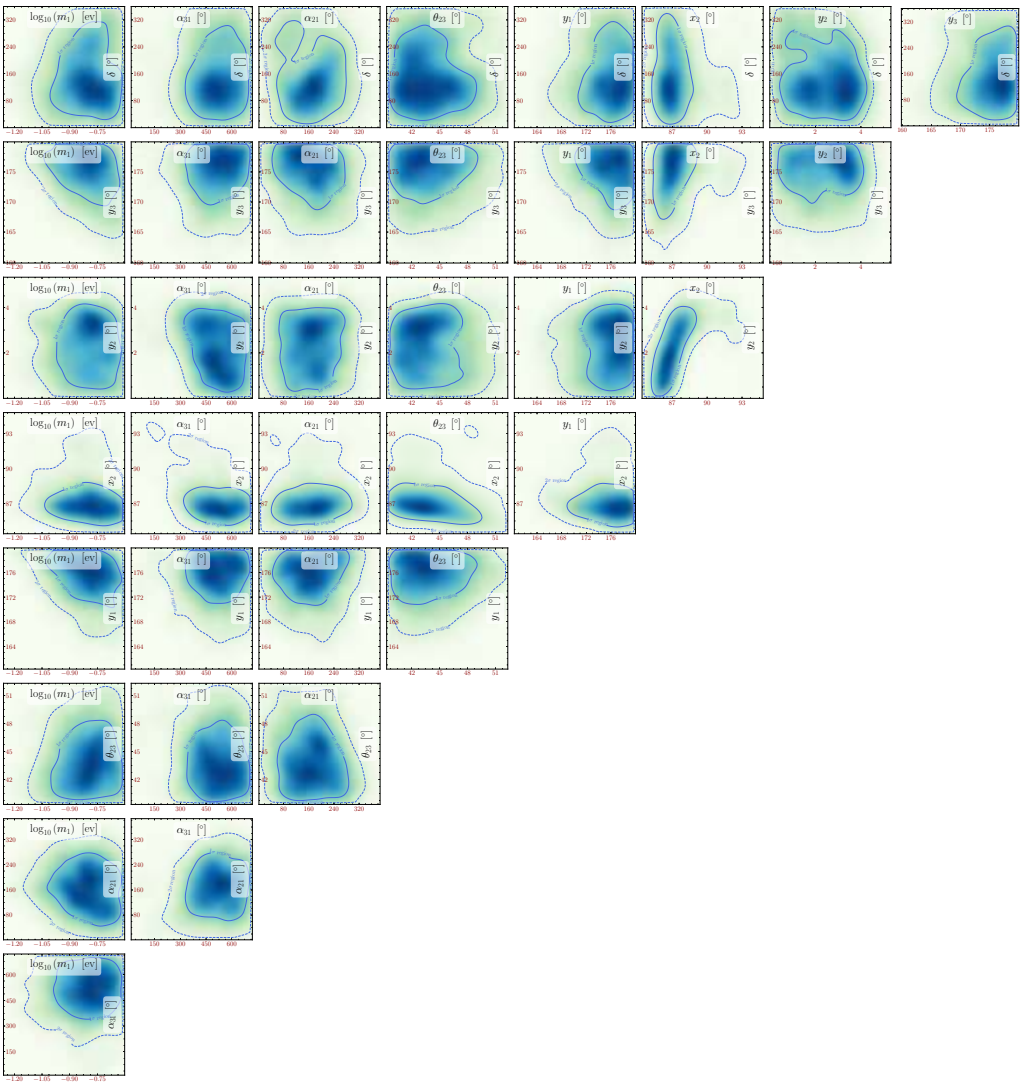

Figure 5.8: S_3: Triangle plot showing the two-dimensional projection of the 11-dimensional model parameter space for posterior distributions using normal ordering with one-decaying heavy Majorana neutrino and heavy Majorana neutrino mass spectrum: $M_1 = 10^{6.5}$ GeV, $M_2 = 5\,M_1$, $M_3 = 5\,M_2$. The contours correspond to 68% and 95% confidence levels respectively.

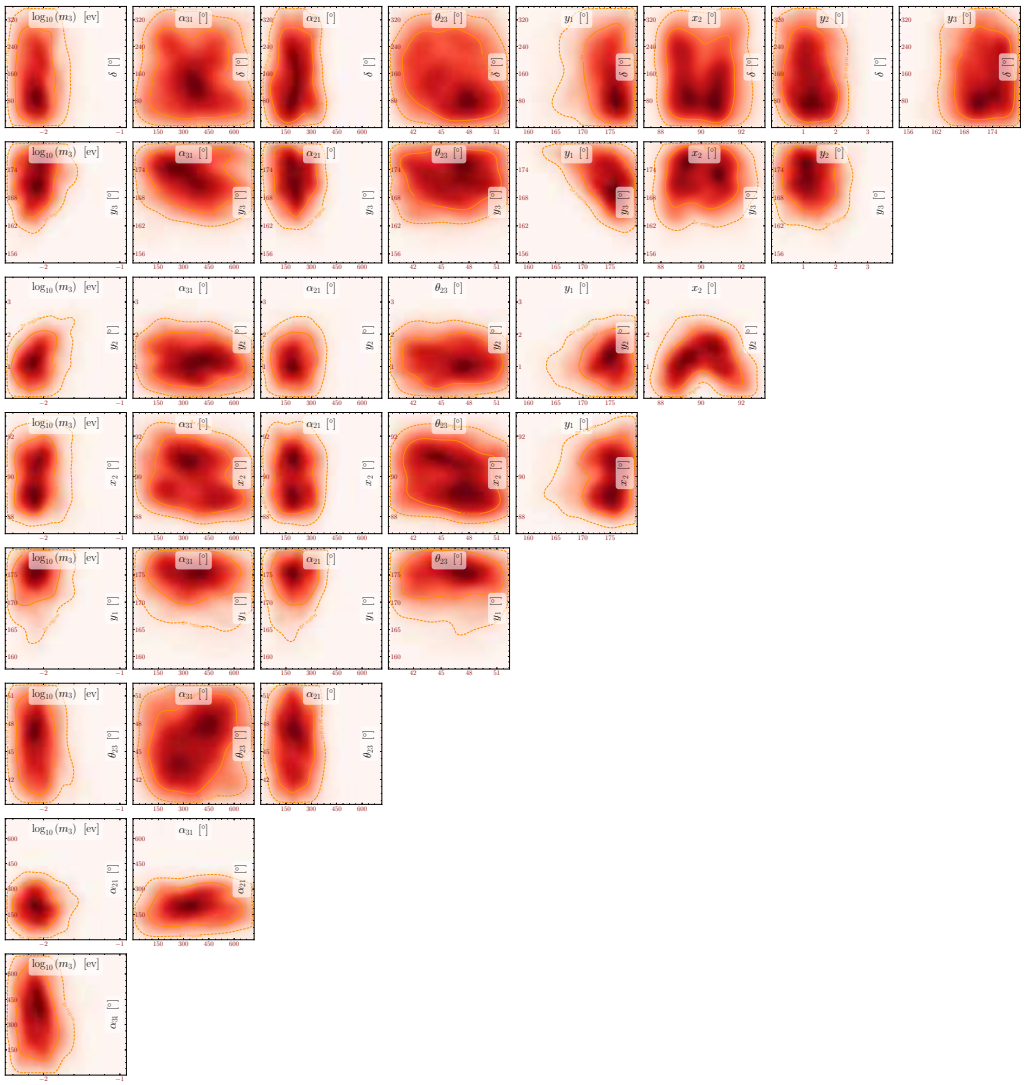

Figure 5.9: $\overline{S_3}$: Triangle plot showing the two-dimensional projection of the 11-dimensional model parameter space for posterior distributions using inverted ordering with one-decaying heavy Majorana neutrino and heavy Majorana neutrino mass spectrum: $M_1 = 10^{6.5}$ GeV, $M_2 = 5\,M_1$, $M_3 = 5\,M_2$. The contours correspond to 68% and 95% confidence levels respectively.

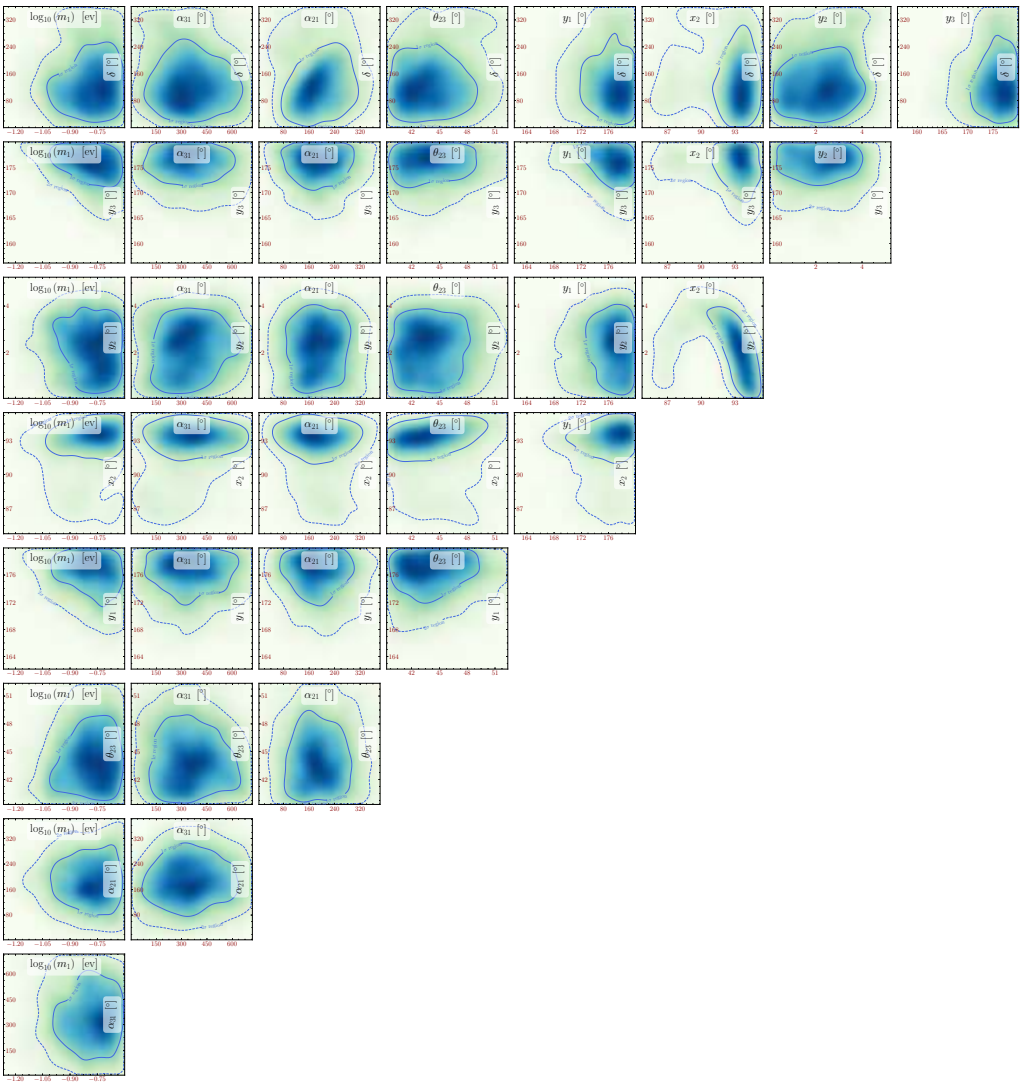

Figure 5.10: S_4: Triangle plot showing the two-dimensional projection of the 11-dimensional model parameter space for posterior distributions using normal ordering, with two-decaying steriles neutrinos and mass spectrum: $M_1 = 10^{6.7}$ GeV, $M_2 = 5.0\,M_1$, $M_3 = 5.0\,M_2$. The contours correspond to 68% and 95% confidence levels respectively.

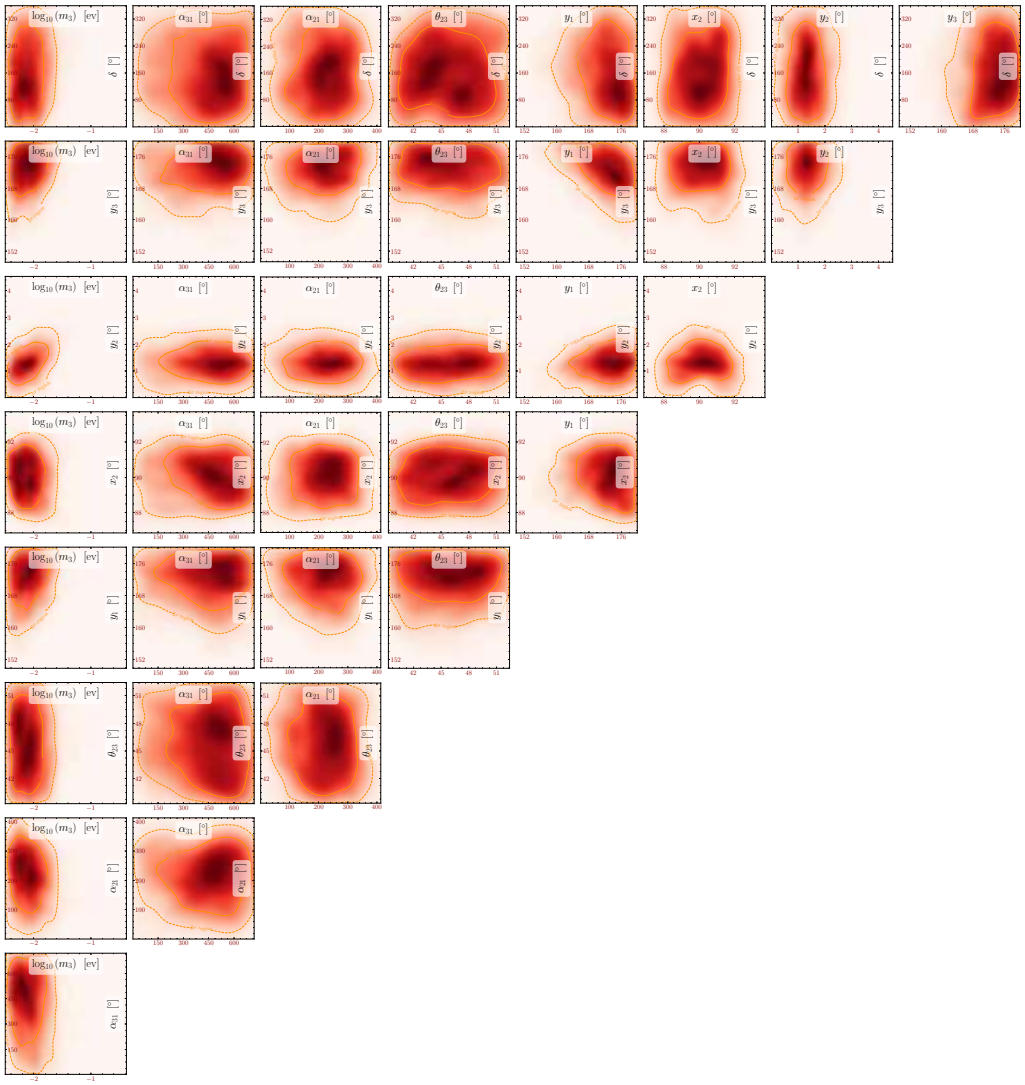

Figure 5.11: $\overline{S_4}$: Triangle plot showing the two-dimensional projection of the 11-dimensional model parameter space for posterior distributions using inverted ordering, with two-decaying steriles and mass spectrum: $M_1 = 10^{6.7}$ GeV, $M_2 = 5.0\, M_1$, $M_3 = 5.0\, M_2$. The contours correspond to 68% and 95% confidence levels respectively.

Chapter 6

Leptogenesis from low-energy CP violation

CP violation is a necessary feature of any theory explaining the creation of a matter-antimatter asymmetry. In thermal leptogenesis, the CP asymmetry comes from the heavy Majorana neutrinos whose decay rates Γ and $\overline{\Gamma}$ are not equal. The source of this CP violation in the Lagrangian is the complex phases of the neutrino Yukawa matrix. Recalling the Casas-Ibarra parametrisation of the Yukawa matrix (Eq. (2.4.21) or Eq. (2.4.24)), we can label two distinct sources of CP violation: the *low-energy CP violating phases* of the PMNS matrix and the *high-scale CP violation* from the R-matrix. In this chapter, we explore the possibility of viable leptogenesis when the CP violation comes only from the low-energy phases.

6.1 Flavour effects and low-energy CP violation

If leptogenesis occurs at high scales, where the temperature $T \gg 10^{12}$ GeV, then it is usually a justifiable approximation to neglect the flavour effects (see Eq. (3.3.19) and the following discussion). A basis may be chosen in which essentially only one flavour of lepton ever appears in the theoretical description. Consequently, it was expected that the low-energy CP-violating phases contained in the neutrino mixing

matrix play no physical role in the production of the lepton and therefore baryon asymmetry [142, 205].

If leptogenesis occurs at temperatures somewhat below 10^{12} GeV (10^{9} GeV), the Yukawa interactions of the tau charged lepton (of the muon) come into thermal equilibrium, causing decoherence between this and the remaining flavour components of the charged lepton state [117, 118, 123, 206, 207] such that two (three) lepton flavour states must be separately considered and the CP-violating phases of the PMNS matrix have physical significance. Historically, the possibility that the CP violation in leptogenesis may be strictly due to Dirac and/or Majorana phases of the PMNS matrix was first apparent in this regime [129–131, 135, 208–211] (for a review see, e.g., [212]).

There have been other works which have investigated the impact of low energy phases on the BAU. Indeed, CP conservation at the high-scale and CP violation at the low-scale in the context of leptogenesis can be theoretically motivated by minimal flavour violation [213, 214], flavour symmetries [215–217] or a generalised CP symmetry [218–220]. Beyond the type I seesaw mechanism, there have been other studies which connect the Dirac phase, δ, with the BAU using an extended Higgs sector [221].

The primary focus of this chapter is to answer the question: *at what scales can low-energy CP-violating phases produce the observed BAU?* We shall show that the scale of successful leptogenesis in the case of interest may indeed vary across many orders of magnitude from $10^{6} - 10^{13}$ GeV, even significantly beyond 10^{12} GeV where it had been previously believed that the low-energy CP violating phases played no role. The observation of low-scale leptonic Dirac CP violation, in combination with the positive determination of the Majorana nature of the massive neutrinos, would make more plausible, but will not be a proof of, the existence of high-scale thermal leptogenesis. These discoveries would indicate that thermal leptogenesis *could* produce the BAU with the requisite CP violation provided by the Dirac CP-violating phase in the neutrino mixing matrix.

6.2 C and CP properties of Majorana neutrinos

As we focus on the possibility that low-scale CP phases are responsible for the BAU, we will investigate the C and CP properties of neutrinos in order to determine the structure of the R-matrices which lead to high-scale CP symmetry. In the type I seesaw, the light (ν_i) and the heavy (N_i) neutrino mass states are both Majorana in nature and thus satisfy the following conditions:

$$\begin{aligned} C\overline{\nu}_i^T &= \nu_i, \\ C\overline{N}_i^T &= N_i, \end{aligned} \tag{6.2.1}$$

where C denotes the charge conjugation matrix.

Following [131], we express the CP-conjugated neutrino fields in terms of the CP operator U_{CP} as

$$\begin{aligned} U_{CP} N_i(x) U_{CP}^\dagger &= i\rho_i^N \gamma_0 N_i(x'), \\ U_{CP} \nu_i(x) U_{CP}^\dagger &= i\rho_i^\nu \gamma_0 \nu_i(x'), \end{aligned} \tag{6.2.2}$$

where x' is the parity-transformed coordinate and $i\rho_i^N = \pm i$ and $i\rho_i^\nu = \pm i$ are the CP parities of the respective Majorana fields. The conditions for CP invariance impose the following restrictions on the elements of the matrix of neutrino Yukawa couplings (setting the unphysical phases in the CP transformations of the lepton and Higgs doublets to 1 and i respectively) is given by,

$$Y_{\alpha i}^* = Y_{\alpha i}\rho_i^N, \tag{6.2.3}$$

and on the elements of the PMNS matrix [222]:

$$U_{\alpha j}^* = U_{\alpha j}\rho_j^\nu, \ j \in \{1,2,3\}, \ \alpha \in \{e,\mu,\tau\}. \tag{6.2.4}$$

From the parametrisation of the Yukawa matrix of Eq. (2.4.24), this imposes the following conditions on the elements of the R-matrix [131]:

$$R_{ij}^* = R_{ij}\rho_i^N\rho_j^\nu, \quad i,j \in \{1,2,3\}. \tag{6.2.5}$$

The leptogenesis scenarios considered in this chapter have CP violation provided

only by the phases of the PMNS matrix. This corresponds to imposing the condition of Eq. (6.2.5) onto the R-matrix but not the condition Eq. (6.2.4) on U. In these scenarios the values of the Dirac and Majorana phases of the PMNS matrix determine the success of leptogenesis. One should bear in mind, however, that there are certain intuitively unexpected possibilities for CP violation in (non-resonant) leptogenesis even when the PMNS- and R-matrices are CP-conserving, i.e., conditions Eq. (6.2.4) and Eq. (6.2.5) are individually fulfilled and the elements $U_{\alpha j}$ and R_{jk} are real or purely imaginary [131].[1]

CP violation due to the Dirac phase δ can only be practically investigated in neutrino oscillation experiments. There has been a slight statistical preference from the existing data for maximally CP-violating $\delta \sim 270°$. This hint has been obtained from the combination of results from long-baseline experiments such as T2K [223] and NOνA [224] with reactor experiments like Daya-Bay [225], RENO [226] and Double-Chooz [227]. In principle, the difference in oscillation probabilities [228–230],

$$A_{CP}^{\alpha,\beta} \equiv P(\nu_\alpha \to \nu_\beta) - P(\overline{\nu}_\alpha \to \overline{\nu}_\beta) \quad (\alpha \neq \beta), \tag{6.2.6}$$

is a measure of CP violation in neutrino oscillations in vacuum and can be measured experimentally. For vacuum oscillations in the three-neutrino case we have [231]

$$A_{CP}^{e,\mu} = 4 J_{CP} F_{\rm osc}^{\rm vac}, \tag{6.2.7}$$

$$F_{\rm osc}^{\rm vac} \equiv \sin\left(\frac{\Delta m_{21}^2}{2E}\mathcal{D}\right) + \sin\left(\frac{\Delta m_{32}^2}{2E}\mathcal{D}\right) + \sin\left(\frac{\Delta m_{13}^2}{2E}\mathcal{D}\right), \tag{6.2.8}$$

$$J_{CP} \equiv \Im\left[U_{e1} U_{\mu 2} U_{e2}^* U_{\mu 1}^*\right]. \tag{6.2.9}$$

J_{CP} is the analogue of the Jarlskog invariant for the lepton sector, which gives a parametrisation-independent measure of CP violation in neutrino oscillations, $\mathcal{D}$ is the distance travelled by the neutrinos and E the neutrino energy. In the case

[1] This unusual possibility is realised when ρ_i^N and ρ_j^ν are fixed by conditions Eq. (6.2.3) and Eq. (6.2.4), but the product of the so fixed values of ρ_i^N and ρ_j^ν differs from the value of $\rho_i^N \rho_j^\nu$ in (Eq. (6.2.5)) [131]. Under these conditions the low energy PMNS matrix U and the high-scale R-matrix are individually CP-conserving, but the interplay between the two in leptogenesis is CP-violating.

of CP-invariance we have $\delta = 0, 180^\circ$ and therefore $J_{CP} = 0$. By measuring, for example, $A_{CP}^{e,\mu}$, one can determine J_{CP} which has the following expression in the standard parametrisation of the PMNS matrix:

$$J_{CP} = \frac{1}{4} \sin 2\theta_{12} \sin 2\theta_{23} \cos^2 \theta_{13} \sin \theta_{13} \sin \delta \,. \tag{6.2.10}$$

The best-fit value and 1σ uncertainty of J_{CP} reported in [202] are

$$J_{CP}^{\max} = 0.0329 \pm 0.0007 \, (\pm 1\sigma). \tag{6.2.11}$$

In the longer term, the next generation of neutrino oscillation experiments such as DUNE [232] and T2HK [233], will be able to measure the Dirac CP-violating phase δ with greater precision and determine whether CP-symmetry is indeed violated in the lepton sector.

As explained in Section 2.2, information on CP-violating Majorana phases can, in principle, be obtained in neutrinoless double beta decay experiments [234–236] (see, however, also [237]). These experiments are the most sensitive probes of the possible Majorana nature of massive neutrinos. They can also provide information on the neutrino mass ordering [238] (see also [236]). The rate of neutrinoless double beta decay is given by (see, e.g., [40])

$$\frac{\Gamma_{0\nu\beta\beta}}{\log 2} = \frac{G_{01}}{m_e^2} |\mathcal{A}|^2, \tag{6.2.12}$$

where G_{01} is a kinematic factor and $\mathcal{A}$ denotes the amplitude which has the following form

$$\mathcal{A} \propto \sum_{i=1}^{3} m_i U_{ei}^2 \mathcal{M}^{0\nu\beta\beta}(m_i) + \sum_{i=1}^{3} M_i V_{ei}^2 \mathcal{M}^{0\nu\beta\beta}(M_i). \tag{6.2.13}$$

The amplitude is dependent on the nuclear matrix elements $\mathcal{M}^{0\nu\beta\beta}$ for which $\mathcal{M}^{0\nu\beta\beta}(m_i) \approx \mathcal{M}^{0\nu\beta\beta}(0) \gg \mathcal{M}^{0\nu\beta\beta}(M_i)$ if $M_i \gg 10^3$ MeV (see, e.g., [40, 42]), which shall always be the case in this work. The mixing elements V_{ei} for the heavy states are $\mathcal{O}\left(m_D/M\right)$ and thus the second term of Eq. (6.2.13) is $\mathcal{O}(m_D^2/M)\mathcal{M}^{0\nu\beta\beta}(M_i)$ $\sim \mathcal{O}(m_i)\mathcal{M}^{0\nu\beta\beta}(M_i)$. As $U_{ei} \sim \mathcal{O}(1)$, the second term is negligible in comparison

with the first and we find [239] (see e.g., [222]):

$$A \propto \langle m_\nu \rangle \equiv m_1 U_{e1}^2 + m_2 |U_{e2}|^2 e^{i\alpha_{21}} + m_3 |U_{e3}|^2 e^{i(\alpha_{31} - 2\delta)}, \tag{6.2.14}$$

where $\langle m_\nu \rangle$ is the neutrinoless double beta decay effective Majorana mass in the case of 3-neutrino mixing. In the case of CP-invariance we have $\alpha_{21} = k\pi$, $\alpha_{31} = q\pi$, $k, q = 0, 1, 2, \ldots$ [240–242].[2] The most stringent upper bound on $|\langle m_\nu \rangle|$ was reported by the KamLAND-Zen collaboration [41] searching for neutrinoless double beta decay of ^{136}Xe:

$$|\langle m_\nu \rangle| < [0.061, 0.165] \text{ eV}, \tag{6.2.15}$$

where the uncertainty in the knowledge of the nuclear matrix element of ^{136}Xe decay have been accounted for. In terms of the half-lives for neutrinoless double beta decay the best lower limits are: for germanium-76, tellurium-130, and xenon-136: $T_{1/2}^{0\nu} > 8.0 \times 10^{25}$ yr (reported by the GERDA-II collaboration), $T_{1/2}^{0\nu} > 1.5 \times 10^{25}$ yr (from the combined results of the Cuoricino, CUORE-0, and CUORE experiments), and $T_{1/2}^{0\nu} > 1.07 \times 10^{26}$ yr (from the KamLAND-Zen collaboration), with all limits given at the 90% CL. Most importantly, a large number of new experiments aim at sensitivities of $|\langle m_\nu \rangle| \sim [0.01, 0.05]$ eV (see, e.g., [42, 43]): CUORE (^{130}Te), SNO+ (^{130}Te), GERDA (^{76}Ge), MAJORANA (^{76}Ge), LEGEND (^{76}Ge), SuperNEMO (^{82}Se, ^{150}Nd), KamLAND-Zen (^{136}Xe), EXO and nEXO (^{136}Xe), PANDAX-III (^{136}Xe), NEXT (^{136}Xe), AMoRE (^{100}Mo), MOON (^{100}Mo), CANDLES (^{48}Ca), XMASS (^{136}Xe), DCBA (^{82}Se, ^{150}Nd), ZICOS (^{96}Zr), etc. The GERDA-II and KamLAND-Zen experiments have already provided the best lower limits on the double beta decay half-lives of ^{76}Ge and ^{136}Xe. The experiments listed above aim to probe the ranges of predictions of $|\langle m_\nu \rangle|$ corresponding to neutrino mass spectra of quasi-degenerate type and with inverted ordering (see, e.g., [44]).

[2] Thus, in order for a value of $\alpha_{21(31)}$ to be CP-violating both $\sin \alpha_{21(31)}/2$ and $\cos \alpha_{21(31)}/2$ at this value should be different from zero.

6.2.1 CP-conserving R-matrix and the structure of the light neutrino mass matrix

If the orthogonal matrix R is allowed to have large elements, then the scale of leptogenesis may be lowered to $M_1 \sim 10^6$ GeV [5, 192, 243]. In such scenarios, care must be taken with the radiative corrections to the light neutrino masses which may grow large (and non-negligible) with the elements of the R-matrix. One can either impose a near-lepton-number-symmetry to prevent this (see [243]), or more generically, incorporate the one-loop contribution to the light neutrino masses (in the manner we have discussed in previous chapters) and remain agnostic about fine-tuned cancellations between the tree-level and one-loop contributions. We proceed with this approach following the attitude taken in Chapter 5 which is based on [5], in which the figure $M_1 \sim 10^6$ GeV was first demonstrated.

As discussed in Chapter 5, when there is a fine-tuned cancellation, the R-matrix takes the form

$$R \approx \begin{pmatrix} R_{11} & R_{12} & R_{13} \\ \pm iR_{22} & R_{22} & R_{23} \\ -R_{22} & \pm iR_{22} & \pm iR_{23} \end{pmatrix}, \tag{6.2.16}$$

$|R_{22}| \gg |R_{1i}|, |R_{23}|$ for $i \in \{1, 2, 3\}$. The cancellation of large tree-level and large one-loop light neutrino mass matrices occurs as a result of relations between the magnitudes and phases of the R-matrix elements which lead to the following structure for the Dirac mass matrix:

$$m_D\sqrt{f} = \begin{pmatrix} \Delta, & u, & \pm iu \end{pmatrix}, \tag{6.2.17}$$

with

$$\Delta = U\left(\sqrt{m_1}R_{11}, \sqrt{m_2}R_{12}, \sqrt{m_3}R_{13}\right)^T$$

and

$$u = U\left(\pm i\sqrt{m_1}R_{22}, \sqrt{m_2}R_{22}, \sqrt{m_3}R_{23}\right)^T,$$

such that $|\Delta_i| \ll |u_j|$, $i, j \in \{1, 2, 3\}$. We may rewrite the tree and one-loop masses

in terms of this relatively simple matrix $m_D\sqrt{f}$, such that

$$m_\nu^0 = \left(m_D\sqrt{f}\right) M^{-1} f^{-1} \left(m_D\sqrt{f}\right)^T, \tag{6.2.18}$$

where the commutativity of the diagonal matrices $\hat{m}_R$ and f has been exploited and

$$m_\nu^1 = \left(m_D\sqrt{f}\right) \left(f - M^{-1}\right) f^{-1} \left(m_D\sqrt{f}\right)^T. \tag{6.2.19}$$

This ensures that the sum of the tree-level and one-loop masses is

$$\begin{aligned} m_\nu &= m_D\sqrt{f} \left(m_D\sqrt{f}\right)^T \\ &= \Delta\Delta^T. \end{aligned} \tag{6.2.20}$$

Due to the relative smallness of the elements of Δ, the matrix m_ν may be considerably smaller than m_ν^0. Immediately, we have

$$m_\nu^0 = -m_\nu^1 + \mathcal{O}(\Delta^2), \tag{6.2.21}$$

which is an explicit expression of the fine-tuned cancellation. As in Chapter 5, we use $\mathcal{F}$ defined as

$$\mathcal{F} \equiv \frac{\sum_{i=1}^3 \hat{m}_{\nu ii}^1}{\sum_{i=1}^3 \hat{m}_{\nu ii}}, \tag{6.2.22}$$

to quantify this fine-tuning.

As the R-matrix structure of Eq. (7.3.1) is required for successful leptogenesis at intermediate scales, we are tasked with finding the R-matrices which assume this form and obey the CP-invariance conditions of Eq. (6.2.5). We intend to translate the conditions in Eq. (7.3.1) and Eq. (6.2.5) into constraints on x_i and y_i. However, we know *a priori* from the work of [5] that one must have $y_2 \sim 0°$ and $y_1 \gtrsim 180°$, $y_3 \gtrsim 180°$ to produce the relative magnitudes of the elements of R in Eq. (7.3.1), crucial to the successful production of the observed baryon asymmetry.

We begin with the elements

$$R_{22} = \cos w_1 \cos w_3 - \sin w_1 \sin w_2 \sin w_3, \tag{6.2.23}$$

and

$$R_{31} = -\cos w_1 \cos w_3 \sin w_2 + \sin w_1 \sin w_3, \tag{6.2.24}$$

which result from the expansion of the R-matrix parametrised as in Eq. (2.4.23). The condition of Eq. (7.3.1) that $R_{22} \approx -R_{31}$ implies that $\sin w_2 \approx 1$, which in turn imposes $\sin x_2 \approx 1$ and $y_2 \approx 0°$. In order to simplify future expressions, we promote the condition on y_2 to the exact equality $y_2 = 0°$. With conditions on x_2 and y_2 determined, we now examine

$$R_{13} = \cos x_2 \left(\cos x_1 \cosh y_1 - i \sin x_1 \sinh y_1\right). \tag{6.2.25}$$

According to the condition Eq. (6.2.5), R_{13} (like all the elements of R) must be purely real or imaginary and thus we should choose one of, $\cos x_1 = 0$ or $\sin x_1 = 0$. We exclude the possibility of $y_1 = 0$ for the reason given above. Likewise, consider

$$R_{11} = \cos x_2 \left(\cos x_3 \cosh y_3 - i \sin x_3 \sinh y_3\right), \tag{6.2.26}$$

and select $\cos x_3 = 0$ or $\sin x_3 = 0$ by the same reasoning.

In summary, we have the following set of constraints

$$\begin{aligned} \cos x_2 \approx 0 \text{ and } y_2 = 0, \\ |\cos x_1| = 0 \text{ or } 1, \\ |\cos x_3| = 0 \text{ or } 1, \end{aligned} \tag{6.2.27}$$

which lead to an R-matrix of purely real and imaginary components and are therefore good candidates for CP-invariant R-matrices. We shall make use of these conditions in considerations where enhancement of the R-matrix is necessary for successful leptogenesis.

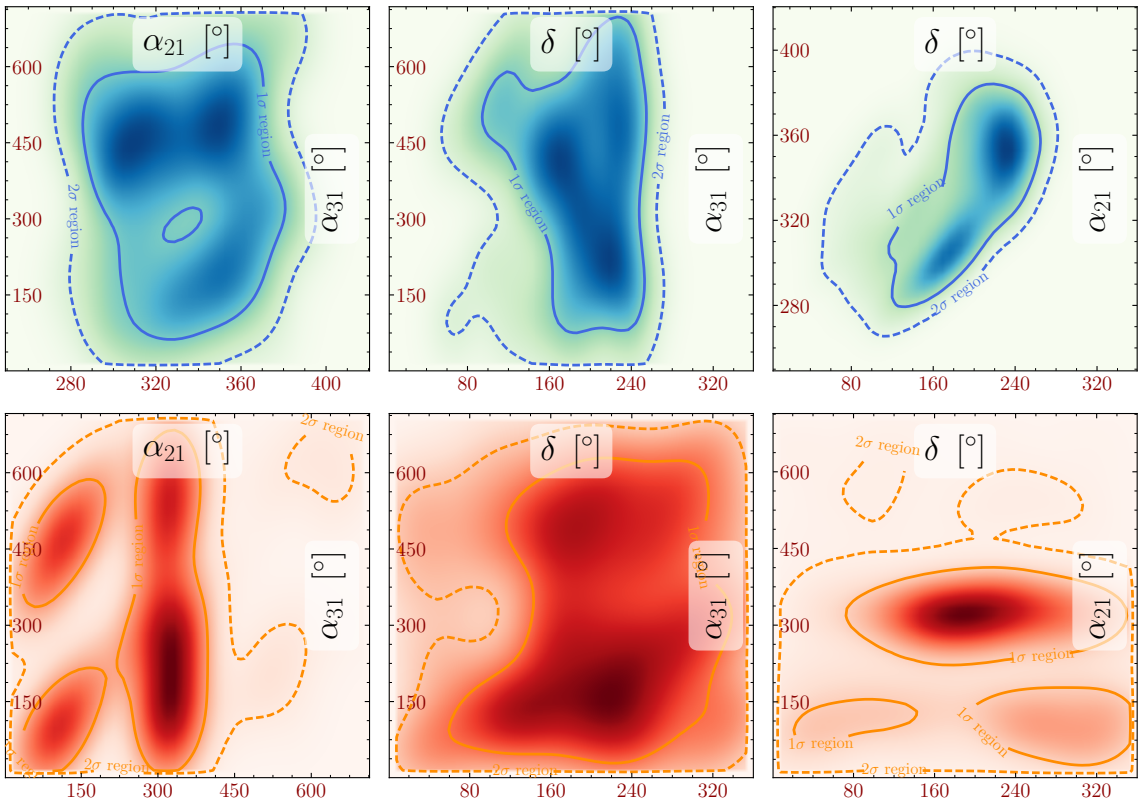

Figure 6.1: The two-dimensional projections for leptogenesis with $M_1 = 10^{10}$ GeV and CP violation provided only by the phases of the PMNS matrix. The NO case is coloured blue/green and the IO one is orange/red. The contours correspond to 68% and 95% confidence levels. This plot was created using SuperPlot [201].

6.3 Leptogenesis in the regime $10^9 < M_1$ (GeV) $< 10^{12}$

In this section, we explore the possibility that successful leptogenesis derives solely from the CP-violating PMNS phases and the mass scale is between $10^9 \leq M_1$ (GeV) $\leq 10^{12}$, which generally corresponds to the two-flavour regime. Historically, the link between low-energy CP violation and the baryon asymmetry was first established in this regime and thus our main purpose in this section is to revisit the scenario with more robust numerical methods than have previously been applied. We shall perform a comprehensive exploration of the parameter space for a model with three heavy Majorana neutrinos in both the normal ordered and inverted ordered scenarios. We shall then investigate a subset of scenarios in which only the Dirac or only the

Majorana phases are varied.

6.3.1 Results of parameter exploration

In this particular exploration of the parameter space, we fix M_1 and vary M_2 and M_3 such that $M_3 > 3M_2 > 9M_1$, ensuring that resonant regimes are avoided [116, 192, 193, 244–246]. We choose to set $M_1 = 10^{10}$ GeV, this being typical of the mass window under consideration.

We fix, $x_1 = 90°$ and $x_3 = 180°$ and $y_2 = 0°$ such that there is a complete leptonic CP-symmetry when $\delta = 0°$, $\alpha_{21} = 180°$ and $\alpha_{31} = 0°$.[3] With the specified parameters fixed or constrained as stated, we explore the parameter space using a flat prior and log-likelihood function evaluated at a point $\mathbf{p} = (\delta, \alpha_{21}, \alpha_{31}, m_{1,3}, M_2, M_3)$ (varying m_1 or m_3 for normal or inverted ordering respectively) by

$$\log L = -\frac{1}{2}\left(\frac{\eta_B^2(\mathbf{p}) - \eta_{B_{\mathrm{CMB}}}^2}{\Delta\eta_{B_{\mathrm{CMB}}}^2}\right), \tag{6.3.1}$$

to define regions of 1σ and 2σ agreement with the observed value of the asymmetry. In addition we impose a bound on the sum of neutrino masses of 1 eV which is consistent with the tritium beta-decay experiments [38, 247, 248] but more conservative than recent constraints from Planck [88]. In the numerical work of this section we allow only for the two lightest heavy Majorana neutrinos to decay (an excellent approximation) and we neglect lepton number-changing scattering processes, spectator effects [206, 249], thermal corrections [113, 250] and the inclusion of quantum statistical factors [251–254] which typically introduces an $\mathcal{O}(10\%)$ error [135, 255–257].

The results of this parameter search are shown in the form of two-dimensional projections in Fig. 6.1. For points in these regions of parameter space for which $\eta_B = \eta_{B_{\mathrm{CMB}}}$, the fine-tuning is $\mathcal{F} \approx 0.23$ which corresponds only to a very slight enhancement of the R-matrix. The values of lightest neutrino mass for NO (IO)

[3] This choice of parameters for the low-energy phases is made such that the CP-symmetry holds for the Yukawa matrix when the R-matrix is taken in to account. It would not suffice to choose, e.g., $\delta = \alpha_{21} = \alpha_{31} = 0°$.

δ (°)	α_{21} (°)	α_{31} (°)	M_1 (GeV)	M_2 (GeV)	M_3 (GeV)	x_1 (°)	x_2 (°)	x_3 (°)	y_2 (°)
228	447	570	2.82×10^{10}	1.00×10^{13}	3.16×10^{13}	90	18	180	0

Table 6.1: A benchmark point for leptogenesis with $M_1 = 2.82 \times 10^{10}$ GeV, with normal ordering. Here, we have $m_1 = 0.02$ eV and $y_1 = y_3 = -33°$, corresponding to $\mathcal{F} = 0.27$. This point produces $\eta_B = 6.1 \times 10^{-10}$.

neutrino mass spectrum corresponding to this case are $m_{1(3)} = 0.0215$ eV. For the best-fit values of the fitted parameters in the NO (IO) case we find: $\delta = 133.8°$ ($139.8°$), $\alpha_{21} = 315.5°$ ($165.3°$), $\alpha_{31} = 551.0°$ ($565.5°$), $M_2 = 4.90$ $(4.97) \times 10^{11}$ GeV, $M_3 = 2.19 \times 10^{12}$ GeV, $x_2 = 113.4°$ ($13.9°$). For the case of a NO light neutrino mass spectrum, we find that the observed baryon asymmetry may be obtained to within 1σ (2σ) with δ between $[95, 265]°$ ($[52, 282]°$). For IO, the 1σ (2σ) range is $[60, 338]°$ ($[8, 360]°$). Both of these scenarios comfortably incorporate the measured bounds on δ (Table 2.2). In what follows, we provide some explanation of these results and plots by introducing an analytical approximation which we use to study the scenarios where only the Dirac or only the Majorana phases provide CP violation.

6.3.2 Dependence of η_B on the Dirac and Majorana Phases

In the scenario $10^9 < M_1(\text{GeV}) < 10^{12}$, it is appropriate to apply the two-flavour Boltzmann equations (namely Eq. (3.3.23) with $\alpha \in \{\beta, \tau\}$). These equations have the following analytical solution [258]

$$n_{B-L} \approx \frac{\pi^2}{6 z_d K_1} n_{N_1}^{\text{eq}}(0) \left(\epsilon_{\tau\tau}^{(1)} \frac{1}{p_{1\tau}} + \epsilon_{\beta\beta}^{(1)} \frac{1}{p_{1\beta}} \right), \tag{6.3.2}$$

where it is assumed that the dominant contribution to the final asymmetry is from the lightest of the heavy Majorana neutrinos and that leptogenesis occurs in the strong washout regime. As we are interested in those scenarios in which CP violation derives only from the phases of the PMNS matrix, we have the supplementary condition

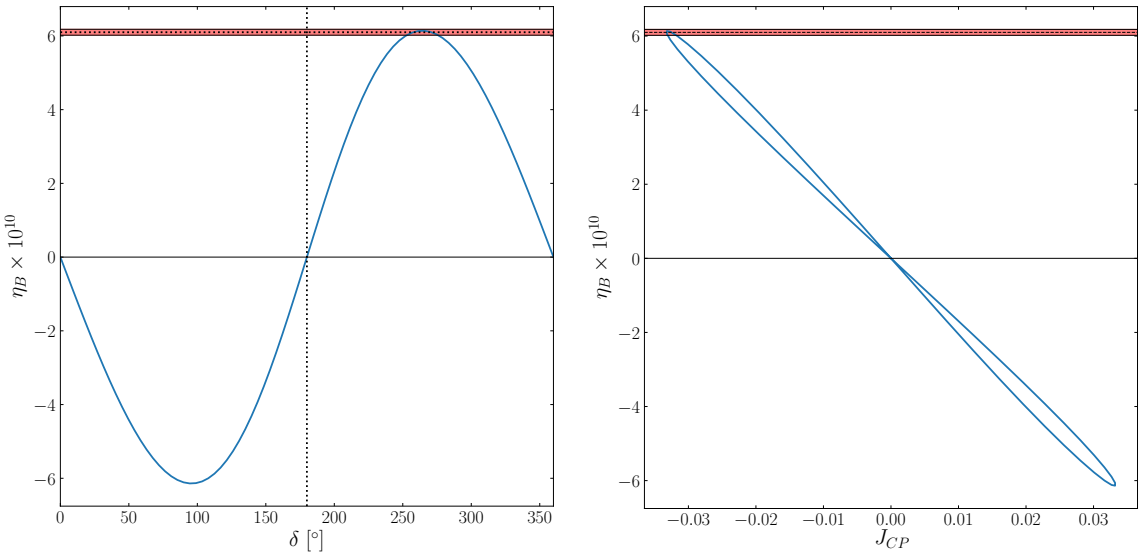

Figure 6.2: The baryon asymmetry with $M_1 = 5.13 \times 10^{10}$ GeV and CP violation provided solely by δ. The Majorana phases are fixed at $\alpha_{21} = 180°$ and $\alpha_{31} = 0°$. The red band indicates the 1σ observed values for $\eta_{B_{\mathrm{CMB}}}$ with the best-fit value indicated by the horizontal black dotted line. Left: The final baryon asymmetry as a function of δ with exact CP-invariance when $\delta = 0°$ and $180°$ (vertical black dotted line). Right: A parametric plot of η_B against J_{CP} as δ is varied. See the text for further details.

$\mathrm{Tr}\,\boldsymbol{\epsilon}^{(1)} = 0$ (or $\epsilon^{(1)}_{\tau\tau} = -\epsilon^{(1)}_{\beta\beta}$) which we may use to simplify the solution to

$$n_{B-L} = \frac{\pi^2}{6 z_d K_1} n^{\mathrm{eq}}_{N_1}(0) \epsilon^{(1)}_{\tau\tau} \Delta F, \tag{6.3.3}$$

with

$$\Delta F \equiv \frac{1}{p_{1\tau}} - \frac{1}{p_{1\beta}} = \frac{1}{p_{1\tau}} - \frac{1}{1 - p_{1\tau}}. \tag{6.3.4}$$

At the benchmark point for normal ordering defined in Table 6.1, which we will use in the further analyses in the present section, we have:

$$\begin{aligned} Y_{\tau 1} &= 1.37 \times 10^{-3} - 1.67 \times 10^{-4} e^{i\delta}, \\ Y_{\tau 1} &= 6.64 \times 10^{-4} - 8.74 \times 10^{-4} e^{i\frac{\alpha_{21}+\pi}{2}}, \\ Y_{\tau 1} &= 4.71 \times 10^{-4} + 1.07 \times 10^{-3} e^{\frac{i\alpha_{31}}{2}}, \end{aligned} \tag{6.3.5}$$

for CP violation from δ, α_{21} and α_{31} respectively. For the case in which δ provides

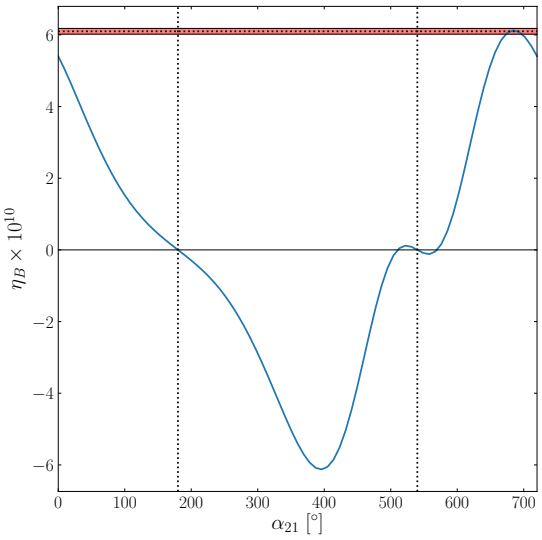

Figure 6.3: The baryon asymmetry with $M_1 = 3.05 \times 10^{10}$ GeV and CP violation provided solely by α_{21} (corresponding to $\delta = \alpha_{31} = 0°$). The red band indicates the 1σ observed values for η_B with the best-fit value indicated by the horizontal black dotted lines. Here we show the baryon asymmetry against α_{21} with exact CP-invariance at $\alpha_{21} = 180°$ and $540°$ (vertical black dotted lines).

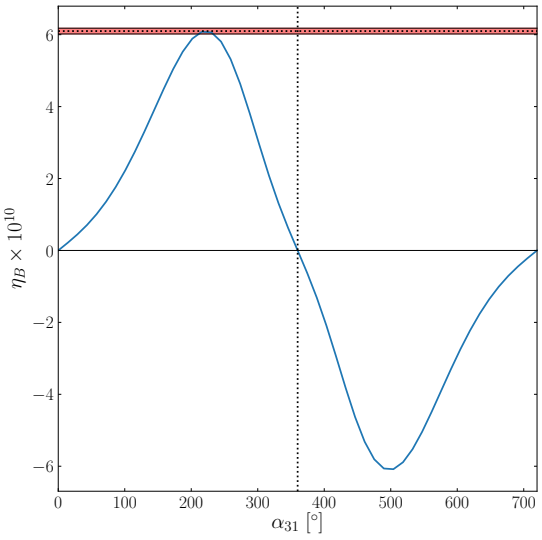

Figure 6.4: The baryon asymmetry with $M_1 = 5.13 \times 10^{10}$ GeV and CP violation provided solely by α_{31} (corresponding to $\delta = 0°$, $\alpha_{21} = 180°$). The red band indicates the 1σ observed values for η_B with the best-fit value indicated by the horizontal black dotted lines. Here we show the baryon asymmetry as a function of α_{31}, exact CP-invariance exists for $\alpha_{31} = 0°$ and $360°$ (vertical black dotted lines).

the CP violation in Eq. (6.3.5), this phase gives a subdominant contribution to $|Y_{\tau 1}|$. As can be shown, $p_{1\tau}$ is similarly weakly dependent on the phases. Thus, the phase dependence of the solutions of Eq. (6.3.3) does not come predominantly from the flavour factor ΔF but from the CP-asymmetry $\epsilon^{(1)}_{\tau\tau}$. However, in the case of α_{21} providing the CP violation, the two terms of Eq. (6.3.5) are similar in magnitude and we may get a strong enhancement in ΔF. The final case where α_{31} provides the CP violation is intermediate and should experience a slight phase-dependent enhancement from ΔF.

Dirac phase CP violation

In this subsection, we consider deviations from the benchmark point of Table 6.1 where we allow δ to vary but fix $\alpha_{21} = 180^\circ$ and $\alpha_{31} = 0^\circ$. Given the pattern of R-matrix angles, this ensures that any CP violation comes solely from δ. In this case, the $\tau\tau$-component of the CP-asymmetry is given by

$$\epsilon^{(1)}_{\tau\tau} = (0.515 - 3.94 c_{13})\, s_{13} \times 10^{-8} \sin\delta = -0.501 \times 10^{-8} \sin\delta. \tag{6.3.6}$$

Thus, given the approximate phase-independence of ΔF, we obtain a sinusoidal dependence of η_B on δ, with $\eta_B = 0$ when $\delta = 0^\circ$ or 180°. Keeping all other parameters fixed, we find that for $M_1 = 2.82 \times 10^{10}$ GeV no value of δ can produce the observed baryon asymmetry of the Universe, the maximum value of η_B as a function of δ is 4.07×10^{-11}. We might scale the heavy Majorana neutrino masses by a constant value, as when the two-flavour approximation of Eq. (6.3.3) is valid, the factor $\epsilon^{(1)}_{\tau\tau}$ scales in proportion with this constant and thus so does η_B. In doing so, we find that the final asymmetry rises until $M_1 = 7.08 \times 10^{11}$ GeV, where η_B takes maximum value 4.01×10^{-10}. After this, the simple scaling fails as one begins to enter the transition to what is usually the single-flavour regime.

Performing a detailed numerical parameter exploration we find that purely Dirac phase CP violation leads to successful leptogenesis for $M_1 = 5.13 \times 10^{10}$ GeV, $M_2 = 2.19 \times 10^{12}$ GeV and $M_3 = 1.01 \times 10^{13}$ GeV. This is illustrated in Fig. 6.2 in

which the plotted η_B comes from solving the full density matrix equations. In this case, we have:

$$Y_{\tau 1} = 1.11 \times 10^{-2} - 2.40 \times 10^{-4} e^{i\delta}. \tag{6.3.7}$$

Given the different orders of magnitude of the two terms in the expression for $Y_{\tau 1}$, the baryon asymmetry should exhibit dependence on δ only from $\epsilon^{(1)}_{\tau\tau}$ and not from ΔF. Our theoretical expectations are borne out by the approximate sinusoidal dependence of η_B on δ seen in Fig. 6.2.

CP violation from the Majorana phase α_{21}

Here, we set $\delta = \alpha_{31} = 0^\circ$ but allow CP violation from α_{21}. Setting all other parameters to their benchmark values we find

$$\epsilon^{(1)}_{\tau\tau} = 3.14 \times 10^{-7} \cos\frac{\alpha_{21}}{2}. \tag{6.3.8}$$

It follows from this expression for $\epsilon^{(1)}_{\tau\tau}$ that at the CP-conserving values for $\alpha_{21} = 0^\circ, 360^\circ$ we have $\epsilon^{(1)}_{\tau\tau} \neq 0$ (see also Fig. 6.3). This corresponds to the case of CP-conserving R-matrix, CP-conserving PMNS matrix, but CP-violating interplay between the R and PMNS matrix elements in leptogenesis [130]. In a similar way to the previous subsection, we find that no value of α_{21} can achieve successful leptogenesis using this combination of phases and the benchmark values from Table 6.1. Thus, we find it necessary to scale all of the heavy Majorana neutrino masses by a common factor such that $M_1 = 3.05 \times 10^{10}$ GeV, as this allows for successful leptogenesis. With this scaling we obtain the results plotted in Fig. 6.3. The deviation from pure (co)sinusoidal behaviour is explained by the α_{21}-dependence of ΔF. For $\alpha_{21} < 360^\circ$, ΔF varies relatively slowly exhibiting a global minimum at $\alpha_{21} = 180^\circ$, resulting in a slightly modified sinusoidal dependence through this point in η_B. A strong peak exists for ΔF around $\alpha_{21} = 540^\circ$, which results in the peak of η_B occurring before 720°, as would be expected from the dependence of $\epsilon^{(1)}_{\tau\tau}$. The small sign-changing fluctuation around the zero at $\alpha_{21} = 540^\circ$ is a feature that does not appear in the solution of two-flavour Boltzmann equations and thus cannot be explained in terms

of the analytic solution Eq. (6.3.3). However, the extra zeros of η_B that are seen in Fig. 6.3 are due only to accidental cancellations and do not correspond to cases of CP-symmetry (unlike those at $\alpha_{21} = 180°$ and $\alpha_{21} = 540°$).

CP violation from the Majorana phase α_{31}

We set $\delta = 0°$ and $\alpha_{21} = 180°$ such that CP violation is provided by α_{31}. Using the benchmark values for the other parameters from Table 6.1 we find:

$$\epsilon^{(1)}_{\tau\tau} = 2.11 \times 10^{-7} \sin \frac{\alpha_{31}}{2}. \tag{6.3.9}$$

Again we find that without scaling the heavy Majorana neutrino masses, no value of α_{31} corresponds to successful leptogenesis. At $M_1 = 5.13 \times 10^{10}$ GeV we obtain the first point for which the observed baryon asymmetry is created and this is plotted in Fig. 6.4. We see that analytical expectation of a sinusoidal dependence of the baryon asymmetry ($\eta_B \propto \epsilon^{(1)}_{\tau\tau} \propto \sin(\alpha_{31}/2)$) from Eq. (6.3.9) is present. ΔF exhibits a broad peak around $\alpha_{31} = 360°$ which results in the slight shift to the centre of the otherwise sinusoidal peaks.

6.3.3 The case of N_3 decoupled

In this section, we review the case that the heaviest Majorana neutrino, N_3, physically decouples. We restrict ourselves to normal ordered light neutrino masses. The resultant scenario with two relevant heavy Majorana neutrinos is the simplest (minimal) type I framework compatible with all neutrino data. In this scenario only two of the light neutrinos have non-zero masses since $m_1 = 0$. For normal ordering, the R-matrix may be parametrised as in Eq. (2.4.25) [204, 259, 260]

$$R = \begin{pmatrix} 0 & \cos\theta & \sin\theta \\ 0 & -\sin\theta & \cos\theta \\ 1 & 0 & 0 \end{pmatrix}. \tag{6.3.10}$$

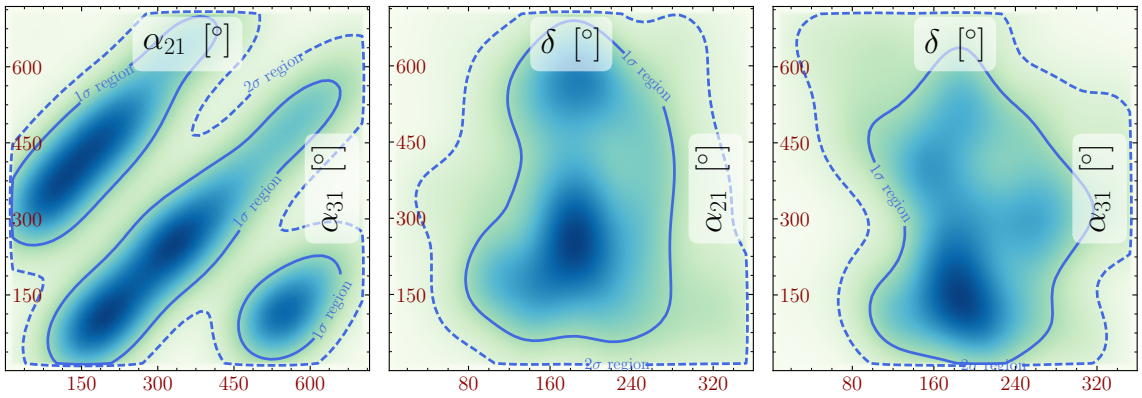

Figure 6.5: The two-dimensional projections for leptogenesis with $M_1 = 10^{11}$ GeV, $M_2 = 10^{12}$ GeV and N_3 decoupled, with CP violation provided only by the phases of the PMNS matrix. Here it is assumed that the light neutrino mass spectrum has normal ordering. Contours correspond to 68% and 95% confidence levels. This plot was created using SuperPlot [201].

The resulting neutrino Yukawa matrix thus has $Y_{\alpha 3} = 0$, consistent with the premise that N_3 has decoupled. We choose to take θ in Eq. (6.3.10) to be real in order to have the condition of Eq. (6.2.5) satisfied. We assume further that at least one of the three phases in the PMNS matrix has a CP-violating value.

As with the previous sections, we have performed an exhaustive exploration of the parameter space where again we are primarily concerned with the situation in which CP violation is provided only by the PMNS phases. We choose to fix $M_1 = 10^{11}$ GeV and $M_2 = 10^{12}$ GeV such that the parameter space to explore is described by $\mathbf{p} = (\delta, \alpha_{21}, \alpha_{31}, \theta)$. In Fig. 6.5, we present the two-dimensional posterior projection for the case of normal ordering. Here, it is seen that with $M_1 = 10^{11}$ GeV, for normal ordering, successful leptogenesis may produce a baryon asymmetry with 1σ (2σ) agreement with the observed value for $\delta \in [95, 315]°$, ($\delta \in [25, 360]°$).

In Table 6.2, we provide a benchmark point for normal ordered leptogenesis, with purely low-energy CP violation and N_3 decoupled. At this point, the observed BAU is produced with a corresponding fine-tuning of $\mathcal{F} = 0.23$. In Fig. 6.6, we illustrate a similar scenario, in which the CP violation is provided only by δ ($\alpha_{21} = 180°$, $\alpha_{31} = 0°$), and where the observed baryon asymmetry is produced near $\delta = 270°$.

δ (°)	α_{21} (°)	α_{31} (°)	M_1 (GeV)	M_2 (GeV)	θ (°)
228	516	100	10^{11}	10^{12}	25.05

Table 6.2: A benchmark point for leptogenesis with $M_1 = 10^{11}$ GeV and N_3 decoupled with a normal ordered light mass spectrum.

We conclude that, even for the minimal type I seesaw scenario with two heavy Majorana neutrinos exhibiting hierarchical mass spectrum, it is possible to generate the observed value of the baryon asymmetry with the requisite CP violation provided exclusively by the Dirac phase δ, and/or by the Majorana phase α_{21} or α_{31}.

Furthermore, we note that, in performing a similar investigation for the inverted ordering scenario, we find no point in the parameter space which corresponds to successful leptogenesis with N_3 decoupled in this mass window[4] with real R-matrix. If, however, e.g., $R_{11}R_{12} = \pm i|R_{11}R_{12}|$ ($R_{13} = 0$ in the case of interest), we can have successful leptogenesis with the CP violation provided by the Dirac and/or Majorana phases in PMNS matrix also for the IO spectrum. These conclusions are in agreement with the results of [130] wherein one may find a detailed discussion of the cases considered in the present subsection.

Finally, in [130] the following necessary condition for successful leptogenesis in the case of NO spectrum with the requisite CP violation provided exclusively by the Dirac phase δ was obtained:

$$|\sin\theta_{13}\,\sin\delta| \gtrsim 0.09\,. \tag{6.3.11}$$

We recall that this condition was derived by using values of the CP-conserving R-matrix elements maximising the lepton asymmetry and assuming that the transition from the two-flavour to one-flavour regime starts at $T \cong 5 \times 10^{11}$ GeV, i.e., that at $M_1 \lesssim 5 \times 10^{11}$ GeV the two-flavour regime is fully effective.

[4] For IO light neutrino mass spectrum the decoupling of N_3 implies $R_{13} = 0$. In this case $m_3 = 0$ as well.

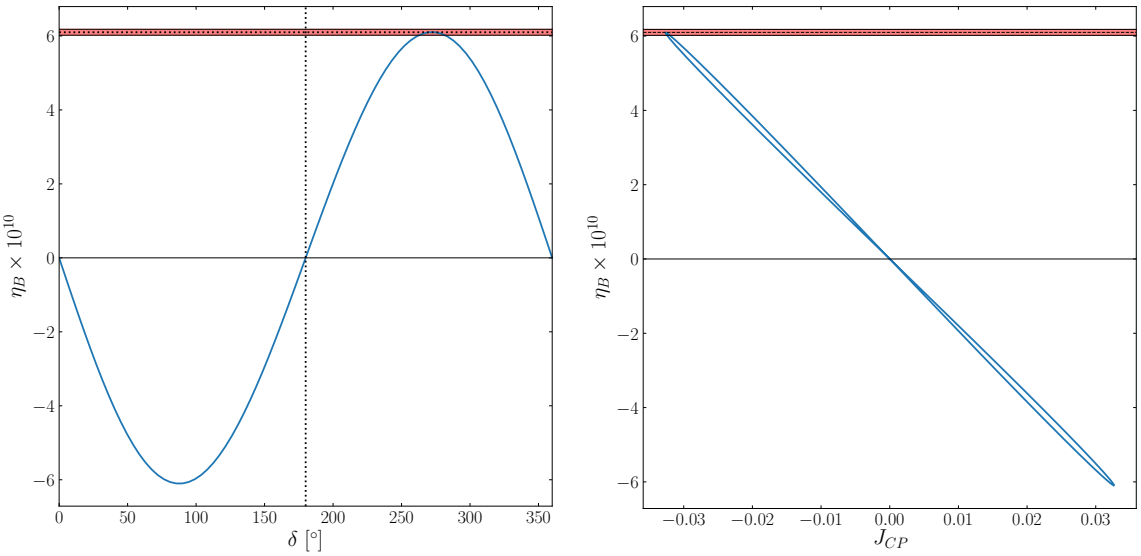

Figure 6.6: The baryon asymmetry from leptogenesis with $M_1 = 10^{11}$ GeV and N_3 decoupled, where CP violation is provided only by the Dirac phase δ. The red bands indicate the values in 1σ agreement with the observed value $\eta_{B_{\rm CMB}}$. Left: A plot of η_B against δ, showing successful leptogenesis near the maximal CP-violating value $\delta = 270°$. Right: The corresponding parametric plot of η_B with J_{CP} as δ is varied. See the text for further details.

6.4 Leptogenesis in the regime $M_1 < 10^9$ GeV

Successful thermal leptogenesis at intermediate scales may be accomplished through the combination of flavour effects and fine-tuned Yukawa matrices with $\mathcal{F} \gtrsim \mathcal{O}(10)$ [5, 261]. In Section 6.2.1, we first review these fine-tuned scenarios and then proceed to determine the subset among them in which the R-matrix is CP-conserving while the PMNS matrix contains CP-violating phases. In Section 6.4.1 we present and analyse the results of a comprehensive search of the model parameter space for regions with successful leptogenesis compatible with these subsets where we have numerically solved the density matrix equations, for two-decaying heavy Majorana neutrinos, exactly. Following this, we consider in detail the scenarios in which CP violation is due solely to the Dirac phase in Section 6.4.2, or due only to the Majorana phases in Section 6.4.2 and Section 6.4.2. In Appendix I, we display results for $M_1 = 10^9$ GeV, where $\mathcal{O}(10)$ fine-tuning is also required.

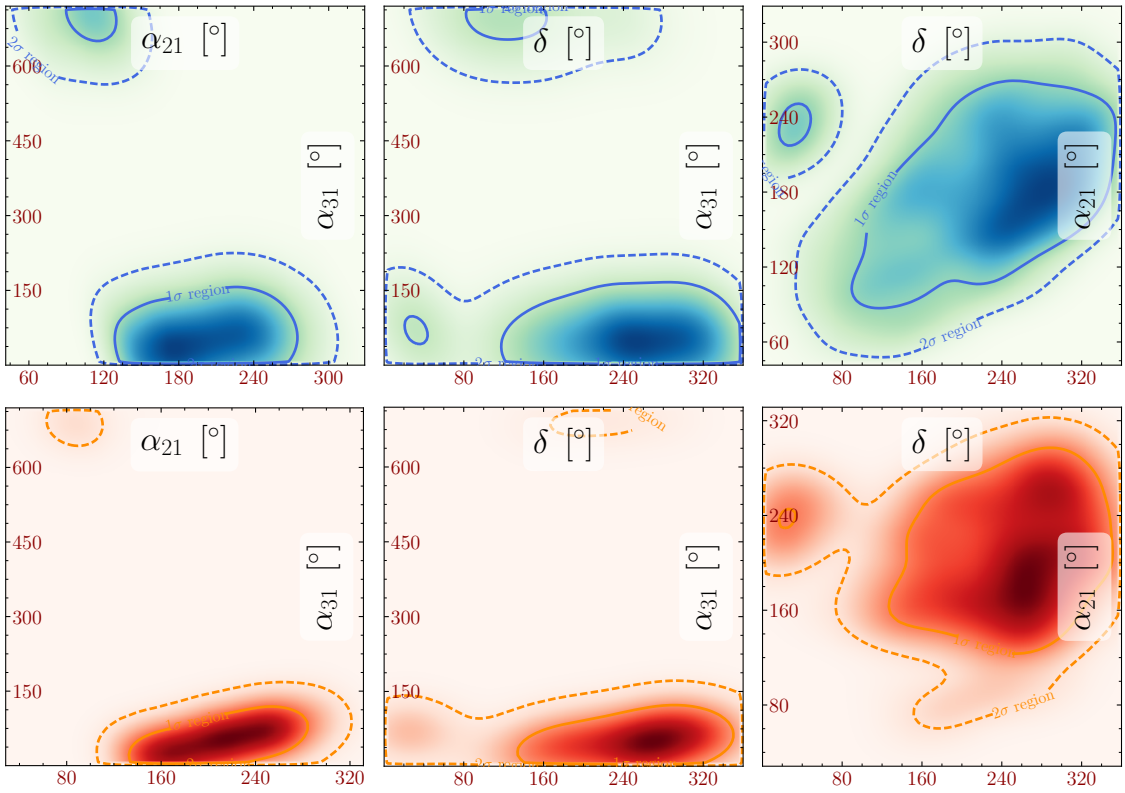

Figure 6.7: The two-dimensional projections for intermediate scale leptogenesis with $M_1 = 3.16 \times 10^6$ GeV for $x_1 = 0$, $y_2 = 0$, $x_3 = 180°$, $y_1 = y_2 = 180°$, with CP violation provided only by the phases of the PMNS matrix. The normal ordered case is coloured blue/green and inverted ordering orange/red and contours correspond to 68% and 95% confidence levels. This plot was created using SuperPlot [201].

We present an analytic approximation of the baryon asymmetry to find that the detailed dependence of the baryon asymmetry on the low energy phases may be roughly explained by the features of $Y_{\tau 1}$ and $Y_{\mu 1}$. We reiterate that we apply these approximation simply to illustrate the qualitative behaviour of the solutions but we numerically solve the density matrix to produce all plots in this chapter.

6.4.1 Results of parameter exploration

The options of Eq. (6.2.27) are satisfied by sixteen distinct R-matrices which may be divided into four classes according to the corresponding parity vectors ρ^ν, ρ^N (see Appendix H for definitions and further details). All such matrices are identical

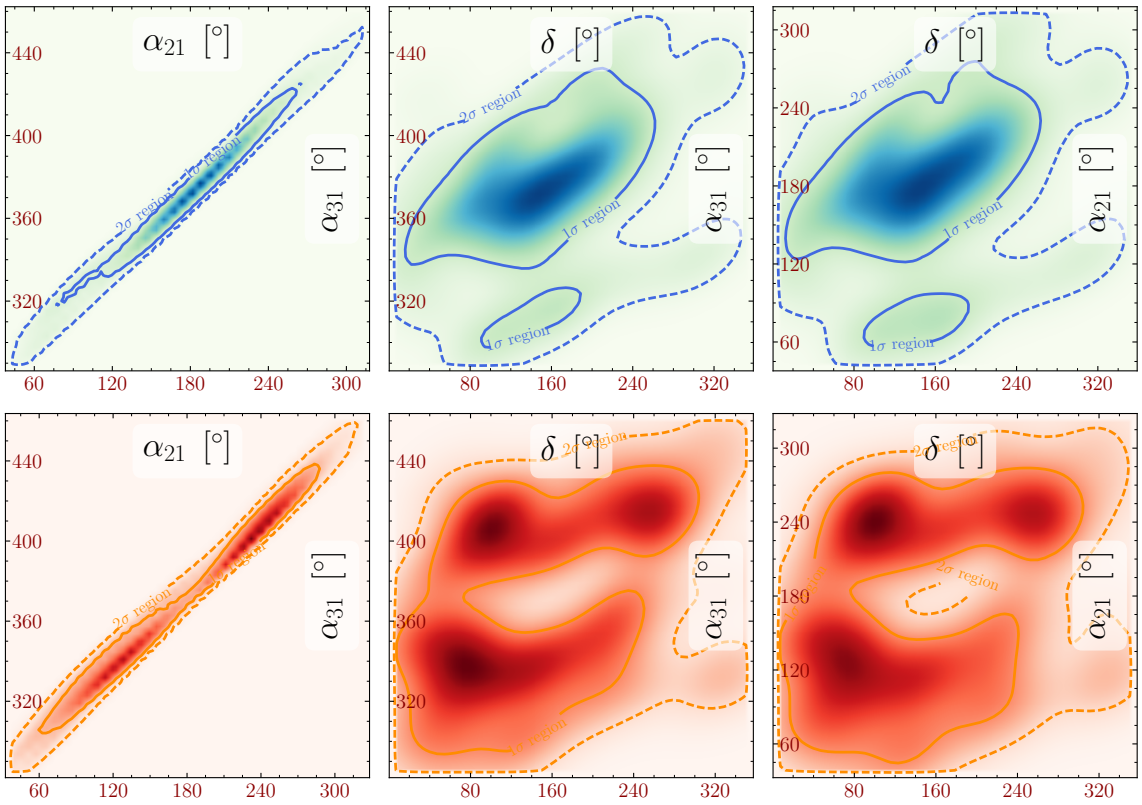

Figure 6.8: The two-dimensional projections for intermediate scale leptogenesis with $M_1 = 1.29 \times 10^8$ GeV for $x_1 = 0$, $y_2 = 0$, $x_3 = 180°$, $y_1 = y_2 = 180°$, with CP violation provided only by the phases of the PMNS matrix. The normal ordered case is coloured blue/green and inverted ordering orange/red and contours correspond to 68% and 95% confidence levels. This plot was created using SuperPlot [201].

except for the placement of factors ± 1 or $\pm i$. The phenomenological implications of each will be qualitatively similar except for the precise positions in parameter space that certain features occur. As we are primarily concerned with demonstrating the viability of leptogenesis with the $\mathcal{O}(100)$ fine-tuned Yukawa matrices (of the type in Eq. (6.2.17)) then we shall focus our numerical efforts on just one possible R-matrix of the set of sixteen. Namely, we choose a scenario corresponding to $\cos x_1 = 0$, $\cos x_3 = -1$ such that $\rho^\nu = \pm(+1, -1, +1)^T$, $\rho^N = \pm(+1, +1, -1)^T$.

For the numerical analysis, we follow the same procedure outlined in Section 6.3.1 with one additional constraint. At values of $\mathcal{F} \gtrsim 1000$, higher-order corrections to the light neutrino mass become important. For this reason we fix $y_1 = y_3 = 180°$

δ (°)	α_{21} (°)	α_{31} (°)	M_1 (GeV)	M_2 (GeV)	M_3 (GeV)	x_1 (°)	x_2 (°)	x_3 (°)	y_2 (°)
228	189	327.6	7.00×10^8	1.55×10^{10}	3.80×10^{10}	90	110	180	0

Table 6.3: A benchmark point for intermediate scale leptogenesis with quasi-degenerate (QD) spectrum of the light neutrino masses. In addition to the parameters listed we have $m_1 = 0.215$ eV and $y_1 = y_3 = -140°$ and corresponding fine-tuning $\mathcal{F} \approx 30$.

and thereby avoid these problematic regions of the model parameter space.

In the parameter searches of this section, we consider two cases, in one we fix $M_1 \sim 10^6$ GeV (Fig. 6.7) and in the other we fix $M_1 \sim 10^8$ GeV (Fig. 6.8). We note that $M_2 = 3.5M_1$ and $M_3 = 3.5M_2$ and $m_1 = 0.21$ eV.[5] This allows for a comparison of the effects of two different degrees of fine-tuning, with the former corresponding usually to $\mathcal{F} \sim 500$. This is close to the maximum fine-tuning (and correspondingly, the smallest non-resonant leptogenesis scale) for which second-order radiative corrections to the mass can be ignored [5].

For the scenario in which $M_1 = 3.16 \times 10^6$ GeV, as anticipated, there is a large fine-tuning of $\mathcal{F} = 745$. In the normal ordered case, we find that the observed baryon asymmetry may be obtained to within 1σ (2σ) with δ between $[84, 360]°$ ($[0, 360]°$). For inverted ordering, the 1σ (2σ) range is $[134, 350]°$ ($[0, 360]°$). With $M_1 = 1.29 \times 10^8$ GeV, the fine-tuning is considerably less, at $\mathcal{F} = 12$. In the normal ordered case, we find that the observed baryon asymmetry may be obtained to within 1σ (2σ) with δ between $[16, 263]°$ ($[0, 360]°$). For inverted ordering, the 1σ (2σ) range is $[0, 305]°$ ($[0, 360]°$). As in the previous section, we may explain these plots in detail by introducing an analytical approximation and then considering the simpler scenarios in which only the Dirac or only the Majorana phases provide CP violation. For brevity, we choose to perform this analysis only for $M_1 \sim 10^8$ GeV in the normal ordered scenario.

[5] In Appendix I, we demonstrate that one may lower m_1 as far as 0.05 eV and still have successful leptogenesis in a albeit rather constrained parameter space.

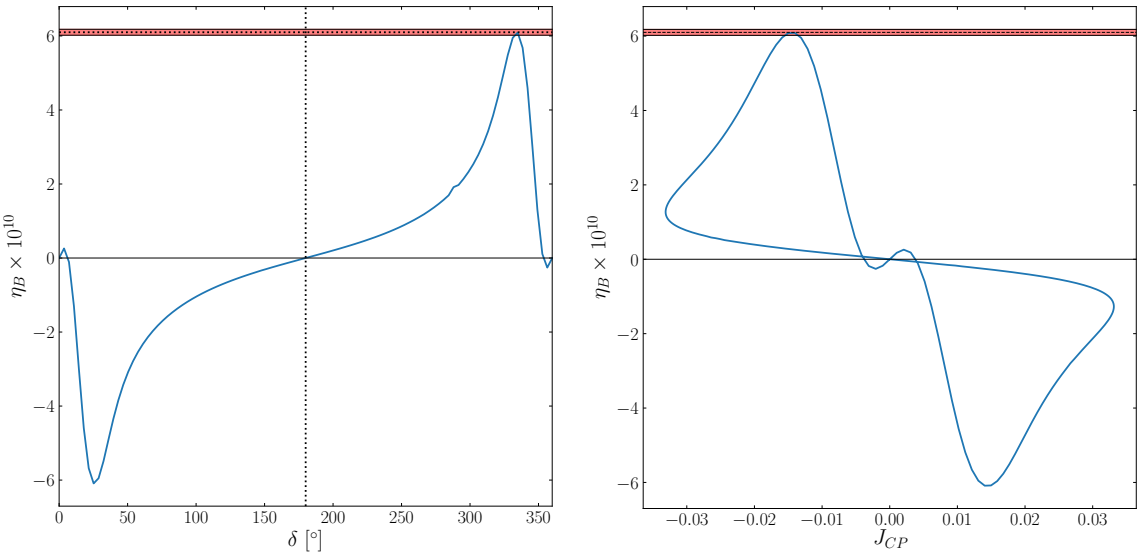

Figure 6.9: Intermediate scale leptogenesis ($M_1 = 7.00 \times 10^8$ GeV), with CP violation provided solely by δ, with $\alpha_{21} = 180°$ and $\alpha_{31} = 0°$. The red band indicates the 1σ observed values for $\eta_{B_{\rm CMB}}$ with the best-fit value indicated by the horizontal black dotted line. Left: The final baryon asymmetry as a function of δ with exact CP-invariance when $\delta = 0°$ and $180°$ (vertical black dotted line). Right: A parametric plot of η_B against J_{CP} as δ is varied at intermediate scales ($M_1 = 7.00 \times 10^8$ GeV). See the text for further details.

6.4.2 Dependence of η_B on Dirac and Majorana phases

In this section, we use the benchmark point given in Table 6.3, in order to analytically study leptogenesis from low-energy CP violation in the case that the lightest heavy Majorana neutrino has mass $M_1 < 10^9$ GeV, such that a relatively high degree of fine-tuning in the light neutrino masses is required. We choose this benchmark point as it allows us to accurately neglect the contributions from decays of the other heavy Majorana neutrinos and thus simplify the analysis.

With $M_1 < 10^9$ GeV, leptogenesis occurs in the three-flavour regime for which the three-flavoured Boltzmann equations are a good approximation to the density matrix equations and have approximate analytical solution [258]:

$$n_{B-L} = \frac{\pi^2}{6 z_d K_1} n_{N_1}^{\rm eq}(0) \left(\frac{\epsilon_{\tau\tau}^{(1)}}{p_{1\tau}} + \frac{\epsilon_{\mu\mu}^{(1)}}{p_{1\mu}} + \frac{\epsilon_{ee}^{(1)}}{p_{1e}} \right), \tag{6.4.1}$$

where we take into account the decays of only the lightest heavy Majorana neutrino.

As we are most interested in the scenarios in which CP violation is due to PMNS phases only, i.e. $\mathrm{Tr}\,\boldsymbol{\epsilon}^{(1)} = 0$, then we can re-express Eq. (6.4.1) as

$$n_{B-L} = \frac{\pi^2}{6 z_d K_1} n_{N_1}^{\mathrm{eq}}(0)\left(\epsilon_{\tau\tau}^{(1)}\Delta F_{\tau e} + \epsilon_{\mu\mu}^{(1)}\Delta F_{\mu e}\right), \tag{6.4.2}$$

where the asymmetry depends on the low-energy phases via $\epsilon_{\tau\tau}^{(1)}$ and $\epsilon_{\mu\mu}^{(1)}$ and from the difference of the inverse flavour projections:

$$\Delta F_{\tau e} \equiv \frac{1}{p_{1\tau}} - \frac{1}{p_{1e}}, \quad \Delta F_{\mu e} \equiv \frac{1}{p_{1\mu}} - \frac{1}{p_{1e}}. \tag{6.4.3}$$

However, for the case of Table 6.3, the two and three-flavour regime Boltzmann equations, to a high degree of accuracy give the same value of η_B. Given the comparative simplicity of the two-flavour solution Eq. (6.3.3), we choose to use this for the practical purpose of simplifying the analysis.

For the benchmark parameter values listed in Table 6.3, we may find analytical approximations for the CP-asymmetries $\epsilon_{\alpha\alpha}^{(1)}$. Under the relatively good approximation, that $m_1 = m_2$ [6], the asymmetry is given by

$$\begin{aligned}\epsilon_{\alpha\alpha}^{(1)} = {} & \frac{3}{16\pi\left(Y^\dagger Y\right)_{11}}\frac{M_1^2}{v^4} m_1\sqrt{m_1 m_3}(e^{y_3}\sin 2x_2)|R_{21}|^2 \\ & \left(\frac{2}{3}\left(\frac{M_1}{M_2}+\frac{M_1}{M_3}\right)\Im\left[e^{-ix_3}\left(U_{\alpha1}+iU_{\alpha2}\right)U_{\alpha3}^*\right] - \frac{5}{9}\frac{M_1^2}{M_2^2}\Im\left[e^{-2i(x_1+x_3)}e^{-ix_3}(U_{\alpha1}+iU_{\alpha2})U_{\alpha3}^*\right]\right).\end{aligned} \tag{6.4.4}$$

Selecting $x_1 = (2k_1+1)\pi/2$ and $x_3 = k_3\pi$ for k_1, $k_3 \in \mathbb{Z}$, such that $\cos x_1 = 0$ and $|\cos x_3| = 1$ and $\cos x_3 = (-1)^{k_3}$ is satisfied, we find the CP-asymmetry $\epsilon_{\alpha\alpha}^{(1)}$ to be

$$\begin{aligned}\epsilon_{\alpha\alpha}^{(1)} = {} & \frac{3}{16\pi\left(Y^\dagger Y\right)_{11}}\frac{M_1^2}{v^4} m_1^{\frac{3}{2}} m_3^{\frac{1}{2}}(e^{y_3}\sin 2x_2)(-1)^{k_3}|R_{21}|^2 \\ & \times\left(\frac{2}{3}\left(\frac{M_1}{M_2}+\frac{M_1}{M_3}\right)+\frac{5}{9}\frac{M_1^2}{M_2^2}\right)\Im\left[\left(U_{\alpha1}+iU_{\alpha2}\right)U_{\alpha3}^*\right],\end{aligned} \tag{6.4.5}$$

where, at our benchmark point, the coefficient of $\Im\left[U_{\alpha3}^*\left(U_{\alpha1}+iU_{\alpha2}\right)\right]$ has magnitude approximately equal to 3.7×10^{-6}. This form is particularly useful in order to isolate the dependence of the CP-asymmetry on the PMNS phases in the factor $\Im\left[U_{\alpha3}^*\left(U_{\alpha1}+iU_{\alpha2}\right)\right]$.

[6] The approximation $m_1 = m_2$ is sufficiently precise as long as $m_1^2 \gg 0.5\Delta m_{21}^2 \cong 3.7\times10^{-5}$ eV^2.

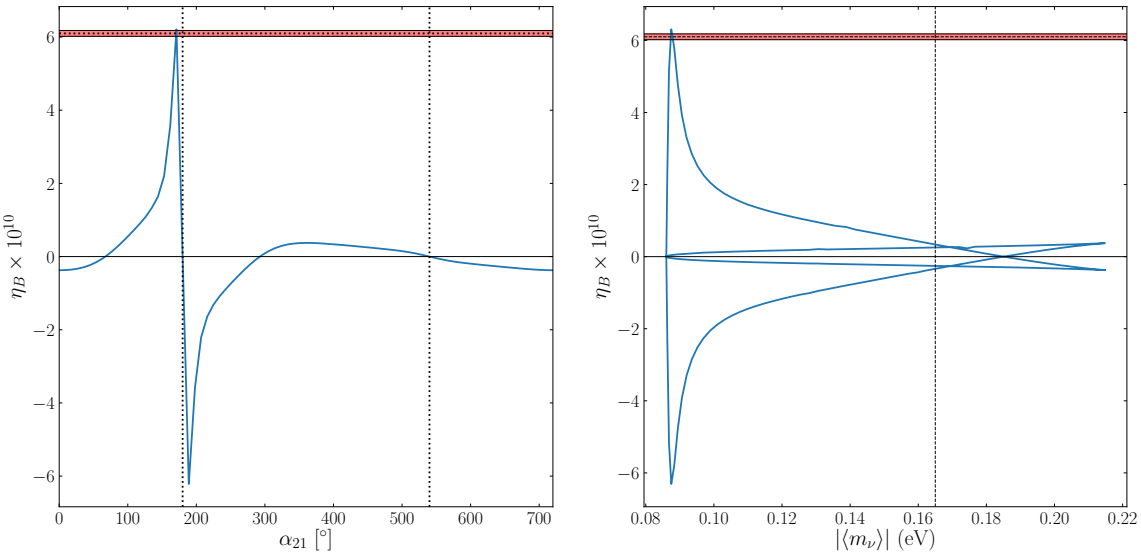

Figure 6.10: Intermediate scale leptogenesis ($M_1 = 7.00 \times 10^8$ GeV) with CP violation provided solely by α_{21} and with $\delta = \alpha_{31} = 0$. The red band indicates the 1σ observed values for η_B with the best-fit value indicated by the horizontal black dotted lines. Left: The baryon asymmetry against α_{21} with exact CP-invariance at $\alpha_{21} = 180°$ and $540°$ (vertical black dotted lines). Right: A parametric plot of η_B against the effective neutrino mass $|\langle m_\nu \rangle|$ as α_{21} is varied with the vertical dashed black line denoting the upper value of the KamLAND-Zen bound 0.165 eV [41]. Successful leptogenesis is achieved for $|\langle m_\nu \rangle| = 0.0877$ eV. See the text for further details.

Dirac phase CP violation

We consider the possibility that the Majorana phases are CP-conserving: $\alpha_{21} = 180°$, $\alpha_{31} = 0°$ (given the R-matrix under consideration). The sole source of CP violation is δ and there is exact CP-invariance if $\delta = 0°, 180°$. The corresponding η_B is plotted in Fig. 6.9 alongside a parametric plot of η_B against J_{CP} with parameter δ.[7]

From the CP-asymmetry, one expects to find η_B proportional to

$$\Im\left[U^*_{\tau 3}\left(U_{\tau 1} + iU_{\tau 2}\right)\right] = s_{13}c_{13}c^2_{23}(s_{12} - c_{12})\sin\delta \approx -0.0178\sin\delta, \tag{6.4.6}$$

and thus sinusoidal in δ. However, the phase-dependent efficiency (flavour-factor)

[7] All plots involving η_B in this chapter have been obtain by solving the full density matrix equations, allowing for the lightest pair of heavy Majorana neutrinos to decay and possibly (if indicated) include scattering effects.

ΔF exhibits a sharp maximum around the region $\delta = 0°$ or $\delta = 360°$. This modifies the sinusoidal dependence from the CP-asymmetries such that the extrema of η_B are shifted towards the extreme values of δ, as in seen in Fig. 6.9. The small fluctuations around $\delta = 0°$, $\delta = 360°$ are not captured by the Boltzmann equations (neither two-flavoured nor three-flavoured) and are only present when solving the full density matrix equations which take account of the finite size of the lepton thermal widths. The result is the addition of some accidental zeros in the variation of η_B which do not correspond to CP-conserving values of δ.

CP violation from the Majorana phase α_{21}

Alternatively, consider the case of CP violation from α_{21}, where $\delta = 0°$, $\alpha_{31} = 0°$ and all other parameters are set to the benchmark values of Table 6.3. The variation of η_B with α_{21} in this scenario is plotted on the left of Fig. 6.10. On the right of the same figure, we parametrically plot η_B against $|\langle m_\nu \rangle|$ with parameter α_{21}. The baryon asymmetry η_B vanishes at the CP-conserving values of $\alpha_{21} = 180°$ and $540°$. However, as is seen in Fig. 6.10, $\eta_B \neq 0$ at the CP-conserving values of $\alpha_{21} = 0°$, $360°$ and $720°$ since at these values the interplay between the CP-conserving R and PMNS matrices leads to CP violation in leptogenesis [130].

The efficiency function ΔF, when plotted as a function of α_{21}, exhibits a very strong narrow peak at $\alpha_{21} = 180°$ and a much less pronounced peak at $\alpha_{21} = 540°$. As a consequence, the corresponding η_B is modified from the simple cosine curve expected from the dependence of $\epsilon^{(1)}_{\tau\tau}$ and $\epsilon^{(1)}_{\mu\mu}$ on α_{21}, which arises in the factors:

$$\Im\left[U^*_{\tau 3}\left(U_{\tau 1} + iU_{\tau 2}\right)\right] = -c_{13}c_{23}(c_{12}s_{23} + s_{12}c_{23}s_{13})\cos\frac{\alpha_{21}}{2} \approx -0.444\cos\frac{\alpha_{21}}{2}, \tag{6.4.7}$$

Thus, there is a sharp transition around $\alpha_{21} = 180°$. We can conclude then that the strong peak in ΔF is what has allowed the observed baryon asymmetry of the Universe to be reproduced. This peak originates in an accidental cancellation of terms in the function $p_{1\tau}$. There is no *a priori* reason to expect such a cancellation

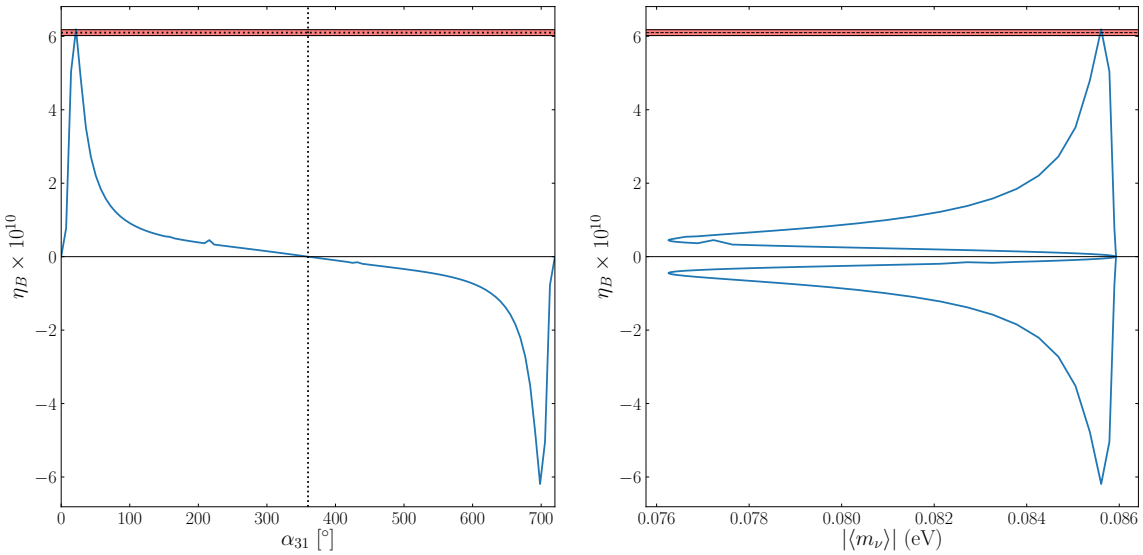

Figure 6.11: Leptogenesis at intermediate scales ($M_1 = 7.00 \times 10^8$ GeV) when CP violation is provided solely by α_{31} with $\delta = 0°$, $\alpha_{21} = 180°$. The red band indicates the 1σ observed values for η_B with the best-fit value indicated by the horizontal black dotted lines. Left: The baryon asymmetry as a function of α_{31}. Exact CP-invariance exists for $\alpha_{31} = 180°$ and $360°$ (vertical black dotted lines). Right: A parametric plot of η_B against the effective neutrino mass $|\langle m_\nu \rangle|$ as α_{31} is varied with successful leptogenesis at $|\langle m_\nu \rangle| = 0.0856$ eV. See the text for further details.

and it should be understood as a feature of the fine-tuned solutions that are being here studied. Thus, we see that the flavour-effects introduce a pair of accidental zeros of η_B, one in the range $[180, 540]°$ and the other in $[0, 180]°$.

CP violation from the Majorana phase α_{31}

Finally, consider the case of CP violation from α_{31} where $\delta = 0°$, $\alpha_{21} = 180°$ and for which the baryon asymmetry is plotted in the left plot of Fig. 6.11 and on the right we show the parametric dependence of the effective neutrino mass $|\langle m_\nu \rangle|$ with α_{31} against that of η_B. The baryon asymmetry η_B vanishes at the CP-conserving values of $\alpha_{31} = 0°$, $360°$ and $720°$.

The efficiency function ΔF in this case is qualitatively similar to that for the case of δ: CP violation only strongly peaks at α_{31} close to $0°$ and to $720°$. Thus, we do

not observe, in the left plot of Fig. 6.11, the simple dependence, $\eta_B \propto \sin(\alpha_{31}/2)$ as may be expected from the expression for $\epsilon_{\tau\tau}$,

$$\begin{aligned}\Im\left[U^*_{\tau 3}\left(U_{\tau 1}+iU_{\tau 2}\right)\right] &= c_{13}c_{23}((c_{12}-s_{12})s_{23}+(c_{12}+s_{12})s_{13}c_{23})\sin\frac{\alpha_{31}}{2}\\ &\approx -0.662\sin\frac{\alpha_{31}}{2}.\end{aligned} \tag{6.4.8}$$

Rather, we find an enhanced positive peak near $\alpha_{31} = 0°$ and an enhanced negative peak near $\alpha_{31} = 720°$.

Summary of fine-tuned solutions with high-energy CP-Symmetry

The fine-tuned solutions we have discussed in this section share the property that they enhance η_B through the production of a peak in the efficiency factor ΔF. In each projection coefficient,

$$p_{1\alpha} = \frac{|Y_{\alpha 1}|^2}{\left(Y^\dagger Y\right)_{11}}, \tag{6.4.9}$$

the PMNS matrix cancels from the denominator such that all phase-dependence comes from that of $|Y_{\alpha 1}|^2$ in the numerator. In this subsection, we may safely use the usual Casas-Ibarra parametrisation (obtained by the replacement of f with $\sqrt{M^{-1}}$ in Eq. (2.4.24)), to obtain

$$Y_{\alpha 1} = \sqrt{M_1}\left(\sqrt{m_1}R_{11}U_{\alpha 1}+\sqrt{m_2}R_{12}U_{\alpha 2}+\sqrt{m_3}R_{13}U_{\alpha 3}\right). \tag{6.4.10}$$

The absolute value $|Y_{\alpha 1}|$ is extremised when each term in the parentheses in Eq. (6.4.10) has a common complex phase or when terms may differ in complex phase by π. This occurs at CP-conserving values of the PMNS phases and so the enhancement expected in the functions ΔF is likely to occur at CP-conserving phases also. As an example, around the benchmark point of Table 6.3, we find that with only α_{21} contributing to CP violation ($\delta = \alpha_{31} = 0°$),

$$Y_{\tau 1} = \left(2.16 + 2.23e^{i\frac{\alpha_{21}+\pi}{2}}\right)\times 10^{-3}. \tag{6.4.11}$$

The absolute value of this function has extrema when $\alpha_{21} = 180°$ or $\alpha_{21} = 540°$ - the CP-conserving values. Moreover, the cancellation that occurs at $\alpha_{21} = 180°$ is

strong because of the similarity in magnitude of the two terms in Eq. (6.4.11). As a result of this there are strong peaks in ΔF which enhance η_B.

This is why the solutions are considered to be fine-tuned as there is no reason to expect these two terms to be so similar in size. At these same points, the asymmetries $\epsilon^{(1)}_{\alpha\alpha}$ are vanishing as CP is a symmetry in the leptonic sector. Thus η_B, being proportional to the product of $\epsilon^{(1)}_{\tau\tau}$ and ΔF, is strongly enhanced on either side of the CP-invariant points (for instance, around $\alpha_{21} = 180^\circ$ in the left plot of Fig. 6.10). Thus the fine-tuned solutions tend to achieve large η_B of one-sign on one side of a CP-invariant point and large η_B of the opposite sign on the other side. Similarly, this effect persists when all phases may contribute together to CP violation (Fig. 6.7 and Fig. 6.8). Thus, successful leptogenesis tends to occur near $\alpha_{21} \sim 180^\circ$, $\alpha_{31} \sim 0^\circ$, 720° when leptogenesis is achieved with fine-tuned light neutrino masses, as it is at intermediate scales ($M_1 \lesssim 10^9$ GeV). Note that although we made these arguments based on the two-flavoured Boltzmann equations, very similar conclusions are reached based on considerations of $\Delta F_{\tau e}$ and $\Delta F_{\mu e}$ for the solutions of the three-flavoured Boltzmann equations. For this reason, one expects similar behaviour to hold even for lower values M_1 such as in Fig. 6.7.

Furthermore, one may usually argue that Dirac-phase leptogenesis suffers a suppression not present in Majorana phase leptogenesis due to the factors of s_{13} that appear in the CP-asymmetries as shown in Eq. (6.4.6). However, for Dirac-phase leptogenesis $\eta_B \propto \sin\delta\Delta F(\delta)$, where the maximum absolute value of $\Delta F(\delta)$ is ~ 408, whereas for α_{21} leptogenesis, $\eta_B \propto \cos\frac{\alpha_{21}}{2}\Delta F(\alpha_{21})$ with maximum absolute value ~ 77. Thus, what is more relevant when leptogenesis occurs intermediate scales, is the degree of enhancement from ΔF that occurs due to fine-tuning.

Finally, as we observe in Fig. 6.8, the contours for α_{21}, α_{31} show a strong dependence on $\alpha_{31} - \alpha_{21}$. A rough explanation of this is given by the dependence of $\epsilon^{(1)}_{\tau\tau}$ on the Majorana phases. With δ fixed at its benchmark value, but α_{21} and α_{31} free to vary,

this CP-asymmetry is given by

$$\epsilon^{(1)}_{\tau\tau} \approx \left(1.46 \cos \frac{(\alpha_{31} - \alpha_{21})}{2} + 0.869 \sin \frac{\alpha_{31}}{2}\right) \times 10^{-7}, \tag{6.4.12}$$

which exhibits a slightly dominant, $(\alpha_{31} - \alpha_{21})$-dependent contribution. This contribution is maximised when $\alpha_{31} = \alpha_{21}$.

6.5 Leptogenesis in the regime $\mathbf{M_1 > 10^{12}}$ GeV

In previous studies in which a connection between low-energy CP violation (CP-conserving R) and leptogenesis was established [131], the scale of leptogenesis was limited to $M_1 \leq 5 \times 10^{11}$ GeV. This allowed for the use of the two-flavour Boltzmann equations (Eq. (3.3.23) with $\alpha \in \{\beta, \tau\}$) where the CP-asymmetries $\epsilon^{(1)}_{\tau\tau}$ and $\epsilon^{(1)}_{\beta\beta}$ appear separately. The expectation had been that for $M_1 \gg 10^{12}$ GeV, the single-flavour Boltzmann equation Eq. (3.2.21) would be appropriate. In this equation, the CP-asymmetries appear only in the factor $\mathrm{Tr}\,\boldsymbol{\epsilon}^{(1)} = 0$ and hence no baryon asymmetry may be produced. In Section 6.5.1 we argue that even at high scales $M_1 \gg 10^{12}$ GeV, if R is CP-conserving, then flavour effects are significant and that the density matrix equations do not reduce to the single flavour Boltzmann equations. Hence we conclude that viable leptogenesis may result from low energy CP violation. Finally, in Section 6.5.2 we proceed to numerically analyse this possibility in detail.

6.5.1 Flavour effects with $M_1 \gg 10^{12}$ GeV and High Energy CP-Symmetry

In Appendix J, we demonstrate that the complete formal solution of the density matrix equations Eq. (3.3.19), with only tau lepton flavour effects and one decaying heavy Majorana neutrino is

$$n_{B-L}(z_f) = \int_0^{z_f} e^{-\int_{z'}^{z_f} W_1(z'')dz''} \left(\mathrm{Tr}\,\boldsymbol{\epsilon}^{(1)} D_1(z')(n_{N_1}(z') - n^{\mathrm{eq}}_{N_1}(z')) + W_1(z')\lambda(z')\right) dz', \tag{6.5.1}$$

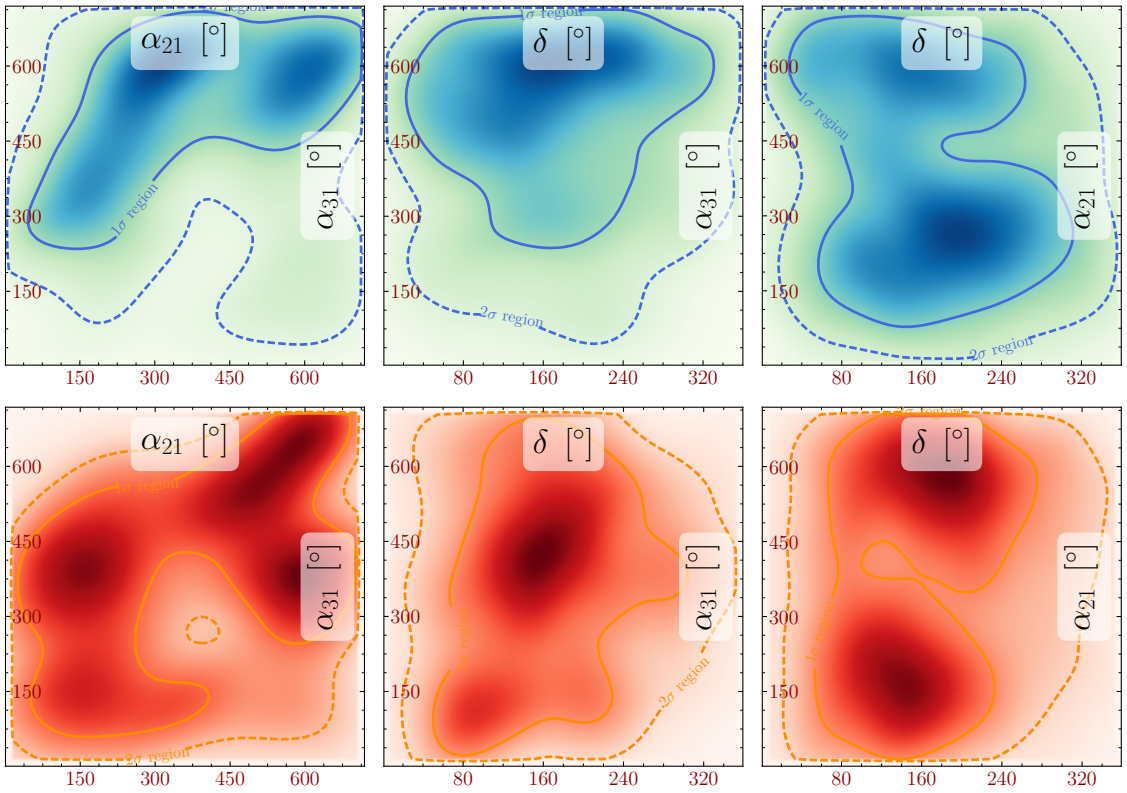

Figure 6.12: The two-dimensional projections for high-scale leptogenesis with $M_1 = 10^{13}$ GeV with CP violation provided only by the phases of the PMNS matrix. The NO case is coloured blue/green and the IO one is orange/red. The contours correspond to 68% and 95% confidence levels. This plot was created using SuperPlot [201].

with

$$\lambda(z) \equiv 2 \int_0^z dz' \Re \left[c_{1\beta} c_{1\tau}^* \frac{\Gamma_\tau}{2Hz'} n_{\tau\beta}(z') \right] . \tag{6.5.2}$$

In a typical leptogenesis scenario, if $M_1 \gg 10^{12}$ GeV, flavour effects are negligible and one obtains the well-known result:

$$n_{B-L}(z_f) = \int_0^{z_f} e^{-\int_{z'}^{z_f} W_1(z'')dz''} \operatorname{Tr} \boldsymbol{\epsilon}^{(1)} D_1(z') (n_{N_1}(z') - n_{N_1}^{\mathrm{eq}}(z')) dz', \tag{6.5.3}$$

which may be found by solving the single flavour Boltzmann equation. However, with a CP-conserving R-matrix, such that CP violation is provided solely by the PMNS phases, one has $\operatorname{Tr} \boldsymbol{\epsilon}^{(1)} = 0$ and so the λ term in Eq. (6.5.1) becomes the

δ (°)	α_{21} (°)	α_{31} (°)	M_1 (GeV)	M_2 (GeV)	M_3 (GeV)	x_1 (°)	x_2 (°)	x_3 (°)
228	200	175	10^{13}	1.2×10^{15}	10^{16}	-96.55	-105.2	141.4

Table 6.4: The benchmark values for high-scale leptogenesis with normal ordering. Here we have $m_1 = 0.0159$ eV and $y_1 = y_2 = y_3 = 0°$.

dominant one:

$$n_{B-L}(z_f) = \int_0^{z_f} e^{-\int_{z'}^{z_f} W_1(z'')dz''} W_1(z')\lambda(z')dz'. \tag{6.5.4}$$

If this is the case, then the baryon asymmetry is produced purely through flavour-effects from $\Gamma_\tau/2Hz$.

The physical effect of $\mathrm{Tr}\,\boldsymbol{\epsilon}^{(1)} = 0$ is that opposite asymmetries are produced in the τ and β flavours due to the decay of N_1: $\epsilon^{(1)}_{\tau\tau} = -\epsilon^{(1)}_{\beta\beta}$. However, with flavour effects, the lepton asymmetries $\epsilon^{(1)}_{\tau\tau}$ and $\epsilon^{(1)}_{\beta\beta}$ produced in the decay experience differing washouts such that $n_{\tau\tau} \neq -n_{\beta\beta}$ and $n_{B-L} = n_{\tau\tau} + n_{\beta\beta} \neq 0$. It is an asymmetry produced by this method that is described in Eq. (6.5.4). The obvious question at this point is whether this can ever be large enough to produce the observed baryon asymmetry when $M_1 \gg 10^{12}$ GeV.

The density matrix equations may be conveniently expressed in terms of the vectors

$$\boldsymbol{n} \equiv (n_{\beta\beta}, n_{\tau\beta}, n_{\beta\tau}, n_{\tau\tau})^T, \tag{6.5.5}$$

$$\boldsymbol{\mathcal{E}^{(1)}} \equiv (\epsilon^{(1)}_{\beta\beta}, \epsilon^{(1)}_{\tau\beta}, \epsilon^{(1)}_{\beta\tau}, \epsilon^{(1)}_{\tau\tau})^T, \tag{6.5.6}$$

as

$$\frac{d\boldsymbol{n}}{dz} = \boldsymbol{\mathcal{E}^{(1)}} D_1 \left(n_{N_1} - n^{\mathrm{eq}}_{N_1}\right) - \frac{1}{2}\mathcal{W}_1 \boldsymbol{n} - \frac{\Gamma_\tau}{2Hz}\mathcal{I}\boldsymbol{n}, \tag{6.5.7}$$

where

$$\mathcal{W}_1 \equiv W_1 \begin{pmatrix} 2|c_{1\beta}|^2 & c_{1\tau}^* c_{1\beta} & c_{1\tau} c_{1\beta}^* & 0 \\ c_{1\tau} c_{1\beta}^* & 0 & 1 & c_{1\tau} c_{1\beta}^* \\ c_{1\tau}^* c_{1\beta} & 0 & 1 & c_{1\tau}^* c_{1\beta} \\ 0 & c_{1\tau}^* c_{1\beta} & c_{1\tau} c_{1\beta}^* & 2|c_{1\beta}|^2 \end{pmatrix} \quad \text{and} \quad \mathcal{I} \equiv \begin{pmatrix} 0 & 0 & 0 & 0 \\ 0 & 1 & 0 & 0 \\ 0 & 0 & 1 & 0 \\ 0 & 0 & 0 & 0 \end{pmatrix}. \tag{6.5.8}$$

In terms of these quantities, the formal solution, with flavour effects neglected is:

$$\boldsymbol{n}\,(z_f) = \int_0^{z_f} e^{\int_{z'}^{z_f} \frac{1}{2}\mathcal{W}_1(z'')dz''} \boldsymbol{\mathcal{E}^{(1)}} D(z')(n_{N_1}(z') - n_{N_1}^{\rm eq}(z'))dz'. \tag{6.5.9}$$

Although flavour effects in high-scale leptogenesis may be negligible, this solution may not be accurately applied for finding η_B in the case that $\mathrm{Tr}\,\boldsymbol{\epsilon}^{(1)} = 0$. This is because there is a strong cancellation of components of the density matrix when computing $n_{B-L} = n_{\beta\beta} + n_{\tau\tau}$, such that the errors made in neglecting flavour effects are dominant. For this reason, we make use of it only for finding the approximate behaviour of individual components of the density matrix and avoid applying it to situations where this cancellation occurs.

If the heavy Majorana neutrino masses M_i are scaled by a common factor x, such that $M_i \to xM_i$, then: $\epsilon^{(1)}$ scales in proportion with x, D_1 and W_1 do not scale with x and $\frac{\Gamma_\tau}{2Hz}$ varies inversely with x. Consequently, according to Eq. (6.5.9), $n_{\alpha\beta}(z)$ scales in proportion to x, (with increasing precision for larger x since we can better neglect the thermal widths). In λ the scaling of $\frac{\Gamma_\tau}{2Hz}$ cancels that of $n_{\tau\beta}$ and so λ does not scale with x if $M_1 \gg 10^{12}$ GeV. Thus, at sufficiently large values of M_1, η_B, given by Eq. (6.5.4), asymptotically approaches a non-zero constant. This is shown in Fig. 6.13 (d) over a range of M_1 values in which the ratios M_1/M_2 and M_2/M_3 are fixed. The curve increases ever more slowly for larger M_1 as the approximation leading to Eq. (6.5.9) becomes ever more precise. This may be interpreted as the transition region between the two flavour regime and the single flavour having grown infinitely large.[8] In each of the plots of Fig. 6.13, we see a dip in the density matrix

[8] If, contrary to our scenario of interest, R is CP-violating ($\mathrm{Tr}\,\boldsymbol{\epsilon}^{(1)} \neq 0$), then the first term in

solution curve near 10^{12} GeV. This feature is due to the difference in sign of the two-flavour solutions, for which $\eta_B \propto \epsilon^{(1)}_{\tau\tau}/p_{1\tau} + \epsilon^{(1)}_{\beta\beta}/p_{1\beta} = 3.99 \times 10^{-4}$, compared to that of the single flavour solutions, where $\eta_B \propto \epsilon^{(1)}_{\tau\tau} + \epsilon^{(1)}_{\beta\beta} = -7.5 \times 10^{-6}$ (where these numbers are valid for plot (a) of Fig. 6.13 corresponding to CP-violating R-matrix). The dip appears as a result of plotting the absolute value of η_B on a logarithmic scale when η_B passes through zero during the transition between these regimes.

In Appendix K, we discuss the robustness of the plateau that forms for large heavy Majorana neutrino masses when the effects of scattering and when a more realistic treatment of the right-handed taus are incorporated. In the next section we explore the parameter space of the three heavy Majorana neutrino type I seesaw with regard to the solutions of Eq. (K.0.1) with CP-conserving R-matrix and $M_1 \gg 10^{12}$ GeV.

6.5.2 Results of parameter exploration

At values of $M_1 \gg 10^{12}$ GeV, fine-tuning through large elements of the R-matrix is not required for successful leptogenesis (if Majorana phases are allowed to play a role, otherwise large fine-tuning is required if only Dirac phases take effect). Thus, in this section we analyse the parameter space corresponding to real, and therefore CP-conserving, R-matrices ($y_i = 0°$), using the same numerical technique as described in Section 6.4.1. In order to perform this analysis we fix $M_1 = 10^{13}$ GeV and again require $M_3 > 3M_2 > 9M_1$ in order to avoid the resonant regime. With a much higher value of M_1, one would need a correspondingly a higher temperature of inflation. For this reason, we choose to illustrate the possibility of successful thermal leptogenesis at just one order of magnitude beyond the two-flavour to single-flavour transition temperature of 10^{12} GeV. In Fig. 6.12, we display the two-dimensional projection plots for both normal ordering and inverted ordering.

In the NO case, we find that the observed baryon asymmetry may be obtained to within 1σ (2σ) with δ between $[240, 331]°$ ($[0, 360]°$). In the IO one, the 1σ (2σ) range

parentheses of Eq. (6.5.1) eventually dominates the second for sufficiently large x and the single flavour regime is entered.

is $[50, 304]^\circ$ ($[20, 352]^\circ$). In what follows, we analyse these results by considering separately the cases of purely Dirac or purely Majorana CP violation. For brevity we consider only the case of NO spectrum.

6.5.3 Dependence of η_B on the Dirac and Majorana phases

As the final value of the baryon asymmetry becomes approximately constant for $M_1 \gg 10^{12}$ GeV (see Fig. 6.13) with a CP-conserving R-matrix, then one can can use the value of η_B that is predicted by the two-flavour Boltzmann equations (2FBE) at the start of the transition $M_1 \sim 10^{12}$ GeV as a proxy for the full solution of the density matrix equations (DME). That is,

$$\eta_B^{\rm DME}\left(M_1 \gg 10^{12}\ {\rm GeV}\right) \approx \eta_B^{\rm 2FBE}\left(M_1 \sim 10^{12}\ {\rm GeV}\right), \tag{6.5.10}$$

provided that the ratios M_2/M_1 and M_3/M_1 are fixed. This has the advantage that we may again make use of the result in Eq. (6.3.3)

$$n_{B-L} \approx n_B^{\rm 2FBE}\left(M_1 \sim 10^{12}\ {\rm GeV}\right) = \frac{\pi^2}{6 z_d K_1} n_{N_1}^{\rm eq}(0)\epsilon_{\tau\tau}^{(1)}\Delta F, \tag{6.5.11}$$

in order to gain an analytical understanding of the numerical solutions.

As in the analysis of Section 6.4.1, we investigate the cases where CP violation comes from precisely one of δ, α_{21} or α_{31}. Unlike the fine-tuned scenario previously considered, $p_{1\tau}$ and consequently ΔF are approximately constant with the PMNS phases as would be expected from our discussion of the fine-tuned solutions in Section 6.4.2. Hence the phase-dependence of the η_B can be understood by reference to $\epsilon_{\tau\tau}^{(1)}$ alone. This may also be understood by reference to the Yukawa couplings when CP violation comes only from δ, α_{21} or α_{31} respectively:

$$\begin{aligned} Y_{\tau 1} &= -0.0476 - 0.000364 e^{i\delta}, \\ Y_{\tau 1} &= -0.0541 + 0.00614 e^{i\frac{\alpha_{21}}{2}}, \\ Y_{\tau 1} &= 0.00972 - 0.0576 e^{i\frac{\alpha_{31}}{2}}. \end{aligned} \tag{6.5.12}$$

The difference in scale of the two terms means that the cancellation is never strong

for any value of the phase and so the peaks in ΔF are not large. In this high scale case, ΔF is approximately constant and thus the plots of η_B exhibit a nearly pure sinusoidal variation given by the CP-asymmetries below.

Dirac phase CP violation

In this case, with a real R, we have $\alpha_{21} = \alpha_{31} = 0^\circ$ such that δ is the sole provider of all CP violation. The asymmetry is given by

$$\epsilon^{(1)}_{\tau\tau} = -1.25 \times 10^{-6} \sin\delta, \tag{6.5.13}$$

in this scenario. Thus we obtain a sinusoidal dependence with $\eta_B = 0$ when $\delta = 0^\circ$ or 180°. Fixing all other parameters at their benchmark value with $y_1 = y_2 = y_3 = 0$, no value of δ can produce the observed baryon asymmetry of the Universe. Unlike in the case of intermediate scale leptogenesis, a small scaling of the heavy Majorana neutrino masses will not much increase the value of η_B because of the plateau of Fig. 6.13. At the best-fit point of Table 6.4, with $\alpha_{21} = \alpha_{31} = 0^\circ$, allowing CP violation only from δ, the largest η_B achieved is a factor ~ 9 smaller than the observed value. This is large enough that even enormously larger scales of the heavy masses cannot make δ-only leptogenesis a viable option.

An alternative for producing the observed baryon asymmetry of the Universe with CP violation only from δ is to work with an R-matrix containing both zero and purely imaginary components which are CP-conserving and may potentially be large in magnitude. If for example, we choose $x_i = 0^\circ$ such that all w_i are either purely imaginary or zero, and take $y_2 = 0^\circ$ also, then by setting $\alpha_{21} = 180^\circ$ and $\alpha_{31} = 0^\circ$, all CP violation will be due to δ. Varying y_1 and y_2 together in this setup, we find that $y_1 = y_2 = 169^\circ$ is the smallest value for which the observed baryon asymmetry of the Universe is produced. With all other parameters equal to the values in Table 6.4, this corresponds to $\mathcal{F} = 105$. Hence a noticeable degree of fine-tuning is required even at high scales to make δ the sole contributor to CP violation with viable leptogenesis. In Fig. 6.14, we plot the variation of η_B with pure δ CP violation for this fine-tuned

scenario in the left plot, and on the right we parametrically plot η_B against J_{CP} as a function of δ.

CP Violation from the Majorana phase α_{21}

Similarly, when $\delta = \alpha_{31} = 0°$, the CP-asymmetry is

$$\epsilon^{(1)}_{\tau\tau} = 1.98 \times 10^{-5} \sin \frac{\alpha_{21}}{2}. \tag{6.5.14}$$

It follows from the preceding expression for $\epsilon^{(1)}_{\tau\tau}$ that at the CP-conserving values of $\alpha_{21} = 180°, 540°$ we have $\epsilon^{(1)}_{\tau\tau} \neq 0$. This corresponds to the case of CP-conserving R-matrix ($y_i = 0$), CP-conserving PMNS matrix, but CP-violating interplay between the R and PMNS matrix elements in leptogenesis [130].

The corresponding η_B, plotted in the left plot of Fig. 6.15 is thus a factor of $\mathcal{O}(10)$ higher and of opposite sign than in the previous case without fine-tuning. Thus, we obtain the observed baryon asymmetry of the Universe (or higher) for values of α_{21} between about 450° and 650°. In the right plot of Fig. 6.15 is η_B for the same scenario parametrically plotted against the effective neutrino mass with parameter α_{21}.

CP Violation from the Majorana phase α_{31}

Finally, we turn to the scenario in which CP violation is provided entirely by α_{31}, plotted on the left in of Fig. 6.16 for which

$$\epsilon^{(1)}_{\tau\tau} = -3.22 \times 10^{-5} \sin \frac{\alpha_{31}}{2}. \tag{6.5.15}$$

Similarly to the case discussed in the preceding subsection, we see that $\epsilon^{(1)}_{\tau\tau} \neq 0$ at the CP-conserving values of $\alpha_{31} = 180°, 540°$. This again corresponds to the case of CP violation in leptogenesis due to the interplay of the CP-conserving R-matrix ($y_i = 0$) and CP-conserving PMNS matrix [130].

Compared with the previous scenario, there is a sign flip and an enhancement by a factor ~ 1.6 of the resulting baryon asymmetry of the Universe. Thus, the observed BAU is achieved and exceeded for smaller values of α_{31}, between about 50° and 300°. On the right of Fig. 6.16, we display a parametric plot for the same scenario with η_B against the effective neutrino Majorana mass with the parameter α_{31}.

6.6 Conclusions

In this chapter we have investigated the connection between leptogenesis and low energy leptonic CP violation over a large range of scales ($10^6 < M_1$ (GeV) $< 10^{13}$). We summarise our main findings below:

- Firstly, we revisited the question of the possibility of successful thermal leptogenesis at scales $10^9 < M_1$ (GeV) $< 10^{12}$. At such scales, tau-Yukawa interactions are in equilibrium, such that there are sufficiently frequent interactions between the leptons and the early Universe plasma causing decoherence between the tau flavour from the other flavour components. We show that successful leptogenesis is indeed possible in this range of scales in the case that the PMNS phases provide all of the CP violation in the model. By performing parameter explorations at $M_1 = 10^9$ GeV and $M_1 = 10^{10}$ GeV, we found that some degree of fine-tuning, $\mathcal{F} \sim 10$, is required for these particular mass scales (with the degree of fine-tuning diminishing as one goes to higher values of M_1).

- By demanding pure Dirac phase or pure Majorana phase CP violation, we found that each phase alone can produce the correct CP-asymmetry, with the cases of Majorana phases requiring, in general, a somewhat lower value of M_1 than those required for the Dirac phase.

- If leptogenesis takes place at scales $M_1 \ll 10^9$ GeV, then all three of the leptonic flavour components involved in leptogenesis will decohere. For masses in this range ($M_1 \sim 10^6$ GeV and $M_1 \sim 10^8$ GeV), we determined the regions of

parameter space in which low energy leptonic CP violation, provided by either the Dirac or the Majorana phases individually, leads to successful intermediate scale leptogenesis. At these scales a large amount of fine-tuning ($\mathcal{F} \sim \mathcal{O}(100)$) is required between the tree-level and one-loop neutrino masses. We restricted ourselves to fine-tuning such that $\mathcal{F} < 1000$ and in doing so have found an approximate lower bound of $M_1 \approx 3 \times 10^6$ GeV (consistent with the conclusions of [5]).

- We studied the possibility of pure Dirac phase CP violation and showed that for $\mathcal{F} < 1000$, $M_1 \gtrsim 8 \times 10^6$ GeV in order to produce the observed baryon asymmetry. Similarly for the purely Majorana phase CP violation and again $\mathcal{F} < 1000$, for α_{21}, we obtain a bound $M_1 \approx 4.5 \times 10^6$ GeV whereas for α_{31} we obtained $M_1 \approx 3 \times 10^6$ GeV. Observables depending on the Dirac and Majorana phases, for example J_{CP} or $\langle m_\nu \rangle$, may be well within experimental bounds in the same parts of parameter space in which leptogenesis is successful. The Dirac phase δ is only very weakly constrained, with the tightest constraint being $\delta \in [16, 263]^\circ$, for 1σ agreement with the observed BAU, which comes from assuming normal ordering and $M_1 = 1.29 \times 10^8$ GeV.

- If leptogenesis takes place at high scales, with $M_1 \gg 10^{12}$ GeV, interactions between the leptons and the early Universe plasma only very weakly decohere the tau flavour from the other flavour components. Normally, this leads to the conclusion that the single flavour Boltzmann equations are an appropriate description of the process. However, we have demonstrated that, if CP violation arises only in the low energy leptonic sector, the effects of decoherence cannot be neglected. Therefore, one should not ignore the phenomenology of high-scale leptogenesis with purely low-energy CP violation.

- We explored the parameter space at $M_1 \sim 10^{13}$ GeV, finding regions in which thermal leptogenesis is a viable explanation of the BAU. We found that the strongest constraint on δ is for normal ordering, for which we require $\delta \in$

$[240, 331]^\circ$ to produce a baryon asymmetry within 1σ of the observed value. With only Dirac phase CP violation, we have concluded that it is not possible produce the observed baryon asymmetry of the Universe unless one introduces significant fine-tuning ($\mathcal{F} \sim 100$) in the light neutrino masses. We argued that there is no scale of the heavy Majorana neutrino masses beyond $M_1 \gg 10^{12}$ GeV for which Dirac phase leptogenesis may be made to work without this fine-tuning. However, with pure Majorana phase violation, we found that successful leptogenesis is possible with essentially no fine-tuning.

The results of this chapter underscore the significance of understanding leptonic CP violation through experimental searches for Dirac and/or Majorana leptonic CP violation. We have departed from previous literature by concluding that low energy leptonic CP-violating phases may always be relevant to the production of the baryon asymmetry in the thermal leptogenesis scenario. It has commonly been thought that their relevance was limited to the window of masses $10^9 \lesssim M_1\ (\text{GeV}) \lesssim 10^{12}$. However, we have shown this window to be significantly wider: Dirac and Majorana phases may be crucial to thermal leptogenesis even at scales as low as $M_1 \sim 10^6$ GeV (provided there are fine-tuned cancellations), or as high as $M_1 \gg 10^{12}$ GeV, where in both cases, the R-matrix is CP-conserving.

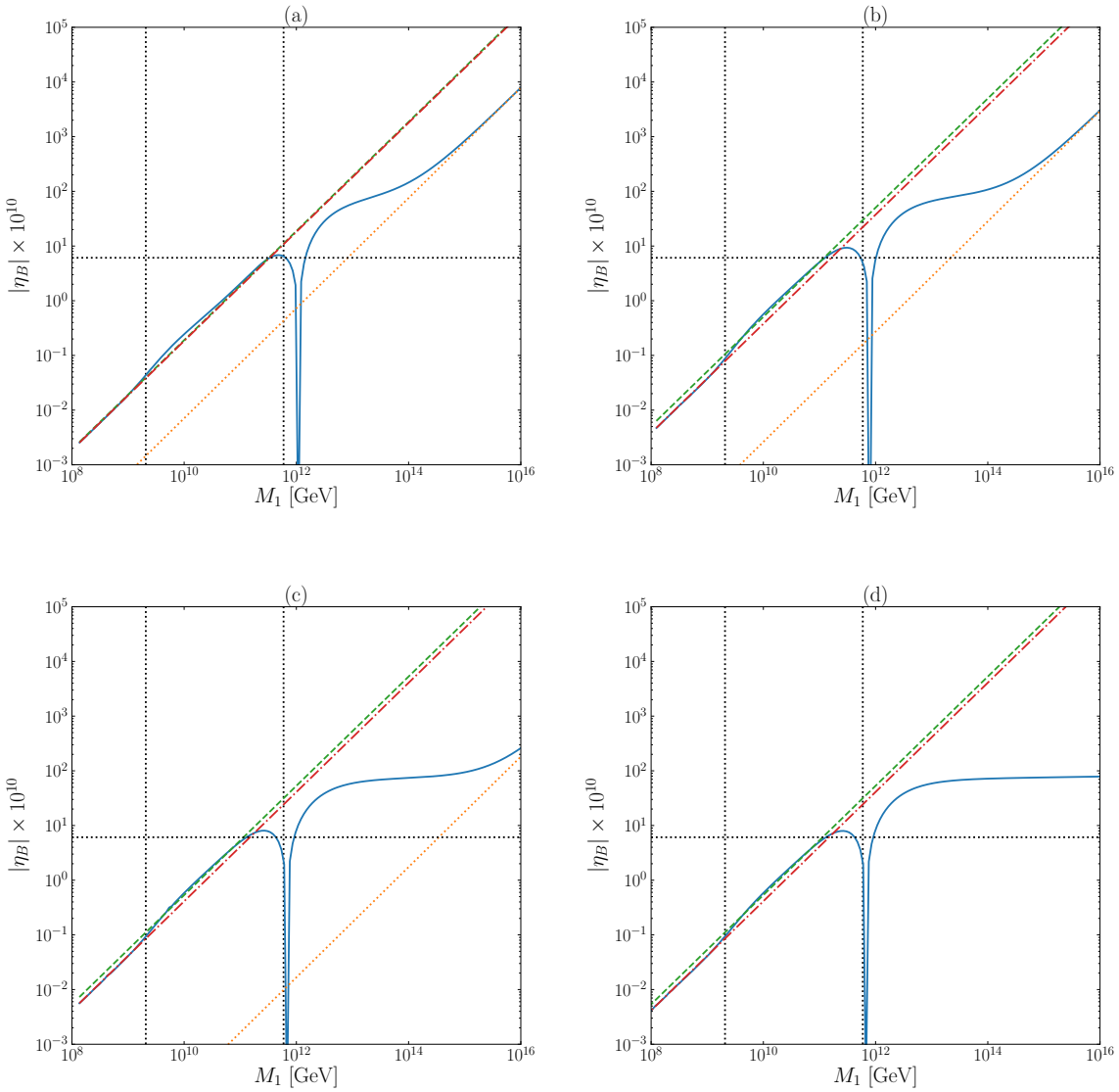

Figure 6.13: The magnitude of the baryon asymmetry as a function of the heavy Majorana neutrino masses at a specific point in parameter space. The dotted orange line corresponds to solutions of the single-flavour Boltzmann equations, the dashed green line to those of the two-flavour Boltzmann equation, the red dot-dashed line to those of the three-flavour Boltzmann equations and the solid blue line to solutions of the density matrix equations. The horizontal black dotted line is the observed value of $\eta_{B_{\rm CMB}}$ and the vertical dotted lines to the values of the muon and tau thermal widths. We vary y_3 such that in (a) $y_3 = 30°$, in (b) $y_3 = 5°$, in (c) $y_3 = 0.3°$ and in (d) $y_3 = 0°$. As y_3 is the only complex parameter of the R-matrix for this parameter point, then plot (d) corresponds to the case of purely low-energy CP violation. As the CP violation becomes solely low energy (going from (a) to (d)), then the transition of the density matrix equations to the single-flavour regime becomes longer. This culminates in an infinite transition width in plot (d) — a plateau in the baryon asymmetry for high-scale leptogenesis. The dip in all of the blue lines occurs as a consequence of the change in sign of the produced asymmetry.

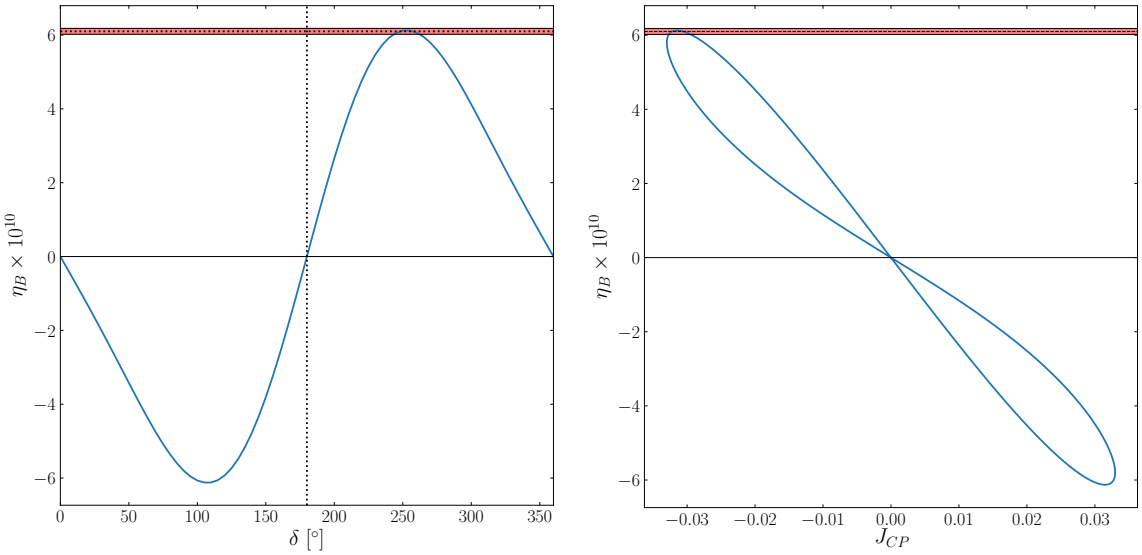

Figure 6.14: Leptogenesis at high scales ($M_1 = 3.16 \times 10^{13}$ GeV) with CP violation provided solely by δ, with $\alpha_{21} = 0°$ and $\alpha_{31} = 0°$. The red band indicates the 1σ observed values for η_B with the best-fit value indicated by the horizontal black dotted lines. Left: The baryon asymmetry as a function of δ with exact CP-invariance exists for $\delta = 0°$ and $180°$ (vertical black dotted lines). In order to make the maximum value touch on the observed baryon asymmetry, an amount of fine-tuning $\mathcal{F} = 105$ is needed. Right: The corresponding variation of η_B against J_{CP} parametrically plotted with δ. See the text for further details.

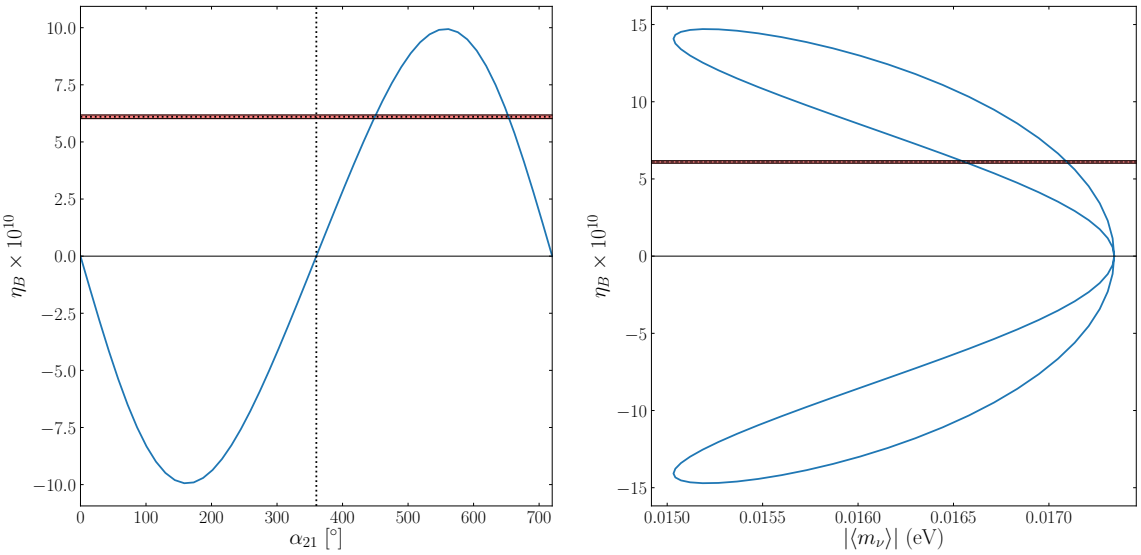

Figure 6.15: Leptogenesis at high scales ($M_1 = 3.16 \times 10^{13}$ GeV) when CP violation is provided solely by α_{21}, with $\delta = 0°$, $\alpha_{31} = 0°$. The red bands indicate the 1σ observed values for η_B with the best-fit value indicated by the horizontal black dotted lines. Left: The baryon asymmetry as a function of α_{21} with exact CP-invariance at $\alpha_{21} = 0°$ and $360°$ (vertical black dotted lines). Right: The variation of η_B against $|\langle m_\nu \rangle|$ parametrically plotted as a function of α_{21}. Successful leptogenesis occurs for $\alpha_{21} \approx 449°$ and $\alpha_{21} \approx 653°$ for which $|\langle m_\nu \rangle| = 0.0171$ eV and $|\langle m_\nu \rangle| = 0.0166$ eV respectively. See text for further details.

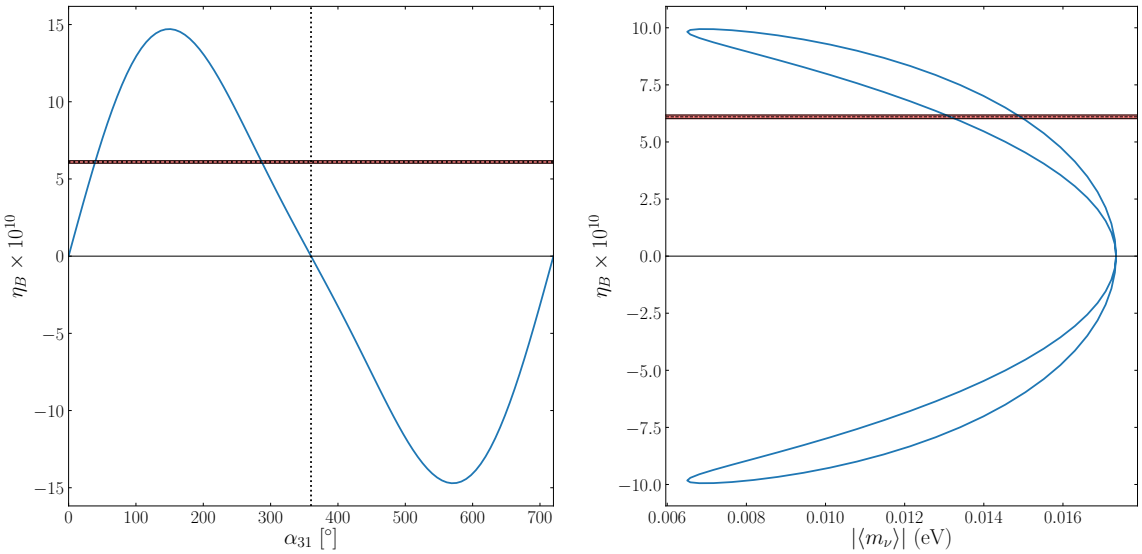

Figure 6.16: High-scale leptogenesis ($M_1 = 3.16 \times 10^{13}$ GeV) with CP violation is provided solely by α_{31}, with $\delta = 0°$, $\alpha_{21} = 0°$. The red bands indicate the 1σ observed values for η_B with the best-fit value indicated by the horizontal black dotted lines. Left: The baryon asymmetry as a function of α_{31}, with exact CP-invariance when $\alpha_{31} = 0°$ and $360°$ (vertical black dotted lines). Right: The parametric plot of η_B against the effective neutrino Majorana mass $|\langle m_\nu \rangle|$ as α_{31} is varied. At the values $\alpha_{31} = 17°, 43°$, η_B takes on its observed values corresponding to $|\langle m_\nu \rangle| = 0.0131$ eV, 0.0149 eV respectively. See the text for further details.

Chapter 7

Leptogenesis in the Neutrino Option

There exists a tension between leptogenesis within the type I seesaw mechanism and the naturalness of the Higgs potential. This is because radiative corrections to the Higgs potential increase monotonically with the mass scale of the heavy Majorana neutrinos. In a natural scenario, where the corrections to the Higgs mass do not exceed 1 TeV, the heavy Majorana neutrino mass scale must satisfy $M < 3 \times 10^7$ GeV [185, 186], which is considerably lower than the Davidson-Ibarra bound for successful leptogenesis $M \gtrsim 10^9$ GeV [1] [119–121].

A different perspective on this problem is brought by the so-called Neutrino Option scenario [2, 8] which is based on the idea that the Higgs potential is generated by the radiative corrections of the heavy Majorana neutrinos, starting from an approximately conformal scalar potential at the seesaw scale. The Neutrino Option scenario can be realised for instance within a conformal UV theory as shown in [262, 263]. In the Neutrino Option framework the heavy Majorana neutrino masses are the only dimensionful parameters of the theory and they effectively control both the breaking of the conformal symmetry and that of lepton number.

[1] We recall that the Davidson-Ibarra bound is valid for hierarchical heavy Majorana neutrino mass spectrum and in the case of absence of flavour effects in leptogenesis.

In this chapter we will investigate the possibility of successful leptogenesis within the Neutrino Option framework and focus on the minimal scenario where there are only two heavy Majorana neutrinos providing both the Higgs mass and the baryon asymmetry. We show that in order for leptogenesis to be successful within the Neutrino Option approach to electroweak symmetry breaking, it is necessary for the two heavy neutrinos to be close in mass (forming a pseudo-Dirac pair [264, 265] at the lowest viable mass scales) and their masses to be in the range $M \sim 10^6 - 10^7$ GeV. From these considerations, we derive an upper and lower bound on this mass scale. The upper bound coincides with that found for the Neutrino Option alone [2], while the lower bound comes from the additional requirement of viable leptogenesis. We explore the naturalness in the neutrino sector in terms of the presence of an approximately conserved lepton charge. We investigate also the production of the baryon asymmetry when the requisite CP violation in leptogenesis is provided exclusively by the low energy phases of the PMNS matrix.

7.1 The Neutrino Option

It has been recently suggested that the heavy Majorana fields, N_i, introduced in the type I seesaw model could be responsible for the dynamical generation of the scalar potential of the Standard Model, in addition to that of neutrino masses [2, 8]. In this scenario, dubbed the Neutrino Option, the classical potential is given by

$$V_0(\phi) = -\frac{m_{H0}^2}{2}\phi^\dagger\phi + \lambda_0(\phi^\dagger\phi)^2, \tag{7.1.1}$$

and is assumed to be nearly conformal at the seesaw scale: $m_{H0}(\mu \gtrsim M) \simeq 0$, $\lambda_0(\mu \gtrsim M) \neq 0$, μ being the renormalisation scale. Radiative corrections to both m_H^2 and λ are generated via the diagrams of Fig. 7.1, thus breaking scale invariance at the quantum level. At scales $\mu < M$ the N_i fields can be integrated out and decoupled from the spectrum. One is then left with an Effective Field Theory (EFT) in which the leading seesaw contributions are encoded in the Weinberg operator for neutrino

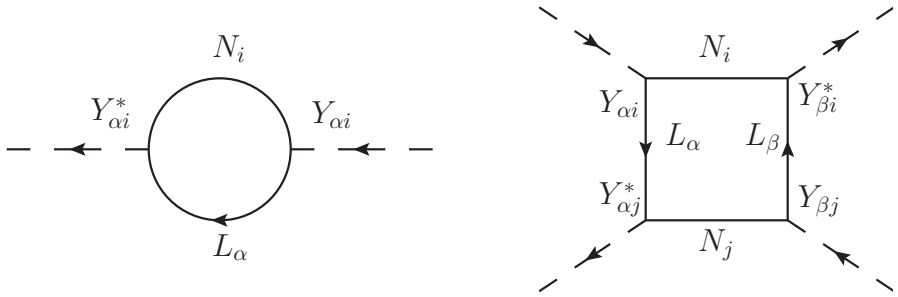

Figure 7.1: The dominant one-loop contribution generating the Higgs potential in the type-I seesaw model.

masses (stemming from the seesaw-EFT matching at tree-level) and in finite *threshold matching contributions* to the Higgs potential parameters Δm_H^2, $\Delta\lambda$ (stemming from the one-loop matching). The latter are identified as the zeroth order term in the E/M expansion of the loops, computed with dimensional regularisation within the $\overline{MS}$ renormalisation scheme. For the case of two heavy Majorana neutrinos with $M_2 = x_M M_1$, $x_M \geq 1$ they read [2]:

$$\begin{aligned}\Delta m_H^2 &= \frac{M_1^2}{8\pi^2}\left(|Y_1|^2 + x_M^2|Y_2|^2\right) , \\ \Delta\lambda &= -\frac{1}{32\pi^2}\left[5|Y_1|^4 + 5|Y_2|^4 + 2\,\mathrm{Re}(Y_1\cdot Y_2^*)^2\left(1 - \frac{2\log x_M^2}{1-x_M}\right)\right. \\ &\quad \left. +2\,\mathrm{Im}(Y_1\cdot Y_2^*)^2\left(1 - \frac{2\log x_M^2}{1+x_M}\right)\right] ,\end{aligned} \tag{7.1.2}$$

with Y_i the ith column of the matrix of neutrino Yukawa couplings. In the limit $M_2 = M_1$ ($x_M = 1$) these reduce to [2]:

$$\begin{aligned}\Delta m_H^2 &= \frac{M_1^2}{8\pi^2}\left(|Y_1|^2 + |Y_2|^2\right) , \\ \Delta\lambda &= -\frac{5}{32\pi^2}\left(|Y_1|^4 + |Y_2|^4 + 2\,\mathrm{Re}(Y_1\cdot Y_2^*)^2\right) - \frac{1}{16\pi^2}\mathrm{Im}(Y_1\cdot Y_2^*)^2 .\end{aligned} \tag{7.1.3}$$

The values of m_H, λ at the EW scale can be extrapolated using the renormalisation group equations (RGEs) of the SM [3] (as the heavy neutrinos are not present in the

[2]Note that although modified Feynman rules must be used when the heavy Majorana neutrinos are nearly degenerate in mass, this is only important when results, such as the CP asymmetry, depend on the difference of masses. In the calculation of the Higgs mass parameter, the contributions from each heavy Majorana neutrino are summed and any correction depending on the difference of the masses is negligible.

spectrum) with the following boundary conditions:

$$m_H^2(\mu = M_1) \equiv \Delta m_H^2 \quad \text{and} \quad \lambda(\mu = M_1) \equiv \Delta\lambda + \lambda_0 \,. \tag{7.1.4}$$

The condition on m_H places the strongest constraint on the parameter space of the Neutrino Option, requiring $M_i \lesssim 10^7$ GeV and $|Y_{\alpha i}| \sim 1\text{TeV}/M_i$ (barring tunings between the Yukawa entries) in order to reproduce the correct Higgs mass and, at the same time, be consistent with the constraints from neutrino oscillation experiments. A similar region of the parameter space has been previously identified as sensitive in relation with the Higgs mass, although in a different approach, in [185, 266]. In fact, as neither m_H nor the light neutrino masses change significantly under RGE running, this result is consistent to a good approximation with the order-of-magnitude estimate

$$m_H^2(\mu = v) \simeq \Delta m_H^2 \sim \frac{M_i^2 |Y_i|^2}{8\pi^2} \quad \text{and} \quad m_\nu(\mu = v) \simeq \frac{v^2 |Y_i|^2}{2M_i} \,. \tag{7.1.5}$$

Within this region of the parameter space the contribution to the Higgs quartic term is $|\Delta\lambda| \leq 10^{-7}$. As a consequence, the threshold matching contribution is always negligible in comparison to the coupling in the classical potential which has to be positive and of loop size ($\lambda_0 \simeq 0.01 - 0.05$) in order to obtain the correct scalar potential at the EW scale [2].

7.2 The framework of resonant leptogenesis

Throughout this chapter we use the flavoured Boltzmann equations for thermal leptogenesis given in Eq. (3.3.23) and restrict ourselves to the case in which only two heavy Majorana neutrinos are present, or equivalently, the case when the third heavy Majorana neutrino, N_3, decouples. For concreteness, we also assume $M_1 \leq M_2$. In the considered scenario, the sum of neutrino masses is $\sum_{i=1}^{3} m_{\nu_i} \cong 0.058\,(0.10)$ eV for NO (IO) neutrino mass spectrum, which is well within the cosmological upper limit reported by the Planck collaboration, $\sum_i m_i < 0.120 - 0.160$ eV at 95% C.L. [36].

As will be discussed in further detail in Section 7.3, we find it necessary to take the two heavy Majorana neutrinos to be nearly-degenerate in mass $\Delta M = M_2 - M_1 \ll M \equiv \frac{1}{2}(M_1 + M_2)$ and thereby $\Delta M \sim \Gamma$. In this case, one is concerned with resonant leptogenesis [193, 245] where the self-energy contribution to the CP asymmetry parameter may become large. Such enhancement of the asymmetry can be significant, allowing the energy scale for successful leptogenesis to be lowered by several orders of magnitude. For this reason, resonant leptogenesis has been most often explored in the literature within scenarios with Majorana masses of the order of a few TeV. Here we apply this paradigm to a wider energy range. The peculiarity of resonant leptogenesis is that non-negligible contributions to the CP-asymmetries can be induced by mixing and oscillation of the heavy Majorana neutrinos. The mixing effects come from the possibility of off-diagonal transitions in the self-energy diagrams at $T = 0$ which are included through use of the resummed Yukawa couplings [267]. In the same regime, $\Delta M \sim \Gamma$, the thermal contributions to the self-energies are also important. This provides an extra contribution to the CP asymmetries in processes where on-shell heavy Majorana neutrinos oscillate in flavour space due to their interactions with a thermal background [268]. The CP asymmetry which takes account of both the mixing and oscillation of the heavy Majorana neutrinos has the form [269]:

$$\epsilon^{(i)}_{\alpha\alpha} = \sum_{j\neq i} \frac{\mathrm{Im}\left[Y^\dagger_{i\alpha} Y_{\alpha j} \left(Y^\dagger Y\right)_{ij}\right] + \frac{M_i}{M_j}\,\mathrm{Im}\left[Y^\dagger_{i\alpha} Y_{\alpha j} \left(Y^\dagger Y\right)_{ji}\right]}{\left(Y^\dagger Y\right)_{ii}\left(Y^\dagger Y\right)_{jj}} \left(f^{\mathrm{mix}}_{ij} + f^{\mathrm{osc}}_{ij}\right) , \quad (7.2.1)$$

where

$$f^{\mathrm{mix}}_{ij} = \frac{\left(M_i^2 - M_j^2\right) M_i \Gamma_j}{\left(M_i^2 - M_j^2\right)^2 + M_i^2 \Gamma_j^2} , \quad (7.2.2)$$

and

$$f^{\mathrm{osc}}_{ij} = \frac{\left(M_i^2 - M_j^2\right) M_i \Gamma_j}{\left(M_i^2 - M_j^2\right)^2 + \left(M_i\Gamma_i + M_j\Gamma_j\right)^2 \frac{\det\left[\mathrm{Re}\left(Y^\dagger Y\right)\right]}{\left(Y^\dagger Y\right)_{ii}\left(Y^\dagger Y\right)_{jj}}} . \quad (7.2.3)$$

7.3 Leptogenesis at the scales required for the Neutrino Option

The largest value of the heavy Majorana neutrino masses compatible with the Standard Model Higgs mass in the Neutrino Option scenario is $M_i \sim 10^7$ GeV. A lower bound on the heavy Majorana neutrino masses can be set by the requirement of perturbativity of the neutrino Yukawa couplings and is $M_i \gtrsim \mathcal{O}(10^2)$ GeV[3]. In such a regime, in order for the neutrino masses to satisfy the existing limits, fine tuned cancellations must exist between the tree level seesaw and the one-loop contributions to the light neutrino masses.

From the lower bound derived from perturbativity arguments to the upper bound from the Neutrino Option itself, there are are two possible mechanisms of leptogenesis viable in the relevant heavy Majorana neutrino mass range:

1. Thermal leptogenesis with enhanced R-matrices [5] (see also [192, 243]).

2. Resonant leptogenesis with nearly degenerate heavy Majorana neutrino masses [128, 193, 213, 270–275].

In this subsection, we shall argue that the fine-tuned scenario (1) is incompatible with the Neutrino Option, and therefore justify our exclusive use the resonant method for the investigations in this work. The arguments we present here are valid in the more general case of three heavy Majorana neutrinos which we consider below.

In the fine-tuned case the elements of the R-matrix elements tend to be large and the one-loop contribution to the light neutrino masses should be incorporated through modification of the Casas-Ibarra parametrisation [72]. In this case, the R-matrix

[3] The lower bound on M_1 as shown in Fig. (3) of [2] comes from the additional assumption that $|\sin(x+iy)| < 1$, that constrains the width of the allowed bands in the figure. This assumption was introduced in order to forbid explicitly fine tunings in the flavour space, but can be relaxed in full generality.

has the structure [5]:

$$R \approx \begin{pmatrix} R_{11} & R_{12} & R_{13} \\ \pm iR_{22} & R_{22} & R_{23} \\ -R_{22} & \pm iR_{22} & \pm iR_{23} \end{pmatrix}, \tag{7.3.1}$$

Here $|R_{22}| \gg |R_{1i}|, |R_{23}|$ for $i \in \{1, 2, 3\}$, which results, in [5]

$$m_\nu^0 \approx -m_\nu^1 . \tag{7.3.2}$$

A typical fine-tuned leptogenesis solution, which allows for partial cancellations between the tree and one-loop level contributions to the light neutrino masses, requires $M_1 \approx 5 \times 10^6$ GeV (see the scenarios of [5]) and correspond to large values $\sqrt{\Delta m_H^2} \sim 8 \times 10^6$ GeV. The latter value owes its magnitude to the dependence of Δm_H^2 on the R-matrix elements which are themselves large in order to provide the fine-tuning of Eq. (7.3.2).

We performed a numerical search of the parameter space with heavy neutrino masses $\sim 10^6$ GeV and found no points which simultaneously satisfy the requirements of the Neutrino Option and leptogenesis even when we allowed m_ν^0 and m_ν^1 to cancel to $\sim 0.1\%$. When no constraint was placed on the levels of fine-tuning it was possible to find solutions with the desired value of η_B and $\sqrt{\Delta m_H^2} \sim 100$ GeV. Such solutions corresponds to an R-matrix with very large entries, $|R_{ij}| \sim 10^{12}$, and very small (physically unreasonable) heavy neutrino masses $M_i \sim 10^{-2}$ GeV. The fine-tuned cancellation between the tree- and one-loop light neutrino masses is so complete that the higher-order radiative corrections to the light neutrino masses dominate and exceed the light neutrino mass bound. Using the estimate that the two-loop contribution to the light neutrino masses is

$$\left|m_\nu^2\right| \sim \frac{1}{16\pi^2} \left|m_\nu^1\right| \text{max.}(|Y|)^2 \approx \frac{1}{16\pi^2} \left|m_\nu^0\right| \text{max.}(|Y|)^2,$$

where max.$(|Y|)$ is the largest element of the matrix of absolute values of neutrino Yukawa couplings, and where we use the approximate equality of Eq. (7.3.2), we

estimate

$$m_\nu^2 \sim 10^3 \text{ GeV},$$

which is well-excluded by the experimental constraints. In summary, we found only physically non-viable solutions involving fine-tuned non-resonant leptogenesis. For this reason, for the remainder of this work we restrict ourselves to resonant leptogenesis in which $M_1 \approx M_2$ and where N_3 is decoupled.

7.4 Results

In this section we present our main results. In Section 7.4.1, we derive the lower bound on the mass scale M for which leptogenesis is viable within the Neutrino Option and explore the available parameter space and in Section 7.4.2 we find the corresponding upper bound.

7.4.1 Lower bound on the heavy Majorana neutrino masses

In this section we determine the range of heavy Majorana neutrino masses in which both the Neutrino Option and leptogenesis are viable. We shall always work in the nearly degenerate case $\Delta M \equiv M_2 - M_1 \ll M$ where $M \equiv (M_1 + M_2)/2$. Evaluating Δm_H^2 at $\mu \sim M$ as is calculated in [2], the threshold correction is

$$\Delta m_H^2 = \frac{1}{8\pi^2} \text{Tr}\left[Y M^2 Y^\dagger\right]. \tag{7.4.1}$$

By substitution of the Casas-Ibarra parametrisation of Eq. (2.4.26) or Eq. (2.4.28), this becomes

$$\Delta m_H^2 = \frac{1}{8\pi^2 v^2} \cosh(2y) M^3 (m_1 + m_2 + m_3), \tag{7.4.2}$$

where the neutrino parameters run with the scale M. This effect amounts to a few percent for the light neutrino masses and is implemented here using the RGEs of Refs. [276, 277]. The remainder of the neutrino parameters change less significantly when RG evolved, so their scale dependence will be neglected. Note that the x

inputs	value (GeV)	RGE boundary conditions at $\mu = m_t$			
v	174.10	λ	0.1258	m_H(GeV)	131.431
m_H	125.09	g_1	0.461	Y_t	0.933
m_t	173.2	g_2	0.644	Y_b	0.024
		g_3	1.22029	Y_τ	0.0102

Table 7.1: Values of the relevant SM parameters adopted in the numerical analysis, consistent with Ref. [2]. The RGE boundary conditions are computed at the highest accuracy provided in Ref. [3].

parameter (the real part of θ which parametrises the R matrix), cancels in (7.4.2) due to the near-diagonality of the heavy Majorana mass matrix. The Neutrino Option is then satisfied if the Standard Model $\overline{MS}$ Higgs mass, when renormalisation group evolved to the scale M, matches the values given by Δm_H^2. The running of the SM parameters is taken into account implementing the RGE of Ref. [3] to the highest available accuracy and with the numerical inputs reported in Table 7.1.

The lower bound on M for leptogenesis in the Neutrino Option is the lowest scale for which the correct baryon asymmetry results whilst still satisfying Eq. (7.4.2). We apply the approximate analytical solution

$$n_{B-L} \approx \frac{\pi^2}{6 z_d} n^{\rm eq}(0) \sum_{\alpha=e}^{\tau} \frac{\epsilon^{(1)}_{\alpha\alpha}}{K_1 p_{1\alpha}}, \tag{7.4.3}$$

in the derivation of which we have eliminated $\epsilon^{(2)}_{\alpha\alpha}$ with the approximation $\epsilon^{(2)}_{\alpha\alpha}/K_2 p_{2\alpha} \approx \epsilon^{(1)}_{\alpha\alpha}/K_1 p_{1\alpha}$. For the lowest heavy Majorana neutrino mass scale M, the value of y (the imaginary part of θ) will be largest as can be seen from inspection of Eq. (7.4.2). Approximating the terms in the sum under the assumption that $e^y \gg e^{-y}$ (to be justified later), we find

$$\begin{aligned} \frac{\epsilon^{(1)}_{\alpha\alpha}}{K_1 p_{1\alpha}} &\approx 16 m_* \left(f_{\rm osc} + f_{\rm mix}\right) \frac{m_2 - m_3}{(m_2 + m_3)^2} e^{-4y} \sin 2x\,, \quad \text{Normal Ordering}\,, \\ \frac{\epsilon^{(1)}_{\alpha\alpha}}{K_1 p_{1\alpha}} &\approx 16 m_* \left(f_{\rm osc} + f_{\rm mix}\right) \frac{m_1 - m_2}{(m_1 + m_2)^2} e^{-4y} \sin 2x\,, \quad \text{Inverted Ordering}\,. \end{aligned} \tag{7.4.4}$$

Using the same approximation, the factor $\propto \det[{\rm Re}(Y^\dagger Y)]$ in the denominator of

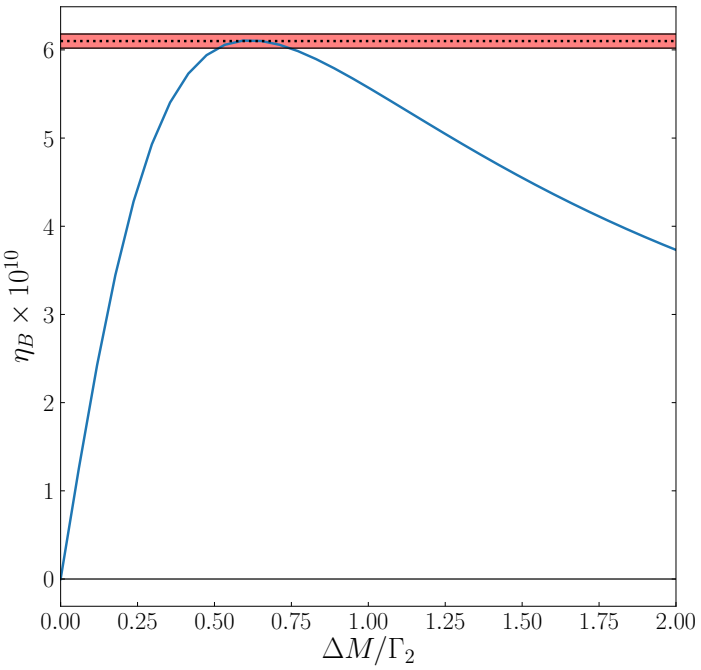

Figure 7.2: The baryon asymmetry as a function of the heavy Majorana neutrino mass splitting divided by the decay rate of N_2 at the lower-bound of M for successful leptogenesis in the Neutrino Option. The plots take an identical form for both normal ordering (for which $\Gamma_2 = 1.62 \times 10^{-2}$ GeV) and inverted ordering (for which $\Gamma_2 = 8.63 \times 10^{-3}$ GeV).

$f_{\rm osc}$ (see Eq. (7.2.3)) becomes

$$\frac{\det\left[\mathrm{Re}\left(Y^\dagger Y\right)\right]}{\left(Y^\dagger Y\right)_{11}\left(Y^\dagger Y\right)_{22}} \approx 1.$$

From Eq. (7.4.4) we observe that the parameter y exponentially suppresses the final asymmetry η_B while enhancing the Higgs mass of Eq. (7.4.2). To the level of accuracy in the approximation, the contribution of each flavour is identical. Although the left-hand side carries a flavour index α, the right-hand side is independent of this index. As the flavour information is contained in the PMNS elements, we expect that at large y, the solutions for successful leptogenesis in the Neutrino Option should have only a weak dependence on the PMNS phases (in terms that have been neglected in Eq. (7.4.4)).

The lower bound on M may be found by maximising the terms in Eq. (7.4.4) with respect to all parameters except y and then finding the largest value of y for which leptogenesis may be successful. From Eq. (7.4.2), we observe the scale of M is determined from y (recalling that the light neutrino masses are to be run to the scale M) and may therefore infer the lower bound for successful leptogenesis in the Neutrino Option. The maximisation of the right-hand side of Eq. (7.4.4) occurs when $x = 135^\circ$ or 315° (note the negative prefactors of the trigonometric factors) and $\Delta M/\Gamma_2 \approx 0.61$. We find that the values of y that give agreement with $\eta_{B_{\rm CMB}}$ are $y = 190.22^\circ$ for normal ordering and $y = 118.21^\circ$ for inverted ordering. These imply lower bounds for viable leptogenesis in the Neutrino Option of

$$M > 1.2 \times 10^6 \text{ GeV} \quad \text{Normal Ordering},$$
$$M > 2.4 \times 10^6 \text{ GeV} \quad \text{Inverted Ordering}.$$

The difference in values for the two bounds is entirely determined by the difference in the factors $(m_2 - m_3)/(m_2 + m_3)^2$ and $(m_1 - m_2)/(m_1 + m_2)^2$ appearing for normal and inverted ordering respectively. We emphasise that the suppression factor e^{-4y} occurring in Eq. (7.4.4) is sufficiently strong that the lower bounds are not strongly affected by the running of the parameters (although the bounds stated include the running of all SM parameters and the light neutrino masses).

As a cross-check we have also determined the lower bound on M for which leptogenesis is viable within the Neutrino Option by numerically solving the resonant Boltzmann equations (we stress we solve the Boltzmann equations and not the analytically approximated equations of Eq. (7.4.4)) for both normal and inverted ordering and scanned the available parameter space for $\eta_B = 6.1 \times 10^{-10}$. We performed the parameter space exploration using MULTINEST [197, 198, 278] for a fixed scale M but varied the splitting ΔM, with y fixed to the value that satisfies $m_H^2(M_1) = \Delta m_H^2(M_1)$. That is, a value of M_1 was chosen and y was fixed to make the Neutrino Option work, then $\delta, \alpha_{21}, \alpha_{31}, x$ and M_2 were varied (none of which can spoil the generation of the Higgs potential once M_1 and y are determined, provided

M_2 does not differ significantly from M_1). We started at the maximum M_1 which was allowed by the Neutrino Option (which occurs when $y = 0°$) and lowered it in small increments, performing a new parameter scan at each of the successively smaller values of M_1. This procedure was stopped when the search no longer yielded points in the parameter space where leptogenesis was successful. The lowest value of M_1 for which leptogenesis was viable was taken as our lower bound.

At the lowest successful value, for both normal and inverted ordering, we found that the numerical results, as shown in Fig. 7.3 and Fig. 7.4 (both of which are placed at lower bound on M), are in broad agreement with the statements made above based on the analytical approximations.

In the inverted ordered case shown in Fig. 7.4, we can see a dependence on α_{21} that is not accounted for in the approximated analytical expressions and that is not present in the normal ordered case of Fig. 7.3. The reason is that the suppression factor e^{-4y} is $\mathcal{O}(100)$ times smaller for inverted ordering, rendering the approximations of Eq. (7.4.4) slightly less accurate than for normal ordering. Terms which were neglected and which depend on α_{21}, contribute to a slight dip in the value of η_B around $\alpha_{21} \sim 300°$. The approximate independence from δ is preserved because terms in δ are multiplied by the relatively small factor s_{13}. Finally, for inverted ordering, independence of α_{31} is exact as it does not appear in the Yukawa matrix when $m_3 = 0$.

Finally, we note that, at the lower bound for both normal ordering and inverted ordering, the heavy Majorana neutrinos form a pseudo-Dirac pair [264, 265]. We can see this for normal-ordering (for example), with $x = 135°$,

$$Y = U \begin{pmatrix} 0 & 0 \\ -\frac{\sqrt{M_1 m_2}}{\sqrt{2}v}\left(\cosh y + i \sinh y\right) & -\frac{\sqrt{M_2 m_2}}{\sqrt{2}v}\left(\cosh y - i \sinh y\right) \\ \frac{\sqrt{M_1 m_3}}{\sqrt{2}v}\left(\cosh y - i \sinh y\right) & -\frac{\sqrt{M_2 m_3}}{\sqrt{2}v}\left(\cosh y + i \sinh y\right) \end{pmatrix},$$

for which $Y_1 \approx iY_2$ when $M_1 \approx M_2$. At the lower bound where $\Delta M \ll M$, as the heavy Majorana neutrino mass matrix is diagonal, this condition implies that the CP

phases of N_1 and N_2 are approximately opposite (see also Eq. (6.2.3)) such that they form a Dirac pair when $M_1 = M_2$. Solutions of this kind may be motivated by assuming an approximate lepton number symmetry [68,73,74,76,77,143,144,157,279–285].

7.4.2 Upper bound on the heavy Majorana neutrino masses

The upper bound on M for the Neutrino Option occurs when $y = 0°$ (Eq. (7.4.2)) . In this case one finds for normal ordering

$$\frac{\epsilon^{(1)}_{\alpha\alpha}}{K_1 p_{1\alpha}} \approx \frac{i m_*(m_2 - m_3)\sqrt{m_2 m_3}\cos x \sin x \left(U^*_{\alpha 2}U_{\alpha 3} - U_{\alpha 2}U^*_{\alpha 3}\right)(f_{\rm osc} + f_{\rm mix})}{(m_2\cos^2 x + m_3 \sin^2 x)(m_3\cos^2 x + m_2\sin^2 x)\left|\sqrt{m_2}\cos x U_{\alpha 2} + \sqrt{m_3}\sin x U_{\alpha 3}\right|^2}, \tag{7.4.5}$$

and for inverted ordering

$$\frac{\epsilon^{(1)}_{\alpha\alpha}}{K_1 p_{1\alpha}} \approx \frac{i m_*(m_1 - m_2)\sqrt{m_1 m_2}\cos x \sin x \left(U^*_{\alpha 1}U_{\alpha 2} - U_{\alpha 1}U^*_{\alpha 2}\right)(f_{\rm osc} + f_{\rm mix})}{(m_2\cos^2 x + m_1 \sin^2 x)(m_1\cos^2 x + m_2\sin^2 x)\left|\sqrt{m_1}\cos x U_{\alpha 1} + \sqrt{m_2}\sin x U_{\alpha 2}\right|^2}. \tag{7.4.6}$$

Unlike for the lower bound where these terms had a maximum value that was largely independent of the PMNS phases, here we find a strong dependence upon these low energy phases and apparently unrestricted enhancement factors. Thus, leptogenesis must be successful at the upper bounds of the Neutrino Option. Combining the lower bounds from requiring the Neutrino Option and leptogenesis to be viable simultaneously with the upper bounds from the Neutrino Option alone results in[4]

$$1.2 \times 10^6 < M\ (\text{GeV}) < 8.8 \times 10^6 \quad \text{Normal Ordering},$$
$$2.4 \times 10^6 < M\ (\text{GeV}) < 7.4 \times 10^6 \quad \text{Inverted Ordering}.$$

In this case the approximate lepton number symmetry need not be so precise as it was for the lower bound.

[4] The upper bounds quoted here are slightly different from the one reported in Ref. [2] owing to the running of light neutrino masses having been neglected in the latter. Numerically the difference amounts to about $\sim 5\%$ and has therefore limited significance.

7.5 Conclusions

The aim of this chapter is to examine resonant leptogenesis in the context of the Neutrino Option thereby taking one further step in constructing a self-consistent theory which simultaneously explains light neutrino masses, the predominance of matter over anti-matter, and the electroweak scale.

We found that the viable parameter space which can satisfy the Neutrino Option and leptogenesis are in the ranges $1.2 \times 10^6 < M \text{ (GeV)} < 8.8 \times 10^6$ and $2.4 \times 10^6 < M \text{ (GeV)} < 7.4 \times 10^6$ for normal and inverted ordering respectively, with successful leptogenesis requiring a pseudo-Dirac pair with masses such that $\Delta M/M = (M_2 - M_1)/M \sim 10^{-8}$. Interestingly, viable solutions for Neutrino Option leptogenesis allows for θ_{23} be to in the lower or upper octant (at the 2 σ level) however for normal ordering there is a slight preference for solutions in the upper octant. In particular, we found that, generally, there is only a weak dependence on the low energy phases of the PMNS matrix δ, α_{21} and α_{31} at the lower bounds on the viable mass range for both normal and inverted ordering (see Fig. 7.3 and Fig. 7.4). The minor exception to this is α_{21} in the case of inverted ordering which must be approximately in the range $[90°, 200°]$ or $[360°, 600°]$ for 1σ agreement with $\eta_{B_{CMB}}$.

We have further shown successful leptogenesis within the framework of the Neutrino Option scenario is possible when the requisite CP violation in leptogenesis is provided exclusively by the Dirac or Majorana low-energy CP violation phases of the PMNS matrix. This is possible only at the upper bound of the viable mass range and provides a stark contrast with leptogenesis at the lower bounds where the low-energy PMNS phases were largely irrelevant.

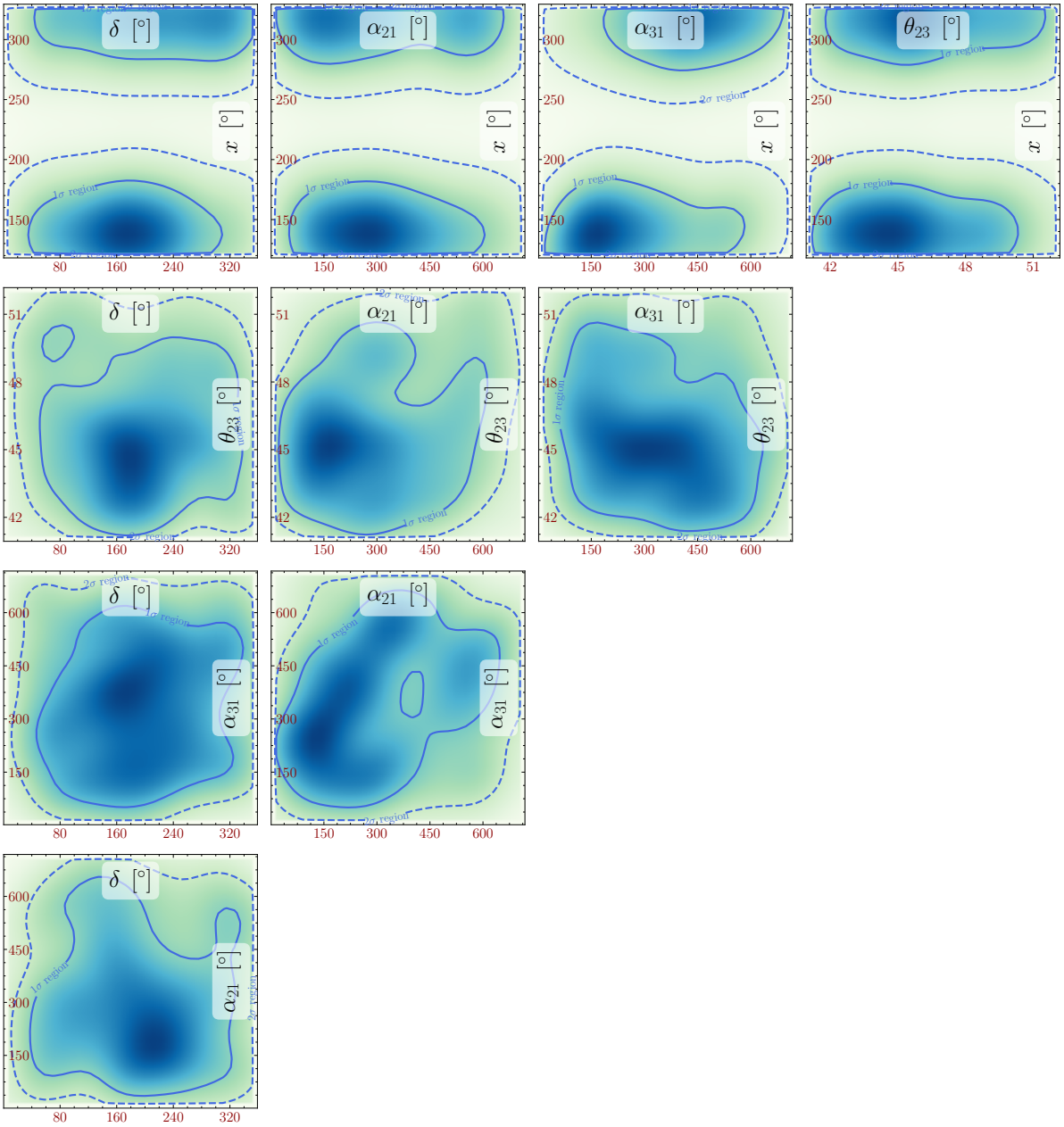

Figure 7.3: The triangle plot shows regions of the model parameter space compatible with the measured η_B within 1σ and 2σ for a normally ordered mass spectrum using resonant leptogenesis with $M = 1.2 \times 10^6$ GeV. The fixed parameters were set to be $y = 190.22°$, $\theta_{12} = 33.63°$ and $\theta_{13} = 8.51°$.

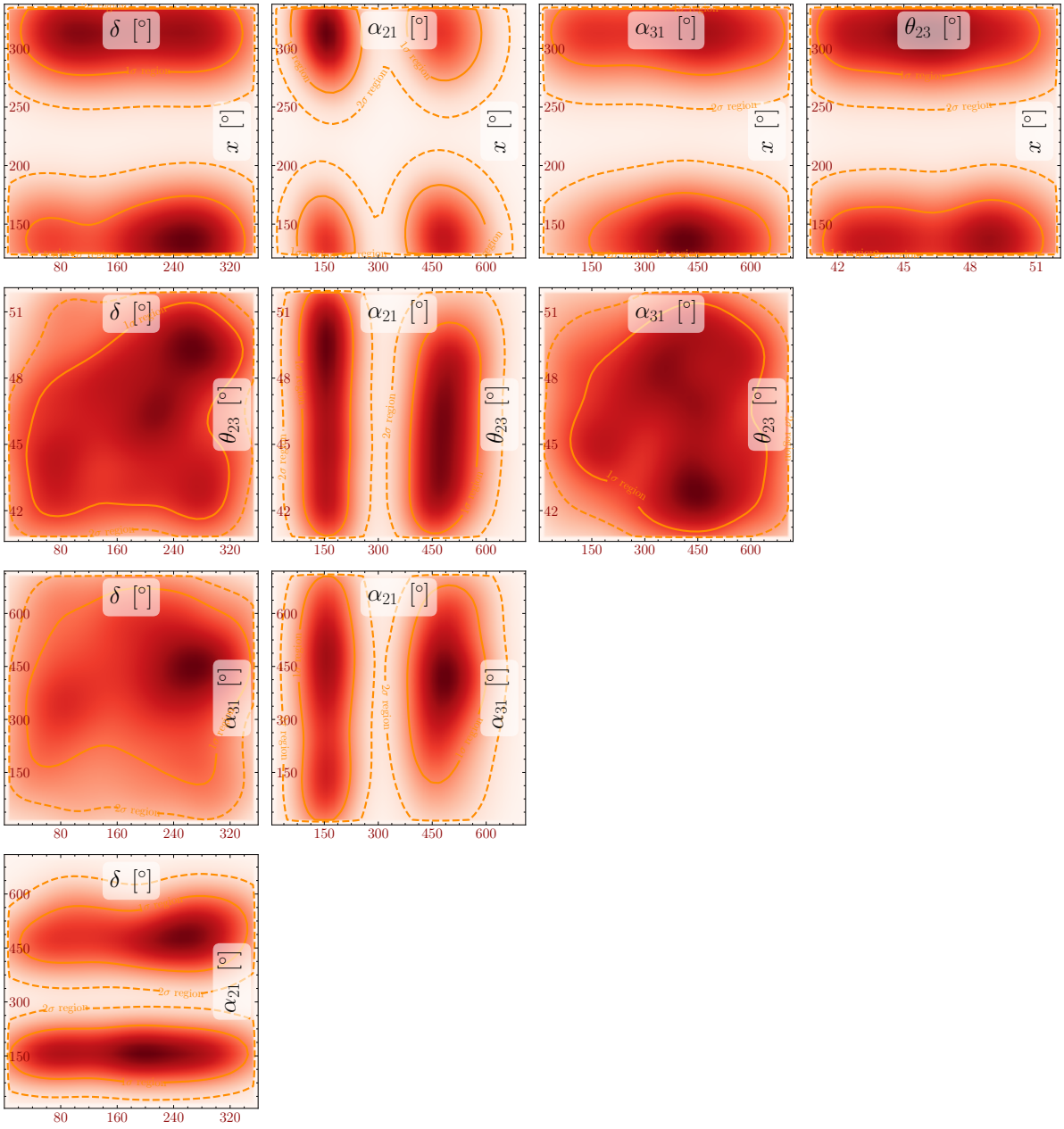

Figure 7.4: The triangle plot shows regions of the model parameter space compatible with the measured η_B within one and two σ for an inverted ordered mass spectrum using resonant leptogenesis with $M = 2.4 \times 10^6$ GeV. The fixed parameters were set to be $y = 118.21°$, $\theta_{12} = 33.63°$ and $\theta_{13} = 8.51°$.

Chapter 8

Outlook

In this thesis I have introduced two of the outstanding problems in modern physics and some of the theoretical attempts to address them: the extreme smallness of neutrino masses (Chapter 2) and the baryon asymmetry (Chapter 3). The later chapters are based on my own work.

In Chapter 4, we argue that the light neutrino masses are tied to lepton number violation in the type I seesaw (although the same arguments appear to hold also for the type III seesaw). If one wants exactly massless light neutrinos, then one must also have an exact lepton number symmetry. This work emphasises the significance of radiative corrections to neutrino masses in lepton number violation studies. In particular, researchers should be careful not to rely on too strong cancellations in the tree-level neutrino masses in order to provide large lepton number violation without excessive light neutrino masses.

In Chapter 5, we apply some heavy numerical machinery to the question of the lower bound on the scale of leptogenesis which had not previously been studied with such numerical rigour. We find that fine-tuned cancellations are necessary to pass much below the 10^9 GeV bound of Davidson and Ibarra, provided one wants to avoid the resonance regime where the CP asymmetries are enhanced by nearly-degenerate heavy Majorana neutrino masses. The parameter space rapidly shrinks with the lowering scale such that we estimate a lower bound $M_1 \sim 10^6$ GeV.

In Chapter 6, we revisited another phenomenological question of leptogenesis — can one have successful leptogenesis when the CP violation is provided solely by the low energy phases? Again applying the machinery developed for the work of Chapter 5, we were able to lower the scale for which this question has a positive answer to 10^6 GeV. More surprisingly, we discovered that flavour effects remain important beyond 10^{12} GeV when CP violation is purely low-energy. This means that all previous phenomenological studies of these scenarios may be extended into the regime $M_1 \gg 10^{12}$ GeV. We also settle a controversy — it is indeed possible to have viable leptogenesis when CP violation comes only from the Dirac phase δ.

In Chapter 7, we looked at the possibility that successful leptogenesis is possible within the Neutrino Option. In this scenario, the heavy Majorana neutrinos are responsible for generating the Higgs potential and thus resolve issues of naturalness in this sector. By demonstrating that leptogenesis is viable in this framework, we have demonstrated that it is possible to resolve the neutrino mass problem, the baryon asymmetry and the naturalness problem all within the type I seesaw. The small range of heavy Majorana neutrino masses for which this is possible gives this explanation an appealing rigidity.

The smallness of neutrino masses is well-explained by the type I seesaw mechanism which is employed throughout this thesis. However, testing the mechanism may be very difficult. Ideally one would look in collider experiments for signatures of lepton number violation such as same-sign dilepton decays. However, as emphasised by the conclusions of Chapter 4, lepton number violation is suppressed by the smallness of the the light neutrino masses. If leptogenesis occurs in the Neutrino Option as in Chapter 7, the range of heavy Majorana neutrino masses must be prohibitively high at $\mathcal{O}(10^6)$ GeV and so it would be difficult to test this idea directly also. Indeed for every major problem in particle physics there exist multiple speculative theories explaining them which are similarly difficult to test. Fundamentally new ideas may be needed if progress is to be achieved in ruling out the many speculations that abound in particle physics today.

Appendix A

Calculation of the one-loop light neutrino masses

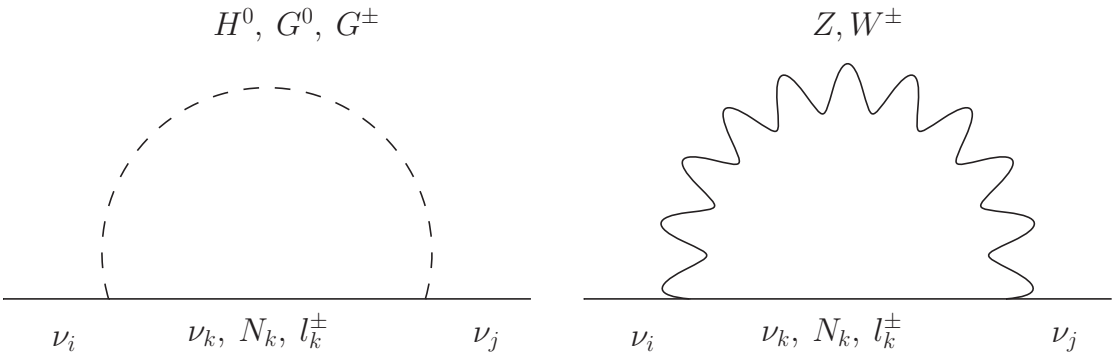

Figure A.1: The one-loop contributions to the light neutrino mass. All permutations of the upper and lower labels compatible with conservation of charge are possible.

The self-energy of the light neutrinos of momentum p may be decomposed as

$$\Sigma(p) = \not{\Sigma}^L\left(p^2\right)\not{p}P_L + \not{\Sigma}^R\left(p^2\right)\not{p}P_R + \Sigma^L\left(p^2\right)P_L + \Sigma^R\left(p^2\right)P_R, \tag{A.0.1}$$

with P_L and P_R the left- and right- chiral projection operators. For simplicity, we shall take $p^2 = 0$ which amounts to setting the neutrino mass to zero — a good approximation for our purposes. This has the additional advantage that our results will be finite, as any counterterm in renormalisation would be proportional to the neutrino mass. The Majorana nature of neutrinos in the type I seesaw places the

conditions $\not{\Sigma}^L = \left(\not{\Sigma}^R\right)^T$, $\Sigma^L = \left(\Sigma^L\right)^T$ and $\Sigma^R = \left(\Sigma^R\right)^T$. When the tree-level mass matrix $\mathcal{M}$ receives loop corrections and is then block-diagonalised, one finds for the light neutrinos,

$$m_\nu = m_\nu^0 + \delta m_L, \tag{A.0.2}$$

where $\delta m_L = U_L^* \Sigma^L U_L^\dagger$ is the correction to the m_L matrix appearing as the $(1,1)$ entry in $\mathcal{M}$ and set to zero at tree-level by symmetry considerations. For this reason we need only compute the left-chiral self-energy correction for the light neutrinos, that is we want Σ^L evaluated with zero external momentum. This may be written

$$\Sigma^L = \Sigma_Z^L + \Sigma_{G^0}^L + \Sigma_{H^0}^L + \underbrace{\Sigma_{G^\pm}^L + \Sigma_{W^\pm}^L}_{\text{equal to zero}}\Bigg|_{p=0}. \tag{A.0.3}$$

In all integrals we may set p, $\not{p}$ and p^2 equal to zero. As a result integrals with $\not{k}$ in the numerator may be immediately set to zero as they will be proportional to $\not{p}$. As we are looking only for Σ^L we extract the coefficient of the left projection operator P_L. The contributions to the self-energy are depicted in Fig. A.1.

Starting with $\Sigma_{G^0}^L$, the vertices give a factor

$$\left(\frac{g}{2m_W}\right)^2 \left(C_{ik} m_i + C_{ik}^* m_k\right)\left(C_{kj} m_k + C_{kj}^* m_j\right). \tag{A.0.4}$$

Since $m_i = m_j = 0$ as they are the masses of external light neutrinos and $p^2 = 0$, we are left with

$$i\Sigma_{ijG^0}^L\big|_{p=0} = \left(\frac{g}{2m_W}\right)^2 C_{ik}^* C_{ik}^* m_k^3 \int \frac{d^D k}{(2\pi)^D} \frac{1}{k^2 - \zeta m_Z^2} \frac{1}{k^2 - m_k^2}. \tag{A.0.5}$$

Next we consider

$$\begin{aligned} i\Sigma_{ijZ}\big|_{p^2=0} =& i^2 \left(-\frac{ig}{2c_W}\right)^2 \left(C_{ik} P_R - C_{ik}^* P_L\right) \gamma^\mu \\ & \int \frac{d^D k}{(2\pi)^D} \frac{m_k}{k^2 - m_k^2} \frac{1}{k^2 - m_k^2} \left[-g^{\mu\nu} + \frac{k^\mu k^\nu (1-\zeta)}{k^2 - \zeta m_Z^2}\right] \gamma^\nu \left(C_{kj} P_L - C_{kj}^* P_R\right). \end{aligned} \tag{A.0.6}$$

Extracting the coefficient of P_L, we get

$$\begin{aligned} i\Sigma^L_{ijZ}\Big|_{p^2=0} =& \left(-\frac{ig}{2c_W}\right)^2 C^*_{ik}C^*_{jk}m_k \\ & \int \frac{d^Dk}{(2\pi)^D}\left(\frac{-\overbrace{\gamma^\mu g^{\mu\nu}\gamma^\nu}^{=D}}{k^2-m_Z^2}+\frac{\overbrace{\not{k}^2}^{=k^2}(1-\zeta)}{(k^2-\zeta m_Z^2)(k^2-m_Z^2)}\right)\frac{1}{k^2-m_k^2} \\ =& \left(\frac{g}{2m_W}\right)^2 C^*_{ik}C^*_{jk}m_k \\ & \int \frac{d^Dk}{(2\pi)^D}\left(\frac{D}{k^2-m_Z^2}+\left(\frac{k^2}{k^2-\zeta m_Z^2}-\frac{k^2}{k^2-m_Z^2}\right)\right)\frac{1}{k^2-m_k^2}, \end{aligned} \tag{A.0.7}$$

where in the second step we make the substitution $c_w = m_W^2/m_Z^2$ and apply $C\hat{m}C^T = 0$.

For the Higgs contribution we have

$$\begin{aligned} i\Sigma^L_{ijH^0}\Big|_{p^2=0} =& \left(-\frac{ig}{2m_W}\right)^2 (C^*_{ik}m_k)(C_{kj}m_k) \\ & \int \frac{d^Dk}{(2\pi)^D}\frac{1}{k^2-m_H^2}\frac{m_k}{k^2-m_k^2} \\ =& m_k^3\left(\frac{g}{2m_W}\right)^2 C^*_{ik}C^*_{jk}\int \frac{d^Dk}{(2\pi)^D}\frac{1}{k^2-m_H^2}\frac{1}{k^2-m_k^2}. \end{aligned} \tag{A.0.8}$$

The sum of the Z and G^0 contributions is

$$\begin{aligned} & i\Sigma^L_{ijZ} + i\Sigma^L_{ijG^0}\Big|_{p=0} = \\ & \left(\frac{g}{2m_W}\right)^2 C^*_{ik}C^*_{jk}m_k\int \frac{d^Dk}{(2\pi)^D}\frac{1}{k^2-m_k^2}\left[\frac{Dm_Z^2}{k^2-m_Z^2}+\left(\frac{k^2}{k^2-\zeta m_Z^2}-\frac{k^2}{k^2-m_Z^2}\right)\right]. \end{aligned} \tag{A.0.9}$$

But we may use the replacement

$$\int \frac{d^Dk}{(2\pi)^D}\frac{k^2}{k^2-m_k^2}\frac{1}{k^2-\zeta m_Z^2} \to \int \frac{d^Dk}{(2\pi)^D}\frac{m_k^2}{k^2-m_k^2}\frac{1}{k^2-\zeta m_Z^2}, \tag{A.0.10}$$

due to $C\hat{m}C^T$.

The total one-loop self-energy is

$$\begin{aligned}
&\left(i\Sigma_Z + i\Sigma_{G^0} + i\Sigma_{H^0}|_{p^2=0}\right)_{ij} \\
&= -\left(\frac{g}{2m_W}\right)^2 C^*_{ik}C^*_{jk}m_k \int \frac{d^Dk}{(2\pi)^D}\left[\frac{Dm_Z^2 - m_k^2}{(k^2-m_k^2)(k^2-m_Z^2)} + \frac{m_k^2}{(k^2-m_k^2)(k^2-m_H^2)}\right] \\
&= -\left(\frac{g}{2m_W}\right)^2 C^*_{ik}C^*_{jk}m_k \int \frac{d^Dk}{(2\pi)^D}\left[\frac{(3-2\epsilon)m_Z^2}{k^2-m_Z^2} + \frac{m_H^2}{k^2-m_H^2} + \underbrace{\frac{m_Z^2-m_k^2}{k^2-m_Z^2}}_{\to -1} + \underbrace{\frac{m_k^2-m_H^2}{k^2-m_H^2}}_{\to 1}\right] \\
&= -\left(\frac{g}{2m_W}\right)^2 C_{ki}C_{kj}m_k \frac{i}{2^4\pi^2}\left(3B_0(0,m_k,m_Z)m_Z^2 + m_H^2 B_0(0,m_H,m_H)\right).
\end{aligned} \tag{A.0.11}$$

Upon substitution of the standard integral B_0, we obtain

$$\begin{aligned}
&\left(i\Sigma_Z + i\Sigma_{G^0} + i\Sigma_{H^0}|_{p^2=0}\right)_{ij} \\
=&i\left(\frac{g}{2m_W}\right)^2 \frac{m_k}{2^4\pi^2}C_{ki}C_{kj}\left(3m_Z^2\left(\frac{m_k^2}{m_k^2-m_Z^2}\log m_k^2 - \frac{m_Z^2\log m_Z^2}{m_k^2-m_Z^2}\right)\right. \\
&\left. + m_H^2\left(\frac{m_k^2}{m_k^2-m_H^2}\log m_k^2 - \frac{m_H^2\log m_H^2}{m_k^2-m_H^2}\right)\right).
\end{aligned} \tag{A.0.12}$$

The terms involving logarithms can be simplified using another replacement

$$\frac{m_k^2}{m_k^2-m_a^2}\log m_k^2 - \frac{m_a^2\log m_a^2}{m_k^2-m_a^2} \to f_{ka} \equiv \frac{m_k^2}{m_k^2-m_a^2}\log m_a^2. \tag{A.0.13}$$

Finally we obtain

$$m^1_{\nu ij} = \delta m_L = \frac{\alpha_W}{16\pi m_W^2}C_{ki}C_{kj}m_k\left(3m_Z^2 f_{kZ} + m_H^2 f_{kH}\right). \tag{A.0.14}$$

Appendix B

CPT and Majorana particles

B.1 The CPT theorem

In $3+1$ dimensions or any space-time with an even number of dimensions, CPT acts on coordinates as the negative identity operation: $x^\mu \to -x^\mu$. This is just a complex Lorentz transformation[1] and thus is a symmetry of a Lorentz invariant theory. According to Wigner's theorem, a symmetry transformation must be represented by a unitary or antiunitary operator — the latter being necessary if there is a reversal of the light-cone as is the case with CPT.

If we have a one-particle state of momentum p, total angular momentum j, spin s and conserved charge Q, then CPT must take $p \to p$, $s \to -s$ and $Q \to Q^c$ with Q^c the conjugate charge. Thus the antiunitary CPT operator Θ must have the action

$$\Theta|p, s, Q\rangle = i^F(-1)^{j-s}|p, -s, Q^c\rangle, \tag{B.1.1}$$

where the phase factor is required for consistency in a Lorentz invariant theory and may not be redefined.

Being antiunitary, we expect the Θ operator to conjugate fields and thus change the sign of their conserved charges. In a classical context, the electrical current densities

[1] In Cartesians, it is a rotation of π around the z-axis and a boost of $i\pi$ along the z-axis that results in a Lorentz transformation matrix $\Lambda = -1$.

transform as $j^\mu \to -j^\mu$ under CPT exactly as would be expected from the change in sign of charge. Meanwhile the stress-energy tensor $T^{\mu\nu}$ sensibly preserves its sign.

B.2 Majorana particles

The concept of an antiparticle is one in which the conserved charges are opposite to that of the corresponding particle. This would appear to make C, CP and CPT all transformations that take particle states into antiparticle states. However, we must remember that of all of these CPT is the only one expected to be a symmetry in general. Thus, given a particle state, the antiparticle state is made by applying CPT to it.

For this reason, in defining Majorana particles, we should say that they are eigenstates not of C or CP but of CPT. [2] Here we must not interpret the word "eigenstate" too narrowly — CPT inverts the spin of a particle. CPT takes a Majorana particle and creates a particle which is identical after some Poincaré transformations. In spite of this, the general condition for a Majorana field is simply

$$\psi = \psi^c. \tag{B.2.1}$$

An equivalent condition is the requirement that there is a basis in which the fields are real. This justifies the occasional use of the term "real fermion" for Majorana particles (although this will be spoiled if one transforms to another basis using a unitary transformation).

The Majorana condition places some restrictions on electromagnetic properties. Consider a particle in a magnetic field. The interaction energy depends on the magnetic moment μ and spin s as

$$E = -\mu s B. \tag{B.2.2}$$

[2] If, for example, one started with a C eigenstate $|\psi\rangle$, such that $C|\psi\rangle = \eta|\psi\rangle$, with η some phase, then there is no guarantee that at a later time, the state is a C eigenstate because of the factor e^{iHt}. This can only be the case if $[C, H] = 0$ and hence if C is a symmetry.

Under CPT, the magnetic field is unchanged but the spin is flipped. Invariance under CPT requires the energy to be unchanged and so the magnetic moment must be opposite for an antiparticle. Majorana particles are supposed to be identical to Majorana antiparticles and so we conclude that they must have magnetic moment equal to zero. An exactly similar argument can be made that the electric dipole is zero.

If a Majorana particle is electrically neutral because it is made of a charge distribution, positive in some places and negative in others summing to zero, then its antiparticle would have the positive and negative parts of its distribution switched and would be distinguishable from the original particle. This would be a contradiction so Majorana particles must be neutral at all points.

Finally, we note that, the CP phase of a Majorana fermion must be $\pm i$. This can be seen by applying the definition of the CP operation on both the original field and the C-conjugated field (which must give the same result).

B.3 Derivation of CPT operator effects

Let us now find explicitly the effect of the antiunitary CPT operator Θ which transforms a field S as $S \to S' = \Theta S \Theta^{\dagger}$. We use the fact that CPT acts on the space-time coordinates like a rotation around the z-axis by π and a boost by $i\pi$ around the same axis. Then we shall insist that amplitudes are invariant under θ.

Let us start by finding the effect of the $x \to -x$ Lorentz transformation on a set of fields. A scalar field transforms as

$$\phi'(x) = \phi(-x). \tag{B.3.1}$$

Fermionic fields transform under rotation θ and boost ϕ as

$$\psi'_L(x) = e^{\frac{1}{2}(i\sigma\cdot\theta - \sigma\cdot\phi)}\psi_L(-x), \tag{B.3.2}$$

and

$$\psi'_R(x) = e^{\frac{1}{2}(i\sigma\cdot\theta+\sigma\cdot\phi)}\psi_R(-x). \tag{B.3.3}$$

which, under the Lorentz transformation we are considering is

$$\psi'_L(x) = -\psi_L(-x), \tag{B.3.4}$$

and

$$\psi'_R(x) = \psi_R(-x). \tag{B.3.5}$$

Similarly, a vector field transforms as

$$A'_\mu(x) = -A_\mu(-x). \tag{B.3.6}$$

Now we look at the effect on amplitudes. We start by recalling that under an antiunitary operator, invariance of amplitudes means that

$$\langle\alpha|\beta\rangle = \langle\overline{\beta}|\overline{\alpha}\rangle = \langle\overline{\alpha}|\overline{\beta}\rangle^*. \tag{B.3.7}$$

Take a generic set of fields S_i to construct

$$\langle 0|S_1(x)\,S_2(x)\ldots S_n(x)\,|0\rangle. \tag{B.3.8}$$

and apply the Lorentz transformation involved in CPT to get

$$(-1)^L\langle 0|S_1(-x)\,S_2(-x)\ldots S_n(-x)\,|0\rangle \tag{B.3.9}$$

with L the total number of left-handed fermions and vector fields. We want to relate this to the conjugate to understand the unitary operator. Complex conjugating twice gives

$$i^F(-1)^L\langle 0|S_1^*(-x)\,S_2^*(-x)\ldots S_n^*(-x)\,|0\rangle^* \tag{B.3.10}$$

where F is the number of fermion fields. This factor came from having to switch the fields back into the original order after complex conjugation and always ends up being $i^F = \pm 1$ as F has to be even (or else the amplitude will be zero). When

comparing with $\langle\alpha|\beta\rangle = \langle\overline{\beta}|\overline{\alpha}\rangle = \langle\overline{\alpha}|\overline{\beta}\rangle^*$, we can interpret

$$\begin{aligned} |\alpha\rangle &= |0\rangle, \\ |\beta\rangle &= S_1(x)\, S_2(x) \ldots S_n(x)\, |0\rangle, \end{aligned} \tag{B.3.11}$$

and

$$\begin{aligned} |\overline{\alpha}\rangle &= \Theta|0\rangle, \\ |\overline{\beta}\rangle &= \Theta S_1(x)\, S_2(x) \ldots S_n(x)\, |0\rangle, \\ &= \Theta S_1(x)\, \Theta^\dagger \Theta S_2(x)\, \Theta^\dagger \Theta \ldots S_n(x)\, \Theta^\dagger \Theta |0\rangle. \end{aligned} \tag{B.3.12}$$

Now it is clear that the antiunitary operator Θ that achieves this acts in the following way:

$$\Theta S(x)\, \Theta^\dagger = (-1)^L\, i^F S^*(-x)\,. \tag{B.3.13}$$

In terms of the Dirac spinor in the Weyl basis $\psi = (\psi_L, \psi_R)^T$

$$\Theta \psi \Theta^\dagger = i\gamma_5 \psi^*(-x)\,. \tag{B.3.14}$$

For a field of any type, the action of Θ on the creation and annihilation operators $a_s(p)$, $b_s(p)$ can be found by explicitly studying the effects of Eq. B.3.13 and is found to have the effect

$$\Theta|p, s, Q\rangle = i^F (-1)^{j-s} |p, -s, Q^c\rangle, \tag{B.3.15}$$

as stated at the beginning of this appendix. The effects on p, s being easily anticipated from the transformation of momentum and angular momentum under space and time reversal.

Appendix C

Sphalerons

C.1 The electroweak sphaleron process

The electroweak interactions include a non-perturbative process called the sphaleron process which is a transition between equilibrium states with differing values of $B+L$. Neglecting fermions, the picture is that the set of all static classical configurations of the Higgs and gauge fields form a torus in a space where one axis (let us make it the vertical axis) corresponds to the energy of the configuration and points that differ by a gauge-transformation have been brought together. The vacuum state is the point of lowest energy and therefore the vertically lowest point on the surface of the torus. A transition from vacuum to vacuum may be drawn as a loop over the surface of the torus which passes through the lowest point. If this loop is non-contractible, then the value of $B+L$ has been altered in the transition. For each non-contractible loop, there is a given maximum energy corresponding to it, and so, from the set of all non-contractible loops, the lowest maximum energy corresponds to the threshold that must be reached in order to make a transition from one vacuum state to another. The static field configuration corresponding to this lowest maximum energy stationary state is called the sphaleron state.

This whole set-up is similar to a classical pendulum. We consider the energy of a static pendulum at any given angle and ask — what is the minimum energy required

to make it swing in a full circle? The answer of course, is given by the potential energy of the highest configuration. The torus is more complicated in that there are multiple paths one can take and so this analogy only considers the circle around the torus (imagined as a 2-torus) that includes the vacuum and sphaleron states.

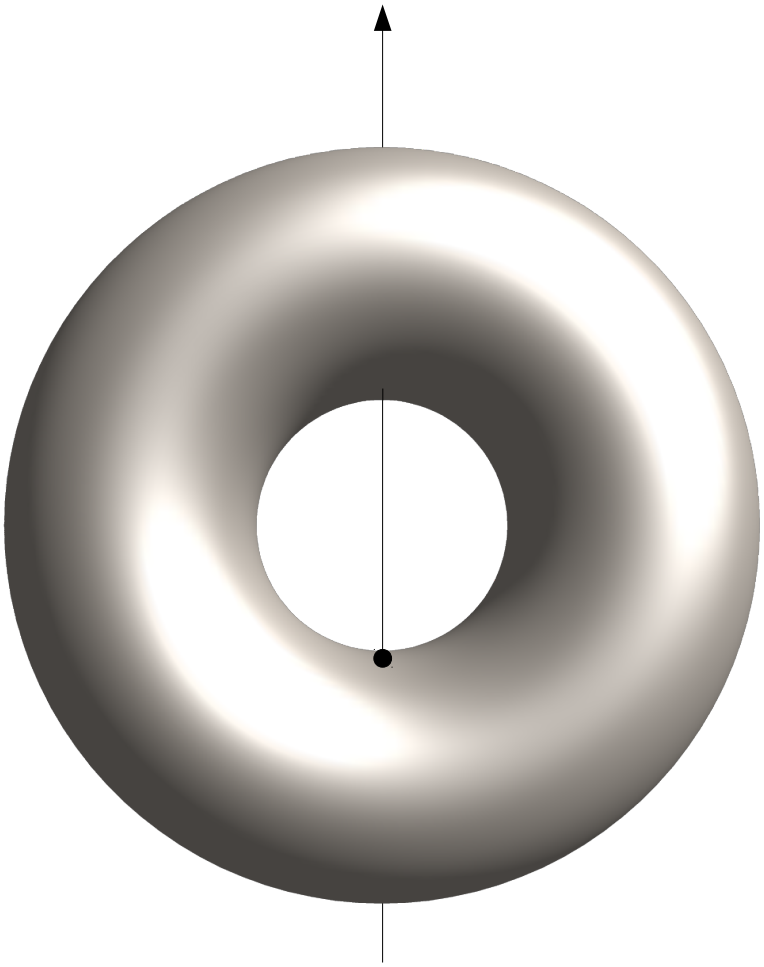

Figure C.1: A cartoon of the surface of the electroweak static field configurations with energy increasing in the direction of the arrow. The black dot represents the sphaleron configuration. The arrow intersects the torus at the lowest energy point (the vacuum), the sphaleron saddle-point, a second saddle-point at the top of the diagram and finally the highest energy field configuration.

C.2 The sphaleron factor in leptogenesis

In the text, we claim that is is possible to obtain the baryonic part of the $B - L$ asymmetry once sphalerons have processed it by multiplication by a factor 28/79.

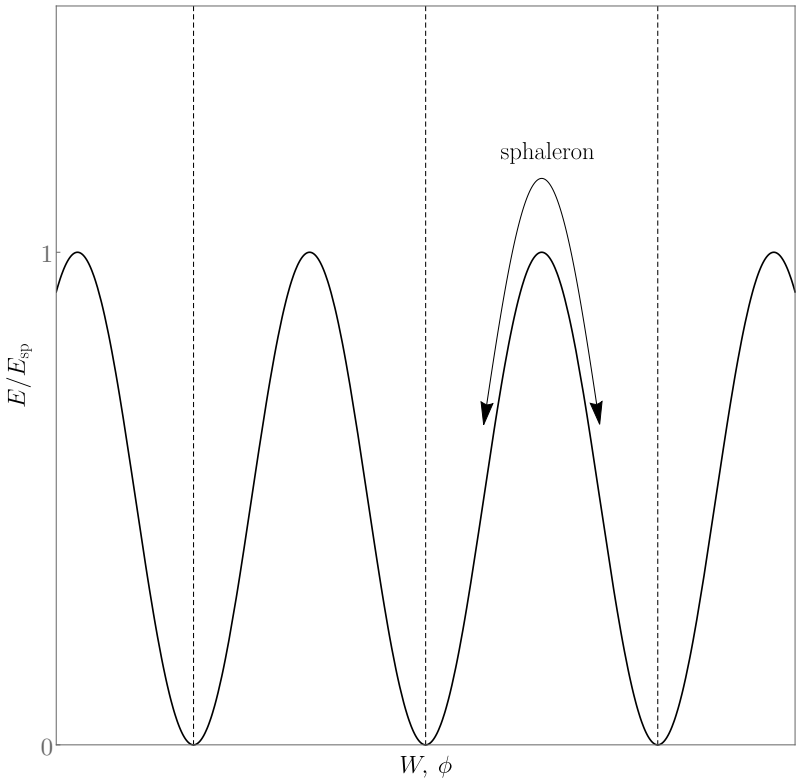

Figure C.2: The energy of transition to different vacua in terms of the sphaleron energy $E_{\rm sp}$. Dashed vertical lines demarcate vacuum states. Sphaleron transitions between them cause a change in $B+L$, $\Delta\left(B+L\right)=3N_g$, with N_g the number of generations.

Let us demonstrate this now.

By expanding the particle densities in $\beta\mu_i$, with β the inverse temperature and μ_i the chemical potential for species i, the matter-antimatter asymmetries are

$$n_i-\overline{n}_i=\frac{g_iT^3}{6}\beta\mu_i, \tag{C.2.1}$$

for fermions and

$$n_i-\overline{n}_i=\frac{g_iT^3}{3}\beta\mu_i, \tag{C.2.2}$$

for bosons (note the factor 2 difference), where g_i is the number of degrees of freedom for species i.

Then baryon number density is

$$n_B=3\left(2\mu_Q+\mu_{u_R}+\mu_{d_R}\right), \tag{C.2.3}$$

and lepton number is

$$n_L = 3\left(2\mu_L + \mu_{l_R}\right), \tag{C.2.4}$$

where we have absorbed factors $gT^3/6$ in the definition for brevity. What we are looking for is the baryonic proportion of n_{B-L}, namely $n_B/(n_B - n_L)$ (so the strange normalisations don't matter).

The reaction $\phi^0 \leftrightarrow \overline{u}_{iL} + u_{iR}$ tells us that

$$\mu_\phi = \mu_{u_R} - \mu_Q. \tag{C.2.5}$$

We also have $\phi^0 \leftrightarrow \overline{d}_{iL} + d_{iR}$ which gives

$$\mu_\phi = \mu_{d_R} - \mu_Q. \tag{C.2.6}$$

Similarly, there is the charged leptonic version of the first reaction $\phi^0 \leftrightarrow \bar{l}_{\alpha R} + l_{\alpha L}$ which gives us

$$\mu_\phi = \mu_{l_R} - \mu_L. \tag{C.2.7}$$

As there are no right-handed neutrinos in the SM we do not have a second leptonic equation of this kind.

The sphalerons which we assume to be in equilibrium as effective operators of the kind $q_L q_L q_L l_L$ and can cause the transition

$$\overline{u} + \overline{d} + \overline{c} \to d + 2s + 2b + t + \nu_e + \nu_\mu + \nu_\tau, \tag{C.2.8}$$

which gives the constraint

$$3\mu_Q + \mu_L = 0. \tag{C.2.9}$$

Finally, we must consider the total hypercharge neutrality of the universe $Y = \Sigma_i Y_i n_i = 0$. We use that $n \propto \mu$ with an extra factor 2 for bosons in comparison with fermions

$$3 \times 3 \times \left(\frac{4}{3}\mu_{u_R} - \frac{2}{3}u_{d_R} + 2 \times \frac{1}{3}u_Q\right) + 3 \times (-2\mu_{l_R} - 2\mu_L) + 2 \times 2 \times \mu_\phi = 0. \tag{C.2.10}$$

All these conditions together give us

$$\frac{n_B}{n_B - n_L} = \frac{28}{79}. \tag{C.2.11}$$

We quickly note that some assumptions have been made here. If we assume that sphalerons remain in equilibrium until after the electroweak phase transition then this factor should be 12/37. Since the two options are numerically similar, we'll stick with the first and not worry about it.

This is part of the conversion factor we need to compute the baryon asymmetry of the universe. There is also an extra piece which is not related to baryon physics. Instead this comes from the change in the photon density at the is proportional to T^3. The temperature is proportional to $g_S^{-1/3}$ where

$$g_S \equiv \sum_i^{\text{bosons}} g_i + \sum_i^{\text{fermions}} \frac{7}{8} g_i. \tag{C.2.12}$$

Thus

$$\eta_{B,r} = \eta_{B,1} \frac{g_{S,r}}{g_{S,l}} \approx \frac{3.94}{106.75} \eta_{B,l} \tag{C.2.13}$$

where subscript l means the quantitiy is evaluated at the time of leptogenesis and subscript r means evaluated at time of recombination. Ultimately,

$$\eta_B = \eta_{B,0} \approx \frac{3.94}{106.75} \frac{28}{79} n_{B-L} = 0.013 n_{B-L}. \tag{C.2.14}$$

Appendix D

Further effects in leptogenesis

In Chapter 3 a number of simplifying approximations were made. Here we will consider what they represent physically and the extent to which they affect the accuracy of the equations.

D.1 Thermal effects in amplitude calculations

There are a number of effects due to temperature that we did not account for in Chapter 3. We briefly summarise these here:

- Couplings should be run with the scale $\Lambda \sim 2\pi T$. These effects will usually be unimportant except that they may shift the points at which cancellations occur for the fine-tuned solutions of Chapter 5 and Chapter 6.
- Thermal particle propagators should be used to compute the CP asymmetry. However, these corrections tend only to be large for $T \gtrsim M$.
- A thermal mass is induced for all the particles. For the lepton doublets and the Higgs, one effect is that the decay rate of a heavy neutrino to these final state particles may be reduced due to their effectively enlarged mass — recall that if the decay products were heavier than the heavy neutrino then there would be no decay at all.

D.2 Spectator processes

There are Standard Model processes that affect the asymmetry densities of leptons and Higgs and thus which indirectly affect the rate of leptogenesis — we call these *spectator processes*. We consider these processes when they are in equilibrium and so when the chemical potentials and densities satisfy

$$\begin{aligned} \sum_{\text{initial}} \mu_i &= \sum_{\text{final}} \mu_i, \\ n_i - \overline{n}_i &= \frac{g_i T^3}{(3)6} \beta \mu_i, \end{aligned} \tag{D.2.1}$$

where the latter applies for fermions (bosons). When spectator processes are added to the description of leptogenesis, one can relate the new particle species to the lepton asymmetry n_{B-L}. Thus spectator effects act to change the numerical coefficients of n_{B-L} in the Boltzmann equations; generically, increasing the washout and thus reducing the final lepton asymmetry by a factor which turns out to be $\mathcal{O}(1)$.

A single example should furnish a full understanding. Take for instance $T \gtrsim 10^{13}$ GeV where the electroweak sphaleron is out of equilibrium and only the fermions with largest Yukawa couplings need to be considered — all others being out of equilibrium. There is no baryon asymmetry because we assume it is vanishing to begin with and no process has created it yet:

$$n_B = 2n_{\Delta Q_3} + n_{\Delta t} = 0. \tag{D.2.2}$$

Similarly, the conservation of hypercharge Y tells us $\sum_i Y_i n_i = 0$ for all relevant n_i:

$$n_{\Delta Q_3} + 2n_{\Delta t} - n_{\Delta l} + n_{\Delta \phi} = 0, \tag{D.2.3}$$

and the top-quark Yukawa coupling gives

$$n_{\Delta Q_3} + \frac{1}{2} n_{\Delta \phi} = n_{\Delta t}. \tag{D.2.4}$$

Then, for instance, in Eq. (3.2.21) had we not set the Higgs asymmetry to zero the

washout term would have been

$$2\left(n_{\Delta\phi}+n_{\Delta l}\right)W,$$

but by solving the simultaneous equations above, we can eliminate $n_{\Delta\phi}$ to get $2\left(n_{\Delta\phi}+n_{\Delta l}\right)=-\frac{5}{3}n_{B-L}$ with $n_{B-L}=-2n_{\Delta l}$. Then we find an equation of the same form as Eq. (3.2.21) but with a numerical factor weighting the washout W. In the general, at different temperature scales there are different processes in equilibrium, so the set of equations to solve will be different but we may always eliminate the other variables for n_{B-L}.[1]

D.3 Scattering effects

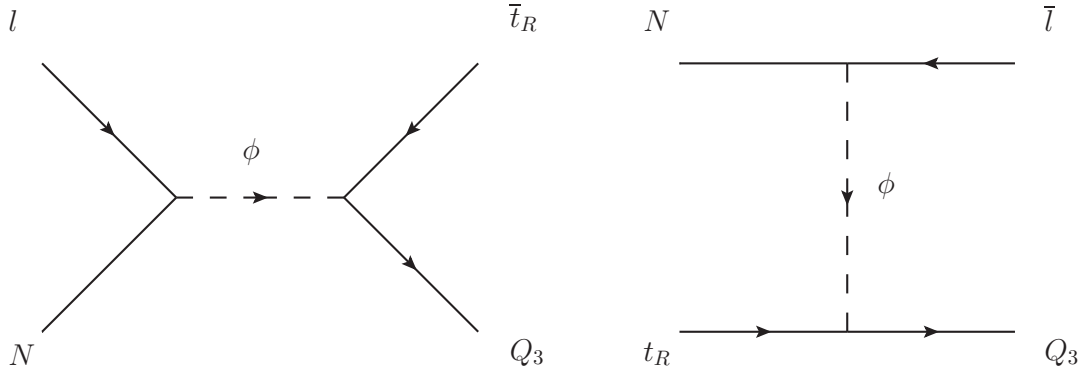

Figure D.1: Some Higgs-mediated scatterings in s- and t-channels.

A class of processes we have neglected but which contribute to lepton number violation are the s- or t-channel Higgs exchanges and top quarks of Fig. D.1. The inclusion of these effects can be incorporated by the replacement $D(z)\to D(z)+S(z)$ with and the washout $W(z)$ is replaced with $j(z)W(z)$ in the equations of Eq. (3.2.21) (see [141] and the references therein for the explicit form of these functions).

It turns out that in the strong washout regime the by the inverse decay process is

[1] See [258], upon which this subsection was based, for a more complete discussion and relevant references.

dominant such that $j(z)W(z) \approx W(z)$. Furthermore, the precise structure of the decay term does not affect the final result (at least in the analytical solution — D or in this case $D + S$ do not appear). This means that the scattering processes are safely neglected in the strong washout scenario.

D.4 Quantum statistical effects

In Eq. (3.2.2) are the factors $1 \pm f$ that we approximated as 1 to arrive at Eq. (3.2.3). These quantum statistical factors result from the exclusion and anti exclusion principles. Consider the bosonic case of n identical particles transitioning to n states. There are $n!$ ways to arrange them in the final states, all of which are identical. Thus, if the amplitude is w for any given arrangement, it is $n!w$ for the sum of all possibilities. The rate, being proportional to the amplitude squared contains a factor $(n!)^2$ but also a $1/n!$ from the phase-space factor to avoid over-counting identical arrangements. This means that there is a factor $n!$ over what we would have classically. Furthermore, to go from n particles in the final state to $n + 1$ requires an extra factor $n + 1$ (to give the $(n + 1)!$). So if there are n particles in the state originally then the probability for another to scatter is $n + 1$ times higher than if they were distinguishable. In a thermal distribution we should use $1 + f$. Similarly, for the fermionic case we should use $1 - f$.

Appendix E

Properties of R^i and f

E.1 Construction of R^i_u, R^i_v, R^i_w

We provide here a procedure for explicitly constructing the matrices R^i_u, R^i_v and R^i_w for given vectors u^i, v^i and w^i. We first construct

$$Y^i = u^{i*}u^{iT} + u^i u^{i\dagger}. \tag{E.1.1}$$

As this is a real symmetric matrix, it is possible to choose a set of n_i real orthogonal eigenvectors b^i. Then

$$R^i_u = \begin{pmatrix} b^{iT}_1 \\ b^{iT}_2 \\ \vdots \\ b^{iT}_{n_i} \end{pmatrix} \tag{E.1.2}$$

will perform the required transformation for generic u^i.

From the relations

$$\text{rank}\left(Y^i\right) \leq \text{rank}\left(u^{i*}u^{iT}\right) + \text{rank}\left(u^i u^{i\dagger}\right) \tag{E.1.3}$$

and

$$\text{rank}\left(u^{i*}u^{iT}\right) = \text{rank}\left(u^i u^{i\dagger}\right) = 0 \text{ or } 1, \tag{E.1.4}$$

it follows that the rank of Y^i may be at most 2. If it is rank 0 then $u^i = 0$ and this is a trivial case. If it is rank 1 then u^i is a real vector and cannot achieve $u^{iT}u^i = 0$ unless $u^i = 0$ in this case. Thus, for non-trivial u^i, Y^i has rank 2. Consequently it has $n_i - 2$ eigenvalues equal to zero.

If b^i_k corresponds to eigenvalue zero then $Y^i b^i_k = 0$. Thus,

$$u^i \left(u^{i\dagger} b^i_k\right) + u^{i*} \left(u^{iT} b^i_k\right) = 0. \tag{E.1.5}$$

Multiplying on the left by u^T yields

$$||u^i||^2 \left(u^{iT} b^i_k\right) = 0. \tag{E.1.6}$$

which implies $u^{iT} b^i_k = 0$ (excluding the trivial solution $u^i = 0$).

Finally,

$$u^{i'} = R^i_u u^i = \begin{pmatrix} b^{iT}_1 u^i \\ b^{iT}_2 u^i \\ \vdots \\ b^{iT}_{n_i} u^i \end{pmatrix} \tag{E.1.7}$$

which has components all zero except for two. Taking these components to be $u^{i'}_1$ and $u^{i'}_2$, the condition $u^{i'T} u^{i'} = 0$ is equivalent to

$$u^{i'2}_1 + u^{i'2}_2 = 0, \tag{E.1.8}$$

which admits the solution

$$u^{i'}_2 = \pm i u^{i'}_1, \tag{E.1.9}$$

and u' thus takes the form of eq.(4.2.42).

The matrices R^i_2 and R^i_3 can then be constructed by analogy. In the case of R^i_2 it is only necessary to repeat the above procedure with the vector

$$\left(v^{i'}_3, v^{i'}_4, \ldots\right)$$

in place of u^i from the start. This works as it gives zero upon taking its scalar

product with itself. Similarly, R_3^i is constructed by repetition of this argument with

$$\left(w_5^{i''}, w_6^{i''}, \ldots\right)$$

in place of u^i.

E.2 Properties of f

The function f is composed of the sum of two terms of the form,

$$h(x) \equiv a\frac{x^3}{x^2-1}\log\left(x^2\right), \tag{E.2.1}$$

for $x > 0$. As h is monotonic increasing and strictly convex then so is f. Since $a > 0$ and is a constant, it will not affect the monotonicity and curvature of h and we will drop it for the rest of this study. We demonstrate that h is monotonic increasing and strictly convex now.

E.2.1 Monotonic increasing

A change of variable $x \to e^u$ gives

$$h\left(u\right) = \frac{2u}{e^{2u}-1}e^{3u}, \tag{E.2.2}$$

for $u \in \mathbb{R}$. From this we obtain

$$h'\left(u\right) = e^{2u}\mathrm{csch}u\left(1-u(\coth u - 2)\right). \tag{E.2.3}$$

Since

$$h'\left(x\right) = u'\left(x\right)h'\left(u\right), \tag{E.2.4}$$

and

$$u'\left(x\right) = \frac{1}{x}, \tag{E.2.5}$$

which is strictly positive for $x > 0$, studying the sign of $h'(x)$, requires us to concern ourselves only with the sign of $h'(u)$. We may drop the factor e^{2u} and consider

$$\operatorname{csch} u \left(1 - u(\coth u - 2)\right),$$

where we recall that

$$\operatorname{sgn}\left(\operatorname{csch} u\right) = \operatorname{sgn}\left(u\right). \tag{E.2.6}$$

Starting with the result that

$$e^{-2u}\left(2u + 1\right) < 1 \tag{E.2.7}$$

for strictly positive u, write

$$e^{-2u}\left(2u + 1\right) - 1 < 0. \tag{E.2.8}$$

Recognising the left-hand side as

$$2ue^{-2u} - \left(1 - e^{-2u}\right), \tag{E.2.9}$$

we write

$$\left(1 - e^{-2u}\right)\left(\frac{2ue^{-2u}}{1 - e^{-2u}} - 1\right) < 0, \tag{E.2.10}$$

for strictly positive u. Using the expression

$$2e^{-2u}u = u\left(1 + e^{-2u} - 1 + e^{-2u}\right) \tag{E.2.11}$$

leads to the conclusion

$$u \coth u - 1 < u \tag{E.2.12}$$

for strictly positive u.

Using the definition of coth, we write

$$\begin{aligned} u \coth u - 1 &= \frac{1 + e^{2u}(u - 1) + u}{e^{2u} - 1} \\ &= \frac{e^{-u}(1 + u) + e^{u}(u - 1)}{e^{u} - e^{-u}}. \end{aligned} \tag{E.2.13}$$

For $u > 0$, we have $e^u - e^{-u} > 0$ and the sign of $u \coth u - 1$ is given by the sign of

$$\lambda(u) = e^{-u}(1+u) + e^u(u-1). \tag{E.2.14}$$

Its derivative is

$$\lambda'(u) = u(e^u - e^{-u}), \tag{E.2.15}$$

which is strictly positive for $u > 0$. Thus λ is a strictly increasing function on $\mathbb{R}^+$ and its minimum on $\mathbb{R}^+$ is

$$\lambda(0) = 0. \tag{E.2.16}$$

From this, we have for $u > 0$

$$u \coth u - 1 > 0 \tag{E.2.17}$$

and since $u \coth u - 1$ is an even function of u, we also learn that

$$u \coth u - 1 > u \tag{E.2.18}$$

for $u < 0$.

From this follows

$$u \coth u - 1 - 2u < 0 \tag{E.2.19}$$

for strictly positive u and

$$u \coth u - 1 - 2u > 0 \tag{E.2.20}$$

for strictly negative u. We can also evaluate

$$\lim_{u \to 0} h'(u) = 2. \tag{E.2.21}$$

Thus $h'(u) > 0$, the function $h(u)$ is monotonic increasing and so is $f(x)$.

E.2.2 Strictly convex

The strict convexivity of h may be demonstrated by considering the sign of its second derivative which may be expressed as

$$\frac{d^2h}{dx^2} = \frac{1}{x^2}\left(\frac{d^2h}{du^2} - \frac{dh}{du}\right). \tag{E.2.22}$$

The content of the parentheses written explicitly as a function of u is

$$\frac{2e^{3u}\left(2e^{2u}(u-3) + e^{4u} + 6u + 5\right)}{\left(e^{2u}-1\right)^3}. \tag{E.2.23}$$

The denominator of this expression has sign equal to the sign of u. Our strategy for proving the convexivity is to prove that this same statement may be made about the numerator.

Owing to the positivity of e^{3u}, we need only consider now the sign of

$$s\left(u\right) = 2e^{2u}(u-3) + e^{4u} + 6u + 5. \tag{E.2.24}$$

Let us observe that at $u = 0$,

$$s\left(0\right) = 0, \tag{E.2.25}$$

$$s'\left(0\right) = 0, \tag{E.2.26}$$

$$s''\left(0\right) = 0, \tag{E.2.27}$$

where the primes denote differentiation with respect to u. Consider now

$$s''\left(u\right) = 8e^{2u}u - 16e^{2u} + 16e^{4u}. \tag{E.2.28}$$

As $e^{4u}/e^{2u} = e^{2u}$, we see that $s''(u)$ is positive for $u > 0$ (since $e^{2u} > 1$) and $s''(u)$ is negative for $u < 0$ (since $e^{2u} < 1$).

This implies that $s'\left(u\right)$ decreases when $u < 0$ to the value 0 at $u = 0$ and increases for all positive u. That is to say that $s'\left(u\right) > 0$ for all $u \neq 0$.

In turn, this implies that $s\left(u\right)$ is an increasing function for all negative and positive values of u. As $s\left(0\right) = 0$, then for $u < 0$ we have $s\left(u\right) < 0$ and for $u > 0$ we have

$s(u) > 0$.

Therefore

$$\frac{2e^{3u}\left(2e^{2u}(u-3)+e^{4u}+6u+5\right)}{\left(e^{2u}-1\right)^3} > 0 \tag{E.2.29}$$

for all $u \neq 0$. Besides,

$$\lim_{u\to 0} \frac{2e^{3u}\left(2e^{2u}(u-3)+e^{4u}+6u+5\right)}{\left(e^{2u}-1\right)^3} = \frac{5}{3}, \tag{E.2.30}$$

and s is always positive. We conclude that $h''(x) > 0$ for all positive x.

Appendix F

Caveats for the theorem

In this section we discuss the two assumptions made in our derivation of the theorem of Chapter 4.[1]

F.1 The cancellation of terms in the seesaw expansion

Alternatives to the condition of eq.(4.2.16) for the tree-level mass involve the cancellation of terms in the seesaw expansion. Consider the light mass matrix to second order in the expansion (denoted $m_\nu^{0(2)}$) [177, 178],

$$m_\nu^{0(2)} = -m_\nu^{0(1)} + \frac{1}{2}\left(m_\nu^{0(1)} Z^\dagger Z + Z^T Z^* m_\nu^{0(1)}\right), \tag{F.1.1}$$

with $m_\nu^{0(1)}$ the first order expression.

If this is set to zero by a cancellation of the two terms (as opposed to setting $m_\nu^{0(1)} = 0$), one finds that

$$0 = -\hat{m}_\nu^{0(1)} + \frac{1}{2}\left(\hat{m}_\nu^{0(1)}\Theta + \Theta^T \hat{m}_\nu^{0(1)}\right), \tag{F.1.2}$$

[1]Both caveats would follow as a consequence of taking the ratio of the electroweak scale v and the heavy Majorana neutrino mass scale m_N, $a \equiv v/m_N$ to be an independent variable and insist that $m_\nu = 0$ no matter the value of a. But I don't know the significance of this.

where Θ is $Z^\dagger Z$ transformed under a unitary transformation.

From the diagonal elements one finds

$$-\hat{m}_{\nu ii}^{0(1)} + \hat{m}_{\nu ii}^{0(1)}\theta_{ii} = 0 \tag{F.1.3}$$

with no summation implied ($i \in \{1,2,3\}$). Thus if one wants to avoid the solution that all three $\hat{m}_{\nu ii}^{0(1)} = 0$, then it follows that at least one $\Theta_{ii} = 1$.

The Frobenius norm of a matrix Θ is defined by

$$||\Theta||_{\mathrm{F}} = \sqrt{\sum_{i=1}^{3}\sum_{j=1}^{3}|\Theta_{ij}|^2} = \sqrt{\mathrm{Tr}\,(\Theta\Theta^\dagger)}. \tag{F.1.4}$$

Now, $Z^\dagger Z$ and Θ differ only by a unitary transformation and thus have the same Frobenius norm.

Using the 2σ upper bounds on $Z^\dagger Z$ from the global fit [286], we find $||\Theta||_{\mathrm{F}} \leq 0.0075$. But the matrices resulting from the cancellation of the first pair of terms in the seesaw expansion have $||\Theta||_{\mathrm{F}} \geq 1$. This naturally precludes the possibility of having a cancellation between different orders of the seesaw expansion.

F.2 Fine-tuning of the cancellation between the tree-level and one-loop contributions to the light neutrino masses

An explicit caveat to our result is the possibility that the smallness of the light neutrino masses results from a cancellation between large tree-level and one-loop contributions as presented in [72]. We will not discuss the radiative stability of this result. Instead we will show that this type of cancellation does not result from the texture of the neutrino mass matrix but from an extremely fine-tuned adjustment of all parameters, including the heavy neutrino masses.

Using the scaling introduced in eq.(4.2.30), we plot in figure F.1 the evolution of the

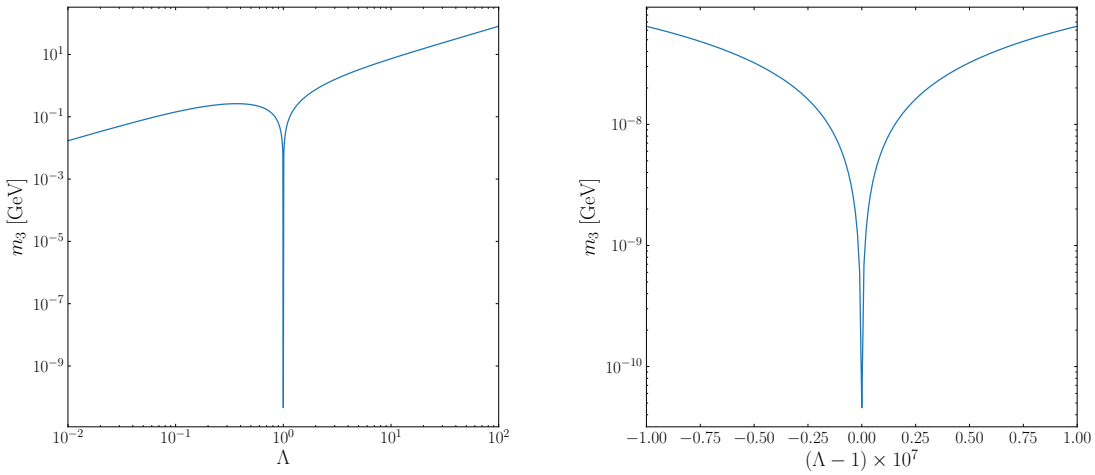

Figure F.1: Evolution of the mass (m_3) of the heaviest of the light neutrinos as a function of the rescaling parameter Λ. Input masses and couplings where chosen to give $m_\nu = m_{\text{tree}} + m_{\text{1-loop}} = 0.046\,\text{eV}$ at $\Lambda = 1$.

mass of the heaviest of the light neutrinos as a function of the rescaling parameter Λ. It is clear that even an extremely small deviation from $\Lambda = 1$, less than 10^{-7} here, is enough to spoil the cancellation and lead to light neutrino masses in contradiction with experimental limits from β decay [38,39] and observational cosmology [88]. This demonstrates that such a cancellation cannot be achieved solely by the choice of a specific texture for the neutrino mass matrix but relies on an extremely fine-tuned choice of the input masses.

It is perhaps not surprising that excluding the cancellation across different orders of the loop expansion lead us to a symmetry. Here is an argument why. If one multiplies a Lagrangian by a factor Λ, $\mathcal{L} \to \Lambda\mathcal{L}$, then in calculating Feynman diagrams the power of Λ depends only on the number of loops (and not the power of the couplings or anything more complicated like that). This follows because, if N is the power of Λ in a diagram, then

$$N = V - P,$$

for P propagators and V vertices. But the number of loops L in a diagram is

$$L = P - V + 1 = -N + 1.$$

So that the number of loops and the power of Λ determine one another.

This means that for our expansion of the neutrino mass

$$m_\nu = m_\nu^0 + m_\nu^1 + m_\nu^2 + \ldots,$$

then a scaled $\mathcal{L}$ would give

$$m_\nu = \Lambda m_\nu^0 + \Lambda^0 m_\nu^1 + \Lambda^{-1} m_\nu^2 + \ldots.$$

So if we impose $m_\nu = 0$ and insist that the condition stays true after $\mathcal{L} \to \Lambda\mathcal{L}$, then we need each contribution $m_i = 0$. But a scaling $\mathcal{L} \to \Lambda\mathcal{L}$ preserves all symmetries at the Lagrangian level so of all the solutions we excluded in insisting we can rescale, none of them set the light neutrino masses to zero as a result of Lagrangian level symmetries.

Appendix G

Higher-order corrections and the Yukawas

G.1 Higher-order radiative corrections and fine-tuning

We have been careful to include the one-loop radiative corrections to the light neutrino masses. In doing so we have expanded the region of the parameter space in which we may accurately explore leptogenesis. Of course, there may also be regions in which the higher-order corrections are important. We may ask the question *how can we be sure that the neglect of two-loops, three-loops etc. was legitimate?*

A pragmatic approach is to perform an order-of-magnitude estimate of the effects of the higher-order corrections for those points in the parameter space of most significance to our result: the best-fit points for the scenarios S_1 to $\overline{S_4}$ and $S_{m_\nu^1}$, $S_{m_\nu^0}$. If, in these scenarios, the higher-order corrections appear small then our main conclusions are left untouched.

Our estimate of the two-loop effect (which we shall assume generically dominates three or more loops) will be given by two extra factors of the Yukawa couplings and

	$\sum_i \left(m_\nu^0 + m_\nu^1\right)_i$ (eV)	$\sum_i m_{\nu i}^2$ (eV)
S_1	3.70×10^{-1}	1.69×10^{-3}
S_2	2.52×10^{-1}	1.12×10^{-3}
S_3	3.53×10^{-1}	4.25×10^{-3}
S_4	6.30×10^{-1}	5.81×10^{-2}
$\overline{S_1}$	1.13×10^{-1}	1.98×10^{-4}
$\overline{S_2}$	1.16×10^{-1}	2.22×10^{-4}
$\overline{S_3}$	1.14×10^{-1}	1.95×10^{-3}
$\overline{S_4}$	1.09×10^{-1}	1.91×10^{-3}
$S_{m_\nu^1}$	8.65×10^{-2}	1.07×10^{-6}
$S_{m_\nu^0}$	6.39×10^{-2}	7.58×10^{-8}

Table G.1: Comparisons of the (sum of singular values of the) tree plus one-loop correct light mass matrix to the two-loop estimate.

the conventional loop factor $(4\pi)^{-2}$ to the one-loop effect. Let us use

$$m_\nu^2 = \frac{1}{(4\pi)^2} |Y_{\text{max.}}|^2 m_\nu^1, \tag{G.1.1}$$

with $|Y_{\text{max.}}|$ the largest element of the matrix of absolute values of the Yukawas, as a conservative estimate (over-estimate) of the second-order radiative correction to neutrino masses. (This is similar to the estimate used in [72].)

From Table G.1, we see that the two-loop contributions generally provide small corrections and therefore that corrections beyond one-loop order are safely neglected at these points.

G.2 Yukawa matrices

Here we provide a table of the absolute values of the Yukawa matrices ($|Y|$) for the best-fit points of each scenario considered in Table 5.1 and Table 5.2.

	$\lvert Y\rvert$
S_1	$\begin{pmatrix} 1.20501\times10^{-5} & 5.84226\times10^{-3} & 1.04449\times10^{-2} \\ 6.50743\times10^{-5} & 2.0441\times10^{-2} & 3.65463\times10^{-2} \\ 7.26332\times10^{-6} & 2.11503\times10^{-2} & 3.78139\times10^{-2} \end{pmatrix}$
S_2	$\begin{pmatrix} 1.78047\times10^{-5} & 1.16361\times10^{-2} & 2.08046\times10^{-2} \\ 1.00881\times10^{-5} & 2.21656\times10^{-2} & 3.96322\times10^{-2} \\ 1.02069\times10^{-4} & 2.55\times10^{-2} & 4.55925\times10^{-2} \end{pmatrix}$
S_3	$\begin{pmatrix} 3.07775\times10^{-5} & 1.59166\times10^{-2} & 2.84583\times10^{-2} \\ 1.23975\times10^{-5} & 3.77326\times10^{-2} & 6.74663\times10^{-2} \\ 1.14533\times10^{-4} & 3.93327\times10^{-2} & 7.03289\times10^{-2} \end{pmatrix}$
S_4	$\begin{pmatrix} 2.54075\times10^{-5} & 3.09962\times10^{-2} & 6.2255\times10^{-2} \\ 1.52369\times10^{-5} & 7.01974\times10^{-2} & 1.40989\times10^{-1} \\ 1.99141\times10^{-4} & 8.33171\times10^{-2} & 1.67344\times10^{-1} \end{pmatrix}$
$\overline{S_1}$	$\begin{pmatrix} 5.37412\times10^{-6} & 3.81344\times10^{-3} & 6.81765\times10^{-3} \\ 4.68081\times10^{-6} & 1.03898\times10^{-2} & 1.85756\times10^{-2} \\ 2.33498\times10^{-5} & 1.28236\times10^{-2} & 2.29271\times10^{-2} \end{pmatrix}$
$\overline{S_2}$	$\begin{pmatrix} 5.37412\times10^{-6} & 3.81344\times10^{-3} & 6.81765\times10^{-3} \\ 4.68081\times10^{-6} & 1.03898\times10^{-2} & 1.85756\times10^{-2} \\ 2.33498\times10^{-5} & 1.28236\times10^{-2} & 2.29271\times10^{-2} \end{pmatrix}$
$\overline{S_3}$	$\begin{pmatrix} 5.37412\times10^{-6} & 3.81344\times10^{-3} & 6.81765\times10^{-3} \\ 4.68081\times10^{-6} & 1.03898\times10^{-2} & 1.85756\times10^{-2} \\ 2.33498\times10^{-5} & 1.28236\times10^{-2} & 2.29271\times10^{-2} \end{pmatrix}$
$\overline{S_4}$	$\begin{pmatrix} 5.37412\times10^{-6} & 3.81344\times10^{-3} & 6.81765\times10^{-3} \\ 4.68081\times10^{-6} & 1.03898\times10^{-2} & 1.85756\times10^{-2} \\ 2.33498\times10^{-5} & 1.28236\times10^{-2} & 2.29271\times10^{-2} \end{pmatrix}$
$S_{m_\nu^1}$	$\begin{pmatrix} 6.27292\times10^{-4} & 1.68158\times10^{-2} & 2.98125\times10^{-2} \\ 2.86893\times10^{-3} & 3.06908\times10^{-2} & 5.56779\times10^{-2} \\ 9.98924\times10^{-4} & 2.62581\times10^{-2} & 4.69331\times10^{-2} \end{pmatrix}$
$S_{m_\nu^0}$	$\begin{pmatrix} 2.08179\times10^{-4} & 3.44059\times10^{-3} & 6.19056\times10^{-3} \\ 3.20671\times10^{-4} & 5.48821\times10^{-3} & 9.63727\times10^{-3} \\ 2.05748\times10^{-4} & 5.38578\times10^{-3} & 9.37847\times10^{-3} \end{pmatrix}$

Table G.2: Absolute values of the Yukawas for each scenario listed in Table 5.1 and Table 5.2.

Appendix H

Classes of CP-conserving R-matrix

With the parameters x_2, y_1 and y_3 left arbitrary, there are 16 possible R-matrices which lead to the fine-tuned light neutrino masses required for successful leptogenesis (Eq. (7.3.1)). For any of these matrices, the absolute values of the elements $|R_{ij}|$ are equal, with the elements themselves differing only by factors ± 1 or $\pm i$. When there is an exact CP-symmetry, then each R-matrix satisfies the condition in Eq. (6.2.5). This allows for a scheme of classification according the phases ρ^ν, ρ^N they correspond to. In this section we present a single example of a matrix for each class[1]:

$\rho^\nu = \pm(-1,+1,+1)^T$, $\rho^N = \pm(+1,+1,-1)^T$ and $x_1 = 90°$ and $x_3 = 90°$:

$$R \approx \begin{pmatrix} -\frac{i}{2}e^{y_3}\cos x_2 & \frac{1}{2}e^{y_3}\cos x_2 & \sin x_2 \\ \frac{i}{4}e^{y_1+y_3}(\sin x_2+1) & -\frac{1}{4}e^{y_1+y_3}(\sin x_2+1) & \frac{1}{2}e^{y_1}\cos x_2 \\ \frac{1}{4}e^{y_1+y_3}(\sin x_2+1) & \frac{i}{4}e^{y_1+y_3}(\sin x_2+1) & -\frac{i}{2}e^{y_1}\cos x_2 \end{pmatrix},$$

in which the second form results from the neglect of terms involving factors e^{-y_1} and e^{-y_3}. $\rho^\nu = \pm(+1,-1,+1)^T$, $\rho^N = \pm(+1,-1,+1)^T$ and $x_1 = 0°$ and $x_3 = 0°$:

$$R \approx \begin{pmatrix} \frac{1}{2}e^{y_3}\cos x_2 & \frac{i}{2}e^{y_3}\cos x_2 & \sin x_2 \\ -\frac{i}{4}e^{y_1+y_3}(\sin x_2+1) & \frac{1}{4}e^{y_1+y_3}(\sin x_2+1) & \frac{i}{2}e^{y_1}\cos x_2 \\ -\frac{1}{4}e^{y_1+y_3}(\sin x_2+1) & -\frac{i}{4}e^{y_1+y_3}(\sin x_2+1) & \frac{1}{2}e^{y_1}\cos x_2 \end{pmatrix},$$

[1]Here we neglect terms involving factors e^{-y_1} or e^{-y_3} such that, as given, these matrices are not strictly orthogonal.

$\rho^\nu = \pm(+1,-1,+1)^T$, $\rho^N = \pm(+1,+1,-1)^T$ and $x_1 = 90^\circ$ and $x_3 = 0^\circ$:

$$R \approx \begin{pmatrix} \frac{1}{2}e^{y_3}\cos x_2 & \frac{i}{2}e^{y_3}\cos x_2 & \sin x_2 \\ -\frac{1}{4}e^{y_1+y_3}(\sin x_2+1) & -\frac{i}{4}e^{y_1+y_3}(\sin x_2+1) & \frac{1}{2}e^{y_1}\cos x_2 \\ \frac{i}{4}e^{y_1+y_3}(\sin x_2+1) & -\frac{1}{4}e^{y_1+y_3}(\sin x_2+1) & -\frac{i}{2}e^{y_1}\cos x_2 \end{pmatrix},$$

$\rho^\nu = \pm(-1,+1,+1)^T$, $\rho^N = \pm(+1,-1,+1)^T$ and $x_1 = 90^\circ$ and $x_3 = 0^\circ$:

$$R \approx \begin{pmatrix} -\frac{i}{2}e^{y_3}\cos x_2 & \frac{1}{2}e^{y_3}\cos x_2 & \sin x_2 \\ -\frac{1}{4}e^{y_1+y_3}(\sin x_2+1) & -\frac{i}{4}e^{y_1+y_3}(\sin x_2+1) & \frac{i}{2}e^{y_1}\cos x_2 \\ \frac{i}{4}e^{y_1+y_3}(\sin x_2+1) & -\frac{1}{4}e^{y_1+y_3}(\sin x_2+1) & \frac{1}{2}e^{y_1}\cos x_2 \end{pmatrix}.$$

Appendix I

Further results for low energy CP-violation leptogenesis

In Fig. I.1 we demonstrate the possibility of fine-tuned leptogenesis in the case of normal ordering with $M_1 = 3.16 \times 10^6$ GeV and $m_1 = 0.05$ eV. This is a variant of the case considered in the main body for which the light neutrino masses are significantly reduced below all present cosmological or current generation direct bounds. We note that lowering the light neutrino masses in this way severely constrains the viable parameter space over that in Fig. 6.7 such that $\delta \approx 296°$, $\alpha_{21} \approx 143°$ and $\alpha_{31} \approx 14°$. Typical fine-tuning in the viable regions is $\mathcal{F} \approx 450$.

In the cases of $m_1 = 0$ and $m_1 = 10^{-3}$ eV with $M_1 = 10^8$ GeV, $M_2 = 3M_1$ and $M_3 = 3M_2$ we did not find a region in the relevant parameter space in which one could have successful leptogenesis.

In Fig. I.2 we present results for $M_1 = 10^9$ GeV. We find that a fine-tuning of the light neutrino masses $\mathcal{F} \approx 14$ at the best-fit points. In the normal ordered case, we find that the observed baryon asymmetry may be obtained to within 1σ (2σ) with δ between $[0, 360]°$ ($[0, 360]°$). While for inverted ordering, the 1σ (2σ) range is $[25, 360]°$ ($[0, 360]°$). This is significantly higher than the case for which $M_1 = 10^{10}$ GeV where the fine-tuning is considerably less at $\mathcal{F} \approx 0.23$. In the normal ordered case, we find that the observed baryon asymmetry may be obtained to within 1σ

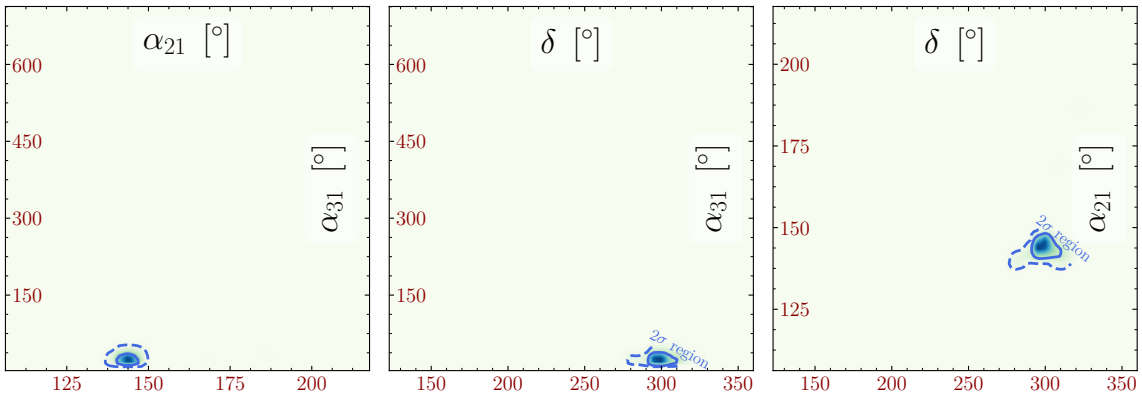

Figure I.1: The two-dimensional projections for intermediate scale leptogenesis with $M_1 = 3.16 \times 10^6$ GeV and $m_1 = 0.05$ eV with CP violation provided only by the phases of the PMNS matrix. Solid lines correspond to 68% confidence level and dashed to 95% confidence level in agreement with the observed value $\eta_{B_{CMB}}$. This plot was created using SuperPlot [201].

(2σ) with δ between $[95, 265]^\circ$ ($[52, 282]^\circ$). For inverted ordering, the 1σ (2σ) range is $[60, 338]^\circ$ ($[8, 360]^\circ$).

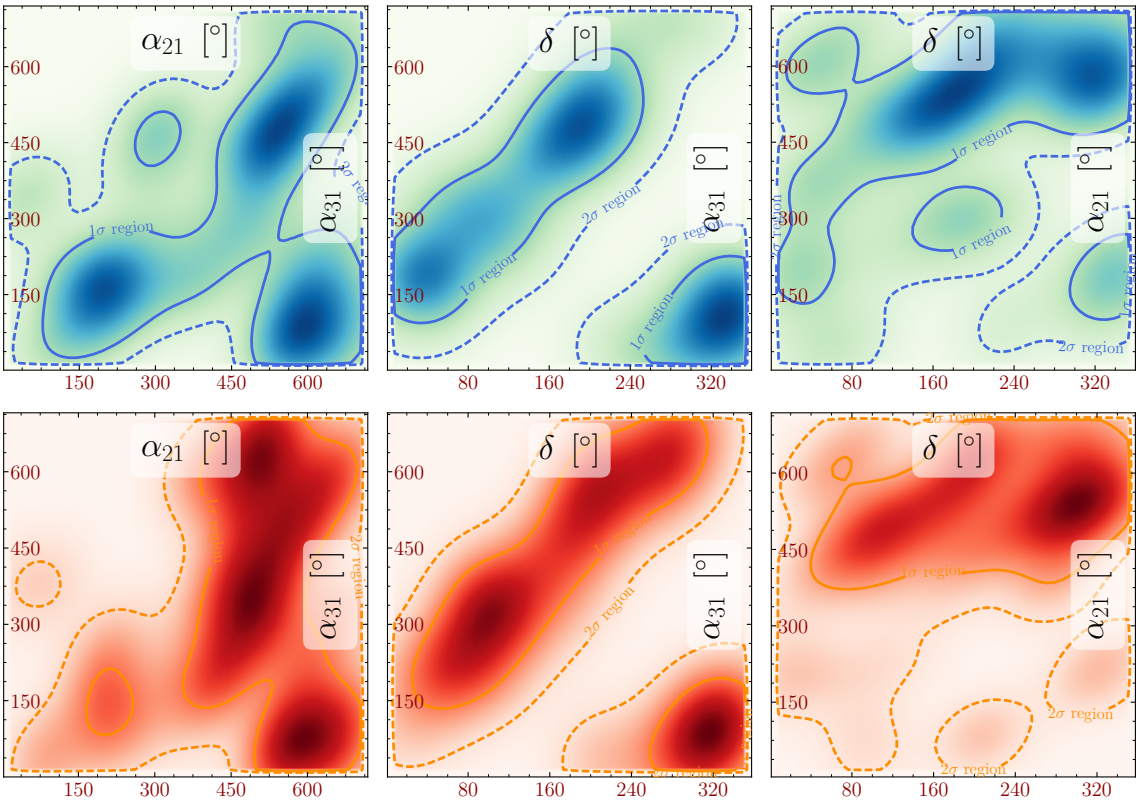

Figure I.2: The two-dimensional projections for leptogenesis with $M_1 = 1.00 \times 10^9$ GeV with CP violation provided only by the phases of the PMNS matrix. The normal ordered case is coloured blue/green and inverted ordering orange/red and contours correspond to 68% and 95% confidence levels. This plot was created using SuperPlot [201].

Appendix J

Single-flavour BE from DMEs

In this appendix we find the conditions under which the density matrix equations (Eq. (3.3.12)) approximate to the single flavour Boltzmann equations. We begin by analysing the criteria under which the single flavour Boltzmann equation

$$\frac{dn_{B-L}}{dz} = \mathrm{Tr}\,\boldsymbol{\epsilon} D(n_N - n_N^{\mathrm{eq}}) - W n_{B-L}, \tag{J.0.1}$$

emerges as an approximation from the density matrix equations, which, written in the (β, τ)-basis are

$$\begin{aligned}
\frac{dn_N}{dz} &= -D\left(n_N - n_N^{\mathrm{eq}}\right) \\
\frac{dn_{\beta\beta}^{B-L}}{dz} &= \epsilon_{\beta\beta} D\left(n_N - n_N^{\mathrm{eq}}\right) - \frac{1}{2} W\left(2|c_{1\beta}|^2 n_{\beta\beta}^{B-L} + c_{1\tau}^* c_{1\beta} n_{\tau\beta}^{B-L} + c_{1\tau} c_{1\beta}^* n_{\beta\tau}^{B-L}\right) \\
\frac{dn_{\tau\tau}^{B-L}}{dz} &= \epsilon_{\tau\tau} D\left(n_N - n_N^{\mathrm{eq}}\right) - \frac{1}{2} W\left(2|c_{1\tau}|^2 n_{\tau\tau}^{B-L} + c_{1\tau}^* c_{1\beta} n_{\tau\beta}^{B-L} + c_{1\tau} c_{1\beta}^* n_{\beta\tau}^{B-L}\right) \\
\frac{dn_{\beta\tau}^{B-L}}{dz} &= \epsilon_{\beta\tau} D\left(n_N - n_N^{\mathrm{eq}}\right) - \frac{1}{2} W\left(n_{\beta\tau}^{B-L} + c_{1\tau}^* c_{1\beta}\left(n_{\beta\beta}^{B-L} + n_{\tau\tau}^{B-L}\right)\right) - \frac{\Gamma_\tau}{Hz} n_{\beta\tau}^{B-L}.
\end{aligned} \tag{J.0.2}$$

As $n_{B-L} = n_{\tau\tau}^{B-L} + n_{\beta\beta}^{B-L}$, we find an equation for the evolution of n_{B-L} by adding the second and third equations together, obtaining

$$\frac{dn_{B-L}}{dz} = D\left(n_N - n_N^{\mathrm{eq}}\right) \mathrm{Tr}\,\boldsymbol{\epsilon} - W\left(|c_{1\tau}|^2 n_{\tau\tau}^{B-L} + |c_{1\tau^\perp}|^2 n_{\beta\beta}^{B-L} + 2\Re[c_{1\beta} c_{1\tau}^* n_{\tau\beta}^{B-L}]\right). \tag{J.0.3}$$

If this were to reproduce the single flavour limit, then we should find that the coefficient of W:

$$|c_{1\tau}|^2 n_{\tau\tau}^{B-L} + |c_{1\beta}|^2 n_{\beta\beta}^{B-L} + 2\Re[c_{1\beta}c_{1\tau}^* n_{\tau\beta}^{B-L}], \tag{J.0.4}$$

is equal to n_{B-L} in the limit that Γ_τ/Hz is small. Recalling that $|c_{1\beta}|^2 + |c_{1\tau}|^2 = 1$, then one should expect, that in the limit of small thermal widths,

$$2\Re\left[c_{1\beta}c_{1\tau}^* n_{\tau\beta}^{B-L}\right] = |c_{1\beta}|^2 n_{\tau\tau}^{B-L} + |c_{1\tau}|^2 n_{\beta\beta}^{B-L}. \tag{J.0.5}$$

In order to demonstrate this equality, first we show that the z-derivative of $2\Re[c_{1\beta}c_{1\tau}^* n_{\tau\beta}^{B-L}]$ equals the z-derivative of $|c_{1\beta}|^2 n_{\tau\tau}^{B-L} + |c_{1\tau}|^2 n_{\beta\beta}^{B-L}$ meaning that the quantities themselves may differ only by a constant. Then we note that, since at $z = z_0$ the quantities are equal, then they must be equal for all z.

By multiplication of the relevant equations in Eq. (J.0.2), we obtain the z-evolution of $|c_{1\beta}|^2 n_{\tau\tau}^{B-L} + |c_{1\tau}|^2 n_{\beta\beta}^{B-L}$:

$$\begin{aligned}
&|c_{1\beta}|^2 \frac{dn_{\tau\tau}^{B-L}}{dz} + |c_{1\tau}|^2 \frac{dn_{\beta\beta}^{B-L}}{dz} = \\
&(|c_{1\beta}|^2\epsilon_{\tau\tau} + |c_{1\tau}|^2\epsilon_{\beta\beta})D(n_N - n_N^{\rm eq}) - W(\Re[c_{1\beta}c_{1\tau}^* n_{\tau\beta}^{B-L}] + |c_{1\beta}|^2|c_{1\tau}|^2(n_{\tau\tau}^{B-L} + n_{\beta\beta}^{B-L})).
\end{aligned} \tag{J.0.6}$$

By similar means we obtain the z-evolution of $\Re[c_{1\beta}c_{1\tau}^* n_{\tau\beta}^{B-L}]$:

$$\begin{aligned}
\Re[c_{1\beta}c_{1\tau}^* \frac{dn_{\tau\beta}^{B-L}}{dz}] =& \Re\left[c_{1\beta}c_{1\tau}^*\epsilon_{\tau\beta}\right] D(n_N - n_N^{\rm eq}) \\
&- \frac{1}{2}W(\Re\left[c_{1\beta}c_{1\tau}^* n_{\tau\beta}^{B-L}\right] + |c_{1\beta}|^2|c_{1\tau}|^2(n_{\tau\tau}^{B-L} + n_{\beta\beta}^{B-L})) \\
&- \Re\left[c_{1\beta}c_{1\tau}^* n_{\tau\beta}^{B-L}\right] \frac{\Gamma_\tau}{Hz}.
\end{aligned}$$

Neglecting Γ_τ/Hz, as we expect this to be small in the single-flavour regime, then we need only show that

$$2\Re\left[c_{1\beta}c_{1\tau}^*\epsilon_{\tau\beta}\right] = |c_{1\beta}|^2\epsilon_{\tau\tau} + |c_{1\tau}|^2\epsilon_{\beta\beta}, \tag{J.0.7}$$

and then it is demonstrated that the coefficient of W in Eq. (J.0.3) is approximately equal to n_{B-L} and thus the single flavour equations are recovered.

The relation of Eq. (J.0.7) can be put into a more suggestive form if we use $|c_{1\beta}|^2 = 1 - |c_{1\tau}|^2$ to re-express it thus

$$2\Re[c_{1\beta}c^*_{1\tau}\epsilon_{\tau\beta}] + |c_{1\beta}|^2\epsilon_{1\beta} + |c_{1\tau}|^2\epsilon_{1\tau} = \epsilon_{\tau\tau} + \epsilon_{\beta\beta}. \tag{J.0.8}$$

The right-hand side of this equation is merely the trace of the CP-asymmetry tensor $\mathrm{Tr}\,\epsilon$ in the (β, τ)-basis. Thus, we suspect that the left-hand side is merely the trace expressed in an unfamiliar basis. This can be confirmed to be the case by construction of the unitary matrix

$$\mathcal{S} = \begin{pmatrix} c_{1\tau} & -c^*_{1\beta} \\ c_{1\beta} & c^*_{1\tau} \end{pmatrix}, \tag{J.0.9}$$

then, by explicit calculation it can be seen that the left-hand side is the result of summing the diagonals (evaluating the trace in a particular basis) of

$$\mathcal{S}^\dagger \boldsymbol{\epsilon} \mathcal{S}. \tag{J.0.10}$$

Thus, we may conclude that, if we set $\Im(\Lambda_\tau) = 0$, we are left with

$$2\Re\left[c_{1\beta}c^*_{1\tau}\frac{dn^{B-L}_{\tau\beta}}{dz}\right] = |c_{1\beta}|^2\frac{dn^{B-L}_{\tau\tau}}{dz} + |c_{1\tau}|^2\frac{dn^{B-L}_{\beta\beta}}{dz}, \tag{J.0.11}$$

and so

$$\frac{d}{dz}(|c_{1\tau}|^2 n^{B-L}_{\tau\tau} + |c_{1\beta}|^2 n^{B-L}_{\beta\beta} + 2\Re[c_{1\beta}c^*_{1\tau}n^{B-L}_{\tau\beta}]) = \frac{dn_{B-L}}{dz}. \tag{J.0.12}$$

Since $n_{\alpha\beta} = 0$ at the initial z, then we may conclude that, if $\Gamma_\tau = 0$, then

$$\frac{dn_{B-L}}{dz} = \mathrm{Tr}\,\boldsymbol{\epsilon} D(n_N - n^{\mathrm{eq}}_N) - W n_{B-L}, \tag{J.0.13}$$

which is the single-flavour limit.

If we don't set $\Gamma_\tau = 0$, then we have

$$\frac{d}{dz}(|c_{1\tau}|^2 n^{B-L}_{\tau\tau} + |c_{1\beta}|^2 n^{B-L}_{\beta\beta} + 2\Re[c_{1\beta}c^*_{1\tau}n^{B-L}_{\tau\beta}]) = \frac{dn_{B-L}}{dz} - 2\Re[c_{1\beta}c^*_{1\tau}\frac{\Gamma_\tau}{Hz}n^{B-L}_{\tau\beta}], \tag{J.0.14}$$

which suggests that we should write the integro-differential equation

$$\frac{dn_{B-L}}{dz} = \mathrm{Tr}\,\boldsymbol{\epsilon} D(n_N - n_N^{\mathrm{eq}}) - W n_{B-L} + 2W \int_{z_0}^{z} dz' \Re \left[c_{1\beta} c_{1\tau}^* \frac{\Gamma_\tau}{H z'} n_{\tau\beta}^{B-L}(z') \right]. \quad \text{(J.0.15)}$$

We define

$$\lambda(z) \equiv 2 \int_{z_0}^{z} dz' \Re \left[c_{1\beta} c_{1\tau}^* \frac{\Gamma_\tau}{H z'} n_{\tau\beta}^{B-L}(z') \right], \quad \text{(J.0.16)}$$

for brevity, then using the integrating factor method, arrive at a solution

$$\begin{aligned} n_{B-L}(z_f) &= e^{-\int_{z_0}^{z_f} W(z) dz} \int_{z_0}^{z_f} e^{\int_{z_0}^{z'} W(z'') dz''} \left(\mathrm{Tr}\,\boldsymbol{\epsilon} D(z')(n_N(z') - n_N^{\mathrm{eq}}(z')) + W(z')\lambda(z') \right) dz' \\ &= \int_{z_0}^{z_f} e^{-\int_{z'}^{z_f} W(z'') dz''} \left(\mathrm{Tr}\,\boldsymbol{\epsilon} D(z')(n_N(z') - n_N^{\mathrm{eq}}(z')) + W(z')\lambda(z') \right) dz'. \end{aligned}$$

For large M, the thermal width is very small and so the term in λ is usually neglected in comparison with the first.

Appendix K

Robustness of the high-scale plateau

In the transition region, the approximation that left-handed τ leptons are produced and destroyed at the same rate by flavour effects is somewhat inaccurate. In fact we should consider a slightly more accurate version of the density matrix equations in which the asymmetry density of right-handed τ leptons, $n_{\tau R}$ is computed. Then, the density matrix equations are

$$\begin{aligned}
\frac{dn_{N_1}}{dz} &= -D_1\left(n_{N_1} - n_{N_1}^{\rm eq}\right) \\
\frac{dn_{\beta\beta}^{B-L}}{dz} &= \epsilon_{\beta\beta}^{(1)} D_1\left(n_{N_1} - n_{N_1}^{\rm eq}\right) - \frac{1}{2}W_1\left(2|c_{1\beta}|^2 n_{\beta\beta}^{B-L} + c_{1\tau}^* c_{1\beta} n_{\tau\beta}^{B-L} + c_{1\tau}c_{1\beta}^* n_{\beta\tau}\right) \\
\frac{dn_{\tau\tau}^{B-L}}{dz} &= \epsilon_{\tau\tau}^{(1)} D_1\left(n_{N_1} - n_{N_1}^{\rm eq}\right) - \frac{1}{2}W_1\left(2|c_{1\tau}|^2 n_{\tau\tau}^{B-L} + c_{1\tau}^* c_{1\beta} n_{\tau\beta}^{B-L} + c_{1\tau}c_{1\beta}^* n_{\beta\tau}\right) \\
&\quad - 2\frac{\Gamma_\tau}{2Hz}(n_{\tau\tau}^{B-L} - 2n_{\tau_R}) \\
\frac{dn_{\beta\tau}}{dz} &= \epsilon_{\beta\tau} D_1\left(n_{N_1} - n_{N_1}^{\rm eq}\right) - \frac{1}{2}W_1\left(n_{\beta\tau} + c_{1\tau}^* c_{1\beta}\left(n_{\beta\beta}^{B-L} + n_{\tau\tau}^{B-L}\right)\right) - \frac{\Gamma_\tau}{2Hz} n_{\beta\tau} \\
\frac{dn_{\tau_R}}{dz} &= 2\frac{\Gamma_\tau}{2Hz}(n_{\tau\tau}^{B-L} - 2n_{\tau_R}).
\end{aligned} \tag{K.0.1}$$

The simpler set we previously considered result from the assumption that $\Gamma_\tau/2Hz$ is large enough to enforce $n_{\tau\tau}^{B-L} = 2n_{\tau_R}$. clearly this is inaccurate for the situation under consideration where $M_1 \gg 10^{12}$ GeV. We should now append to $\lambda(z)$ an extra

term such that

$$\lambda(z) \to \lambda'(z) = 2\int_{z_0}^{z} dz' \left(\Re \left[c_{1\beta} c_{1\tau}^{*} \frac{\Gamma_\tau}{2Hz'} n_{\tau\beta}^{B-L}(z') \right] - 2\frac{\Gamma_\tau}{2Hz'} (n_{\tau\tau}^{B-L}(z') - 2n_{\tau R}(z')) \right). \tag{K.0.2}$$

Now in this solution, there is a term in $n_{\tau\tau}^{B-L}\Gamma_\tau/2Hz$ which scales approximately as $xx^{-1} = x^0$ and a term $n_{\tau R}\Gamma_\tau/2Hz$ in which, it may be shown $n_{\tau R} \propto x$ and thus $\lambda'(z)$ exhibits a approximate invariance under a scaling x as does $\lambda(z)$.

It may be added that scattering effects can be incorporated by modifying the decay function $D_1(z) \to D_1'(z) = D_1(z) + S_1(z)$ and the washout $W_1(z) \to W_1'(z) = j(z)W_1(z)$ [142]. The new decay function $D_1'(z)$ which depends on a scattering part $S_1(z)$ is still multiplied by zero in the $\mathrm{Tr}\,\epsilon = 0$ case and is thus unimportant. The new washout function is multiplied by $j(z)$ which depends on M_1 through $\log(M_1/m_H)$. Thus, the plateau demonstrated in Fig. 6.13 picks up some unimportant logarithmic dependence on M_1 in addition to the small variation when scattering is neglected. In the numerical calculations of Section 6.5, the effects of scattering are included.

Bibliography

[1] I. Esteban, M. C. Gonzalez-Garcia, A. Hernandez-Cabezudo, M. Maltoni and T. Schwetz, *Global analysis of three-flavour neutrino oscillations: synergies and tensions in the determination of θ_{23}, δ_{CP}, and the mass ordering*, *JHEP* **01** (2019) 106, [1811.05487].

[2] I. Brivio and M. Trott, *Examining the neutrino option*, *JHEP* **02** (2019) 107, [1809.03450].

[3] D. Buttazzo, G. Degrassi, P. P. Giardino, G. F. Giudice, F. Sala, A. Salvio et al., *Investigating the near-criticality of the Higgs boson*, *JHEP* **12** (2013) 089, [1307.3536].

[4] K. Moffat, S. Pascoli and C. Weiland, *Equivalence between massless neutrinos and lepton number conservation in fermionic singlet extensions of the Standard Model*, 1712.07611.

[5] K. Moffat, S. Pascoli, S. T. Petcov, H. Schulz and J. Turner, *Three-Flavoured Non-Resonant Leptogenesis at Intermediate Scales*, 1804.05066.

[6] K. Moffat, S. Pascoli, S. T. Petcov and J. Turner, *Leptogenesis from Low Energy CP Violation*, *JHEP* **03** (2019) 034, [1809.08251].

[7] I. Brivio, K. Moffat, S. Pascoli, S. T. Petcov and J. Turner, *Leptogenesis in the Neutrino Option*, 1905.12642.

[8] I. Brivio and M. Trott, *Radiatively Generating the Higgs Potential and Electroweak Scale via the Seesaw Mechanism*, *Phys. Rev. Lett.* **119** (2017) 141801, [1703.10924].

[9] M. Gell-Mann, *A Schematic Model of Baryons and Mesons*, *Phys. Lett.* **8** (1964) 214–215.

[10] G. Zweig, *An SU(3) model for strong interaction symmetry and its breaking. Version 1*, .

[11] G. Zweig, *An SU(3) model for strong interaction symmetry and its breaking. Version 2*, in *DEVELOPMENTS IN THE QUARK THEORY OF HADRONS. VOL. 1. 1964 - 1978* (D. Lichtenberg and S. P. Rosen, eds.), pp. 22–101. 1964.

[12] M. Gell-Mann, *Symmetries of baryons and mesons*, *Phys. Rev.* **125** (1962) 1067–1084.

[13] Y. Ne'eman, *Derivation of strong interactions from a gauge invariance*, *Nucl. Phys.* **26** (1961) 222–229.

[14] M. L. Perl et al., *Evidence for Anomalous Lepton Production in e+ - e- Annihilation*, *Phys. Rev. Lett.* **35** (1975) 1489–1492.

[15] UA1 collaboration, G. Arnison et al., *Experimental Observation of Isolated Large Transverse Energy Electrons with Associated Missing Energy at s**(1/2) = 540-GeV*, *Phys. Lett.* **B122** (1983) 103–116.

[16] UA2 collaboration, M. Banner et al., *Observation of Single Isolated Electrons of High Transverse Momentum in Events with Missing Transverse Energy at the CERN anti-p p Collider*, *Phys. Lett.* **B122** (1983) 476–485.

[17] UA1 collaboration, G. Arnison et al., *Experimental Observation of Lepton Pairs of Invariant Mass Around 95-GeV/c**2 at the CERN SPS Collider*, *Phys. Lett.* **B126** (1983) 398–410.

[18] UA2 collaboration, P. Bagnaia et al., *Evidence for Z0 —> e+ e- at the CERN anti-p p Collider*, *Phys. Lett.* **B129** (1983) 130–140.

[19] CDF collaboration, F. Abe et al., *Observation of top quark production in $\bar{p}p$ collisions*, *Phys. Rev. Lett.* **74** (1995) 2626–2631, [hep-ex/9503002].

[20] D0 collaboration, S. Abachi et al., *Observation of the top quark*, *Phys. Rev. Lett.* **74** (1995) 2632–2637, [hep-ex/9503003].

[21] ATLAS Collaboration collaboration, G. Aad et al., *Observation of a new particle in the search for the Standard Model Higgs boson with the ATLAS detector at the LHC*, *Phys.Lett.* **B716** (2012) 1–29, [1207.7214].

[22] CMS collaboration, S. Chatrchyan et al., *Combined results of searches for the standard model Higgs boson in pp collisions at $\sqrt{s} = 7$ TeV*, *Phys. Lett.* **B710** (2012) 26–48, [1202.1488].

[23] E. Fermi, *Tentativo di una teoria dell'emissione dei raggi beta*, *Ric. Sci.* **4** (1933) 491–495.

[24] Particle Data Group collaboration, M. Tanabashi, K. Hagiwara, K. Hikasa, K. Nakamura, Y. Sumino, F. Takahashi et al., *Review of particle physics*, *Phys. Rev. D* **98** (Aug, 2018) 030001.

[25] R. Davis, Jr., D. S. Harmer and K. C. Hoffman, *Search for neutrinos from the sun*, *Phys. Rev. Lett.* **20** (1968) 1205–1209.

[26] H. Fritzsch and P. Minkowski, *Vector-Like Weak Currents, Massive Neutrinos, and Neutrino Beam Oscillations*, *Phys. Lett.* **62B** (1976) 72–76.

[27] B. Pontecorvo, *Mesonium and anti-mesonium*, *Sov. Phys. JETP* **6** (1957) 429.

[28] B. Pontecorvo, *Inverse beta processes and nonconservation of lepton charge*, *Sov. Phys. JETP* **7** (1958) 172–173.

[29] B. Pontecorvo, *Neutrino Experiments and the Problem of Conservation of Leptonic Charge*, *Sov. Phys. JETP* **26** (1968) 984–988.

[30] V. N. Gribov and B. Pontecorvo, *Neutrino astronomy and lepton charge*, *Phys. Lett.* **28B** (1969) 493.

[31] Z. Maki, M. Nakagawa and S. Sakata, *Remarks on the unified model of elementary particles*, *Prog. Theor. Phys.* **28** (1962) 870–880.

[32] N. Cabibbo, *Unitary Symmetry and Leptonic Decays*, *Phys. Rev. Lett.* **10** (1963) 531–533.

[33] M. Kobayashi and T. Maskawa, *CP Violation in the Renormalizable Theory of Weak Interaction*, *Prog. Theor. Phys.* **49** (1973) 652–657.

[34] S. M. Bilenky and B. Pontecorvo, *Lepton Mixing and Neutrino Oscillations*, *Phys. Rept.* **41** (1978) 225–261.

[35] S. M. Bilenky and B. Pontecorvo, *Again on Neutrino Oscillations*, *Lett. Nuovo Cim.* **17** (1976) 569.

[36] Planck collaboration, N. Aghanim et al., *Planck 2018 results. VI. Cosmological parameters*, 1807.06209.

[37] G. B. Franklin, *The KATRIN Neutrino Mass Measurement: Experiment, Status, and Outlook*, in *13th Conference on the Intersections of Particle and Nuclear Physics (CIPANP 2018) Palm Springs, California, USA, May 29-June 3, 2018*, 2018, 1809.10603.

[38] C. Kraus et al., *Final results from phase II of the Mainz neutrino mass search in tritium beta decay*, *Eur. Phys. J.* **C40** (2005) 447–468, [hep-ex/0412056].

[39] Troitsk collaboration, V. N. Aseev et al., *An upper limit on electron antineutrino mass from Troitsk experiment*, *Phys. Rev.* **D84** (2011) 112003, [1108.5034].

[40] M. Blennow, E. Fernandez-Martinez, J. Lopez-Pavon and J. Menendez, *Neutrinoless double beta decay in seesaw models*, *JHEP* **07** (2010) 096, [1005.3240].

[41] KamLAND-Zen collaboration, A. Gando et al., *Search for Majorana Neutrinos near the Inverted Mass Hierarchy Region with KamLAND-Zen*, *Phys. Rev. Lett.* **117** (2016) 082503, [1605.02889].

[42] J. D. Vergados, H. Ejiri and F. Šimkovic, *Neutrinoless double beta decay and neutrino mass*, *Int. J. Mod. Phys.* **E25** (2016) 1630007, [1612.02924].

[43] S. Dell'Oro, S. Marcocci, M. Viel and F. Vissani, *Neutrinoless double beta decay: 2015 review*, *Adv. High Energy Phys.* **2016** (2016) 2162659, [1601.07512].

[44] K. Nakamura and S. Petcov, *(Particle Data Group)*, *Phys. Rev.* **D98** (2018) 030001.

[45] S. Weinberg, *Baryon and Lepton Nonconserving Processes*, *Phys. Rev. Lett.* **43** (1979) 1566–1570.

[46] S. Weinberg, *Varieties of Baryon and Lepton Nonconservation*, *Phys. Rev.* **D22** (1980) 1694.

[47] P. W. Angel, N. L. Rodd and R. R. Volkas, *Origin of neutrino masses at the LHC: $\Delta L = 2$ effective operators and their ultraviolet completions*, *Phys. Rev.* **D87** (2013) 073007, [1212.6111].

[48] P. Minkowski, *$\mu \to e\gamma$ at a Rate of One Out of 10^9 Muon Decays?*, *Phys. Lett.* **B67** (1977) 421–428.

[49] M. Magg and C. Wetterich, *Neutrino Mass Problem and Gauge Hierarchy*, *Phys. Lett.* **B94** (1980) 61–64.

[50] J. Schechter and J. W. F. Valle, *Neutrino Masses in SU(2) x U(1) Theories*, *Phys. Rev.* **D22** (1980) 2227.

[51] R. Foot, H. Lew, X. G. He and G. C. Joshi, *Seesaw Neutrino Masses Induced by a Triplet of Leptons*, *Z. Phys.* **C44** (1989) 441.

[52] A. Zee, *A Theory of Lepton Number Violation, Neutrino Majorana Mass, and Oscillation*, *Phys. Lett.* **93B** (1980) 389.

[53] K. S. Babu, *Model of 'Calculable' Majorana Neutrino Masses*, *Phys. Lett.* **B203** (1988) 132–136.

[54] J. C. Pati and A. Salam, *Lepton Number as the Fourth Color*, *Phys. Rev.* **D10** (1974) 275–289.

[55] R. N. Mohapatra and J. C. Pati, *A Natural Left-Right Symmetry*, *Phys. Rev.* **D11** (1975) 2558.

[56] G. Senjanovic and R. N. Mohapatra, *Exact Left-Right Symmetry and Spontaneous Violation of Parity*, *Phys. Rev.* **D12** (1975) 1502.

[57] Y. Chikashige, R. N. Mohapatra and R. D. Peccei, *Spontaneously Broken Lepton Number and Cosmological Constraints on the Neutrino Mass Spectrum*, *Phys. Rev. Lett.* **45** (1980) 1926.

[58] R. N. Mohapatra and P. B. Pal, *Massive Neutrinos in Physics and Astrophysics*. WORLD SCIENTIFIC, 3rd ed., 2004, 10.1142/5024.

[59] J. A. Harvey, D. B. Reiss and P. Ramond, *Mass Relations and Neutrino Oscillations in an SO(10) Model*, *Nucl. Phys.* **B199** (1982) 223–268.

[60] V. D. Barger, M. S. Berger, T. Han and M. Zralek, *Test of the Dimopoulos-Hall-Raby ansatz for fermion mass matrices*, *Phys. Rev. Lett.* **68** (1992) 3394–3397, [hep-ph/9203220].

[61] L. J. Hall and S. Raby, *A Complete supersymmetric SO(10) model*, *Phys. Rev.* **D51** (1995) 6524–6531, [hep-ph/9501298].

[62] C. S. Aulakh and R. N. Mohapatra, *Neutrino as the Supersymmetric Partner of the Majoron*, *Phys. Lett.* **119B** (1982) 136–140.

[63] L. J. Hall and M. Suzuki, *Explicit R-Parity Breaking in Supersymmetric Models*, *Nucl. Phys.* **B231** (1984) 419–444.

[64] G. G. Ross and J. W. F. Valle, *Supersymmetric Models Without R-Parity*, *Phys. Lett.* **151B** (1985) 375–381.

[65] Y. Grossman and M. Neubert, *Neutrino masses and mixings in nonfactorizable geometry*, *Phys. Lett.* **B474** (2000) 361–371, [hep-ph/9912408].

[66] N. Arkani-Hamed, S. Dimopoulos, G. R. Dvali and J. March-Russell, *Neutrino masses from large extra dimensions*, *Phys. Rev.* **D65** (2001) 024032, [hep-ph/9811448].

[67] G. Moreau and J. I. Silva-Marcos, *Neutrinos in warped extra dimensions*, *JHEP* **01** (2006) 048, [hep-ph/0507145].

[68] A. Pilaftsis, *Radiatively induced neutrino masses and large Higgs neutrino couplings in the standard model with Majorana fields*, *Z. Phys.* **C55** (1992) 275–282, [hep-ph/9901206].

[69] W. Grimus and L. Lavoura, *One-loop corrections to the seesaw mechanism in the multi-Higgs-doublet standard model*, *Phys. Lett.* **B546** (2002) 86–95, [hep-ph/0207229].

[70] D. Aristizabal Sierra and C. E. Yaguna, *On the importance of the 1-loop finite corrections to seesaw neutrino masses*, *JHEP* **08** (2011) 013, [1106.3587].

[71] J. A. Casas and A. Ibarra, *Oscillating neutrinos and muon —> e, gamma*, *Nucl. Phys.* **B618** (2001) 171–204, [hep-ph/0103065].

[72] J. Lopez-Pavon, E. Molinaro and S. T. Petcov, *Radiative Corrections to Light Neutrino Masses in Low Scale Type I Seesaw Scenarios and Neutrinoless Double Beta Decay*, *JHEP* **11** (2015) 030, [1506.05296].

[73] R. N. Mohapatra, *Mechanism for Understanding Small Neutrino Mass in Superstring Theories*, *Phys. Rev. Lett.* **56** (1986) 561–563.

[74] R. N. Mohapatra and J. W. F. Valle, *Neutrino Mass and Baryon Number Nonconservation in Superstring Models*, *Phys. Rev.* **D34** (1986) 1642.

[75] J. Bernabéu, A. Santamaria, J. Vidal, A. Mendez and J. Valle, *Lepton flavour non-conservation at high energies in a superstring inspired standard model*, *Physics Letters B* **187** (1987) 303 – 308.

[76] E. K. Akhmedov, M. Lindner, E. Schnapka and J. W. F. Valle, *Left-right symmetry breaking in NJL approach*, *Phys. Lett.* **B368** (1996) 270–280, [hep-ph/9507275].

[77] E. K. Akhmedov, M. Lindner, E. Schnapka and J. W. F. Valle, *Dynamical left-right symmetry breaking*, *Phys. Rev.* **D53** (1996) 2752–2780, [hep-ph/9509255].

[78] L. Canetti, M. Drewes and M. Shaposhnikov, *Matter and Antimatter in the Universe*, *New J. Phys.* **14** (2012) 095012, [1204.4186].

[79] G. Steigman, *Observational tests of antimatter cosmologies*, *Ann. Rev. Astron. Astrophys.* **14** (1976) 339–372.

[80] F. Iocco, G. Mangano, G. Miele, O. Pisanti and P. D. Serpico, *Primordial Nucleosynthesis: from precision cosmology to fundamental physics*, *Phys. Rept.* **472** (2009) 1–76, [0809.0631].

[81] G. Steigman, *Primordial Nucleosynthesis in the Precision Cosmology Era*, *Ann. Rev. Nucl. Part. Sci.* **57** (2007) 463–491, [0712.1100].

[82] G. Steigman, *Primordial nucleosynthesis: successes and challenges*, *Int. J. Mod. Phys.* **E15** (2006) 1–36, [astro-ph/0511534].

[83] R. H. Cyburt, B. D. Fields, K. A. Olive and E. Skillman, *New BBN limits on physics beyond the standard model from ^4He*, *Astropart. Phys.* **23** (2005) 313–323, [astro-ph/0408033].

[84] K. A. Olive, G. Steigman and T. P. Walker, *Primordial nucleosynthesis: Theory and observations*, *Phys. Rept.* **333** (2000) 389–407, [astro-ph/9905320].

[85] W. Hu and S. Dodelson, *Cosmic microwave background anisotropies*, *Ann. Rev. Astron. Astrophys.* **40** (2002) 171–216, [astro-ph/0110414].

[86] S. Dodelson, *Modern Cosmology*. Academic Press, Amsterdam, 2003.

[87] Particle Data Group collaboration, C. Patrignani et al., *Review of Particle Physics*, *Chin. Phys.* **C40** (2016) 100001.

[88] Planck collaboration, P. A. R. Ade et al., *Planck 2015 results. XIII. Cosmological parameters*, *Astron. Astrophys.* **594** (2016) A13, [1502.01589].

[89] A. D. Sakharov, *Violation of CP Invariance, c Asymmetry, and Baryon Asymmetry of the Universe*, *Pisma Zh. Eksp. Teor. Fiz.* **5** (1967) 32–35.

[90] G. 't Hooft, *Symmetry Breaking Through Bell-Jackiw Anomalies*, *Phys. Rev. Lett.* **37** (1976) 8–11.

[91] V. A. Kuzmin, V. A. Rubakov and M. E. Shaposhnikov, *On the Anomalous Electroweak Baryon Number Nonconservation in the Early Universe*, *Phys. Lett.* **155B** (1985) 36.

[92] S. Yu. Khlebnikov and M. E. Shaposhnikov, *The Statistical Theory of Anomalous Fermion Number Nonconservation*, *Nucl. Phys.* **B308** (1988) 885–912.

[93] C. Jarlskog, *Commutator of the Quark Mass Matrices in the Standard Electroweak Model and a Measure of Maximal CP Violation*, *Phys. Rev. Lett.* **55** (1985) 1039.

[94] M. E. Shaposhnikov, *Possible Appearance of the Baryon Asymmetry of the Universe in an Electroweak Theory*, *JETP Lett.* **44** (1986) 465–468.

[95] M. B. Gavela, M. Lozano, J. Orloff and O. Pene, *Standard model CP violation and baryon asymmetry. Part 1: Zero temperature*, *Nucl. Phys.* **B430** (1994) 345–381, [hep-ph/9406288].

[96] M. B. Gavela, P. Hernandez, J. Orloff, O. Pene and C. Quimbay, *Standard model CP violation and baryon asymmetry. Part 2: Finite temperature*, *Nucl. Phys.* **B430** (1994) 382–426, [hep-ph/9406289].

[97] P. Huet and E. Sather, *Electroweak baryogenesis and standard model CP violation*, *Phys. Rev.* **D51** (1995) 379–394, [hep-ph/9404302].

[98] K. Kajantie, M. Laine, K. Rummukainen and M. E. Shaposhnikov, *The Electroweak phase transition: A Nonperturbative analysis*, *Nucl. Phys.* **B466** (1996) 189–258, [hep-lat/9510020].

[99] K. Kajantie, M. Laine, K. Rummukainen and M. E. Shaposhnikov, *Is there a hot electroweak phase transition at m(H) larger or equal to m(W)?*, *Phys. Rev. Lett.* **77** (1996) 2887–2890, [hep-ph/9605288].

[100] K. Rummukainen, M. Tsypin, K. Kajantie, M. Laine and M. E. Shaposhnikov, *The Universality class of the electroweak theory*, *Nucl. Phys.* **B532** (1998) 283–314, [hep-lat/9805013].

[101] F. Csikor, Z. Fodor and J. Heitger, *Endpoint of the hot electroweak phase transition*, *Phys. Rev. Lett.* **82** (1999) 21–24, [hep-ph/9809291].

[102] Y. Aoki, F. Csikor, Z. Fodor and A. Ukawa, *The Endpoint of the first order phase transition of the SU(2) gauge Higgs model on a four-dimensional isotropic lattice*, *Phys. Rev.* **D60** (1999) 013001, [hep-lat/9901021].

[103] V. A. Rubakov and M. E. Shaposhnikov, *Electroweak baryon number nonconservation in the early universe and in high-energy collisions*, *Usp. Fiz. Nauk* **166** (1996) 493–537, [hep-ph/9603208].

[104] M. Trodden, *Electroweak baryogenesis*, *Rev. Mod. Phys.* **71** (1999) 1463–1500, [hep-ph/9803479].

[105] T. Yanagida, *HORIZONTAL SYMMETRY AND MASSES OF NEUTRINOS*, *Conf. Proc.* **C7902131** (1979) 95–99.

[106] M. Gell-Mann, P. Ramond and R. Slansky, *Complex Spinors and Unified Theories*, *Conf. Proc.* **C790927** (1979) 315–321, [1306.4669].

[107] R. N. Mohapatra and G. Senjanovic, *Neutrino Masses and Mixings in Gauge Models with Spontaneous Parity Violation*, *Phys. Rev.* **D23** (1981) 165.

[108] M. Fukugita and T. Yanagida, *Barygenesis without grand unification*, *Physics Letters B* **174** (1986) 45 – 47.

[109] E. W. Kolb and S. Wolfram, *Baryon Number Generation in the Early Universe*, *Nucl. Phys.* **B172** (1980) 224.

[110] S. Blanchet, P. Di Bari, D. A. Jones and L. Marzola, *Leptogenesis with heavy neutrino flavours: from density matrix to Boltzmann equations*, *JCAP* **1301** (2013) 041, [1112.4528].

[111] M. Plumacher, *Baryogenesis and lepton number violation*, *Z. Phys.* **C74** (1997) 549–559, [hep-ph/9604229].

[112] L. Covi, N. Rius, E. Roulet and F. Vissani, *Finite temperature effects on CP violating asymmetries*, *Phys. Rev.* **D57** (1998) 93–99, [hep-ph/9704366].

[113] G. F. Giudice, A. Notari, M. Raidal, A. Riotto and A. Strumia, *Towards a complete theory of thermal leptogenesis in the SM and MSSM*, *Nucl. Phys.* **B685** (2004) 89–149, [hep-ph/0310123].

[114] M. Flanz, E. A. Paschos and U. Sarkar, *Baryogenesis from a lepton asymmetric universe*, *Phys. Lett.* **B345** (1995) 248–252, [hep-ph/9411366].

[115] M. Fukugita and T. Yanagida, *Baryogenesis Without Grand Unification*, *Phys. Lett.* **B174** (1986) 45–47.

[116] L. Covi, E. Roulet and F. Vissani, *CP violating decays in leptogenesis scenarios*, *Phys. Lett.* **B384** (1996) 169–174, [hep-ph/9605319].

[117] R. Barbieri, P. Creminelli, A. Strumia and N. Tetradis, *Baryogenesis through leptogenesis*, *Nucl. Phys.* **B575** (2000) 61–77, [hep-ph/9911315].

[118] A. Abada, S. Davidson, F.-X. Josse-Michaux, M. Losada and A. Riotto, *Flavor issues in leptogenesis*, *JCAP* **0604** (2006) 004, [hep-ph/0601083].

[119] S. Davidson and A. Ibarra, *A Lower bound on the right-handed neutrino mass from leptogenesis*, *Phys. Lett.* **B535** (2002) 25–32, [hep-ph/0202239].

[120] W. Buchmuller, P. Di Bari and M. Plumacher, *Cosmic microwave background, matter - antimatter asymmetry and neutrino masses*, *Nucl. Phys.* **B643** (2002) 367–390, [hep-ph/0205349].

[121] J. R. Ellis and M. Raidal, *Leptogenesis and the violation of lepton number and CP at low-energies*, *Nucl. Phys.* **B643** (2002) 229–246, [hep-ph/0206174].

[122] E. Nardi, Y. Nir, E. Roulet and J. Racker, *The Importance of flavor in leptogenesis*, *JHEP* **01** (2006) 164, [hep-ph/0601084].

[123] A. Abada, S. Davidson, A. Ibarra, F. X. Josse-Michaux, M. Losada and A. Riotto, *Flavour Matters in Leptogenesis*, *JHEP* **09** (2006) 010, [hep-ph/0605281].

[124] T. Endoh, T. Morozumi and Z.-h. Xiong, *Primordial lepton family asymmetries in seesaw model*, *Prog. Theor. Phys.* **111** (2004) 123–149, [hep-ph/0308276].

[125] A. Abada, H. Aissaoui and M. Losada, *A Model for leptogenesis at the TeV scale*, *Nucl. Phys.* **B728** (2005) 55–66, [hep-ph/0409343].

[126] O. Vives, *Flavor dependence of CP asymmetries and thermal leptogenesis with strong right-handed neutrino mass hierarchy*, *Phys. Rev.* **D73** (2006) 073006, [hep-ph/0512160].

[127] T. Fujihara, S. Kaneko, S. K. Kang, D. Kimura, T. Morozumi and M. Tanimoto, *Cosmological family asymmetry and CP violation*, *Phys. Rev.* **D72** (2005) 016006, [hep-ph/0505076].

[128] A. Pilaftsis and T. E. J. Underwood, *Electroweak-scale resonant leptogenesis*, *Phys. Rev.* **D72** (2005) 113001, [hep-ph/0506107].

[129] G. C. Branco, R. Gonzalez Felipe and F. R. Joaquim, *A New bridge between leptonic CP violation and leptogenesis*, *Phys. Lett.* **B645** (2007) 432–436, [hep-ph/0609297].

[130] S. Pascoli, S. T. Petcov and A. Riotto, *Connecting low energy leptonic CP-violation to leptogenesis*, *Phys. Rev.* **D75** (2007) 083511, [hep-ph/0609125].

[131] S. Pascoli, S. T. Petcov and A. Riotto, *Leptogenesis and Low Energy CP Violation in Neutrino Physics*, *Nucl. Phys.* **B774** (2007) 1–52, [hep-ph/0611338].

[132] S. Antusch, S. F. King and A. Riotto, *Flavour-Dependent Leptogenesis with Sequential Dominance*, *JCAP* **0611** (2006) 011, [hep-ph/0609038].

[133] S. Antusch and A. M. Teixeira, *Towards constraints on the SUSY seesaw from flavour-dependent leptogenesis*, *JCAP* **0702** (2007) 024, [hep-ph/0611232].

[134] S. Antusch, *Flavour-dependent type II leptogenesis*, *Phys. Rev.* **D76** (2007) 023512, [0704.1591].

[135] S. Blanchet and P. Di Bari, *Flavor effects on leptogenesis predictions*, *JCAP* **0703** (2007) 018, [hep-ph/0607330].

[136] S. Blanchet, P. Di Bari and G. G. Raffelt, *Quantum Zeno effect and the impact of flavor in leptogenesis*, *JCAP* **0703** (2007) 012, [hep-ph/0611337].

[137] V. Cirigliano, A. De Simone, G. Isidori, I. Masina and A. Riotto, *Quantum Resonant Leptogenesis and Minimal Lepton Flavour Violation*, *JCAP* **0801** (2008) 004, [0711.0778].

[138] V. Cirigliano, C. Lee, M. J. Ramsey-Musolf and S. Tulin, *Flavored Quantum Boltzmann Equations*, *Phys. Rev.* **D81** (2010) 103503, [0912.3523].

[139] C. S. Fong, M. C. Gonzalez-Garcia, E. Nardi and J. Racker, *Supersymmetric Leptogenesis*, *JCAP* **1012** (2010) 013, [1009.0003].

[140] A. De Simone and A. Riotto, *On the impact of flavour oscillations in leptogenesis*, *JCAP* **0702** (2007) 005, [hep-ph/0611357].

[141] S. Blanchet, *A New Era of Leptogenesis*, Ph.D. thesis, Munich, Tech. U., 2008. 0807.1408.

[142] W. Buchmuller, P. Di Bari and M. Plumacher, *Leptogenesis for pedestrians*, *Annals Phys.* **315** (2005) 305–351, [hep-ph/0401240].

[143] J. Bernabeu, A. Santamaria, J. Vidal, A. Mendez and J. W. F. Valle, *Lepton Flavor Nonconservation at High-Energies in a Superstring Inspired Standard Model*, *Phys. Lett.* **B187** (1987) 303–308.

[144] A. Ilakovac and A. Pilaftsis, *Flavor violating charged lepton decays in seesaw-type models*, *Nucl. Phys.* **B437** (1995) 491, [hep-ph/9403398].

[145] S. M. Barr, *A Different seesaw formula for neutrino masses*, *Phys. Rev. Lett.* **92** (2004) 101601, [hep-ph/0309152].

[146] M. Malinský, J. C. Romão and J. W. F. Valle, *Novel supersymmetric SO(10) seesaw mechanism*, *Phys. Rev. Lett.* **95** (2005) 161801, [hep-ph/0506296].

[147] G. C. Branco, W. Grimus and L. Lavoura, *The Seesaw Mechanism in the Presence of a Conserved Lepton Number*, *Nucl. Phys.* **B312** (1989) 492–508.

[148] W. Buchmuller and C. Greub, *Heavy Majorana neutrinos in electron - positron and electron - proton collisions*, *Nucl. Phys.* **B363** (1991) 345–368.

[149] T. Asaka, S. Blanchet and M. Shaposhnikov, *The nuMSM, dark matter and neutrino masses*, *Phys. Lett.* **B631** (2005) 151–156, [hep-ph/0503065].

[150] T. Asaka and M. Shaposhnikov, *The nuMSM, dark matter and baryon asymmetry of the universe*, *Phys. Lett.* **B620** (2005) 17–26, [hep-ph/0505013].

[151] W. Chao, Z.-g. Si, Y.-j. Zheng and S. Zhou, *Testing the Realistic Seesaw Model with Two Heavy Majorana Neutrinos at the CERN Large Hadron Collider*, *Phys. Lett.* **B683** (2010) 26–32, [0907.0935].

[152] P. Chattopadhyay and K. M. Patel, *Discrete symmetries for electroweak natural type-I seesaw mechanism*, *Nucl. Phys.* **B921** (2017) 487–506, [1703.09541].

[153] R. Adhikari and A. Raychaudhuri, *Light neutrinos from massless texture and below TeV seesaw scale*, *Phys. Rev.* **D84** (2011) 033002, [1004.5111].

[154] P. S. B. Dev and A. Pilaftsis, *Minimal Radiative Neutrino Mass Mechanism for Inverse Seesaw Models*, *Phys. Rev.* **D86** (2012) 113001, [1209.4051].

[155] S. K. Kang and C. S. Kim, *Extended double seesaw model for neutrino mass spectrum and low scale leptogenesis*, *Phys. Lett.* **B646** (2007) 248–252, [hep-ph/0607072].

[156] X.-G. He, S. Oh, J. Tandean and C.-C. Wen, *Large Mixing of Light and Heavy Neutrinos in Seesaw Models and the LHC*, *Phys. Rev.* **D80** (2009) 073012, [0907.1607].

[157] A. Ibarra, E. Molinaro and S. T. Petcov, *TeV Scale See-Saw Mechanisms of Neutrino Mass Generation, the Majorana Nature of the Heavy Singlet Neutrinos and $(\beta\beta)_{0\nu}$-Decay*, *JHEP* **09** (2010) 108, [1007.2378].

[158] N. Haba, T. Horita, K. Kaneta and Y. Mimura, *TeV-scale seesaw with non-negligible left-right neutrino mixings*, 1110.2252.

[159] E. Ma, *Deciphering the Seesaw Nature of Neutrino Mass from Unitarity Violation*, *Mod. Phys. Lett.* **A24** (2009) 2161–2165, [0904.1580].

[160] D. Wyler and L. Wolfenstein, *Massless Neutrinos in Left-Right Symmetric Models*, *Nucl. Phys.* **B218** (1983) 205–214.

[161] Y. Chikashige, R. N. Mohapatra and R. D. Peccei, *Are There Real Goldstone Bosons Associated with Broken Lepton Number?*, *Phys. Lett.* **98B** (1981) 265–268.

[162] G. B. Gelmini and M. Roncadelli, *Left-Handed Neutrino Mass Scale and Spontaneously Broken Lepton Number*, *Phys. Lett.* **99B** (1981) 411–415.

[163] C. N. Leung and S. T. Petcov, *A Comment on the Coexistence of Dirac and Majorana Massive Neutrinos*, *Phys. Lett.* **125B** (1983) 461–466.

[164] S. T. Petcov and S. T. Toshev, *Conservation of Lepton Charges, Massive Majorana and Massless Neutrinos*, *Phys. Lett.* **143B** (1984) 175–178.

[165] M.-C. Chen and J. Huang, *TeV scale models of neutrino masses and their phenomenology*, *Mod. Phys. Lett. A* **26** (2011) 1147–1167, [1105.3188].

[166] S. M. Boucenna, S. Morisi and J. W. F. Valle, *The low-scale approach to neutrino masses*, 1404.3751.

[167] Particle Data Group collaboration, C. Patrignani et al., *Review of Particle Physics*, *Chin. Phys.* **C40** (2016) 100001.

[168] ATLAS collaboration, G. Aad et al., *Search for heavy Majorana neutrinos with the ATLAS detector in pp collisions at $\sqrt{s} = 8$ TeV*, *JHEP* **07** (2015) 162, [1506.06020].

[169] CMS collaboration, V. Khachatryan et al., *Search for heavy Majorana neutrinos in $e^{\pm}e^{\pm}$+ jets and $e^{\pm}$ $\mu^{\pm}$+ jets events in proton-proton collisions at $\sqrt{s} = 8$ TeV*, *JHEP* **04** (2016) 169, [1603.02248].

[170] LHCb collaboration, R. Aaij et al., *Search for Majorana neutrinos in $B^- \to \pi^+\mu^-\mu^-$ decays*, *Phys. Rev. Lett.* **112** (2014) 131802, [1401.5361].

[171] B. Shuve and M. E. Peskin, *Revision of the LHCb Limit on Majorana Neutrinos*, *Phys. Rev.* **D94** (2016) 113007, [1607.04258].

[172] NA48/2 collaboration, J. R. Batley et al., *Searches for lepton number violation and resonances in $K^{\pm} \to \pi\mu\mu$ decays*, *Phys. Lett.* **B769** (2017) 67–76, [1612.04723].

[173] G. Cacciapaglia, A. Deandrea and S. De Curtis, *Nearby resonances beyond the Breit-Wigner approximation*, *Phys. Lett.* **B682** (2009) 43–49, [0906.3417].

[174] J. Kersten and A. Yu. Smirnov, *Right-Handed Neutrinos at CERN LHC and the Mechanism of Neutrino Mass Generation*, *Phys. Rev.* **D76** (2007) 073005, [0705.3221].

[175] G. Ingelman and J. Rathsman, *Heavy Majorana neutrinos at e p colliders*, *Z. Phys.* **C60** (1993) 243–254.

[176] J. Gluza, *On teraelectronvolt Majorana neutrinos*, *Acta Phys. Polon.* **B33** (2002) 1735–1746, [hep-ph/0201002].

[177] W. Grimus and L. Lavoura, *The Seesaw mechanism at arbitrary order: Disentangling the small scale from the large scale*, *JHEP* **11** (2000) 042, [hep-ph/0008179].

[178] J. G. Korner, A. Pilaftsis and K. Schilcher, *Leptonic CP asymmetries in flavor changing H0 decays*, *Phys. Rev.* **D47** (1993) 1080–1086, [hep-ph/9301289].

[179] J. Lopez-Pavon, S. Pascoli and C.-f. Wong, *Can heavy neutrinos dominate neutrinoless double beta decay?*, *Phys. Rev.* **D87** (2013) 093007, [1209.5342].

[180] S. Pascoli, M. Mitra and S. Wong, *Effect of cancellation in neutrinoless double beta decay*, *Phys. Rev.* **D90** (2014) 093005, [1310.6218].

[181] N. Haba, H. Ishida and Y. Yamaguchi, *Naturalness and lepton number/flavor violation in inverse seesaw models*, *JHEP* **11** (2016) 003, [1608.07447].

[182] P. Hernández, M. Kekic, J. López-Pavón, J. Racker and J. Salvado, *Testable Baryogenesis in Seesaw Models*, *JHEP* **08** (2016) 157, [1606.06719].

[183] M. Drewes and S. Eijima, *Neutrinoless double β decay and low scale leptogenesis*, *Phys. Lett.* **B763** (2016) 72–79, [1606.06221].

[184] W. Buchmuller, P. Di Bari and M. Plumacher, *The Neutrino mass window for baryogenesis*, *Nucl. Phys.* **B665** (2003) 445–468, [hep-ph/0302092].

[185] F. Vissani, *Do experiments suggest a hierarchy problem?*, *Phys. Rev.* **D57** (1998) 7027–7030, [hep-ph/9709409].

[186] J. D. Clarke, R. Foot and R. R. Volkas, *Electroweak naturalness in the three-flavor type I seesaw model and implications for leptogenesis*, *Phys. Rev.* **D91** (2015) 073009, [1502.01352].

[187] J. Racker, M. Pena and N. Rius, *Leptogenesis with small violation of B-L*, *JCAP* **1207** (2012) 030, [1205.1948].

[188] M. Raidal, A. Strumia and K. Turzynski, *Low-scale standard supersymmetric leptogenesis*, *Phys. Lett.* **B609** (2005) 351–359, [hep-ph/0408015].

[189] M. Yu. Khlopov and A. D. Linde, *Is It Easy to Save the Gravitino?*, *Phys. Lett.* **138B** (1984) 265–268.

[190] J. R. Ellis, J. E. Kim and D. V. Nanopoulos, *Cosmological Gravitino Regeneration and Decay*, *Phys. Lett.* **145B** (1984) 181–186.

[191] M. Kawasaki, K. Kohri, T. Moroi and A. Yotsuyanagi, *Big-Bang Nucleosynthesis and Gravitino*, *Phys. Rev.* **D78** (2008) 065011, [0804.3745].

[192] S. Blanchet and P. Di Bari, *New aspects of leptogenesis bounds*, *Nucl. Phys.* **B807** (2009) 155–187, [0807.0743].

[193] A. Pilaftsis and T. E. J. Underwood, *Resonant leptogenesis*, *Nucl. Phys.* **B692** (2004) 303–345, [hep-ph/0309342].

[194] W. Weckesser, *odeintw: Complex and matrix differential equations.*, 2014–.

[195] "A. C. Hindmarsh, "ODEPACK, A Systematized Collection of ODE Solvers," in Scientific Computing, R. S. Stepleman et al. (eds.), North-Holland, Amsterdam, 1983 (vol. 1 of IMACS Transactions on Scientific Computation), pp. 55-64.."

[196] E. Jones, T. Oliphant, P. Peterson et al., *SciPy: Open source scientific tools for Python*, 2001–.

[197] F. Feroz, M. P. Hobson and M. Bridges, *MultiNest: an efficient and robust Bayesian inference tool for cosmology and particle physics*, *Mon. Not. Roy. Astron. Soc.* **398** (2009) 1601–1614, [0809.3437].

[198] F. Feroz and M. P. Hobson, *Multimodal nested sampling: an efficient and robust alternative to MCMC methods for astronomical data analysis*, *Mon. Not. Roy. Astron. Soc.* **384** (2008) 449, [0704.3704].

[199] F. Feroz, M. P. Hobson, E. Cameron and A. N. Pettitt, *Importance Nested Sampling and the MultiNest Algorithm*, *ArXiv e-prints* (June, 2013) , [1306.2144].

[200] Buchner, J., Georgakakis, A., Nandra, K., Hsu, L., Rangel, C., Brightman, M. et al., *X-ray spectral modelling of the agn obscuring region in the cdfs: Bayesian model selection and catalogue*, *A&A* **564** (2014) A125.

[201] A. Fowlie and M. H. Bardsley, *Superplot: a graphical interface for plotting and analysing MultiNest output*, *Eur. Phys. J. Plus* **131** (2016) 391, [1603.00555].

[202] I. Esteban, M. C. Gonzalez-Garcia, M. Maltoni, I. Martinez-Soler and T. Schwetz, *Updated fit to three neutrino mixing: exploring the accelerator-reactor complementarity*, *JHEP* **01** (2017) 087, [1611.01514].

[203] E. Molinaro, S. T. Petcov, T. Shindou and Y. Takanishi, *Effects of Lightest Neutrino Mass in Leptogenesis*, *Nucl. Phys.* **B797** (2008) 93–116, [0709.0413].

[204] S. Antusch, P. Di Bari, D. A. Jones and S. F. King, *Leptogenesis in the Two Right-Handed Neutrino Model Revisited*, *Phys. Rev.* **D86** (2012) 023516, [1107.6002].

[205] W. Buchmuller, R. D. Peccei and T. Yanagida, *Leptogenesis as the origin of matter*, *Ann. Rev. Nucl. Part. Sci.* **55** (2005) 311–355, [hep-ph/0502169].

[206] E. Nardi, Y. Nir, J. Racker and E. Roulet, *On Higgs and sphaleron effects during the leptogenesis era*, *JHEP* **01** (2006) 068, [hep-ph/0512052].

[207] H. B. Nielsen and Y. Takanishi, *Baryogenesis via lepton number violation and family replicated gauge group*, *Nucl. Phys.* **B636** (2002) 305–337, [hep-ph/0204027].

[208] A. Anisimov, S. Blanchet and P. Di Bari, *Viability of Dirac phase leptogenesis*, *JCAP* **0804** (2008) 033, [0707.3024].

[209] E. Molinaro and S. T. Petcov, *The Interplay Between the 'Low' and 'High' Energy CP-Violation in Leptogenesis*, *Eur. Phys. J.* **C61** (2009) 93–109, [0803.4120].

[210] E. Molinaro and S. T. Petcov, *A Case of Subdominant/Suppressed 'High Energy' Contribution to the Baryon Asymmetry of the Universe in Flavoured Leptogenesis*, *Phys. Lett.* **B671** (2009) 60–65, [0808.3534].

[211] M. J. Dolan, T. P. Dutka and R. R. Volkas, *Dirac-Phase Thermal Leptogenesis in the extended Type-I Seesaw Model*, *JCAP* **1806** (2018) 012, [1802.08373].

[212] C. Hagedorn, R. N. Mohapatra, E. Molinaro, C. C. Nishi and S. T. Petcov, *CP Violation in the Lepton Sector and Implications for Leptogenesis*, 1711.02866.

[213] G. C. Branco, A. J. Buras, S. Jager, S. Uhlig and A. Weiler, *Another look at minimal lepton flavour violation, $l_i \to l_{j\gamma}$, leptogenesis, and the ratio M_ν/Λ_{LFV}*, *JHEP* **09** (2007) 004, [hep-ph/0609067].

[214] L. Merlo and S. Rosauro-Alcaraz, *Predictive Leptogenesis from Minimal Lepton Flavour Violation*, *JHEP* **07** (2018) 036, [1801.03937].

[215] C. C. Nishi, B. L. Sánchez-Vega and G. Souza Silva, *$\mu\tau$ reflection symmetry with a high scale texture-zero*, 1806.07412.

[216] A. Meroni, E. Molinaro and S. T. Petcov, *Revisiting Leptogenesis in a SUSY SU(5) x T' Model of Flavour*, *Phys. Lett.* **B710** (2012) 435–445, [1203.4435].

[217] R. N. Mohapatra and C. C. Nishi, *Implications of $\mu - \tau$ flavored CP symmetry of leptons*, *JHEP* **08** (2015) 092, [1506.06788].

[218] C. Hagedorn and E. Molinaro, *Flavor and CP symmetries for leptogenesis and $0\nu\beta\beta$ decay*, *Nucl. Phys.* **B919** (2017) 404–469, [1602.04206].

[219] P. Chen, G.-J. Ding and S. F. King, *Leptogenesis and residual CP symmetry*, *JHEP* **03** (2016) 206, [1602.03873].

[220] C.-C. Li and G.-J. Ding, *Implications of residual CP symmetry for leptogenesis in a model with two right-handed neutrinos*, *Phys. Rev.* **D96** (2017) 075005, [1701.08508].

[221] L. Covi, J. E. Kim, B. Kyae and S. Nam, *Leptogenesis with high-scale electroweak symmetry breaking and an extended Higgs sector*, *Phys. Rev.* **D94** (2016) 065004, [1601.00411].

[222] S. M. Bilenky and S. T. Petcov, *Massive Neutrinos and Neutrino Oscillations*, *Rev. Mod. Phys.* **59** (1987) 671.

[223] T2K collaboration, K. Abe et al., *The T2K Experiment*, *Nucl. Instrum. Meth.* **A659** (2011) 106–135, [1106.1238].

[224] NOvA collaboration, D. S. Ayres et al., *NOvA: Proposal to Build a 30 Kiloton Off-Axis Detector to Study $\nu_\mu \to \nu_e$ Oscillations in the NuMI Beamline*, *n/a* (2004) , [hep-ex/0503053].

[225] Daya Bay collaboration, F. P. An et al., *Observation of electron-antineutrino disappearance at Daya Bay*, *Phys. Rev. Lett.* **108** (2012) 171803, [1203.1669].

[226] RENO collaboration, J. K. Ahn et al., *Observation of Reactor Electron Antineutrino Disappearance in the RENO Experiment*, *Phys. Rev. Lett.* **108** (2012) 191802, [1204.0626].

[227] Double Chooz collaboration, F. Ardellier et al., *Double Chooz: A Search for the neutrino mixing angle theta(13)*, *n/a* (2006) , [hep-ex/0606025].

[228] N. Cabibbo, *Time reversal violation in neutrino oscillation*, *Physics Letters B* **72** (1978) 333 – 335.

[229] S. Bilenky, J. Hošek and S. Petcov, *On the oscillations of neutrinos with dirac and majorana masses*, *Physics Letters B* **94** (1980) 495 – 498.

[230] V. D. Barger, K. Whisnant and R. J. N. Phillips, *CP Violation in Three Neutrino Oscillations*, *Phys. Rev. Lett.* **45** (1980) 2084.

[231] P. I. Krastev and S. T. Petcov, *Resonance Amplification and t Violation Effects in Three Neutrino Oscillations in the Earth*, *Phys. Lett.* **B205** (1988) 84–92.

[232] DUNE collaboration, R. Acciarri et al., *Long-Baseline Neutrino Facility (LBNF) and Deep Underground Neutrino Experiment (DUNE)*, 1512.06148.

[233] Hyper-Kamiokande Proto-Collaboration collaboration, K. Abe et al., *Physics potential of a long-baseline neutrino oscillation experiment using a J-PARC neutrino beam and Hyper-Kamiokande*, *PTEP* **2015** (2015) 053C02, [1502.05199].

[234] S. M. Bilenky, S. Pascoli and S. T. Petcov, *Majorana neutrinos, neutrino mass spectrum, CP violation and neutrinoless double beta decay. 1. The Three neutrino mixing case*, *Phys. Rev.* **D64** (2001) 053010, [hep-ph/0102265].

[235] S. Pascoli, S. T. Petcov and L. Wolfenstein, *Searching for the CP violation associated with Majorana neutrinos*, *Phys. Lett.* **B524** (2002) 319–331, [hep-ph/0110287].

[236] S. Pascoli, S. T. Petcov and T. Schwetz, *The Absolute neutrino mass scale, neutrino mass spectrum, majorana CP-violation and neutrinoless double-beta decay*, *Nucl. Phys.* **B734** (2006) 24–49, [hep-ph/0505226].

[237] V. Barger, S. L. Glashow, P. Langacker and D. Marfatia, *No go for detecting CP violation via neutrinoless double beta decay*, *Phys. Lett.* **B540** (2002) 247–251, [hep-ph/0205290].

[238] S. Pascoli and S. T. Petcov, *The SNO solar neutrino data, neutrinoless double beta decay and neutrino mass spectrum*, *Phys. Lett.* **B544** (2002) 239–250, [hep-ph/0205022].

[239] M. Doi, T. Kotani, H. Nishiura, K. Okuda and E. Takasugi, *Cp violation in majorana neutrinos*, *Physics Letters B* **102** (1981) 323 – 326.

[240] L. Wolfenstein, *CP Properties of Majorana Neutrinos and Double beta Decay*, *Phys. Lett.* **107B** (1981) 77–79.

[241] S. M. Bilenky, N. P. Nedelcheva and S. T. Petcov, *Some Implications of the CP Invariance for Mixing of Majorana Neutrinos*, *Nucl. Phys.* **B247** (1984) 61–69.

[242] B. Kayser, *CPT, CP, and c Phases and their Effects in Majorana Particle Processes*, *Phys. Rev.* **D30** (1984) 1023.

[243] S. Antusch, S. Blanchet, M. Blennow and E. Fernandez-Martinez, *Non-unitary Leptonic Mixing and Leptogenesis*, *JHEP* **01** (2010) 017, [0910.5957].

[244] L. Covi and E. Roulet, *Baryogenesis from mixed particle decays*, *Phys. Lett.* **B399** (1997) 113–118, [hep-ph/9611425].

[245] A. Pilaftsis, *CP violation and baryogenesis due to heavy Majorana neutrinos*, *Phys. Rev.* **D56** (1997) 5431–5451, [hep-ph/9707235].

[246] W. Buchmuller and M. Plumacher, *CP asymmetry in Majorana neutrino decays*, *Phys. Lett.* **B431** (1998) 354–362, [hep-ph/9710460].

[247] C. Weinheimer, *Direct neutrino mass experiments: Present and future*, *Nucl. Phys. Proc. Suppl.* **118** (2003) 279–286.

[248] V. M. Lobashev et al., *Direct search for neutrino mass and anomaly in the tritium beta-spectrum: Status of 'Troitsk neutrino mass' experiment*, *Nucl. Phys. Proc. Suppl.* **91** (2001) 280–286.

[249] W. Buchmuller and M. Plumacher, *Spectator processes and baryogenesis*, *Phys. Lett.* **B511** (2001) 74–76, [hep-ph/0104189].

[250] C. P. Kiessig, M. Plumacher and M. H. Thoma, *Decay of a Yukawa fermion at finite temperature and applications to leptogenesis*, *Phys. Rev.* **D82** (2010) 036007, [1003.3016].

[251] A. De Simone and A. Riotto, *Quantum Boltzmann Equations and Leptogenesis*, *JCAP* **0708** (2007) 002, [hep-ph/0703175].

[252] M. Beneke, B. Garbrecht, C. Fidler, M. Herranen and P. Schwaller, *Flavoured Leptogenesis in the CTP Formalism*, *Nucl. Phys.* **B843** (2011) 177–212, [1007.4783].

[253] A. Anisimov, W. Buchmüller, M. Drewes and S. Mendizabal, *Quantum Leptogenesis I*, *Annals Phys.* **326** (2011) 1998–2038, [1012.5821].

[254] M. Beneke, B. Garbrech, M. Herranen and P. Schwaller*Nucl. Phys.* **B838** (2010) 1–27, [1002.1326].

[255] T. Frossard, A. Kartavtsev and D. Mitrouskas, *Systematic approach to ΔL=1 processes in thermal leptogenesis*, *Phys. Rev.* **D87** (2013) 125006, [1304.1719].

[256] E. Nardi, J. Racker and E. Roulet, *CP violation in scatterings, three body processes and the Boltzmann equations for leptogenesis*, *JHEP* **09** (2007) 090, [0707.0378].

[257] B. Garbrecht and P. Schwaller, *Spectator Effects during Leptogenesis in the Strong Washout Regime*, *JCAP* **1410** (2014) 012, [1404.2915].

[258] C. S. Fong, E. Nardi and A. Riotto, *Leptogenesis in the Universe*, *Adv. High Energy Phys.* **2012** (2012) 158303, [1301.3062].

[259] A. Ibarra and G. G. Ross, *Neutrino phenomenology: The Case of two right-handed neutrinos*, *Phys. Lett.* **B591** (2004) 285–296, [hep-ph/0312138].

[260] S. Blanchet, *Dirac phase leptogenesis*, *J. Phys. Conf. Ser.* **120** (2008) 022007, [0710.0570].

[261] S. Lavignac, I. Masina and C. A. Savoy, *Large solar angle and seesaw mechanism: A Bottom up perspective*, *Nucl. Phys.* **B633** (2002) 139–170, [hep-ph/0202086].

[262] V. Brdar, Y. Emonds, A. J. Helmboldt and M. Lindner, *Conformal Realization of the Neutrino Option*, *Phys. Rev.* **D99** (2019) 055014, [1807.11490].

[263] V. Brdar, A. J. Helmboldt and J. Kubo, *Gravitational Waves from First-Order Phase Transitions: LIGO as a Window to Unexplored Seesaw Scales*, *JCAP* **1902** (2019) 021, [1810.12306].

[264] L. Wolfenstein, *Different Varieties of Massive Dirac Neutrinos*, *Nucl. Phys.* **B186** (1981) 147–152.

[265] S. T. Petcov, *On Pseudodirac Neutrinos, Neutrino Oscillations and Neutrinoless Double beta Decay*, *Phys. Lett.* **110B** (1982) 245–249.

[266] H. Davoudiasl and I. M. Lewis, *Right-Handed Neutrinos as the Origin of the Electroweak Scale*, *Phys. Rev.* **D90** (2014) 033003, [1404.6260].

[267] P. S. Bhupal Dev, P. Millington, A. Pilaftsis and D. Teresi, *Flavour Covariant Transport Equations: an Application to Resonant Leptogenesis*, *Nucl. Phys.* **B886** (2014) 569–664, [1404.1003].

[268] P. S. Bhupal Dev, P. Millington, A. Pilaftsis and D. Teresi, *Kadanoff–Baym approach to flavour mixing and oscillations in resonant leptogenesis*, *Nucl. Phys.* **B891** (2015) 128–158, [1410.6434].

[269] G. Bambhaniya, P. S. Bhupal Dev, S. Goswami, S. Khan and W. Rodejohann, *Naturalness, Vacuum Stability and Leptogenesis in the Minimal Seesaw Model*, *Phys. Rev.* **D95** (2017) 095016, [1611.03827].

[270] T. Hambye, *Leptogenesis at the TeV scale*, *Nucl. Phys.* **B633** (2002) 171–192, [hep-ph/0111089].

[271] T. Hambye, J. March-Russell and S. M. West, *TeV scale resonant leptogenesis from supersymmetry breaking*, *JHEP* **07** (2004) 070, [hep-ph/0403183].

[272] V. Cirigliano, G. Isidori and V. Porretti, *CP violation and Leptogenesis in models with Minimal Lepton Flavour Violation*, *Nucl. Phys.* **B763** (2007) 228–246, [hep-ph/0607068].

[273] Z.-z. Xing and S. Zhou, *Tri-bimaximal Neutrino Mixing and Flavor-dependent Resonant Leptogenesis*, *Phys. Lett.* **B653** (2007) 278–287, [hep-ph/0607302].

[274] E. J. Chun and K. Turzynski, *Quasi-degenerate neutrinos and leptogenesis from L(mu) - L(tau)*, *Phys. Rev.* **D76** (2007) 053008, [hep-ph/0703070].

[275] T. Kitabayashi, *Remark on the minimal seesaw model and leptogenesis with tri/bi-maximal mixing*, *Phys. Rev.* **D76** (2007) 033002, [hep-ph/0703303].

[276] J. A. Casas, J. R. Espinosa, A. Ibarra and I. Navarro, *General RG equations for physical neutrino parameters and their phenomenological implications*, *Nucl. Phys.* **B573** (2000) 652–684, [hep-ph/9910420].

[277] S. Antusch, J. Kersten, M. Lindner and M. Ratz, *Running neutrino masses, mixings and CP phases: Analytical results and phenomenological consequences*, *Nucl. Phys.* **B674** (2003) 401–433, [hep-ph/0305273].

[278] F. Feroz, M. P. Hobson, E. Cameron and A. N. Pettitt, *Importance Nested Sampling and the MultiNest Algorithm*, 1306.2144.

[279] A. Abada, G. Bhattacharyya, D. Das and C. Weiland, *A possible connection between neutrino mass generation and the lightness of a NMSSM pseudoscalar*, *Phys. Lett.* **B700** (2011) 351–355, [1011.5037].

[280] A. Abada, D. Das and C. Weiland, *Enhanced Higgs Mediated Lepton Flavour Violating Processes in the Supersymmetric Inverse Seesaw Model*, *JHEP* **03** (2012) 100, [1111.5836].

[281] R. Alonso, E. Fernandez Martinez, M. B. Gavela, B. Grinstein, L. Merlo and P. Quilez, *Gauged Lepton Flavour*, *JHEP* **12** (2016) 119, [1609.05902].

[282] M. B. Gavela, T. Hambye, D. Hernandez and P. Hernandez, *Minimal Flavour Seesaw Models*, *JHEP* **09** (2009) 038, [0906.1461].

[283] A. G. Dias, C. A. de S. Pires and P. S. R. da Silva, *How the Inverse See-Saw Mechanism Can Reveal Itself Natural, Canonical and Independent of the Right-Handed Neutrino Mass*, *Phys. Rev.* **D84** (2011) 053011, [1107.0739].

[284] F. Bazzocchi, *Minimal Dynamical Inverse See Saw*, *Phys. Rev.* **D83** (2011) 093009, [1011.6299].

[285] E. Ma, *Radiative inverse seesaw mechanism for nonzero neutrino mass*, *Phys. Rev.* **D80** (2009) 013013, [0904.4450].

[286] E. Fernandez-Martinez, J. Hernandez-Garcia and J. Lopez-Pavon, *Global constraints on heavy neutrino mixing*, *JHEP* **08** (2016) 033, [1605.08774].